UNCLASSIFIED

MARTIN MARIETTA ENERGY SYSTEMS LIBRARIES
3 4456 0350537 5

CENTRAL RESEARCH LIBRARY
DOCUMENT COLLECTION

ORNL-2386
Chemistry-General
TID-4500 (13th ed)

cy. 6

REFERENCE COPY

DO NOT REMOVE FROM LIBRARY

CHEMISTRY DIVISION

ANNUAL PROGRESS REPORT

FOR PERIOD ENDING JUNE 20, 1957

CENTRAL RESEARCH LIBRARY
DOCUMENT COLLECTION
LIBRARY LOAN COPY
DO NOT TRANSFER TO ANOTHER PERSON
If you wish someone else to see this document, send in name with document and the library will arrange a loan.

OAK RIDGE NATIONAL LABORATORY
OPERATED BY
UNION CARBIDE NUCLEAR COMPANY
A Division of Union Carbide and Carbon Corporation
UCC
POST OFFICE BOX P · OAK RIDGE, TENNESSEE

UNCLASSIFIED

Printed in USA. Price $4.00 cents. Available from the

Office of Technical Services
U. S. Department of Commerce
Washington 25, D. C.

LEGAL NOTICE

This report was prepared as an account of Government sponsored work. Neither the United States, nor the Commission, nor any person acting on behalf of the Commission:

A. Makes any warranty or representation, express or implied, with respect to the accuracy, completeness, or usefulness of the information contained in this report, or that the use of any information, apparatus, method, or process disclosed in this report may not infringe privately owned rights; or

B. Assumes any liabilities with respect to the use of, or for damages resulting from the use of any information, apparatus, method, or process disclosed in this report.

As used in the above, "person acting on behalf of the Commission" includes any employee or contractor of the Commission to the extent that such employee or contractor prepares, handles or distributes, or provides access to, any information pursuant to his employment or contract with the Commission.

UNCLASSIFIED

ORNL-2386
Chemistry-General
TID-4500 (13th ed)

Contract No. W-7405-eng-26

CHEMISTRY DIVISION

ANNUAL PROGRESS REPORT

for Period Ending June 20, 1957

E. H. Taylor, Director
M. A. Bredig, Associate Director

DATE ISSUED

OCT 4 1957

OAK RIDGE NATIONAL LABORATORY
Operated by
UNION CARBIDE NUCLEAR COMPANY
A Division of Union Carbide and Carbon Corporation
Post Office Box X
Oak Ridge, Tennessee

UNCLASSIFIED

MARTIN MARIETTA ENERGY SYSTEMS LIBRARIES
3 4456 0350537 5

Chemistry Division progress reports previously issued in this series are as follows:

ORNL-65	March, April, May, 1948
ORNL-176	June, July, August, 1948
ORNL-229	September, October, November, 1948
ORNL-336	December, 1948, January and February, 1949
ORNL-286	Period Ending June 30, 1949
ORNL-499	Period Ending September 30, 1949
ORNL-607	Period Ending December 31, 1949
ORNL-685	Period Ending March 31, 1950
ORNL-795	Period Ending June 30, 1950
ORNL-870	Period Ending September 30, 1950
ORNL-1036	Period Ending December 31, 1950
ORNL-1053	Period Ending March 31, 1951
ORNL-1116	Period Ending June 30, 1951
ORNL-1153	Period Ending September 30, 1951
ORNL-1260	Period Ending December 31, 1951
ORNL-1285	Period Ending March 31, 1952
ORNL-1344	Period Ending June 30, 1952
ORNL-1432	Period Ending September 30, 1952
ORNL-1482	Period Ending December 31, 1952
ORNL-1587	Period Ending June 20, 1953
ORNL-1674	Period Ending December 20, 1953
ORNL-1755	Period Ending June 20, 1954
ORNL-1832	Period Ending December 20, 1954
ORNL-1940	Period Ending June 20, 1955
ORNL-2046	Period Ending December 20, 1955
ORNL-2159	Period Ending June 20, 1956

ORNL-2386
Chemistry-General
TID-4500 (13th ed)

INTERNAL DISTRIBUTION

1. C. E. Center
2. Biology Library
3. Health Physics Library
4-6. Central Research Library
7-12. Laboratory Records Department
13. Laboratory Records, ORNL R.C.
14. Reactor Experimental Engineering Library
15. A. M. Weinberg
16. L. B. Emlet (K-25)
17. J. P. Murray (Y-12)
18. J. A. Swartout
19. E. H. Taylor
20. E. J. Murphy
21. E. D. Shipley
22. S. C. Lind
23. M. L. Nelson
24. W. H. Jordan
25. R. R. Dickison
26. F. L. Culler
27. A. H. Snell
28. A. Hollaender
29. M. T. Kelley
30. R. A. Charpie
31. K. Z. Morgan
32. T. A. Lincoln
33. A. S. Householder
34. C. S. Harrill
35. C. E. Winters
36. D. W. Cardwell
37. D. Phillips
38. J. A. Lane
39. G. E. Boyd
40. M. A. Bredig
41. R. W. Stoughton
42. R. B. Briggs
43. G. W. Parker
44. C. J. Borkowski
45. G. H. Jenks
46. K. A. Kraus
47. H. A. Levy
48. R. S. Livingston
49. T. E. Willmarth
50. C. H. Secoy
51. C. J. Hochanadel
52. W. H. Baldwin
53. A. R. Brosi
54. R. N. Lyon
55. S. A. Reynolds
56. P. F. Thomason
57. E. G. Bohlmann
58. C. P. Keim
59. C. D. Susano
60. A. S. Dworkin
61. P. M. Reyling
62. R. Livingston
63. G. H. Cartledge
64. E. R. Van Artsdalen
65. G. C. Williams
66. R. W. Johnson
67. J. R. McNally, Jr.
68. G. D. O'Kelley
69. S. J. Cromer
70. M. J. Skinner
71. D. S. Billington
72. H. G. MacPherson
73. J. L. Gabbard
74. R. H. Busey
75. J. J. Panajian
76. D. W. Sherwood
77. P. H. Emmett (consultant)
78. H. Eyring (consultant)
79. J. Bigeleisen (consultant)
80. G. T. Seaborg (consultant)
81. C. E. Larson (consultant)
82. E. P. Wigner (consultant)

EXTERNAL DISTRIBUTION

83. R. F. Bacher, California Institute of Technology
84. Division of Research and Development, AEC, ORO
85. Boeing Airplane Company
86. Union Carbide and Carbon Chemical Company (South Charleston)
87. North America Aviation, Inc.

88-602. Given distribution as shown in TID-4500 (13th ed.) under Chemistry-General category (75 copies – OTS)

CONTENTS

CHEMISTRY DIVISION PUBLICATIONS FROM JUNE 20, 1956 TO JUNE 20, 1957 ix

SUMMARY 1

NUCLEAR CHEMISTRY 9
Decay Schemes of Sm^{145} and Pm^{145} 9
Decay of Dy^{159} 9
Nuclear Decay of Br^{84} and the Level Scheme in Kr^{84} 9
Half Life of Tc^{98} and Its Abundance in Fission-Product Technetium 12
Fission-Product "Solubilities" in In-Pile Loops 12
Effective Reactor Cross Sections in MTR Fuel Assemblies 16
Neutron Cross Sections of U^{234}, Pu^{239}, and Pu^{240} 20
Calculated Thermal Cross Section of Pu^{240} and Calculated and Experimental Effective Reactor Cross Sections of Pu^{239} and Pu^{240} 20
Measurement of the Thermal-Neutron Capture Cross Section of Pu^{240} with the Pile Oscillator 21
Remeasurement of the Thermal Capture Cross Section of U^{234} 22
Survey of Thorium Breeder Blankets 22
Effect of Nitrite on Neptunium Extraction 22
Absorption Spectra of Neptunium Oxidation States 22
Investigation of Nitrite Catalysis 23
Examination of Hanford-recovered Uranium for Neptunium Content 24
Volatilization of Fission Products by the Melting of Reactor Fuel Plates 25

ISOLATION AND CHEMICAL PROPERTIES OF SYNTHETIC ELEMENTS 26
Chemistry of Technetium 26
Search for Technetium in Terrestrial Materials 26
Solvent Extraction of Heptavalent Technetium 26
Heat Capacity of Potassium Pertechnetate from 16 to 310°K 26
Low-Temperature Heat Capacity of Potassium Hexachlororhenate 29

CHEMICAL SEPARATION OF ISOTOPES 31
Enrichment of Oxygen Isotopes 31
Carbon Dioxide Exchange Systems 31
Nitric Oxide Exchange Systems 31
Carbon Monoxide Exchange Systems 31
Enrichment of Sulfur Isotopes 32
Separation of Boron Isotopes 32
Laboratory-Scale Anco System 32
Heat of Reaction of Anisole with Boron Trifluoride 33
N^{15} Separation 33

RADIATION CHEMISTRY 34
Effect of Ionizing Radiation on Heterogeneous Catalysts 34
Gas-Phase Irradiation 34
Retardation of Alpha-Ray-Induced Acetylene Polymerization by Benzene Vapor 34
Photoreduction of Ceric Ion in Sulfuric Acid Solutions – Effect of Thallous Ion 35
Warming Curves for the Condensed Product of Dissociated Water Vapor and for Hydrogen Peroxide Glass 36

Free-Radical and Molecular Yields in the Gamma-Ray Decomposition of Heavy Water 36
Radiation-induced Nitrite Formation from Concentrated Nitrate Solutions 37
Effect of Uranyl Ion on the Oxidation of Ferrous Sulfate by Gamma Radiation 37
Radiolyses of Compounds Dispersed in Alkali-Halide Matrices 37

ORGANIC CHEMISTRY 39
The Pinacol Rearrangement 39
The Phenyl-di-*p*-tolyl System 39
The Diphenyl-*o*-tolyl System 44
The Amino-Alcohol Rearrangement 50
The Deamination of 1,1-Diphenyl-2-amino-1-propanol 50
The Hydrogen/Deuterium Isotope Effect (k_H/k_D) in the Rearrangement of Triarylethylene Glycols 52
Stereochemistry of the Solvolytic and Deamination Reactions of 1,2,2-Triphenylethyl Derivatives 54
Stereochemical Study of the Acetoxyl Exchange Reaction of 1,2,2-Triphenylethyl Acetate 55
Kinetic Determinations 56
Study of the Absolute and Relative Rates of Decarbonylation of Formic Acid and Formic-*d* Acid in Concentrated Sulfuric Acid 57
Cracking Patterns of Formic Acid, Formic Acid-*d*, and Formic-*d* Acid in the Mass Spectrometer 59
Preparation of Alkyl Phosphinates by the Grignard Reaction 59
Acid Formation During the Radiolysis of Organophosphorus Compounds 59
Dibutyl Phosphonoacetic Acid 61
Composition of Amsco 125-82 61
Preparation and Properties of Uranium- and Thorium-Containing Organic Compounds 62

CHEMISTRY OF AQUEOUS SYSTEMS 64
Spectrophotometry of Aqueous Solutions 64
Adaptation of a Cary Model 14M Recording Spectrophotometer for Measurements of Aqueous Spectra at Elevated Temperatures and Pressures 64
Differential Temperature Absorption of Heavy and Light Water in the Visible and Near-Infrared Regions 67
A Spectrophotometric Method for Determination of H_2O in D_2O 69
Extension of Measurements of the Aqueous Absorption Spectra of Neptunium Ions 70
The Cell Pt, H_2, $HCl_{(m)}$, AgCl, Ag at High Temperatures 71
A High-Temperature Glass Electrode 73
The Cell Pt, PbO_2, $PbSO_4$, $H_2SO_{4(m)}$, Ag_2SO_4, Ag as a Function of Temperature 73
A High-Temperature Isopiestic Unit 74
The Apparatus 75
Operability and Results 77
The Base-saturated Region of the System CuO-UO_3-SO_3-H_2O at 100°C 80
Characterization of Slurry Flocculation by pH Measurements 81
Homogeneous Catalysis of the Hydrogen-Oxygen Reaction in Aqueous Solutions 83
Studies in the Perchlorate System 83
Studies in the Sulfate System 84
Studies in the Deuterium–Heavy-Water System 86
Critical Phenomenon in Binary Aqueous Solutions – The System SO_3-H_2O 87
The Densities of Heavy-Water Liquid and Saturated Vapor at Elevated Temperatures 91

Anion Exchange Studies 92
Adsorption of Metals from HCl-HF Solutions 92
Adsorption from EDTA Solutions 93
Adsorption of Gaseous $GeCl_4$ by Anion Exchangers 95
General Separations Scheme 96
Activity Coefficients of Strong Electrolytes in the Resin Phase 97
Adsorption of HF by Anion Exchangers 98
Ultracentrifugation of Inorganic Systems 99
Interference Optical System 99
Silicotungstic Acid 99
Polymerization of Sn(IV) 100
Polymerization of Th(IV) in Perchlorate and Chloride Solutions 100
Pb(II) in Acidic Solutions 101
Search for Hydrolytic Copolymers 101
Temperature Coefficients of Ion Exchange Equilibria 101
Trace-Metal Adsorption on a Sulfonic Acid Cation Exchanger 101
Adsorption of Acids and Bases by Hydrous Zirconium Oxide 103
Solubility of Chloroaurates in HCl and in LiCl Solutions 104
Dispersions of Thorium Oxide 104
Adsorption on Inorganic Materials 105
Anion and Cation Exchange Properties of Hydrous Oxides 105
Acid Dependence of Selectivities – Group Separation of Alkali Metals and Alkaline Earths 106

CHEMISTRY OF CORROSION 108
Electrochemistry of Corrosion Systems 108
Studies on Corrosion Systems Involving Independent, Simultaneous Electrochemical Reactions 110
Electrochemistry of Zirconium 114
Evidence for a Flade Potential on Inhibited Iron Electrodes 116

NONAQUEOUS SYSTEMS AT HIGH TEMPERATURES 117
Heterogeneous Isotopic Exchange Reactions of Fluorine-Containing Compounds 117
Self-Diffusion in Molten Salts 117
Liquid Metal–Salt Solutions 119
High-Temperature Region of the Sodium–Sodium Halide Systems 119
Rubidium–Rubidium Halide Systems 122
Electrical Conductivity in Molten Salt–Metal Solutions 122
Effusiometric Determination of the Vapor Pressure of NaCl and KCl. Effect of Vapor Phase Association 125

CHEMICAL PHYSICS 128
Microwave and Radio-Frequency Spectroscopy 128
Hydrogen Gas and Atomic Hydrogen Yields from Irradiated Acids 128
Paramagnetic Resonance Studies 129
Nuclear Magnetic Resonance 130
Neutron and X-Ray Diffraction Studies 130
Effect of Thermal Motion on the Diffraction Measurement of Bond Lengths in Crystals 130
Crystal Structure of Acetylglycine 132
Neutron and X-Ray Diffraction Studies on Urea 134
Preliminary Neutron Diffraction Study of Solid H_2O_2 137

Mass Spectrometry and Related Techniques 138
Dissociation of CO^+ and CO^{++} Ions by Collision with Neutral Molecules 138
Research Mass Spectrometer, RS 1 139
Two-Stage Mass Spectrometer, RS 2 139
Fundamental Vibrational-Rotational Band of $N^{15}O$ 141
Beam Studies in Chemical Kinetics 142

CHEMISTRY DIVISION PUBLICATIONS FROM JUNE 20, 1956, TO JUNE 20, 1957

NUCLEAR CHEMISTRY

B. H. Ketelle, H. Thomas, and A. R. Brosi, "Decay of the Cerium-139 Isomers," *Phys. Rev.* **103**, 190 (1956).

A. R. Brosi and B. H. Ketelle, "Radioactive Decay of La^{137} and Ce^{137}," *Phys. Rev.* **103**, 917 (1956).

G. D. O'Kelley and Q. V. Larson, "Half-life of Tc^{98} and Its Abundance in Fission-Product Technetium," presented at the Southwide Chemical Conference, Memphis, Tennessee, December 6, 1956; *Southern Chemist* **16**, 113 (1956).

G. D. O'Kelley, Q. V. Larson, and G. E. Boyd, "Decay Chain Mo^{101}-Tc^{101}," *Bull. Am. Phys. Soc.* **2**, 24 (1957).

N. R. Johnson and G. D. O'Kelley, "Decay of Br^{84}," *Bull. Am. Phys. Soc.* **2**, 24 (1957).

N. R. Johnson, J. B. Cumming, and M. Izawa, "Decay of Se^{72}," *Bull. Am. Phys. Soc.* **2**, 230 (1957).

E. C. Campbell and F. Nelson, "Rapid Ion-Exchange Techniques for Radiochemical Separations," *J. Inorg. Nuclear Chem.* **3**, 233 (1956).

J. Halperin and R. W. Stoughton, "Batch Versus Continuous Processing in Fluidized Nuclear Reactors," *Ind. Eng. Chem.* **48**, 2115 (1956).

R. W. Stoughton and J. Halperin, "Heavy Isotope Buildup in the Core of a U-233 Breeder," *J. Nuclear Energy* **4**, 279 (1957).

M. H. Lietzke and R. W. Stoughton, "Feasible Chemical Forms for Thorium Breeder Blanket," *Ind. Eng. Chem.* **49**, 202 (1957).

L. I. Katzin and R. W. Stoughton, "A Manganese Dioxide Procedure for Isolation and Concentration of Protoactinium from Irradiated Thorium Compounds," *J. Inorg. Nuclear Chem.* **3**, 229 (1956).

R. W. Stoughton, book review, *Gmelin's Handbook of Inorganic Chemistry: Thorium and Isotopes*, *J. Chem. Educ.* **34**(3), A135 (1957).

CHEMICAL SEPARATION OF ISOTOPES

G. M. Begun, "Nitrogen Isotope Effect in the Distillation of N_2O_4," *J. Chem. Phys.* **25**, 1279 (1956).

G. M. Begun and C. E. Melton, "Nitrogen Isotopic Fractionation Between NO and NO_2 and Mass Discrimination in Mass Analysis of NO_2," *J. Chem. Phys.* **25**, 1292 (1956).

G. M. Begun, L. L. Brown, L. B. Yeatts, N. C. Bradley, and E. F. Joseph, *Chemical and Isotopic Studies of the Nitrox System for N^{15} Enrichment*, ORNL-2291 (June 6, 1957).

A. A. Palko, L. L. Brown, G. M. Begun, and E. F. Joseph, *Chemical and Isotopic Studies of the Closed-Cycle Carbonate System for N^{15} Enrichment*, ORNL-2138 (Nov. 8, 1956).

RADIATION CHEMISTRY

E. H. Taylor and H. W. Kohn, "An Enhancement of Catalytic Activity by Gamma Radiation," *J. Am. Chem. Soc.* **79**, 252 (1957).

S. C. Lind and P. S. Rudolph, "Retardation of a Radiochemical Reaction by Charge Transfer in a Bimolecular Mixture of Gases," *J. Chem. Phys.* **26**, 1768 (1957).

J. A. Ghormley, "Warming Curves for the Condensed Product of Dissociated Water Vapor and for Hydrogen Peroxide Glass," *J. Am. Chem. Soc.* **79**, 1862 (1957).

J. A. Ghormley and A. C. Stewart, "Effects of Gamma-Radiation on Ice," *J. Am. Chem. Soc.* **78**, 2934 (1956).

J. A. Ghormley, "Thermal Behavior of Amorphous Ice," *J. Chem. Phys.* **25**, 599 (1956).

J. A. Ghormley, "Lifetime of Intermediates in Water Subjected to Electron Irradiation," *Radiation Research* **5**, 247 (1956).

T. J. Sworski, "Mechanism for the Reduction of Ceric Ion by Thallous Ion Induced by Cobalt-60 Gamma Radiation," *Radiation Research* **4**, 483 (1956).

T. J. Sworski, "Relative Rate Constants for Reaction of OH Radical with Sulfuric Acid, Formic Acid and Cerous Ion," *J. Am. Chem. Soc.* **78**, 1768 (1956).

C. J. Hochanadel and S. C. Lind, "Radiation Chemistry," *Ann. Rev. Phys. Chem.* **7**, 83 (1956).

C. J. Hochanadel, "Radiation Decomposition of Water Used as a Reactor Moderator or Coolant" (Material for Revised Reactor Handbook), ORNL CF-56-12-32 (Dec. 10, 1956).

C. J. Hochanadel, "Radiation Stability of Aqueous Fuel Solutions" (Material for Revised Reactor Handbook), ORNL CF-56-11-54 (Nov. 13, 1956).

ORGANIC CHEMISTRY

A. J. Weinberger, J. B. Davidson, and G. A. Ropp, "Liquid Scintillation Counter for Carbon-14 Employing Automatic Sample Alternation," *Anal. Chem.* **28**, 110 (1956).

G. A. Ropp and E. M. Hodnett, "Isotopic Fractionation Studies of Reactions with Cleavage of a Carbon-14 to Hydrogen Bond in the Rate-Determining Step," *J. Chem. Phys.* **25**, 587 (1956).

C. E. Higgins and W. H. Baldwin, "Ester Interchange for the Preparation of P^{32}-Labeled Butyl Phosphates," *J. Org. Chem.* **21**, 1156 (1956).

J. F. Eastham, J. E. Huffaker, V. F. Raaen, and C. J. Collins, "A Reinvestigation of the Alkaline Cleavage of α-Arylbenzoins," *J. Am. Chem. Soc.* **78**, 4323 (1956).

B. M. Benjamin and C. J. Collins, "Molecular Rearrangements. VIII. A Mechanistic Correlation of the Aldehyde-Ketone and Pinacol Rearrangements," *J. Am. Chem. Soc.* **78**, 4329 (1956).

G. A. Ropp, "Errors in Quantitative Tracer Studies," *J. Chem. Educ.* **34**, 60 (1957).

B. M. Benjamin and C. J. Collins, "Molecular Rearrangements. IX. The *p*-Tolyl/Phenyl Migration Ratio in Deamination Reactions," *J. Am. Chem. Soc.* **78**, 4952 (1956).

W. A. Bonner and C. J. Collins, "Molecular Rearrangements. X. Rearrangement During the Deamination of 1,2,2-Triphenylethylamine with Nitrous Acid," *J. Am. Chem. Soc.* **78**, 5587 (1956).

W. H. Baldwin, *Acid Formation in the Radiolysis of Phosphorus Esters*, ORNL CF-57-4-9 (April 3, 1957).

CHEMISTRY OF AQUEOUS SYSTEMS

J. S. Johnson and K. A. Kraus, "Hydrolytic Behavior of Metal Ions. VI. Ultracentrifugation of Zirconium(IV) and Hafnium(IV); Effect of Acidity on the Degree of Polymerization," *J. Am. Chem. Soc.* **78**, 3937 (1956).

R. W. Holmberg, K. A. Kraus, and J. S. Johnson, "Hydrolytic Behavior of Metal Ions. VIII. Ultracentrifugation of Bismuth(III) in Perchlorate Solution," *J. Am. Chem. Soc.* **78**, 5506 (1956).

J. S. Johnson and K. A. Kraus, "Equilibrium Ultracentrifugations of Acidic Hg(I), Hg(II), In(III), and Au(III) Solutions," *J. Am. Chem. Soc.* **79**, 2034 (1957).

M. H. Lietzke and R. W. Stoughton, "The Thermodynamics of Indium Sulfate Solutions," *J. Am. Chem. Soc.* **78**, 4520 (1956).

E. V. Jones, M. H. Lietzke, and W. L. Marshall, "The Solubility of Several Metal Sulfates at High Temperature and Pressure in Water and in Aqueous Uranyl Sulfate Solution," *J. Am. Chem. Soc.* **79**, 267 (1957).

M. H. Lietzke and R. W. Stoughton, "On the Solubility of Ag_2SO_4 in Various Electrolyte Media. Effects of the Solubility of Ag_2SO_4 and AgCl on the Ag, Ag_2SO_4 and the Ag, AgCl Electrodes," *J. Am. Chem. Soc.* **79**, 2067 (1957).

W. L. Marshall and J. S. Gill, "A Synthetic Uranyl Silicate Hydrate," *J. Am. Chem. Soc.* **79**, 1300 (1957).

B. A. Soldano, review of book by G. H. Osborne, *Synthetic Ion Exchangers. Recent Developments in Theory and Application*, *J. Am. Chem. Soc.* **79**, 1521 (1957).

CHEMISTRY OF CORROSION

G. H. Cartledge, "The Electrode Potential of the OsO_2-OsO_4 Couple," *J. Phys. Chem.* **60**, 1468 (1956).

G. H. Cartledge, "The Passivation of Iron by Osmium(VIII) Oxide and the Origin of the Flade Potential," *J. Phys. Chem.* **60**, 1571 (1956).

R. F. Sympson and G. H. Cartledge, "The Mechanism of the Inhibition of Corrosion by the Pertechnetate Ion. IV. Comparison with Other XO_4^{n-} Inhibitors," *J. Phys. Chem.* **60**, 1037 (1956).

NONAQUEOUS SYSTEMS AT HIGH TEMPERATURE

M. A. Bredig, "Salt-Metal Liquid-Phase Equilibria," *Proceedings of the Symposium on "High-Temperature—A Tool for the Future,"* p 111–116, at Berkeley, California, June 25, 26, 27, 1956, Stanford Research Institute, Stanford University, California.

CHEMICAL PHYSICS

S. Datz and E. H. Taylor, "Ionization on Platinum and Tungsten Surfaces. I. The Alkali Metals," *J. Chem. Phys.* **25**, 389 (1956).

S. Datz and E. H. Taylor, "Ionization on Platinum and Tungsten Surfaces. II. The Potassium Halides," *J. Chem. Phys.* **25**, 395 (1956).

S. W. Peterson and H. A. Levy, "Proton Positions in $CuCl_2 \cdot 2H_2O$ by Neutron Diffraction," *J. Chem. Phys.* **26**, 220 (1957).

S. W. Peterson and H. A. Levy, "A Single-Crystal Neutron Diffraction Study of Heavy Ice," *Acta Cryst.* **10**, 70 (1957).

W. R. Busing and H. A. Levy, "High Speed Computation of the Absorption Correction for Single-Crystal Diffraction Measurements," *Acta Cryst.* **10**, 180 (1957).

W. R. Busing and H. A. Levy, "Neutron Diffraction Study of Calcium Hydroxide," *J. Chem. Phys.* **26**, 563 (1957).

J. E. Worsham, Jr., H. A. Levy, and S. W. Peterson, "The Positions of Hydrogen Atoms in Urea by Neutron Diffraction," *Acta Cryst.* **10**, 319 (1957).

T. A. Gens, J. A. Wethington, Jr., A. R. Brosi, and E. R. Van Artsdalen, "The Exchange of F^{18} Between Metallic Fluorides and Gaseous Fluorine Compounds," *J. Am. Chem. Soc.* **79**, 1001 (1957).

R. Livingston and H. Zeldes, "Zeeman Effect on the Quadrupole Spectrum of Iodic Acid," *J. Chem. Phys.* **26**, 351 (1957).

H. Zeldes and R. Livingston, "Zeeman Effect on the Quadrupole Spectra of Sodium, Potassium, and Barium Chlorates," *J. Chem. Phys.* **26**, 1102 (1957).

J. H. Burns and M. A. Bredig, "Transformation of Calcite to Aragonite by Grinding," *J. Chem. Phys.* **25**, 1281 (1956).

H. M. Rosenstock and C. E. Melton, "Metastable Transitions and Collision-Induced Dissociations in Mass Spectra," *J. Chem. Phys.* **26**, 314 (1957).

C. E. Melton and H. M. Rosenstock, "Collision-Induced Dissociations in the Mass Spectrum of Methane," *J. Chem. Phys.* **26**, 568 (1957).

C. E. Melton, M. M. Bretscher, and R. Baldock, "Collision-Induced Dissociations in the Mass Spectrum of Acetylene," *J. Chem. Phys.* **26**, 1302 (1957).

CHEMISTRY DIVISION ANNUAL PROGRESS REPORT

SUMMARY

NUCLEAR CHEMISTRY

The decay schemes of Sm^{145}, Pm^{145}, and Dy^{159} were studied.

The decay properties of 31.80-min Br^{84} were studied by means of single-crystal and coincidence scintillation spectrometry. It was possible to formulate an energy-level scheme in Kr^{84} with excited states at 0.88, 1.90, 2.17, 2.36, 2.62, 2.71, 2.91, 3.35, 3.70, 3.91, and 4.18 Mev.

A preliminary half life of $(1.5 \pm 0.7) \times 10^6$ years was measured for Tc^{98}. The gamma rays characteristic of Tc^{98} were detected in a sample of fission-product technetium, from which the atomic ratio Tc^{98}/Tc^{99} was calculated to be 3×10^{-8}.

Although the resonance parameters of U^{234} suggested a thermal capture cross section much smaller than 92 ± 7 barns, obtained by Pomerance, a redetermination by the pile oscillator method with a different sample of enriched U^{234} confirmed the 90-barn value, and hence negative resonances must exist. An effective reactor capture cross section of 500 barns was calculated for Pu^{239} from experimental data in a graphite reactor, as compared with a value of 490 barns calculated from the resonance parameters and the cross section vs energy curve. The results of irradiations in a graphite reactor, in the light-water-moderated MTR, and in the heavy-water-moderated Chalk River reactor were all consistent, with an effective reactor capture cross section for Pu^{240} at low concentrations of about 1200 barns, as contrasted with values of about 500 barns reported previously by other investigators. An effective reactor cross section of 1200 barns was also calculated for Pu^{240} from recent resonance parameter data and the cross section vs energy curve, assuming a thermal-to-resonance flux ratio of 12. Also, by using the resonance parameter data, a thermal (2200-m/s) cross section of about 340 barns and an "effective" thermal cross section (reflecting the non-$1/v$ dependence) of about 370 barns for 500°K neutrons were calculated. By using the pile oscillator, a thermal cross section of about 360 barns was determined for Pu^{240}.

Twelve highly irradiated MTR fuel assemblies were analyzed by chemical, radiochemical, and mass spectrographic methods for the relative concentrations of U^{234}, U^{235}, U^{236}, U^{238}, Np^{237}, Pu^{238}, Pu^{239}, Pu^{240}, Pu^{241}, Pu^{242}, and Pu^{244}. By using flux-time values based on U^{236}/U^{235} and U^{238}/U^{235} ratios, effective cross sections of 34 ± 6 and 23 ± 3 barns were found for U^{236} and U^{238}, respectively. From the known thermal cross sections and resonance integrals for these two nuclides, a thermal-to-resonance flux ratio of 12 was obtained. By using this figure and the known thermal cross sections and resonance integrals for the other nuclides, reactor cross sections were calculated for them. The calculated relative concentrations of heavy nuclides based on these values agreed remarkably well with the experimental values.

In order to get some idea of the behavior of the more prevalent fission products and heavy nuclides under homogeneous reactor conditions, analyses were made as a function of time on several in-pile loop solutions for the following nuclides: Np^{239}, Cs^{137}, Ce^{144}, Sr^{89}, Ba^{140}, Mo^{99}, I^{131}, Zr^{95}, Nb^{95}, and Ru^{103}. Analyses for Pu^{239}, Tc^{99}, and Y^{91} are still under way. While the behavior of these species varies with conditions, in general, Np, Cs, and Ce apparently remain in solution; Sr and Ba initially remain in solution and then appear to reach saturation concentrations, with the concentration of Sr higher than that of Ba, as expected; Zr, Nb, and Ru are relatively "insoluble," and after extended irradiation only about 1% or less remains in solution; the fraction of the Mo and I remaining in solution tends to level off after a while at from 0.1 to 0.5 of the amounts formed (the iodine is somewhat volatile and tends to deposit elsewhere in the system); preliminary plutonium data indicate a low "solubility." In order to explain the quantities of Np^{239} found in various loops, it was necessary to use effective U^{238} capture cross sections of 8 to 50 barns (as contrasted with the thermal value of 2.8 barns), depending on the closeness of the loop to the reactor fuel.

A survey was made of the feasible chemical forms for a thorium breeder blanket. The only blanket form which has so far been demonstrated to be practical consists of aluminum-jacketed metal slugs. Of the other systems, a thorium oxide slurry in D_2O, and thorium nitrate (with N^{15}) dissolved in D_2O now appear to be the most promising.

The beneficial effect of nitrite ion on the extraction of Np(V) in process solutions was studied. When less than the stoichiometric ratio of nitrite to neptunium was present in 4 *N* HNO_3, an increase in TBP distribution coefficients by an order of magnitude was observed. The extractable state has been identified as Np(VI), and a nitrite-catalyzed oxidation by nitrate ion is proposed to explain the results.

Sampling and determination of the neptunium content of 19.5 tons of uranium oxide ashes from Hanford (tower, cyclone, and barrier filter ashes) indicated a total of 130 g of neptunium, which is presently being recovered in the ORNL Metal Recovery Plant.

Data are presented from the initial phase of the investigation of fission-product volatility when various reactor fuel elements, such as STR-type zirconium alloy, MTR-type aluminum alloy, and APPR plate, are melted in air or steam.

ISOLATION AND CHEMICAL PROPERTIES OF SYNTHETIC ELEMENTS

A search for the occurrence of technetium in nature failed to disclose any traces of this element in a variety of terrestrial materials. This negative result, together with recent information on a hitherto missing Tc^{98} isotope, supports the conclusion that technetium is truly an extinct element.

Measurements of the solvent extraction of heptavalent technetium from aqueous solutions by a variety of organic liquids revealed the general superiority of cyclic ketones and alcohols and of organophosphorus and alkyl amines dissolved in hydrocarbons as extractants. Many of the results could be explained in terms of three factors: solvent basicity, steric hindrance, and dielectric constant. The assumption of "onium" salt formation proved to be useful in the interpretation of the extraction of pertechnetate ion from acid solutions. Extraction from neutral and alkaline solutions could be partially understood in terms of "ion association" in the organic phase.

The low-temperature heat capacity of $KTcO_4$ was determined from 16 to 310°K. From these and other selected thermochemical measurements, the following thermodynamic properties were computed: $S^0(KTcO_4, c) = 39.74$ cal·deg^{-1}·mole^{-1}, $S^0(TcO_4^-, aq) = 43.2$ cal·deg^{-1}·mole^{-1}, $\Delta F_f^0(KTcO_4, c) = -218.4$ kcal·mole^{-1}, and $\Delta F_f^0(TcO_4^-, aq) = -149.7$ kcal·mole^{-1}.

Additional heat capacity measurements on K_2ReCl_6 were compared with previous measurements made. It is concluded that the three heat capacity anomalies exhibited by the samples arise from the K_2ReCl_6 itself and not from some impurity or impurities therein.

CHEMICAL SEPARATION OF STABLE ISOTOPES

Because of the importance of the oxygen isotope, O^{17}, especially for tracer studies in systems of biological interest, various systems involving CO_2, CO, and NO were studied for separating the isotope by decomposing and re-forming gas-liquid addition compounds. Sulfur dioxide addition compounds that can be readily decomposed appear to give little enrichment of sulfur isotopes.

The heat of reaction of anisole with BF_3 at 30°C was determined by vapor pressure measurements as 12.3 ± 0.4 kcal/mole. It was found feasible to operate a Nitrox cascade for the continuous automatic production of high-purity N^{15}.

RADIATION CHEMISTRY

Various influences of catalyst poisons on the radiation effect on heterogeneous catalysts were observed.

The first example of a gas-phase reaction induced by alpha particles being retarded by the addition of a foreign gas is described in experiments on the polymerization of acetylene in the presence of benzene.

Evidence is presented for the OH radical being an intermediate in the photoreduction of ceric ion in H_2SO_4 solutions.

Experiments with the product condensed at −196°C from the gases resulting in an electric discharge through water vapor indicate the presence of a highly endothermic, as yet unidentified, species such as H_2O-O, H_2O_3, or H_2O_4.

It was found convenient for studying the action of high-energy radiation on chemical compounds by means of infrared absorption spectra to suspend milligram samples in potassium bromide as a

matrix, which does not suffer changes in infrared absorption on radiation.

The free-radical and molecular yields in the decomposition of heavy water were determined. The formation of nitrite in solutions of magnesium, zinc, aluminum, and thorium nitrates was found to obey the equation

$$G(NO_2^-) = 1.22 \pm 0.02 \log [NO_3^-] + 1.70 \pm 0.01 \ .$$

The decrease, in the presence of uranyl ion, in the yield of ferric ion is attributed to the competition of the UO_2^{++} ion for H atoms produced by the decomposition of the water.

ORGANIC CHEMISTRY

The mechanism originally proposed for the pinacol rearrangement of the phenyl-di-*p*-tolyl system of glycols and the corresponding aldehyde was confirmed by means of multiple-labeling techniques with C^{14}.

The *o*-tolyl/phenyl migration ratio in the rearrangement of diphenyl-*o*-tolylacetaldehyde was determined to be about 3, whereas in the deamination of 2,2-diphenyl-2-*o*-tolylethyl-1-C^{14} amine, the ratio is 0.8. These results are explained on the basis of conformational control of the deamination reaction, as contrasted with complete rotational equilibrium of the ionic conformations in the rearrangement of diphenyl-*o*-tolylacetaldehyde.

Additions of phenylmagnesium bromide (C^{14}-labeled) and of *p*-tolylmagnesium bromide to α-aminopropiophenone were shown to be 98 to 99% stereospecific. The rearrangement, in the presence of nitrous acid, of (+)- or (–)-1,1-diphenyl-2-aminopropanol (IV) stereospecifically labeled with C^{14} in only one of the two phenyls produces α-phenylpropiophenone (VII), which has undergone approximately 88% inversion (with 12% retention) at the migration terminus. These results are in agreement with the literature. The product from the deamination of (+)-IV was resolved into a (–)-fraction ($[\alpha]_D^{24} = -210$ deg) and a very nearly racemic ($[\alpha]_D^{24} = -1.6$ deg) fraction. Degradation of these two fractions followed by radioactivity assay of the degradation products disclosed that migration of the labeled phenyl resulted in inversion to produce (–)-VII, whereas migration of the unlabeled phenyl resulted in retention to produce (+)-VII. The present study of the deamination of labeled 2-amino-1,1,2-triphenylethanol refutes the *cis*-transition state of the literature. The results are explained in terms of open carbonium ion intermediates whose rotation about the $C\text{-}C^+$ bond is restricted, and whose phenyl groups migrate solely through *trans*-transition states.

The hydrogen/deuterium isotope effect for the acid-catalyzed rearrangements of several triarylethylene glycols was determined as 2.8 ± 0.6. From these data and from the fact that, under the conditions of the reaction, threo and erythro 1,2-diphenyl-1-*p*-tolylethylene glycol are interconverted, it is concluded that the mechanism of the rearrangement involves a pre-equilibrium of rapid, reversible hydroxyl removal, followed by rate-determining migration of hydrogen or aryl group.

The solvolytic and deamination reactions of 1,2,2-triphenylethanol and its derivatives were studied stereochemically. The products of hydrolysis and acetolysis of 1,2,2-triphenylethyl tosylate and the deamination product from the reaction between 1,2,2-triphenylethylamine and nitrous acid are formed with some racemization plus *retention of configuration*. The (–)-1,2,2-triphenylethanol-1,2-C_1^{14} obtained from deamination of the (–)-amine at 36.5°C was resolved into a fraction of $[\alpha]_D^{25} = -119$ deg and into a racemic fraction. The extent of C^{14} rearrangement of the former (20.6%) and of the racemic (24.5%) fraction was consistent with a mechanism involving the equilibrating of classical carbonium intermediates. These data, however, exclude bridged ions as the cause of configuration retention. Evidence is thus presented that the rate of rotation about the carbon-carbon bond is comparable with the rate of phenyl migration.

The rate of racemization (k_r) of 1,2,2-triphenylethyl acetate was determined under conditions previously used to study the rates of isotope position isomerization (k_I and k_{II}) and acetoxyl exchange (k_{III}) of this same compound. Possible explanations for finding that $k_r/k_I = 1.23$ are (1) steric shielding by the leaving group to front-side attack and (2) internal return, without rearrangement and without solvent exchange, during which some of the ion pairs collapse to yield a product of inverted configuration.

In the decarbonylation of formic acid in 96.2% sulfuric acid, substitution of deuterium for the hydrogen attached to carbon results in isotope effects, k_H/k_D, of 1.49 at 25°C and 1.72 at 0°C;

a tentative explanation is possible in terms of a reaction mechanism suggested by Hammett.

Mass spectrometric cracking patterns of formic-*d* acid and formic acid-*d* indicate that the peak of mass 45 in formic acid may arise from loss of hydrogen, both from carbon and from oxygen.

It was found that, in general, carboxylate salts of uranium and thorium are only slightly soluble in diphenyl. Chelates are more soluble, but around 200°C show signs of decomposition (darkening and increased visocosity). Addition compounds between uranyl salts and phosphine oxides are appreciably soluble in diphenyl.

The Grignard reagent reacts with alkyl dichlorophosphates to yield phosphinate esters [$R_2P(O)OR$]. Trialkyl phosphine oxides (R_3PO) are sometimes formed as by-products in this reaction when the alkoxy group reacts with the Grignard reagent.

In the radiolysis of organophosphorus compounds, the formation of a strong acid, dibutyl hydrogen phosphate, and, in the presence of oxygen, of a weaker acid, carboxylic, was observed.

The compound dibutylphosphonoacetic acid, $(BuO)_2P(O)CH_2COOH$, was synthesized and shown to be a solvent for the extraction of uranium. The uranium salt is associated, containing 10 to 15 units in the polymer.

The progress of the separation, by fractionation, of Amsco 125-82, which is expected to consist of highly branched hydrocarbons, is being followed by means of gas chromatography.

CHEMISTRY OF AQUEOUS SYSTEMS

A study is under way on the cell Pt, H_2, $HCl_{(m)}$, AgCl, Ag at elevated temperatures in order to determine HCl activities as a function of concentration and temperature above 100°C and in order to determine the usefulness of the hydrogen electrode under these conditions. Solubility measurements on AgCl also are being made under the same conditions.

A high-temperature glass electrode pH meter, recently purchased and subjected to several modifications in its electronic setup, appears to behave reproducibly with 0.01 *m* HCl and H_2SO_4 over the range 25 to 135°C. The cell Pt, PbO_2, $PbSO_4$, $H_2SO_{4(m)}$, Ag_2SO_4, Ag was studied over a range of concentrations of H_2SO_4 and of temperature up to 125°C. This cell behaved in a sufficiently reproducible manner over this temperature range to justify further study.

The high-temperature isopiestic unit described previously was tested further, and initial data were obtained up to 105°C. Relative osmotic coefficients (compared with KCl) were obtained for the alkali chlorides and bromides, NaF, Na_2SO_4, $MgSO_4$, UO_2SO_4, etc., for a particular set of conditions at 91.5 and 104.6°C. From a comparison with literature values for 25°C, it is concluded that the osmotic coefficients of the alkali chlorides and bromides (except for the lithium salts) change very little with temperature; that the coefficients of lithium chloride, bromide, and perchlorate, as well as those for sodium fluoride and sulfate, increase appreciably with temperature; and that those of magnesium and uranyl sulfate decrease markedly with increasing temperature.

A Cary model 14M recording spectrophotometer was adapted for precision measurement of aqueous spectra (particularly of the transuranic elements) at elevated temperatures and pressures. The first cell operated successfully over a range of 0 to 250°C and 0 to 1000 psi.

The absorption spectra of heavy and light water were measured as a function of temperature in the ranges 6 to 85°C and 0.6 to 1.8 μ. Measurements with D_2O are being extended to 250°C. The significance of the data for high-temperature aqueous spectrophotometry and their relation to the structure of water are discussed.

A spectrophotometric method for determination of H_2O in D_2O is described. Possible applications to rapid estimation of H_2O in D_2O solutions of inorganic ions are indicated.

Measurements of the absorption spectra of aqueous Np(III), (IV), (V), and (VI) ions were extended from 1 to 1.85 μ by using deuterated aqueous solutions. New absorption bands were identified for each of the four valences. Discovery of an Np(VI) band at 1.224 μ allows, for the first time, an independent spectrophotometric determination of the neptunyl ion. The uranyl ion does not absorb appreciably between 0.5 and 1.85 μ and presumably will not interfere with the estimation of either transuranic ions or H_2O in deuterated aqueous media.

Preliminary steps were taken in a study, by means of pH measurements, of ThO_2 slurries to which acid is added for control of peptization.

Study was resumed of the homogeneous hydrogen-oxygen reaction, catalyzed by dissolved copper salts, in aqueous solutions at elevated temperatures. The findings in the cupric sulfate–sulfuric acid–water system at 175 and 200°C indicate that the involvement of copper is not simple; it appears possible to separate a solubility parameter from a catalytic activity parameter. These parameters are affected differently by changes in copper concentration, acidity, and temperature. The deuterium-oxygen reaction in a heavy-water system is analogous to the hydrogen-oxygen reaction, but is slower.

The densities of heavy-water liquid and saturated vapor at elevated temperatures up to the critical point have been determined from observations of the fractional filling of quartz tubes at elevated temperature as a function of fractional filling at room temperature.

The base-saturated region of the system CuO-UO_3-SO_3-H_2O was investigated at 100°C. The effect of some slight reaction with the walls of the pyrex vessel, which led to the formation of the compound $(UO_2)SiO_4 \cdot 3H_2O$, needs further evaluation.

Knowledge of critical phenomena in aqueous solution is rather limited because of the high temperatures and pressures involved. Experimental techniques were developed for obtaining data on the SO_3-H_2O system, whose highly corrosive nature posed special difficulties, which were overcome. Critical temperatures are reported as a function of SO_3 concentration and show a maximum of 666°C at 40 mole % SO_3.

In the study of anion exchange of metal complexes, principal emphasis was placed on extension of adsorption studies to complexing systems which had received little attention in the past, on a preliminary general ion exchange separations scheme, on studies of the properties of exchangers in concentrated electrolyte solutions, and on utilization of exchangers for the determination of equilibrium constants and activity coefficients in the aqueous phase.

Measurements of the adsorbability of 20 elements from HF-HCl solutions are summarized. These solutions appear to be attractive for separations, because fluoride ions effectively prevent hydrolytic reactions to which highly charged metal ions tend to be subject in the absence of complexing agents.

After a study of adsorbabilities in EDTA (ethylendiaminetetraacetic acid) solutions, a very large number of separations has become possible through control of EDTA concentration, pH, and eluting ion concentration. A combination of gas sweeping and anion exchange adsorption of $GeCl_4$ from the gas stream permits isolation of Ge(IV) from a large number of elements. The technique used here should be applicable in many cases, and in particular should permit adsorption of acidic gases by anion exchangers in suitable salt forms.

On the basis of what has been learned in the last few years about anion exchange behavior of metallic elements, a general separations scheme appears to be feasible. As a beginning, such a scheme is presented for the metallic elements of the first long period of the periodic system.

Measurements of the activity coefficients of the strong electrolytes HCl, LiCl, and NaCl, in the resin phase, showed the similarity to their coefficients in the aqueous phase. The high adsorbabilities of complex ions imply interactions with the resin that are very much greater than those of "simple," strong electrolytes.

The acid-base reaction $F^-_{(r)} + HF_{(r)} \rightleftharpoons HF_{2(r)}^-$ was found to provide a mechanism by which substantial amounts of HF can be adsorbed by the fluoride form of an anion exchanger. Examples are given in which this HF uptake may be utilized for separations. A study of the temperature coefficient of ion exchange equilibria, both with organic and inorganic cation and anion exchangers, was initiated. Columns made of glass and stainless steel were designed for operation up to 150°C. Temperature-dependent enthalpies for the exchange reaction,

$$M^{z+} + zH^+_{(resin)} \longrightarrow M^{z+}_{(resin)} + zH^+ ,$$

on Dowex 50 × 12 are given for Na^+, K^+, Ba^{++}, Co^{++}, and Zn^{++} in the temperature range from 0 to 200°C. Between 27 and 85°C, heats of adsorption of HCl and KOH on zirconium oxide were found to be –6.9 and –3.8 kcal, respectively.

Interference optics were added to the ultracentrifuge, which permitted observation of refractive-index differences of considerable theoretical advantage in nonideal polycomponent systems, and which yielded substantially more accurate data

than the "schlieren" method. By assuming a charge of –4 for the silicotungstate ion, the molecular weight of silicotungstic acid was found by ultracentrifugation to be within ±4% of the formula weight, $H_4SiW_{12}O_{40}$. The hydrolytic polymerization of Sn(IV), Th(IV), and Pb(II) was studied in a variety of solutions, including HCl, $HClO_4$, and NaOH. In many such systems, no indication was found of the formation of copolymers.

Studies on the properties of concentrated (1 to 2 kg/liter) dispersions of thorium oxide in water continued. Attempts to stabilize these dispersions at high temperatures were only partially successful. Most promising as an additive is W(VI), with which dispersions stable at 250°C for one to two days were prepared.

With packed-column techniques the solubilities of a number of substituted ammonium chloroaurates and of $CsClO_4$ were determined in HCl (0.1 to 16 *m*) and in LiCl (0.1 to 19 *m*) solutions. For some of these salts, solubilities differ widely in concentrated HCl and in LiCl solutions even though the activity coefficients of HCl and LiCl in binary mixtures are approximately the same if compared at the same molality.

The systematic investigation of adsorption and ion exchange properties of inorganic materials continued. The comparative study of the relative importance of anion and cation exchange properties of hydrous oxides now includes data on Ti(IV), Zr(IV), Th(IV), Sn(IV), V(V), Nb(V), Ta(V), and U(VI), as well as on Fe(III) and Bi(III). The hydrous oxide of U(VI) was found to be an interesting cation exchanger with which various separations could be carried out. For the cation exchangers such as zirconium phosphate, molybdate, and tungstate, an interesting change of selectivity with pH was established. This change of selectivity makes group separations possible with essentially the same materials which, under other conditions, permit separation of elements within groups.

CHEMISTRY OF CORROSION

A review is given of the three chief lines of investigation in the fundamental electrochemistry related to corrosion. In recent work the absolute rate theory of electrode processes was amplified to cover multiple electrode reactions occurring independently and simultaneously at an electrode, and with activation energies that vary over the surface of the electrode. The resulting equations were applied to the data obtained in potentiostatic and galvanostatic measurements on stainless steel in sulfuric acid. Conclusions regarding the mechanism of action of added ions, such as Cu^{++}, can be derived. The polarization experiments were extended to zirconium in sulfuric acid.

In the work on inhibitors and passivation, it was shown that, in aerated inhibitor solutions, the film formed by oxygen has the same electrochemical behavior as that produced by passivation in concentrated nitric acid or by anodic polarization.

NONAQUEOUS SYSTEMS AT HIGH TEMPERATURES

Isotopic fluorine exchange between solid inorganic fluorides and gaseous fluorocarbons was studied for the first time. The exchange appears to proceed by two distinct mechanisms. In an initial stage of an immeasurably fast reaction rate, the fractionation of fluorine atoms that exchange was an exponential function of temperature, and transport appears to be in the form of fluorine atoms moved through crystal lattice defects. In the second step, self-diffusion of fluoride ions seems to control the rate of exchange. The self-diffusion coefficients of both cations and anions in fused alkali-metal nitrates $NaNO_3$, KNO_3, and $CsNO_3$ were determined. Both radioactive and stable isotopes (O^{18} and N^{15}) were used. For the ratios of the coefficient in each salt, the relative sizes of cation and anion appear to be more important than the relative masses. Heats of activation for self-diffusion are 5 to 6 kcal/mole.

The use of thermal analysis in a pressurized tank system, in extending measurements of the liquid phase equilibria in the four sodium metal–sodium halide systems to higher temperatures (up to 1200°C), led to the elimination of difficulties previously encountered with the equilibration-and-sampling method. The phase diagrams as established now suggest relationships between solubility and size of the atoms and ions of the components, such that the solubility in the component with the larger atoms is greater than the solubility in the component with the smaller atoms.

The *specific* electric conductances of solutions of sodium or potassium in their chlorides and

bromides were found to increase monotonically from concentrations as low as 0.25 mole % metal. On the other hand, the *equivalent* conductance of sodium is distinquished from that of potassium by an initial decrease, with a minimum in the range of 5 to 10 mole % at 2×10^3 to 8×10^3 $ohm^{-1} \cdot cm^2 \cdot equiv^{-1}$. This behavior may be connected with the greater tendency of sodium to associate, at the test temperatures 750 to 900°C, perhaps forming Na_2 molecules as is indicated by the equilibrium phase diagrams and the known relative stability of the diatomic molecules in the gas phase.

A detailed report is in preparation on measurements, by means of a specially designed x-ray diffractometer and by neutron diffraction, of the radial distribution function of the ions in molten alkali halides. In the salts studied thus far, namely, CsCl, CsBr, CsI, NaI, LiCl, LiBr, and LiI, the average number of nearest neighbors of opposite charge was found to range between 4.0 and 5.5. Of special interest, and in agreement with these figures, is the observation that the average, or the most frequent, distance between such neighbors, is considerably smaller than the corresponding one in the crystal at the melting point. The occurrence in molten LiBr and LiI of the highest coordination numbers observed here, 5.5 and 5.0 respectively, may perhaps be taken as the result of the greater ease with which the smallest cation Li^+ can enter the basal plane of a regular trigonal bipyramid of large anions.

Vapor pressure measurements on alkali halides by means of the Knudsen effusion method were extended in temperature up through the melting point of the salts and appeared to be in good agreement with known calorimetric heats of fusion. However, the assumption of associated salt molecules, such as Na_2Cl_2, in the vapor would destroy this agreement.

CHEMICAL PHYSICS

Results are reported of paramagnetic resonance studies of various substances in the form of single crystals irradiated at 77°K. The kinetics of the disappearance reaction were determined for various species produced by the irradiation.

Hydrogen and oxygen gas yields from irradiation, at 77°K, of glassy and crystalline aqueous acids were found to have the same concentration dependence as the hydrogen-atom yields measured by paramagnetic resonance. The yields from glassy material were much higher than from crystalline material. A new type of irradiation experiment, the observation of the paramagnetic resonance spectrum of a substance during irradiation at room temperature, is in the stage of preparation. A survey study of the applicability of nuclear magnetic resonance for elucidating basic properties of fused salt systems was started. Both the hydrogen and sodium resonances were seen in molten sodium hydroxide.

A careful comparison of neutron and x-ray diffraction for urea showed good agreement in position parameters, but left a pronounced disagreement in the parameters describing thermal motion. It was shown further that this disagreement is not principally a reflection of distortion of the atoms on bonding or hybridization of orbitals.

The results of a weighted least-squares refinement of previous neutron diffraction measurements on acetylglycine are reported. Expressions that take account of various modes of thermal motion in crystals were derived for use in correcting bond-length values obtained from diffraction data.

A preliminary neutron diffraction study of solid H_2O_2 yielded atomic positions that are in good agreement with those from an x-ray study.

The results of an analysis of the fundamental vibrational and rotational spectrum of $N^{15}O$ are presented.

Ion-molecule reactions of various types between the ions of CO, CO^+, and CO^{++} and the neutral molecules He, D_2, H_2, N_2, CO, A, and Kr were investigated with a single-stage 6-in.-radius mass spectrometer as a function of the energy of the ions over a range from 1000 to 5100 ev. The operating characteristics of this research spectrometer, RS 1, are described. The studies indicate that the fragmentation of a molecule is dependent on the structure of the molecule rather than on the method of excitation.

A new branch of study was undertaken in which a beam of low-energy simple ions will be made to collide with a molecular beam. The composition and angular distribution of products will be observed by a small mass analyzer, rotating about the scattering center. The first ion-molecule study will be the reaction of the protium ion with the deuterium molecule.

NUCLEAR CHEMISTRY

DECAY SCHEMES OF Sm^{145} AND Pm^{145}

A. R. Brosi B. H. Ketelle
H. C. Thomas[1] R. J. Kerr[2]

Radioactive decay of Sm^{145} was first observed[3] in a mass spectrographic study of reactor-irradiated samarium. This work indicated that the Sm^{145} half life was greater than 72 days and that the Pm^{145} half life was an order of magnitude different from that of the Sm^{145} parent. In a study of reactor-bombarded samarium, Butement[4] found the Sm^{145} half life to be 410 days. From the relative intensity of the *K* x rays associated with the promethium daughter, he calculated a half life of 30 years for Pm^{145}. He reported no other radiations associated with either of these mass-145 isotopes.

Rutledge, Cork, and Burson[5] found a 61.3-kev gamma ray associated with Sm^{145}. They reported a *K/L* conversion ratio of 1 for this gamma ray. In work with samarium enriched in Sm^{144} which had been bombarded for a year at a neutron flux of 3.6×10^{13} neutrons·cm^{-2}·sec^{-1}, Parker and Martin[6] found the Sm^{145} half life to be about one year and the Pm^{145} half life to be much longer. They also found low-energy gamma radiation (70 to 80 kev) associated with Pm^{145} decay.

In the present study the gamma radiation emitted by Pm^{145} was resolved into two gamma rays with energies of 68 and 72 kev. A new but very-low-intensity gamma ray was found to be emitted in Sm^{145} decay. Coincidence measurements were made by using magnetic-lens, scintillation-counter, or proportional-counter spectrometers for energy discrimination. From the data obtained, *L/K* electron capture ratios, branching ratios, and conversion coefficients were computed. In the case of Sm^{145} the energy end points of x-ray and gamma-ray coincident inner bremsstrahlung radiation were determined. Half lives for both Sm^{145} and Pm^{145} were remeasured.

Energy-level diagrams with spin and parity assignments consistent with the experimental data will be published for both isotopes.

DECAY OF Dy^{159}

B. H. Ketelle A. R. Brosi

Previous work[7,8] has indicated that electron-capture decay of 134-day Dy^{159} occurs only to the ground state of Tb^{159}. However, beta decay of Gd^{159} has been shown[9] to populate a complex energy-level system in Tb^{159}.

In the present work, coincidence measurements showed that *L* capture in low intensity occurred to a 345-kev level in Tb^{159}. However, *K* capture did not occur to this level. Neither *L* nor *K* capture populated a 362-kev level which is observed in the beta decay of Gd^{159}. Analysis of the Dy^{159} inner bremsstrahlung energy spectrum indicates that the decay energy is too low to permit these unobserved electron-capture transitions. All the levels in Tb^{159} below 345 kev which have been observed to follow beta decay of Gd^{159} were observed in this work to follow electron-capture decay of Dy^{159}.

NUCLEAR DECAY OF Br^{84} AND THE LEVEL SCHEME IN Kr^{84}

G. D. O'Kelley N. R. Johnson

The decay properties of fission-product Br^{84} have been studied by scintillation methods. Measurements on the decay of Br^{84} gamma rays above an energy of 0.1 Mev and the decay of the most intense gamma-ray peak (0.879 Mev) were analyzed by the method of least squares and yielded closely agreeing values for the half life. It is felt that an accurate representation of the Br^{84} half life is given by 31.80 ± 0.08 min, where the deviation includes both the standard statistical error and an estimate of systematic errors.

---

[1] Temporary summer employee (1956), Bradley University, Peoria, Ill.

[2] Instrumentation and Controls Division, now of the Applied Nuclear Physics Division.

[3] M. G. Inghram, R. J. Hayden, and D. C. Hess, Jr., *Phys. Rev.* **71**, 643 (1947).

[4] F. D. S. Butement, *Nature* **167**, 400 (1951).

[5] W. C. Rutledge, J. M. Cork, and S. B. Burson, *Phys. Rev.* **86**, 775 (1952).

[6] G. W. Parker and W. J. Martin, *Chem. Quar. Prog. Rep. Sept. 30, 1952*, ORNL-1432, p 18.

[7] B. H. Ketelle, *Phys. Rev.* **76**, 1256 (1949).

[8] F. D. S. Butement, *Proc. Phys. Soc. (London)* **64A**, 428 (1951).

[9] R. Ballini and R. Barloutaud, *J. phys. radium* **17**, 534 (1956).

By means of single-crystal and coincidence gamma-ray spectroscopy, 23 gamma rays were established, with a possibility of other weak transitions. The gamma-ray results are summarized in Table 1.

The beta-ray transition energy to the ground state of Kr^{84} was established as 4.71 ± 0.08 Mev and includes 31.9 ± 5.0% of the beta-ray transitions. A beta-ray group of 3.83 ± 0.07 Mev was found in coincidence with the 0.879-Mev gamma ray; two beta-ray groups of energy 2.80 ± 0.10 and 1.81 ± 0.06 Mev were in coincidence with 1.90-Mev gamma rays; a group of 1.39 ± 0.10 and possibly 0.83 ± 0.08 Mev was coincident with the 2.47-Mev gamma ray. Table 2 lists the various beta-ray groups and their intensities, calculated from the decay scheme of Fig. 1, the relative gamma-ray intensities, and the branching to the ground state.

A decay scheme consistent with the majority of the Br^{84} observations is presented in Fig. 1. The 2^- assignment to the ground state of Br^{84} is based on the shell model and the log *ft* value of 7.7 for the beta-ray transitions to the 0^+ ground state of Kr^{84} and to the 2^+ first excited state. The log *ft* value of 7.1 for the beta decay to the 1.90-Mev state in Kr^{84}, the relative intensities of the 1.01- and 1.90-Mev gamma rays, and the anisotropy of the 1.01-0.879-Mev cascade are

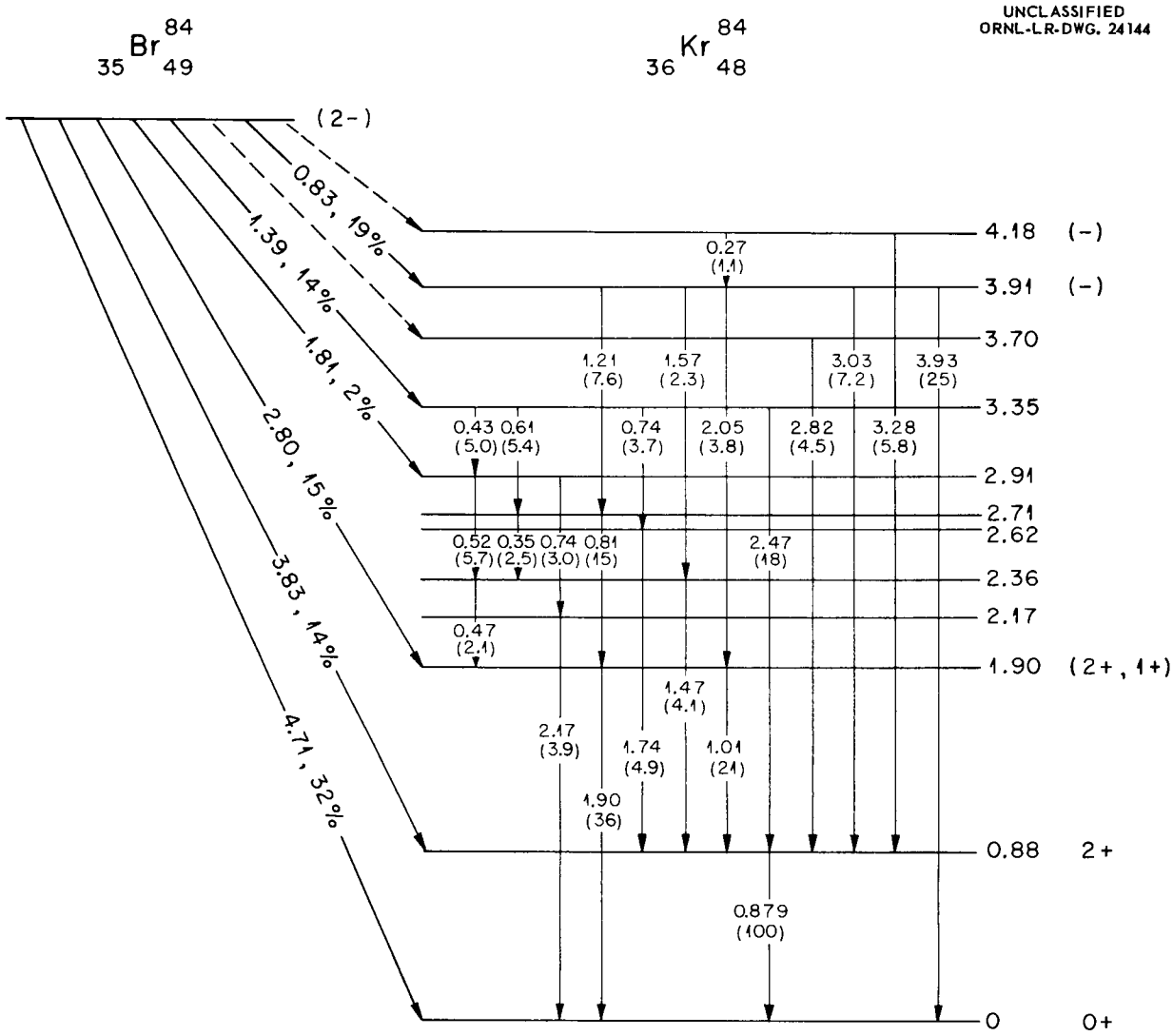

Fig. 1. Decay Scheme Proposed for Br^{84}.

Table 1. Summary of Br^{84} Gamma-Ray Data

Gamma-Ray Energy (Mev)	Intensities Relative to 0.879-Mev Gamma Ray as 100 Units		Gamma Ray Appeared in Coincidence with:			
	From Single-Crystal Data	Best Value from Coincidence Data	0.879 Mev	1.90 Mev	2.47 Mev	3.93 Mev
0.27 ± 0.04	*a*	1.1 ± 0.4	Yes	Yes	?	Yes
0.35 ± 0.03	3.5 ± 1.7	2.5 ± 1.0	Yes	Yes	?	No
0.43 ± 0.04	~1[b]	5.0 ± 2.0	Yes	Yes	No	No
0.47 ± 0.04	2.0 ± 1.0	2.1 ± 0.5	?	Yes	?	No
0.52 ± 0.03	7.3 ± 2.0	5.7 ± 1.7	Yes	Yes	?	No
0.61 ± 0.03	5 ± 2	5.4 ± 1.6	Yes	?	?	No
0.74 ± 0.03	6.7 ± 2.5	3.7 ± 1.0[c]	Yes	No	?	No
0.81 ± 0.03	20 ± 4	15 ± 4	Yes	Yes	No	No
0.879 ± 0.007	100		No	No	Yes	No
1.01 ± 0.02	20 ± 3	21 ± 2	Yes	?[d]	No	No
1.21 ± 0.02	7.6 ± 0.8	7.7 ± 1.0	Yes	Yes	No	No
1.47 ± 0.03	4.2 ± 1.1	4.1 ± 0.8	Yes	No	No	No
1.57 ± 0.05	2.3 ± 1.1	2.3 ± 1.1	Yes	Yes	No	No
1.74 ± 0.05	3.6 ± 1.3	4.9 ± 1.0	Yes	No	No	No
1.90 ± 0.02	36 ± 4		No	No	No	No
2.05 ± 0.05	3.8 ± 1.3	3.8 ± 1.0	?	Yes	No	No
2.17 ± 0.04	3.9 ± 1.0		No	No	No	No
2.47 ± 0.03	18 ± 3	13 ± 3	Yes	No	No	No
2.82 ± 0.05	4.0 ± 1.6	4.5 ± 1.3	Yes	No	No	No
3.03 ± 0.05	9.8 ± 3.0	7.2 ± 1.5	Yes	No	No	No
3.28 ± 0.05	5.8 ± 2.0	5.6 ± 1.2	Yes	No	No	No
3.93 ± 0.03	25 ± 4		No	No	No	No

[a] This peak appeared so near the "backscatter" peak that its analysis was not possible.

[b] Since it was difficult to subtract the Compton background, no attempt was made to determine the limit of error in the intensity.

[c] Another 0.74-Mev gamma ray which would not have appeared in any of the coincidence data is proposed elsewhere in the decay scheme.

[d] There were slight indications for a very small coincidence contribution from a 1.01-Mev gamma ray which could be accommodated at several positions above the 1.90-Mev level.

Table 2. Intensities and Comparative Half Lives of Br^{84} Beta-Ray Transitions

(Beta-ray subscripts denote final states)

Beta-Ray Group	Experimental Energies (Mev)	Intensity	Log ft
β_0	4.71 ± 0.08	0.319 ± 0.050	7.7 ± 0.1
$\beta_{0.88}$	3.83 ± 0.07	0.144 ± 0.029	7.7 ± 0.1
$\beta_{1.90}$	2.80 ± 0.10	0.150 ± 0.060	$7.1^{+0.2}_{-0.1}$
$\beta_{2.17}$		~0	
$\beta_{2.36}$		~0	
$\beta_{2.62}$		~0	
$\beta_{2.71}$		~0	
$\beta_{2.91}$	1.81 ± 0.06	(0.015)*	(7.3)
$\beta_{3.35}$	1.39 ± 0.10	0.136 ± 0.035	5.9 ± 0.1
$\beta_{3.70}$		(0.019)*	(6.0)
$\beta_{3.91}$	0.83 ± 0.08	0.187 ± 0.038	5.0 ± 0.1
$\beta_{4.18}$		0.029 ± 0.010	$5.4^{+0.2}_{-0.1}$
β_{total}		1.00	

*Intensity value was uncertain due to possibility of additional weak gamma rays decaying to or from this level.

consistent with an assignment of 1^+ or 2^+ to the second excited state at 1.90 Mev. Negative parity assignments to the 3.91- and 4.18-Mev levels are based on the log ft values of about 5.

HALF LIFE OF Tc^{98} AND ITS ABUNDANCE IN FISSION-PRODUCT TECHNETIUM

G. D. O'Kelley Q. V. Larson

By the use of gamma-gamma coincidence counting of the 0.65- and 0.75-Mev gamma rays from the decay of Tc^{98}, it has been possible to measure the specific activity of Tc^{98} in a sample of cyclotron-produced technetium isotopes[10] containing 17.3% Tc^{98}. A preliminary half life of $(1.5 \pm 0.7) \times 10^6$ years was calculated from these measurements.

Gamma rays characteristic of Tc^{98} were also detected in a sample containing 3.12 g of fission-product technetium, by using the gamma-gamma coincidence method of assay. If the half life of Tc^{98} is taken as 1.5×10^6 years, the atomic ratio Tc^{98}/Tc^{99} is $(3 \pm 1) \times 10^{-8}$.

[10] G. E. Boyd *et al.*, *Phys. Rev.* 99, 1030 (1955).

FISSION-PRODUCT "SOLUBILITIES" IN IN-PILE LOOPS

J. Halperin J. O. Oliver[11]
R. W. Stoughton

Of some interest to the HRP are the chemistry and, particularly, the apparent solubility[12] behavior of the various fission products under the conditions of an operating reactor. Since the in-pile loops closely simulate reactor conditions, a study of fission-product "solubilities" has been undertaken in the loops in order to gain some experience preparatory to carrying out a similar study in HRE-2 upon its startup. Some results are now available, and a summary of some of these data is presented in Figs. 2 through 5. The data of experiments L-4-13 and L-2-14 are the results of the most careful analysis up to this time. The data shown for experiments DD and FF represent older work not subject to as complete an analysis as that in L-4-13.

Most of the high-yield fission products were analyzed radiochemically in periodic samplings of the in-pile loop experiments. Analyses were carried out on Np^{239} (not a fission product but present in high yield), Cs^{137}, Ce^{144}, Sr^{89}, Ba^{140}, Mo^{99}, I^{131}, Zr^{95}, Nb^{95}, and Ru^{103}; Pu^{239}, Tc^{99}, and Y^{91} are also under study, but relatively few data have as yet been collected for these species.

The radiochemical analyses were largely carried out by the Radioisotope Analysis Group headed by E. I. Wyatt, with some assistance by the Radiochemical Analysis Group headed by S. A. Reynolds. The Pilot Plant Control Group headed by C. E. Lamb carried out the plutonium analyses.

The data are presented in the form of ratios of the amount of each species experimentally found in solution to that calculated on the basis of complete solubility, by using fission yield data and total integrated fissions obtained from Cs^{137} analyses. Thus this ratio of "exp/calc" for a soluble fission product would be expected to be

[11] Analytical Chemistry Division.

[12] "Solubility" is used here in the sense of an effective or an apparent solubility, regardless of mechanism of removal from solution, that is, including adsorption and coprecipitation processes.

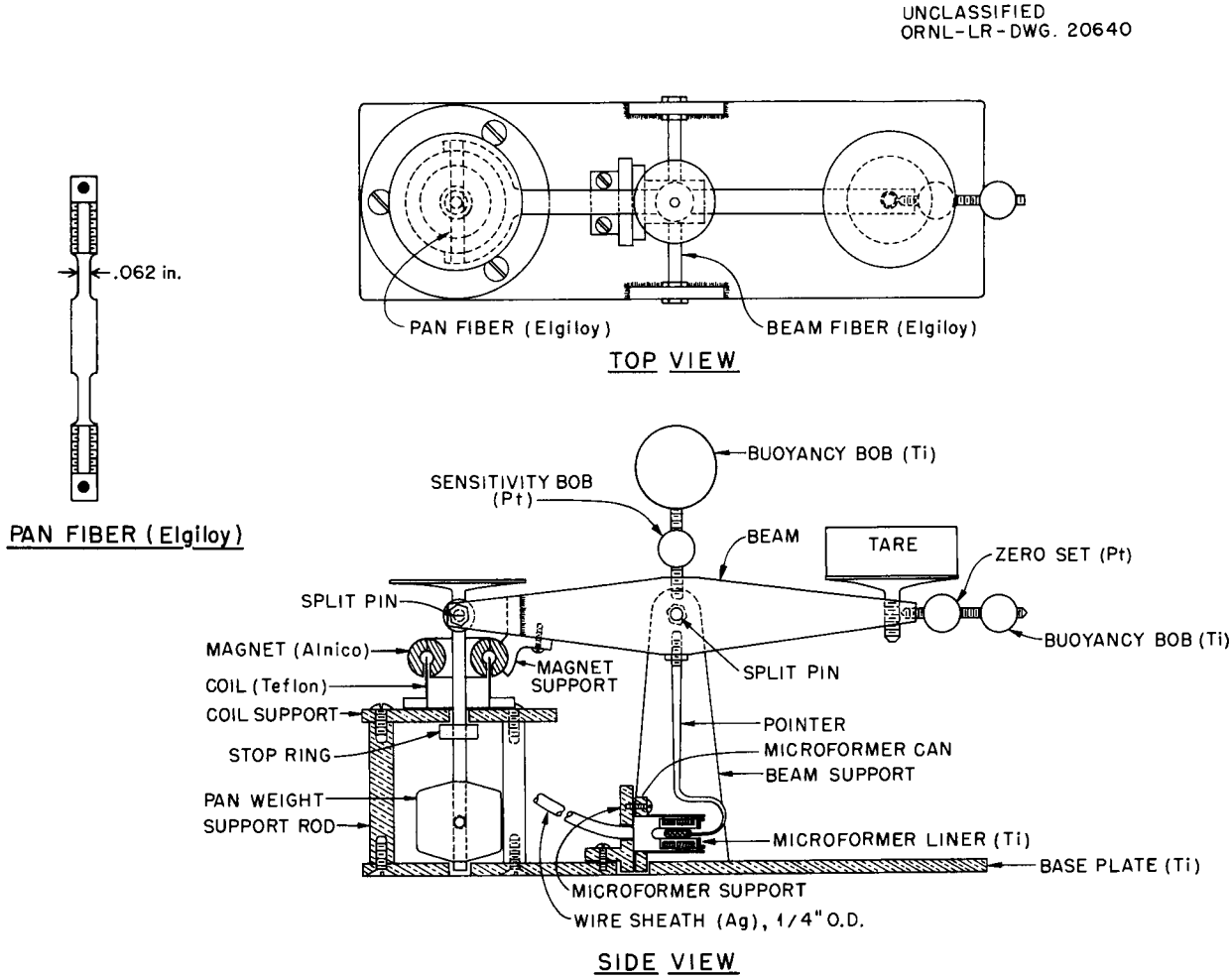

Fig. 2. Radiochemical Behavior (Apparent Solubilities) of Fission Products in In-Pile Loop DD.

1.0 or 100% at all times; it has been plotted against reactor megawatt-hours in Figs. 2 through 5 for convenience of presentation. The neutron flux level has varied from run to run, and the variation of flux has been very great within each loop, so that no simple correlation of flux level with solubility behavior seems to be possible, and no such attempt has been made here. Each of these three experiments was carried out with a uranium concentration of about 40 g/liter circulated in stainless steel loops at 250°C except for L-2-14, which was in a titanium loop. Experiments DD, FF, L-4-13, and L-2-14 had excess H_2SO_4 concentrations of 0.008, 0.04, 0.02, and 0.4 *M*, respectively. Experiment L-4-13 was carried out in D_2O rather than in H_2O.

Cesium-137 analyses have been used as a measure of the fission rate in the solution. All the points plotted in the figures are therefore relative to the cesium analyses. Since the completed cesium analyses are not available for months following the experiment, the proper normalization has not been possible in run L-4-13. Therefore the data for L-4-13 have yet to be properly normalized, and the ordinate is only proportional to the correct value, although all the fission products are correctly plotted relative to each other.

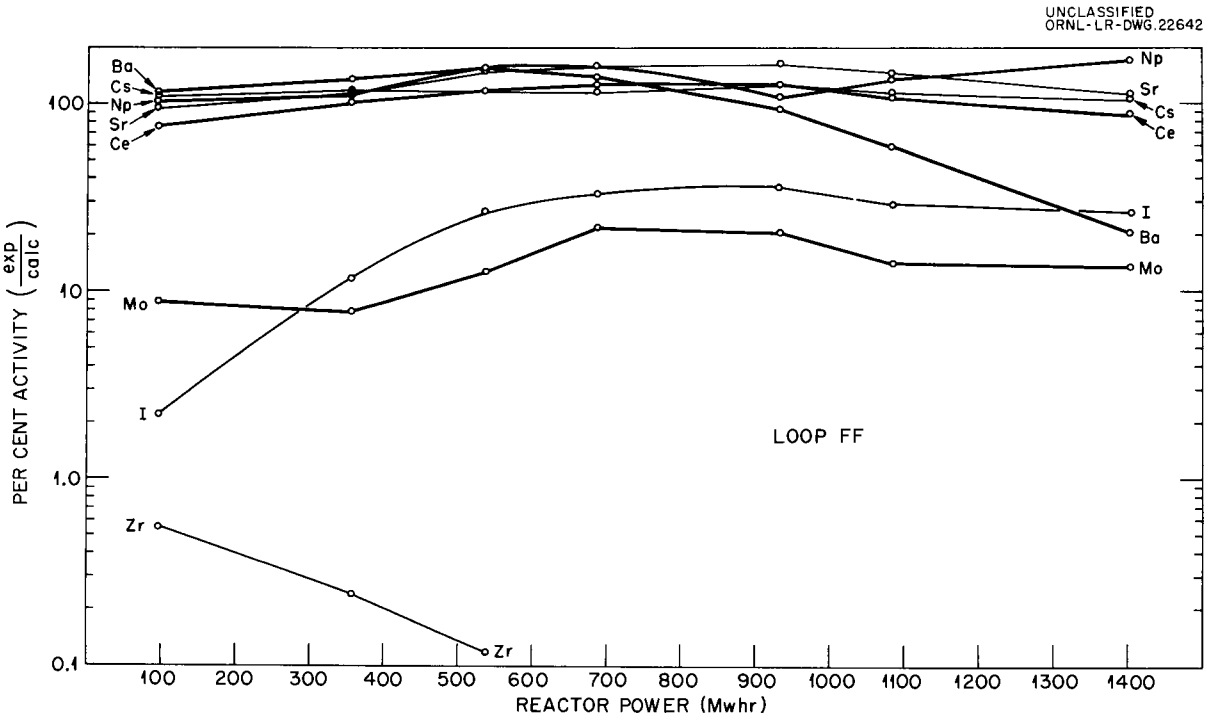

Fig. 3. Radiochemical Behavior (Apparent Solubilities) of Fission Products in In-Pile Loop FF.

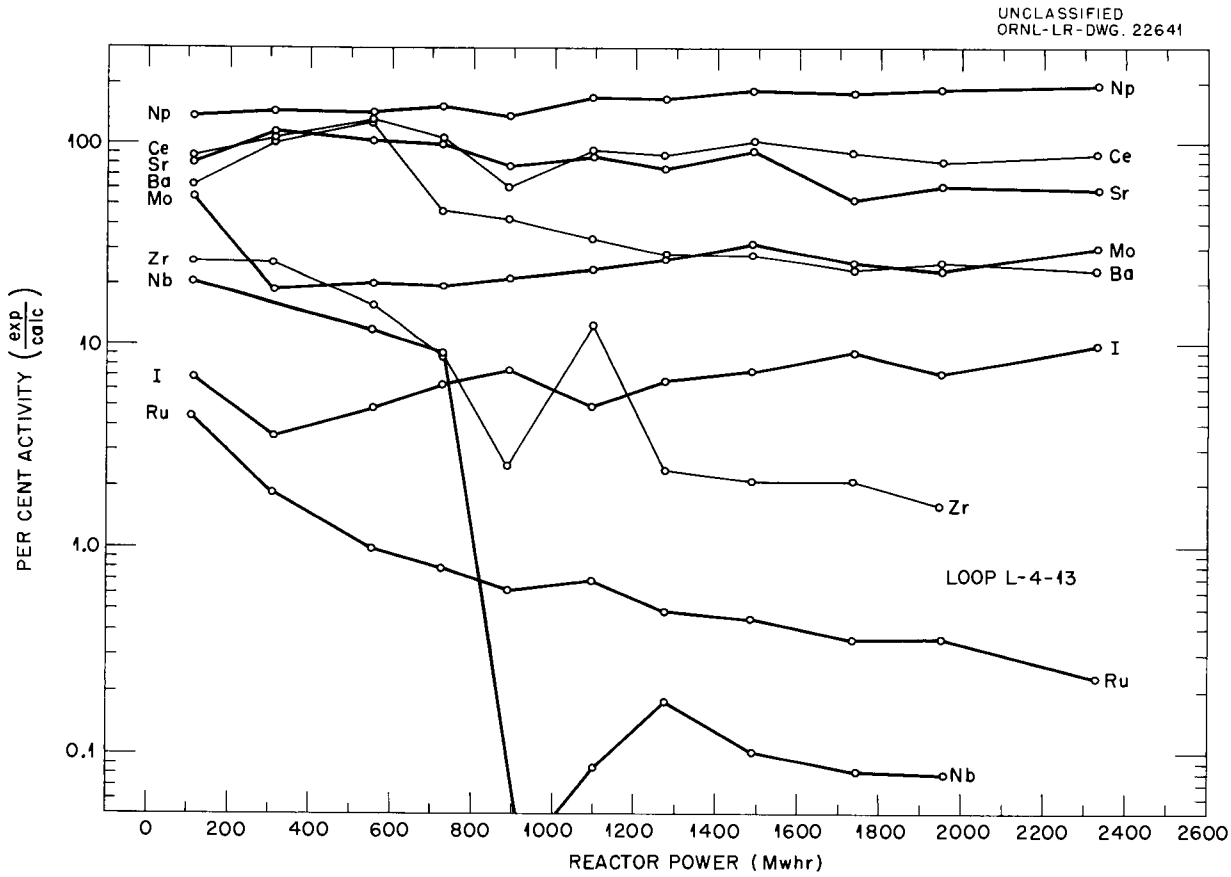

Fig. 4. Radiochemical Behavior (Apparent Solubilities) of Fission Products in In-Pile Loop L-4-13.

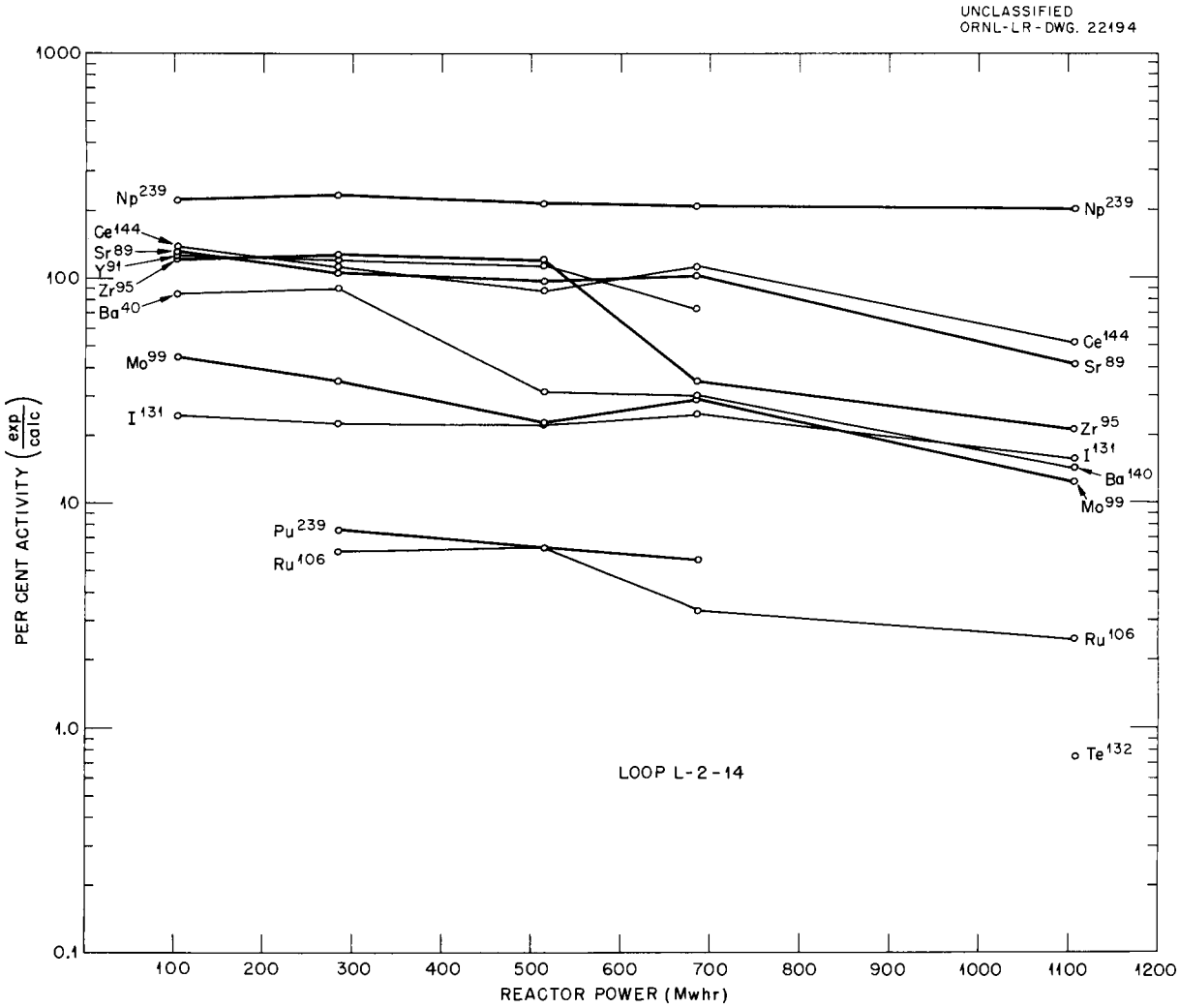

Fig. 5. Radiochemical Behavior (Apparent Solubilities) of Fission Products in In-Pile Loop L-2-14.

It would appear from the scatter of the points that the experimental errors are not small. However, a smoothed curve through the points gives a fair indication of the apparent solubility behavior of each species. The various curves may be conveniently divided into three groups: those approximately completely soluble, those partially soluble, and those relatively insoluble.

The elements Np, Cs, Ce, Sr, and Ba are initially completely or almost completely soluble. The value of the "exp/calc" ratio for Np^{239} is directly proportional to the value of $\sigma_c(U^{238})$ chosen for the calculation. A value of 25 barns was used for L-2-14, L-4-13, and FF; and 8 barns was used in DD. The position of the loop in DD was presumably farther from fuel elements, giving a lower fast flux. From the data these cross sections appear to be low, and an even higher effective cross section is suggested. Surprisingly, L-2-14 appears to require an effective cross section of about 50 barns for U^{238}. Strontium and barium both appear to reach a limiting solubility in solution, which suggests a solubility-product relationship when the data are plotted as solubility vs time. Strontium, as expected, saturates at an appreciably greater flux-time than does the barium.

The "exp/calc" ratios of molybdenum and iodine tend to level off at intermediate values ranging from about 10 to 50% after a period of time. Of course the iodine can be expected to volatilize and

deposit elsewhere in the system. The solution, however, is not purged and has a static overpressure of about 100 psi of O_2 and about 12 psi of H_2, together with a steam pressure of about 1000 psi.

The elements Zr, Nb, and Ru are relatively insoluble, and after an extended irradiation approach "apparent solubilities" of 1% or less. Although not shown in Fig. 5, the niobium concentration in L-2-14 was below the limit of detectability, that is, less than 0.5%. Plutonium data, although as yet very limited (and not shown in the figures), indicate a low "solubility."

EFFECTIVE REACTOR CROSS SECTIONS IN MTR FUEL ASSEMBLIES[13]

J. Halperin J. O. Blomeke[14]
D. A. Mrkvicka[15]

The ORNL chemical pilot plant in operation Neptex[16] has been used to process 12 highly irradiated MTR fuel assemblies primarily to recover the Np^{237} that had been formed. Incidental to this operation it became possible to carry out certain analyses which permitted the measurement and correlation of a number of heavy-element cross sections. Regrettably, due to the nature of this operation, it was not possible to carry out all the analyses which might have proved to be valuable. However, within the accuracy of the measurements, the data yielded cross-section values which are consistent and can be correlated with other known determinations.

The 12 irradiated assemblies consisted of four fuel elements and eight shim rods (i.e., control rods containing fuel) that had been exposed to integrated flux-times ranging from about 8×10^{20} to 2×10^{21} neutrons/cm^2.

Eight of the assemblies were individually dissolved in nitric acid and sampled. The remaining four were dissolved together and analyzed as one batch. Chemical analyses were carried out for uranium, neptunium, and plutonium. The uranium was analyzed fluorimetrically, and the results are thought to be accurate to ±3%. The neptunium and plutonium were separated by a TTA extraction technique of controlled oxidation states and were finally alpha-counted. The plutonium analyses are considered to be accurate to within ±10%, and the neptunium analyses are thought to be accurate to within ±15%. A chemical yield of 98% was taken for the plutonium, and 85% was taken for the neptunium.

A sample of the uranium separated in each of the nine runs was mass-analyzed. Three samples of plutonium (runs M-0, M-3, and M-5) were also mass-analyzed. The uranium analyses were carried out in the Stable Isotopes Division by measuring UO_2^+ ions on an 8-in.-radius, 60-deg Nier-type mass spectrometer equipped with a single-filament thermal ionization source. The plutonium analyses were carried out at the Argonne National Laboratory on a 12-in.-radius, 60-deg Nier-type mass spectrometer with a multiple-filament[17] ionization source. The analyses and estimated uncertainties are shown in Tables 3 and 4. From the mass spectrographic and chemical analyses it was possible to estimate the effective reactor cross sections[18] of U^{236} and U^{238} and to check approximately the plutonium cross sections in the MTR core. The irradiation data are summarized in Table 5. The average values of flux-time products computed from the U^{236}/U^{235} and U^{238}/U^{235} mass ratios differed by about 3%; however, the two methods were not entirely independent.

The effective reactor cross section of U^{236}, derived from the Np^{237} analyses, is shown in Table 6. The average of the nine batches processed is $\sigma'(U^{236}) = 34 \pm 6$ barns. It may be

[13]The authors wish to acknowledge the cooperation and help of E. M. Shank of the Chemical Technology Division, who was responsible for the pilot-plant operation, and of L. T. Corbin, J. H. Cooper, C. E. Lamb, and co-workers in the Analytical Chemistry Division, who carried out the numerous chemical analyses under sometimes trying circumstances. The writers wish to acknowledge the help of S. Fried of Argonne National Laboratory for purification of plutonium samples for mass analyses, and also wish to express indebtedness to L. O. Gilpatrick, J. R. Sites, J. R. Walton, and C. R. Baldock for the mass spectrographic analyses of the uranium samples.

[14]Chemical Technology Division.

[15]Argonne National Laboratory.

[16]*Oak Ridge National Laboratory Status and Progress Report, January 1956*, ORNL-2044, p 19.

[17]M. G. Inghram and W. A. Chupka, *Rev. Sci. Instr.* **24**, 518 (1953).

[18]The effective reactor cross section, σ', is here defined as

$$\sigma' = \frac{\text{reaction rate}}{\phi_{th}} = \sigma_{th} + \frac{\phi_{res}}{\phi_{th}} \int \sigma d(\ln E) \ .$$

Table 3. Mass Spectrographic Analyses of Irradiated Uranium (at. %)

Sample	U^{234}	U^{235}	U^{236}	U^{238}
M-0	1.27 ± 0.05	80.7 ± 0.3	9.41 ± 0.13	8.65 ± 0.17
M-1	1.61 ± 0.08	70.7 ± 0.3	16.9 ± 0.1	10.8 ± 0.2
M-2	2.03 ± 0.08	60.6 ± 0.5	24.4 ± 0.3	13.0 ± 0.2
M-3	Not measured	74.71 ± 0.11	14.76 ± 0.14	10.53 ± 0.06
M-4	1.39 ± 0.07	72.3 ± 0.4	15.4 ± 0.3	11.0 ± 0.2
M-5	1.39 ± 0.06	73.0 ± 0.4	14.7 ± 0.4	10.9 ± 0.3
M-6	1.54 ± 0.09	70.5 ± 0.8	17.1 ± 0.5	10.8 ± 0.5
M-7	1.41 ± 0.08	71.2 ± 0.2	16.1 ± 0.1	11.3 ± 0.2
M-8	1.54 ± 0.07	65.4 ± 0.4	20.8 ± 0.2	12.4 ± 0.2

Table 4. Mass Spectrographic Analyses of Separated Plutonium (at. %)

Sample	Pu^{238}	Pu^{239}	Pu^{240}	Pu^{241}	Pu^{242}	Pu^{244}
M-0	$6.07^{+0.06}_{-0.15}$	76.8 ± 0.2	13.5 ± 0.2	3.12 ± 0.06	0.48 ± 0.01	0.001
M-3	13.5 ± 0.2	64.6 ± 0.2	15.3 ± 0.2	5.23 ± 0.06	1.38 ± 0.02	
M-5	$12.1^{+0.1}_{-1.4}$	65.4 ± 0.2	16.9 ± 0.2	4.52 ± 0.05	1.11 ± 0.02	0.003

Table 5. Irradiation Data and Derived Values of Flux-Time

Sample*	Irradiation Time (days)	Cooling Time (months)	Initial U^{235} Content (g)	U (mg/ml)	Np (counts/min/ml)	Pu (counts/min/ml)	ϕt Based on U^{236}/U^{235}	ϕt Based on U^{238}/U^{235}
						$\times 10^5$	$\times 10^{21}$	$\times 10^{21}$
M-0(F)	74	35	169	0.258	259	4.09	0.835	0.824
M-1(F)	127	27	169	0.422	1050	32.1	1.393	1.361
M-2(F)	179	21	168	0.269	1130	47.6	1.918	1.875
M-3(S)	82	28	131	0.273	664	17.4	1.226	1.238
M-4(S)	79	24	109	0.215	592	17.9	1.291	1.354
M-5(F)	122	33	169	0.336	562	16.9	1.242	1.326
M-6(S)	100	27	131	0.244	749	24.3	1.407	1.365
M-7(S)	99	20	131	0.274	800	34.1	1.343	1.418
M-8(S)	186	17	131	0.573	2330	16.5	1.669	1.688
	121	17	130					
	115	23	109					
	178	21	109					

*(F) indicates fuel rod, (S) indicates shim rod.

Table 6. Effective Cross Section of U^{236}

Sample	$\sigma'(U^{236})$ Based on Pu^{238} (barns)	$\sigma'(U^{236})$ Based on Np^{237} (barns)
M-0(F)	33.2	37.1
M-1(F)	35.2	30.4
M-2(F)	31.4	25.5
M-3(S)	42.1	38.0
M-4(S)	45.2	37.8
M-5(F)	30.1	25.3
M-6(S)	45.6	37.0
M-7(S)	60.5	36.6
M-8(S)	76.3	32.6
	Av	33.6

significant that the average for the fuel assemblies M-0, M-1, M-2, and M-5 was $\sigma' = 30$ barns, in contrast with an average $\sigma' = 36$ barns for the shim rods M-3, M-4, M-6, M-7, and M-8. However, this distinction did not appear to be justified (because of the large uncertainties), and the over-all average has been taken as representative of the core cross section.

The effective reactor cross section of U^{236}, based on the Pu^{238} yield, is also shown in Table 6. Mass analyses for the plutonium were available in only runs M-0, M-3, and M-5. However, since greater than 90% of the alpha count was due to the Pu^{238} in these samples, it was possible to use the values based on the alpha count, with minor corrections for the Pu^{239} and Pu^{240} content, to compute the U^{236} cross section in these samples also. The results of runs M-7 and M-8 are unexplainably high and inconsistent with the other analyses. The average of the seven runs, excluding M-7 and M-8, is $\sigma' = 37.5$ barns. Here again there appears to be a difference between the fuel elements and the shim rods.

The 34-barn value based on the Np^{237} analyses has been taken here as the better measure of the effective reactor cross section of U^{236}, in view of the higher-order reaction for the formation of Pu^{238}, the greater scatter of the data from the plutonium measurements, and the unaccountably high values found in M-7 and M-8.

In a manner analogous to the U^{236} measurement, from the plutonium yields and the mass analyses of the three samples M-0, M-3, and M-5, the effective reactor cross section of U^{238} was calculated. These results are shown in Table 7. The mean of the three values is rounded off as $\sigma'(U^{238}) = 23 \pm 3$ barns.

Table 7. Effective Cross Section of U^{238}

Sample	$\sigma'(U^{238})$ Based on Pu^{239} (barns)
M-0(F)	23.2
M-3(S)	25.1
M-5(F)	21.0
Av	23

The ratio of the resonance flux per unit ln E to thermal flux, ϕ_r/ϕ_{th}, in the MTR core may be estimated from the effective cross section, σ', from the effective resonance integral, $[\int \sigma d(\ln E)]_{eff}$, and from the thermal cross section, σ_{th}, of U^{238} and U^{236}. The resonance integral of infinitely dilute U^{238} has been measured as 280 barns.[19] Although the U^{238} is very dilute in the MTR core, there is a small amount of self-absorption. An exact calculation of the effective integral is difficult, but a reasonable estimate[20,21] can be made that the effective integral will be about 10% less than the infinitely dilute value. A value of

$$\left[\int_{0.4}^{E_f} \sigma d(\ln E)\right]_{eff} = 250 \text{ barns}$$

was therefore adopted for U^{238}. On this basis,

$$\frac{\phi_r}{\phi_{th}} = \frac{\sigma' - \sigma_{th}}{[\int \sigma d(\ln E)]_{eff}} = 0.080 \ .$$

[19] R. L. Macklin and H. S. Pomerance, *Proc. Intern. Conf. Peaceful Uses Atomic Energy, Geneva, 1955* **5**, 96 (1956).

[20] L. Dresner, *J. Nuclear Energy* **2**, 118 (1955).

[21] L. Dresner, *Nuclear Sci. and Eng.* **1**, 68 (1956).

A similar calculation can be carried out for U^{236}. From the data of Pilcher, Hughes, and Harvey,[22] it is possible to compute the resonance integral of infinitely dilute U^{236} as $\int \sigma d(\ln E) = 320$ barns. Since the U^{236} content is initially zero, the average effective integral is taken equal to the 320-barn value within the accuracy of the measurement; then taking $\sigma_{th}(U^{236}) = 6$ barns, $\phi_r/\phi_{th} = 0.087$. Thus the mean of the U^{238} and U^{236} measurements is 0.835, or about $1/12$. This may be compared with the value of $1/16$ found in the moderator of graphite reactors discussed by Hughes.[23]

By making use of the value of $\phi_r/\phi_{th} = 1/12$, effective reactor cross sections were estimated for the MTR core, and the bases for these estimates are shown in Table 8. By using these cross-section values, the yields of the plutonium isotopes were computed and were compared with the experimental data. The results are summarized in Table 9. The agreement is well within the experimental uncertainties involved in such an estimate.

[22] V. E. Pilcher, D. J. Hughes, and J. A. Harvey, *Bull. Am. Phys. Soc.* 1, Series II, 187 (1956).

[23] D. J. Hughes, *Pile Neutron Research*, p 63, Addison-Wesley, Cambridge, 1953.

Table 8. Effective Reactor Cross Sections

Isotope	Process	σ_0	σ_{th}	$\int_{0.4} \sigma d(\ln E)$	$\frac{[\int \sigma d(\ln E)]_{eff}}{12}$	σ'^a	Reference
U^{235}	Capture	107	105^b	50	4	110	*c, d*
	Fission	580	568^b	270	23	590	*c*
	Absorption	687	673^b	320	27	700	*c, e*
U^{236}	Capture	6		320	27	33	*f*
U^{238}	Capture	2.8	3	280	21	24	*c, e*
Np^{237}	Capture	170		600^g	50	220	*c*
Pu^{238}	Capture	454	454	950	79	530	*h*
Pu^{239}	Capture	315	360^b	1600^g	133	500	*c, d, i*
	Fission	750	840^b	2000^g	167	1000	*c, i*
	Absorption	1065	1200^b	3600^g	300	1500	*c, i*
Pu^{240}	Capture	500		9600	800	1300	*c, i*
Pu^{241}	Capture	400				500^j	*c, k*
	Fission	950				1100^j	*c, k*
	Absorption	1350				1600^j	*c, k*
Pu^{242}	Capture	23	23	870	72	95	*h*

[a] Unless the accuracy warranted, values of σ' have been rounded off.

[b] For a Maxwellian distribution only.

[c] D. J. Hughes and J. A. Harvey, *Neutron Cross Sections*, BNL-325 (July 1, 1955).

[d] J. A. Harvey, *Thermal Neutron Cross Sections and Definition of the f-Factor in BNL-325*, ORNL CF-56-6-41 (June 7, 1956).

[e] R. L. Macklin and H. S. Pomerance, *Proc. Intern. Conf. Peaceful Uses Atomic Energy, Geneva, 1955* **5**, 96 (1956).

[f] V. E. Pilcher, D. J. Hughes, and J. A. Harvey, *Bull. Am. Phys. Soc.* 1, Series II, 187 (1956).

[g] The lower limit of the integral is taken from about 0.15 ev and estimated from resonance parameters or graphical integration.

[h] J. P. Butler, M. Lounsbury, and J. Merritt, *Determination of the Neutron Capture Cross-Sections of Pu^{242}, Pu^{238}, and Am^{243}*, CRC-628 (Jan. 1956).

[i] F. W. Cornish and M. Lounsbury, *Cross Sections of Pu^{239} and Pu^{240} in the Thermal and Epi-Cadmium Regions*, CRC-633 (March 1, 1956).

[j] Estimated.

[k] P. R. Kasten, *Summary of Some New Nuclear Data*, ORNL-2142 (Aug. 7, 1956).

Table 9. Comparison of Calculated and Experimental Plutonium Yields

Sample	Pu^{239}/U^{238}		Pu^{240}/U^{238}		Pu^{241}/U^{238}		Pu^{242}/U^{238}	
	Calculated	Experimental	Calculated	Experimental	Calculated	Experimental	Calculated	Experimental
	$\times 10^{-2}$	$\times 10^{-2}$	$\times 10^{-3}$	$\times 10^{-3}$	$\times 10^{-3}$	$\times 10^{-3}$	$\times 10^{-4}$	$\times 10^{-4}$
M-0	1.20	1.17	2.01	2.06	0.652	0.60	0.798	0.731
M-3	1.42	1.56	3.34	3.71	1.42	1.52	2.79	3.34
M-5	1.43	1.35	3.45	3.49	1.51	1.16	3.08	2.28

NEUTRON CROSS SECTIONS OF U^{234}, Pu^{239}, AND Pu^{240}

J. Halperin
J. Oliver[24]
H. S. Pomerance[25]
R. W. Stoughton

Calculated Thermal Cross Section of Pu^{240} and Calculated and Experimental Effective Reactor Cross Sections of Pu^{239} and Pu^{240}

The large resonance absorption (in excess of 10^5 barns) of Pu^{240} at about 1 ev (refs 26 and 27) indicates that the effective reactor cross section of this nuclide should vary markedly with its concentration and the size of the sample irradiated. It may be expected that in very small concentrations or in very small samples the effective cross section will be appreciably larger than the thermal value and that it will decrease with increasing concentration or sample size. Previously reported values[26,28] for the reactor effective capture cross section of Pu^{240} have been around 500 barns, and little attention appears to have been given to the effect of concentration and amounts of the Pu^{240} in the samples irradiated. The following is a comparison of the values of the reactor effective capture cross section of Pu^{240} at low dilution, as calculated from the resonance parameters[27] and from experimental mass ratios resulting from two special sets of irradiations in graphite reactors and from one set in the Chalk River heavy-water reactor. As will be seen, these values are mutually consistent and average around 1200 barns, as contrasted with the 500-barn values previously reported. Since this work has been accepted for publication in *Nuclear Science and Engineering*, only the results will be given here.

One of the sets of graphite-reactor irradiations and the heavy-water reactor irradiation involved starting with natural uranium. The total plutonium/uranium ratio varied from about 2×10^{-4} to 6×10^{-4} in the former irradiations and over a much wider range in the latter. The results obtained in the former irradiations depended on the value used for the effective cross section for U^{238} capture; this was 3.5 barns. By using this value and the experimental results from the graphite-reactor irradiations, an effective capture cross section of 500 barns was obtained for Pu^{239}, as compared with a value of 490 barns calculated from the resonance parameters, the thermal value, and the experimental curve for cross section vs neutron energy in the near-epithermal range as given in BNL-325.[26] The values for the effective Pu^{240} capture cross section in this set varied from 1000 to 1370 barns, with an average of 1160 barns. The values for the heavy-water reactor varied from 960 to 1530 barns, with an average of 1140 barns, based on an assumed effective capture cross section of 500 barns for Pu^{239}. (Actually, both these effective reactor cross sections may be a little too high for a heavy-water reactor, where the resonance-to-thermal flux ratio may be expected to be lower than in a graphite reactor.)

The other set of graphite-reactor irradiations involved the reirradiation of small plutonium

[24] Analytical Chemistry Division.

[25] Education Division.

[26] D. J. Hughes and J. A. Harvey, *Neutron Cross Sections*, BNL-325 (July 1, 1955).

[27] J. A. Harvey, private communication; D. J. Hughes and R. B. Schwartz, *Neutron Cross Sections*, Supplement No. 1, BNL-325 (Jan. 1, 1957).

[28] W. C. Bentley *et al.*, *Proc. Intern. Conf. Peaceful Uses Atomic Energy, Geneva, 1955* **7**, 261 (1956).

samples. Values of 1030 to 1550 barns were obtained for the effective Pu^{240} capture cross section (with an average of 1360 barns), based on an assumed Pu^{239} effective capture cross section of 500 barns.

Also, it should be pointed out that Halperin, Blomeke, and Mrkvicka (see section entitled "Effective Reactor Cross Sections in MTR Fuel Assemblies," in this report) found it necessary to use an effective capture cross section of about 1300 barns for Pu^{240} in order to explain the plutonium isotopic composition in highly irradiated fuel assemblies in the light-water-moderated MTR at Arco. A cross section for Pu^{240} of a significantly lower value would not have given calculated results consistent with the experimental ones.

The effective capture cross section of Pu^{240} at high dilution was then calculated by adding a thermal value and a resonance contribution. By using presently accepted values for the resonance parameters for the 1-ev resonance[27] only, a value of 8300 barns was obtained for the resonance integral. The corresponding effective contribution to the neutron absorption in a graphite reactor is then about 830 barns, based on the assumption of a thermal-to-resonance flux ratio of 10. The thermal (2200-m/s) value calculated from the resonance parameters for the 1-ev resonance[27] only, by use of the Breit-Wigner formula, was about 340 barns. Since this resonance peak[26] is so large and so near the thermal region, its contribution alone, as calculated from the Breit-Wigner formula, probably represents by far the major part of the thermal cross section. Also, because of this resonance the Pu^{240} cross section does not vary as $1/v$ in the thermal region, and the "effective" thermal cross section is about 10% higher than the 2200-m/s value, as can be verified by integrating both the actual curve and a $1/v$ curve over a Maxwellian neutron distribution at a neutron temperature of 500°K; hence the calculated "effective" thermal cross section is about 370 barns (whereas a thermal fission cross section of U^{235} of 582 barns would be used for the same flux). By adding the "effective" thermal value and the resonance contribution, a value of 1200 barns is obtained for the effective reactor cross section, which is in good agreement with the experimental value.

This calculated thermal (2200-m/s) cross section of 340 barns is in very good agreement with an experimental value of 360 barns obtained with the pile oscillator (see the following section). These values may be compared with a relatively recent Canadian[27,29] thermal cross section for Pu^{240} of 240 ± 35 barns and a Russian[30] value of 460 ± 45 barns.

The authors conclude that a thermal (2200-m/s) cross section of about 350 barns and an effective reactor cross section of about 1200 barns at high dilution, with a thermal-to-resonance flux ratio of about 10, now appear to be the best values for Pu^{240}.

Measurement of the Thermal-Neutron Capture Cross Section of Pu^{240} with the Pile Oscillator

A measurement of the thermal cross section of Pu^{240} has been made with the pile oscillator.[31] The experiment was carried out with a sample of plutonium containing 80.08% Pu^{240}, 18.64% Pu^{239}, 1.14% Pu^{241}, and 0.14% Pu^{242}. About 20 mg of the PuO_2 was deposited on an aluminum foil over an area of approximately 5 cm^2. This deposit is sufficiently thin to provide negligible self-absorption. A similar sample containing pure Pu^{239} was prepared in order to correct the measurement of the Pu^{240}-containing sample for its Pu^{239} and Pu^{241} content. Gold was used as a standard in the pile oscillator measurement; the cross section used for gold was 99.4 barns (i.e., 98.8 barns for the thermal contribution plus 0.6 barn for the resonance contribution). The 2200-m/s value found for the cross section of Pu^{240} was 360 ± 30 barns, after a small correction was made because of the departure from the $1/v$ law due to the strong resonance at 1 ev. This correction depends on the characteristic temperature of the assumed Maxwellian distribution and on the energy dependence of the efficiency of the boron counter, as well as on the resonance parameters, and is about 3% of the observed effect.

---

[29] F. W. Cornish and M. Lounsbury, *Cross Sections of Pu^{239} and Pu^{240} in the Thermal and Epi-Cadmium Regions*, CRC-633 (March 1, 1956).

[30] P. A. Krupchitskii, *Atomnaya Energ.* **2**, 240–246 (1957).

[31] J. I. Hoover *et al.*, *Phys. Rev.* **74**, 864 (1948).

Remeasurement of the Thermal Capture Cross Section of U^{234}

The inconsistency of the reported[32] thermal cross sections of U^{234} (60 to 90 barns) with the cross section deduced from the resonance parameter[33] (about 20 barns) prompted a remeasurement of the thermal value. A new preparation of a sample containing about 80% U^{234} was measured on the pile oscillator and was found to yield a cross section of about 90 barns, as compared with the gold standard. This value is in excellent agreement with the value reported previously by Pomerance,[34] 92 ± 7 barns. Thus the discrepancy in the measured and calculated values of this cross section apparently is due to negative resonances.

SURVEY OF THORIUM BREEDER BLANKETS

M. H. Lietzke R. W. Stoughton

A survey has been made of the feasible chemical forms for a thorium breeder blanket. The information has been published in a paper[35] describing the thorium blanket systems which have been seriously considered and the general nuclear and chemical considerations involved in choosing a thorium breeder blanket. It was pointed out that the only blanket form which has been demonstrated to be practical consists of aluminum-jacketed metal slugs, although reprocessing and refabrication methods used for such slugs are undesirably elaborate. Of the other systems, a thorium oxide slurry in D_2O, and thorium nitrate (with N^{15}) dissolved in D_2O now appear to be the most promising in the long run.

EFFECT OF NITRITE ON NEPTUNIUM EXTRACTION

G. W. Parker P. M. Lantz W. J. Martin

Some beneficial effect on neptunium extraction coefficients has been previously observed by both Sheppard[36] and Siddall,[37] and this led the authors to a further study of the oxidation states of neptunium in the presence of nitrite ion and nitric acid. Since it can be demonstrated that Np(VI) is readily reduced by nitrite,[38] a mechanism for reduction of Np(V) to Np(IV), or reoxidation to Np(VI), must be found in order to explain improved extractability.

Absorption Spectra of Neptunium Oxidation States

The first experiment designed to aid in interpretation of this phenomenon was the measurement of the absorption spectra of a sample of neptunium extracted into TBP in the presence of nitrous acid. The bands for Np(VI) at 1230 mμ (Fig. 6) and for Np(V) at 1105 mμ were especially helpful. It was found in this instance that only Np(VI) was present in the organic phase.

In a study of extraction coefficients, it was noted that initially the extraction for Np(IV) with TBP was reduced by the addition of nitrite but that subsequent extraction was obtained with improved coefficients. This suggests immediate reduction of Np(VI), followed by gradual reoxidation. In seeking an explanation for the nitrite behavior, the following possibilities have been investigated:

1. A rapid reduction of Np(VI) or a rapid oxidation of Np(IV) may be followed by a disproportionation of Np(V) to Np(IV) and (VI). The rate of disproportionation of Np(V) is expected to follow fourth-power hydrogen ion dependence, and nitrate complexing should also contribute to this mechanism; however, the reaction is slow at low acidities.
2. Separate nitrite oxidation-reduction reactions of first and second order may occur. This mechanism implies that the reduction of Np(VI) to Np(V) would vary as the reciprocal of the nitrite concentration and that the oxidation of Np(IV) should follow the log of the nitrite concentrations. On the other hand, it also implies that nitrite should be consumed in the reaction.
3. Nitrate oxidation may be catalyzed by a threshold concentration of nitrite.[39] In strong (16 *M*) nitric acid, Np(V) is readily oxidized to Np(VI). In dilute nitric acid this does not occur.[38] If this same reaction catalyzed by nitrite at low acid

[32] D. J. Hughes and J. A. Harvey, *Neutron Cross Sections*, BNL-325 (July 1, 1955).

[33] D. J. Hughes and R. B. Schwartz, *Neutron Cross Sections*, Supplement No. 1, BNL-325 (Jan. 1, 1957).

[34] H. Pomerance, *Thermal Neutron Capture Cross Sections of Uranium*, ORNL CF-51-12-151.

[35] M. H. Lietzke and R. W. Stoughton, *Ind. Eng. Chem.* 49, 202 (1957).

[36] J. C. Sheppard, *Path of Neptunium in the Hanford Process*, Proceedings of Neptunium Information Meeting, USAEC (to be published).

[37] T. H. Siddall, *Path of Neptunium in the Savannah River Process* (to be published).

[38] D. A. Orth, *Isotopes of Neptunium and Plutonium*, UCRL-1059, p 7 (March 17, 1952).

[39] Suggested by G. H. Cartledge, private communication.

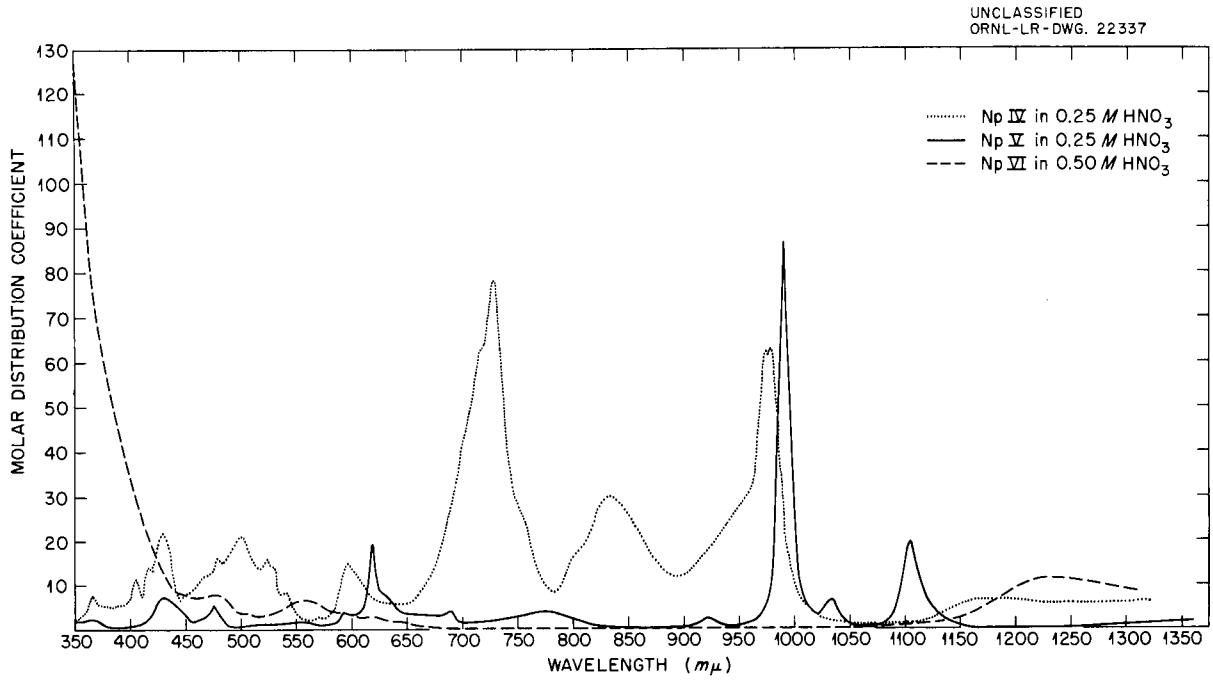

Fig. 6. Adsorption Spectra of Neptunium Ions in HNO_3 Taken with Beckman Spectrophotometer, Model DU.

strength should be responsible for the oxidation of Np(V), there should be little effect of increasing neptunium concentration. In addition, there should be no oxidation by nitrite in other acids such as $HClO_4$.

Investigation of Nitrite Catalysis

For the purpose of measuring the extent to which Np(V) is oxidized in the presence of nitrite, a specially prepared Np^{239} tracer solution 10^{-4} *M* in Np^{237} [both as Np(V)] was allowed to react at different concentrations of nitrite (10^{-6} to 10^{-1} *M*), and the Np(VI) produced was measured by coprecipitation with $NaZnUO_2(C_2H_3O_2)_5$. In Table 10 a summary is given of a comparison of the relative amounts of neptunium oxidized in the two acids. There was no oxidation (above trace impurity) in 4 *N* $HClO_4$ and only a minor amount in 2 *N* HNO_3. In 4 *N* HNO_3 a large effect was observed.

Effect of Neptunium Concentration on Per Cent of Np(V) Oxidized. – In order to determine whether the neptunium concentration affected the per cent of Np(V) oxidized at a threshold concentration of nitrite (2.5×10^{-5} *M*), amounts of Np^{237} as Np(V) were added to the Np^{239} tracer over the range from 10^{-5} to 4×10^{-3} *M*. Table 11 shows that an almost constant yield of Np(VI) at nearly 50 times the stoichiometric amount of nitrite resulted.

Table 10. Np(V) Oxidation in HNO_3-HNO_2 Systems

Np^{237} conc = 10^{-6} *M*; warmed to 50°C for 30 min

$NaNO_2$ (*M*)	Np(VI) [% Np Carried by $NaZnUO_2(C_2H_3O_2)_5$]		
	4 *N* $HClO_4$	2 *N* HNO_3	4 *N* HNO_3
0	6.2	4.5	6.1
2.5×10^{-5}	7.6	6.2	31.6
1.25×10^{-4}	4.5	7.7	41.8
2.5×10^{-4}	4.5	7.4	35.8
2.5×10^{-3}	4.6	5.5	28.2
2.5×10^{-2}	4.3	4.5	6.4
2.5×10^{-1}	4.4	4.5	2.6

The simplest representation of the catalytic oxidation reaction, which does not consume nitrite, may be written as follows:

$$NpO_2^{+} + NO_3^{-} \xrightarrow[H^+]{NO_2^-} NpO_2^{++} + NO_2^{-}$$

Effect of Nitrite on Np(V) Extraction in TBP. – Since it had been shown that oxidation occurred at low nitrite concentrations, diminishing significantly at higher concentrations, it was decided to measure the extraction coefficients of the mixed states corresponding to those found in the plant solutions. Since the oxidation effect was less pronounced at low acid concentrations, it was measured only in 4 N HNO_3. The results in Fig. 7 clearly substantiate plant experience (shown in Fig. 8) that nitrite control is of primary importance to neptunium extractability.

The reason for the failure of the larger quantities of nitrite to reduce extractability into TBP to the extent expected from the uranyl acetate precipitation test is not clear; however, it may perhaps be explained as the result of nitrite complexing.

Table 11. Np^{237} Oxidized by 4 N HNO_3, HNO_2-catalyzed

$NaNO_2$ conc = 2.5×10^{-5} M

Np^{237} (M)	Per Cent Oxidized*
4×10^{-3}	39
4×10^{-4}	39
4×10^{-5}	45
1×10^{-5}	42

*Carried on $NaZnUO_2(C_2H_3O_2)_5$.

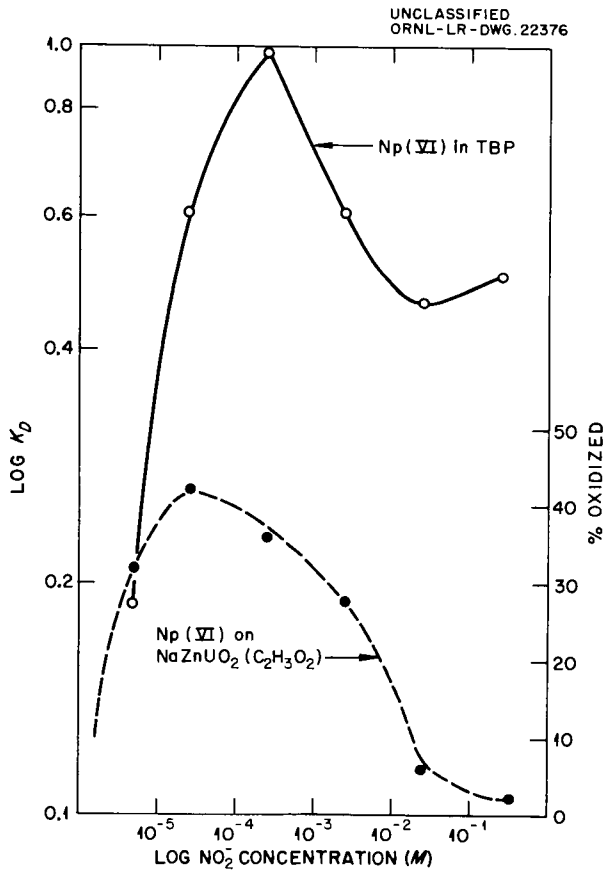

Fig. 7. Effect of Nitrite on Np(V) Extraction into TBP.

EXAMINATION OF HANFORD-RECOVERED URANIUM FOR NEPTUNIUM CONTENT

G. W. Parker P. M. Lantz

In connection with the neptunium isolation program at ORNL, a cursory analysis of Savannah River and Hanford processed uranium last year resulted in the discovery of a moderate amount of Np^{237} in the uranium oxide[40] at K-25. An initial analysis of Hanford uranium at Paducah in April 1956 revealed that little of the neptunium was contained in the former Redox process material. Subsequently, the Hanford Purex process has been

[40] G. W. Parker *et al.*, *Chem. Semiann. Prog. Rep. Dec. 20, 1955*, ORNL-2046, Table 20, p 65.

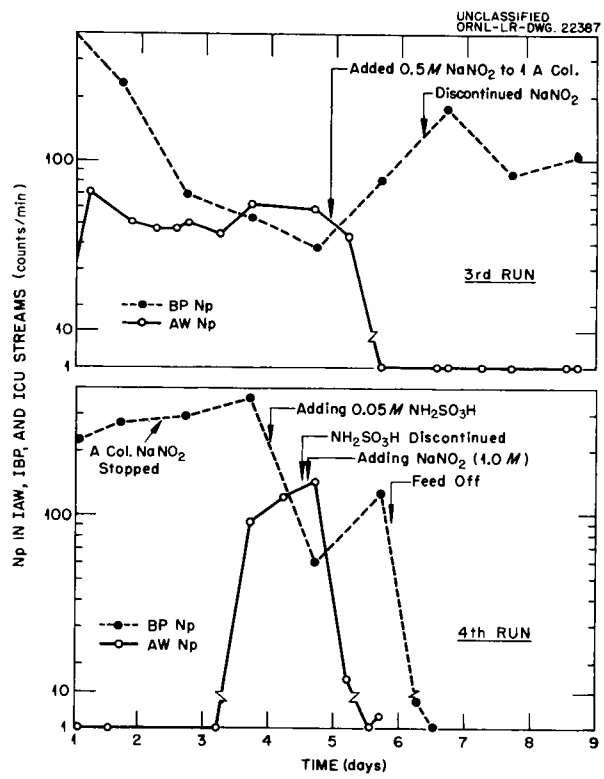

Fig. 8. Effect of Nitrite Addition on Neptunium Extraction in Plant Process.

contributing an increasing proportion of the processed uranium.

Early this year the technical section at Paducah became concerned over the high alpha count in the uranium oxide being received from Hanford. As a result they submitted to this laboratory for Np^{237} analysis several samples of the oxide and ash accumulated from the tower, cyclone separator, and barrier filter. The oxide contained approximately the theoretical yield of Np^{237} expected from Hanford-irradiated natural uranium, indicating that most of the neptunium was following the uranium in the metal recovery process. The drums of ash were divided into six lots, with random distribution of tower, cyclone separator, and barrier filter ashes. Sampling of the drums was conducted by removing portions relative to the drum weight and combining them for each lot. Results of the oxide and separator ash analyses are given in Table 12.

Table 12. Neptunium Content of Paducah Fluoride Ash

Composite No.	Total Weight of Ash (tons)	Total Weight of Np^{237} (g)
1	4.0	19.68
2	5.0	3.3
3	5.0	7.1
4	2.0	41.2
5	1.0	6.47
6	2.5	52.6
	19.5	130.35

The six lots of ash, a total of 19.5 tons, whose neptunium content varied from 0.7 to 21.0 g/ton, contained a total of 130 g of neptunium. Lots 1 and 4 are currently being processed by the Metal Recovery Plant of the Laboratory for neptunium recovery, and it is anticipated that lots 5 and 6 will also be processed.

VOLATILIZATION OF FISSION PRODUCTS BY THE MELTING OF REACTOR FUEL PLATES

G. W. Parker G. E. Creek

The initial phase of the investigation of fission-product volatility has been completed with the following results: At trace concentration of fission products, slow melting of the APPR plate at 1525°C in air or steam effected the release of 50% of the rare gases, 33% of the iodine, 9% of the cesium, and traces of strontium. After 25% burnup, the cesium value increased to about 60%. When aluminum alloy of the MTR type, also at trace concentration of fission products, was melted at 700°C, it released up to 2% of the iodine, 10% of the rare gases, and negligible portions of other fission products. When zirconium alloy of the STR type, after 15% burnup, was melted at 1850°C, it released up to 95% of the iodine and only a trace of strontium. This information has been reported in detail elsewhere.[41]

[41] G. W. Parker and G. E. Creek, *The Volatilization of Fission Products by Melting of Reactor Fuel Plates*, ORNL CF-57-6-87 (July 15, 1957).

ISOLATION AND CHEMICAL PROPERTIES OF SYNTHETIC ELEMENTS

CHEMISTRY OF TECHNETIUM

Search for Technetium in Terrestrial Materials

G. E. Boyd Q. V. Larson

An extensive search for primordial technetium in various rocks, minerals, and meteorites was concluded during this past year, and a report covering this work has appeared.[1]

No traces of this element were found by using a variety of sensitive detection methods including optical spectrometry, neutron activation analysis, and isotope dilution in which fission-product Tc^{99} and a mass spectrometer were employed. Nuclear chemical researches on technetium radioisotopes conducted at the Laboratory have shown that technetium possesses no beta-stable nuclear species, although the existence of three very-long-lived isotopes, Tc^{97}, Tc^{98}, and Tc^{99}, has been established. Both Tc^{97} and Tc^{99} have been shown to possess half lives of less than one million years and hence, if initially present at the time of the earth's formation, would have disappeared in the approximately 4.5×10^9 years since then. Quite recently (cf. "Half Life of Tc^{98} and Its Abundance in Fission-Product Technetium," this report), a preliminary value of $(1.5 \pm 0.7) \times 10^6$ years has been determined for Tc^{98}. This result is consistent with our failure to find technetium in terrestrial materials. The existence[2] of an isomeric state of Tc^{98} with a half life exceeding 10^8 years has not been excluded by nuclear chemical investigations. Such a possibility is considered to be unlikely, however.

Solvent Extraction of Heptavalent Technetium

G. E. Boyd Q. V. Larson

Measurements of the extraction of heptavalent technetium from aqueous solutions by a variety of organic solvents were continued during the report period.[3] This investigation is now completed, and the findings will be submitted for publication at an early date.

Survey measurements of the extraction of pertechnetate ion from normal H_2SO_4, Na_2SO_4, and NaOH solutions were performed with a wide variety of alcohols, ketones, ethers, esters, organophosphorus compounds, organonitrogen compounds, and miscellaneous hydrocarbons and their halogenated derivatives. Interesting correlations of extraction with chain length, chain branching, ring formation, and other steric factors were observed. The interplay of the basicity and the dielectric constant, ϵ, of the organic solvent was of importance, as shown by ethers, which have relatively high basicity but low ϵ values and are not good extractants compared with the less basic ketones and alcohols, which possess higher ϵ values and extract pertechnetate efficiently. The hypothesis of "onium" salt formation proved to be useful in understanding the extraction of pertechnetate ion from acid solutions. The differences in pertechnetate extraction from 1 *N* H_2SO_4, HCl, HBr, HNO_3, HI, and $HClO_4$ could be explained in terms of an anion exchange competition with the oxonium salt formed with $HTcO_4$. The retrograde extraction of technetium found with increasing concentrations of the same acids may also be explained in this manner.

Detailed studies were conducted by using tributyl phosphate and trioctylphosphine oxide, both of which extract technetium efficiently from acid solutions. Additionally, a variety of tertiary amines and quaternary ammonium compounds were studied. Good extraction from strongly basic solutions was observed only with the latter compounds, as was expected. A number of specific "salt effects" were noted in other measurements conducted by using cyclohexanol, cyclohexanone, methyl ethyl ketone, and tributyl phosphate.

Heat Capacity of Potassium Pertechnetate from 16 to 310°K

R. H. Busey Q. V. Larson

The low-temperature heat capacity of potassium pertechnetate, $KTcO_4$, was measured to provide values of the entropy and free-energy functions of this important compound of technetium. These measurements, in combination with other selected thermochemical measurements, make possible an accurate calculation of the free energy of formation of the pertechnetate ion, TcO_4^-.

---

[1] G. E. Boyd and Q. V. Larson, *J. Phys. Chem.* **60**, 707 (1956).

[2] E. Anders, R. N. Sen Sarma, and P. H. Kato, *J. Chem. Phys.* **24**, 622 (1956).

[3] G. E. Boyd and Q. V. Larson, *Chem. Semiann. Prog. Rep. June 20, 1956*, ORNL-2159, p 16.

Potassium Pertechnetate Sample. – The technetium sample was isolated from fission products by W. J. Martin and G. W. Parker and was furnished as $KTcO_4$. The sample was further purified by several recrystallizations from water and was dried for two weeks in an evacuated desiccator charged with P_2O_5. Subsequent heat capacity measurements through the ice-point region showed that this treatment is insufficient for removing all the water apparently trapped in the crystals. Attempts to analyze for the water content by loss in weight on ignition were unsuccessful because of decomposition of the sample. (Subsequent work on $KTcO_4$ shows that this decomposition must have been due to some minor, undetected impurity apparently catalyzing the decomposition, since $KTcO_4$ has now been prepared that is extremely stable to heat; $KTcO_4$ can be melted and sublimed without apparent decomposition.) Spectrographic analysis revealed a trace of Ca and faint traces of Mg, Si, and Sn.

Apparatus and Temperature Scale. – The cryostat has been described previously.[4] The calorimeter used was a 10-ml gold calorimeter with a combination thermometer-heater wound on the outside. A standard copper-constantan thermocouple is attached to the adiabatic shield, and in conjunction with the differential thermocouple makes possible the calibration of the resistance thermometer concurrently with the heat capacity measurements.

Heat Capacity Data. – The weight of $KTcO_4$ in the calorimeter was 9.1738 g (*in vacuo*), representing 0.045389 mole of $KTcO_4$ (with 99.00 used for the atomic weight of Tc). The heat capacity observations determined by the adiabatic method are given in Tables 13 and 14. Table 13 gives the

[4] R. H. Busey, *A Combination Isothermal-Adiabatic Low-Temperature Calorimeter*, ORNL-1828 (Jan. 26, 1955).

Table 13. Heat Capacity ($cal \cdot deg^{-1} \cdot mole^{-1}$) of $KTcO_4$

T_{av} (°K)	C_p	T_{av} (°K)	C_p	T_{av} (°K)	C_p
Series 1		Series 2		Series 3	
273.26	28.94	52.14	9.544	184.08	24.10
279.80	29.13	61.08	11.31	190.44	24.45
287.02	29.48	64.30	11.89	197.47	24.79
294.41	29.80	67.52	12.46	204.65	25.26
302.29	30.20	70.75	12.92	211.54	25.63
310.51	30.70	74.00	13.45	218.16	25.95
		77.23	13.96	223.14	26.21
Series 2		79.96	14.38	236.75	26.87
16.31	1.046	83.35	14.87	243.92	27.31
17.50	1.251	86.77	15.29	251.28	27.70
18.76	1.527	90.27	15.75	258.92	28.30
20.33	1.846	93.87	16.19	284.12	29.35
21.12	2.003	97.55	16.63	292.27	29.70
23.16	2.496	101.33	17.09		
25.26	3.032	109.54	18.05	Series 4	
27.68	3.631	113.87	18.46	124.00	19.49
30.25	4.336			132.45	20.32
32.96	5.063	Series 3		138.86	20.88
35.80	5.865	148.96	21.76	145.59	21.50
38.53	6.546	154.68	22.08	151.94	21.94
41.14	7.169	160.75	22.59	158.54	22.40
43.77	7.795	166.55	22.93	165.40	22.87
46.50	8.412	172.10	23.38	172.42	23.41
49.29	8.952	177.95	23.76	179.60	23.86

Table 14. Excess Heat Absorption in the Region of the Ice Point of a 9.2502-g (*In Vacuo*) Sample of $KTcO_4 + H_2O$

T_1	T_2	ΔH (cal)
Series 5		
258.430	266.645	11.025
266.645	266.662	0.029*
266.662	275.122	17.354
275.122	275.151	0.050*
275.151	284.105	12.803
Observed heat absorption from 258.430 to 284.105°K		41.261
$\int C_p\, dT$		34.916
Excess heat absorption		6.345
Series 6		
262.058	268.980	9.381
268.980	268.995	0.041*
268.995	279.690	20.990
Observed heat absorption from 262.058 to 279.690°K		30.396
$\int C_p\, dT$		23.941
Excess heat absorption		6.455
Series 7		
262.234	271.564	12.967
271.564	271.664	0.156*
271.664	289.524	30.833
Observed heat absorption from 262.234 to 289.524°K		43.956
$\int C_p\, dT$		37.547
Excess heat absorption		6.409

*Estimated values.

heat capacity results corrected for the water content, calculated below. The results are expressed in terms of the defined thermochemical calorie equal to 4.1840 j (abs). The ice point was taken to be 273.16°K.

Table 14 gives the excess heat absorption, in the region of the ice point, arising from fusion of ice in the sample. The excess heat absorption was computed as follows. Given in the table are those determinations which showed abnormal absorption of heat. By applying small corrections for the temperature regions not actually observed, there is obtained a total observed heat absorption (by summing the individual heat observations) in going from a temperature below to a temperature above the ice point. By extrapolation of the normal heat capacity curve from well below the ice point to 273.16°K, and again from well above to 273.16°K, there is obtained an estimation of the heat absorption that would have been observed had no melting of ice occurred. This latter calculated heat absorption over the specified temperature region is designated in Table 14 as $\int C_p\, dT$. The difference between these two summations gives the excess heat absorption arising from fusion of ice to form a solution of $KTcO_4$. The average of the three determinations is 6.40 ± 0.04 cal.

A difficulty arises in computing how much water this represents because of the uncertainty in the composition of the final product, that is, the concentration of the $KTcO_4$ solution formed. The two extremes are 80.3 mg of H_2O for formation of pure water, and 74.7 mg of H_2O for formation of a saturated solution at 25°C. This difference arises from the fact that $KTcO_4$ has appreciable solubility in water, 0.63 *M* at 25°C. By assuming the formation of a saturated solution at the final temperature given, the following amounts of H_2O are calculated: 75.7, 77.6, and 76.0 mg for series 5, 6, and 7, respectively, giving the average value of 76.4 mg. This average value was used to correct the data for H_2O content; thus the sample had 0.826% H_2O by weight, or 8.55 mole %. This water content is probably correct to only ±3%.

The observed heat capacities below the ice point were corrected for ice content by using the data of Giauque and Stout.[5] Above the ice point a constant correction for H_2O of 0.95 $cal \cdot deg^{-1} \cdot g^{-1}$ was employed. These corrections to the observed heat capacities amounted to approximately 2% from the lowest temperatures up to 150°K, to 2.5% from 200 to 250°K, and to 5% above the ice point. Since the water content is known to only 3%, this represents an uncertainty in the heat capacities which arises from the water content of 0.06, 0.08, and 0.15% over the above temperature ranges, respectively.

The heat capacities are believed to be accurate to within 5% at 15°K, 1% at 25°K, 0.2% above

[5] W. F. Giauque and J. W. Stout, *J. Am. Chem. Soc.* **58**, 1144 (1936).

40°K, and 0.5% above the ice point. These estimates were made by consideration of the thermometer sensitivity, sample size, and uncertainties in the water content of the measured sample.

Entropy of $KTcO_4$ and $TcO_4^-(aq)$. – The entropy of $KTcO_4$ is 39.74 cal·deg^{-1}·mole^{-1} at 298.16°K, obtained by application of the third law of thermodynamics to the heat capacity data and utilization of the Debye T^3 law for an estimation of the entropy at 15°K, namely, 0.29 cal·deg^{-1}·mole^{-1}.

Parker and Martin[6] have determined the solubility of $KTcO_4$ at 7 and at 27°C. For the solubility reaction the following thermochemical quantities at 298.16°K may be computed:

$$KTcO_4(c) = KTcO_4(aq),$$
$$m = 0.63 \text{ mole·liter}^{-1},$$
$$\gamma_{\pm} = 0.57 \text{ (estimate)},$$
$$\Delta F^0 = -RT \ln (\gamma m)^2 = 1214 \text{ cal·mole}^{-1},$$
$$\Delta H^0 = 9550 \text{ cal·mole}^{-1} \text{ (temperature coefficient of solubility)},$$
$$\Delta S^0 = (\Delta H^0 - \Delta F^0)/T = 28.0 \text{ cal·deg}^{-1}\text{·mole}^{-1}.$$

By using 24.5 cal·deg^{-1}·mole^{-1} for the entropy of $K^+(aq)$ and the above value for the entropy of $KTcO_4(c)$ the following can be computed:

$$S^0(TcO_4^-, aq) = \Delta S^0 + S^0(KTcO_4) - S^0(K^+) = 43.2 \text{ cal·deg}^{-1}\text{·mole}^{-1} .$$

Free Energy of Formation of $KTcO_4(c)$ and $TcO_4^-(aq)$; the Tc-TcO_4^- Couple. – Cobble, Smith, and Boyd[7] give –242.5 kcal·mole^{-1} for the heat of formation of $KTcO_4(c)$ at 298.16°K. By using 39.74 cal·deg^{-1}·mole^{-1} for the entropy of $KTcO_4(c)$, –81.1 cal·deg^{-1}·mole^{-1} is obtained for the entropy of formation and –218.4 kcal·mole^{-1} is obtained for the free energy of formation.

Cobble *et al.*[7] also give –173.0 kcal·mole^{-1} for the heat of formation of $HTcO_4(aq)$. By using the above value of 43.2 cal·deg^{-1}·mole^{-1} for the entropy of $HTcO_4(aq)$, –78.0 cal·deg^{-1}·mole^{-1} is obtained for the entropy of formation and –149.7 kcal·mole^{-1} is obtained for the free energy of formation. From the last value the potential of the Tc-TcO_4^- couple is calculated to be –0.477 v.

[6] G. W. Parker and W. J. Martin, *Chem. Quar. Prog. Rep. June 30, 1951*, ORNL-1116, p 26.

[7] J. W. Cobble, Wm. T. Smith, Jr., and G. E. Boyd, *J. Am. Chem. Soc.* **75**, 5777 (1953).

Low-Temperature Heat Capacity of Potassium Hexachlororhenate

R. H. Busey R. B. Bevan, Jr.

Additional low-temperature heat capacity measurements have been made on a sample of K_2ReCl_6 prepared by a different procedure than that used for the first measurements reported previously.[8] These measurements were made to reduce the possibility that one or more of the three anomalies previously observed in the heat capacity at 76, 103.5, and 111°K were due to an impurity such as $K_2Re(OH)Cl_5$. It seems unlikely that the two preparations would contain the same concentrations of impurities.

The second sample was prepared[9] by hypophosphorous acid reduction of potassium perrhenate according to the procedure of Rulfs and Meyer.[10] Table 15 gives the analysis of the sample, along with that obtained on the first sample for comparison purposes.

Table 15. Analytical Data on K_2ReCl_6 Samples (wt %)

	Sample No.		Theoretical Values
	1	2	
Cl	44.53	44.55	44.58
Re	39.04	39.24	39.03

The significant information wanted is the agreement between the two sets of measurements, and this will be given rather than the individual heat capacity determinations. The second sample exhibited three peaks, the same as the first sample but with small and possibly significant differences. At the 76°K anomaly the two sets of data agreed to within 0.1%, except at the trough on the high-temperature side of the anomaly, where the second sample gave results 0.2 to 0.3% lower. The most significant difference appeared at the 103.5°K anomaly. Here again the agreement was within 0.1% on the low-temperature side of the anomaly, but the second sample exhibited its maximum at

[8] R. H. Busey, H. H. Dearman, and Q. V. Larson, *Chem. Semiann. Prog. Rep. June 20, 1956*, ORNL-2159, p 11.

[9] D. E. LaValle, Analytical Chemistry Division.

[10] C. L. Rulfs and R. J. Meyer, *J. Am. Chem. Soc.* **77**, 4505 (1955).

103°K and approximately 1% lower in height than the first sample. The second sample gave a trough approximately 0.5% lower for this anomaly. At the 111°K anomaly the second sample gave results 0.1 to 0.2% lower on the low-temperature side of the anomaly, essentially perfect agreement at the maximum, and 0.4 to 0.5% lower results at the trough on the high-temperature side of the anomaly. Outside the region of the anomalies the two sets of data agree to within 0.1 to 0.2% in general, with the second sample fairly consistently giving somewhat higher heat capacities.

It is difficult to ascertain the significance of the differences exhibited by the two samples in the anomalous regions. A cursory search of the literature revealed no compound having a heat capacity anomaly which has been the subject of precise duplicate measurements, either by one or by different investigators. It is believed, however, that the data on the second sample do give strong evidence that the three anomalies shown by the K_2ReCl_6 samples arise from the K_2ReCl_6 itself and not from an impurity or impurities in the samples.

CHEMICAL SEPARATION OF ISOTOPES

ENRICHMENT OF OXYGEN ISOTOPES

L. L. Brown L. B. Yeatts, Jr.

There is considerable interest in O^{17} (normal abundance 0.04%), since this isotope can be detected by nuclear magnetic-resonance methods with little disturbance to the system under study, and for this reason it would be a useful tracer in biological systems of interest.

Since both the normal-abundance and isotopic-separation factors for O^{17} are fairly low, many stages and a high reflux ratio are required to enrich O^{17} to a useful level. For this reason systems are being sought in which there is little or no net consumption of chemicals in the reflux reactions. In the systems described in this report, a gas-liquid addition compound is decomposed by heating and is re-formed by reacting the two constituents at or below room temperature. The separation factors reported in the following experiments give the isotopic fractionation in terms of the O^{16}/O^{18} ratio in the two phases. This factor is more readily measured by the mass spectrometer than is the corresponding factor in terms of the O^{16}/O^{17} ratio, since O^{18} is more abundant than O^{17}, and the enrichment factor $(\alpha - 1)$ in terms of O^{18} fractionation should be about double the O^{17} enrichment factor.

Carbon Dioxide Exchange Systems

Experiments[1] on amine–carbon dioxide complexes have continued during the past year. The carbamates of mono- and diethanolamine were found to be soluble in alcohols of low molecular weight. Heating of a butyl alcohol solution of CO_2 and diethanolamine removed essentially all the CO_2. Monoethanolamine carbamate in butyl alcohol was equilibrated with CO_2 gas in a three-stage batch experiment. A single-stage separation factor of 1.013 ± 0.002 (95% C.I.) was measured with O^{18} enriching in the gas phase.

Carbon dioxide solubility in acetone has a strong temperature dependence which is favorable for a thermally refluxed separation system. One gram of acetone contains 300 cc (STP) of CO_2 at –73°C and only 8 cc at 20°C, but there is no hint of a definite complex. A solution of CO_2 in acetone immersed in a dry ice–acetone bath was equilibrated with CO_2 gas for 3 hr. A separation factor of 1.006 ± 0.005 (95% C.I.) was measured, showing a slight enrichment of O^{18} in the liquid phase at –78°C.

Nitric Oxide Exchange Systems

In previous work[2] the separation factor for nitrogen isotopes in the nitric oxide–ferronitroso ion system was determined. The same type of experiment has been repeated for the oxygen separation factor. A modified version of the previous[2] contactor was used. Ninety milliliters of 0.89 *M* $FeSO_4$ saturated with NO at 14°C (Fe/NO $\simeq$ 2.7) was contacted for $2\frac{2}{3}$ hr with NO at a pressure of 72 cm Hg. No oxygen enrichment was found (α = 1.000 ± 0.002, 95% C.I.), but the nitrogen separation factor was 1.011 ± 0.004 (95% C.I.) with N^{15} enriching in the liquid phase.

Oxygen isotope fractionation has also been investigated in the exchange between gaseous NO and liquid NOCl. The NOCl was distilled at –5.5°C in a dry, oxygen-free, helium atmosphere. Oxygen must be completely excluded from the system, since O_2^{16} has the same mass as $N^{14}O^{18}$ and would interfere with the mass spectrometer analysis. Purified NO gas was equilibrated with liquid NOCl for 4 hr at –50°C and 700 mm Hg pressure. A previous exchange experiment with $N^{15}O$ showed exchange to be complete in this period. An oxygen separation factor of 1.011 ± 0.002 (95% C.I.) and a nitrogen separation factor of 1.013 ± 0.003 (95% C.I.) were measured with O^{18} and N^{15} enriching in the liquid phase.

Carbon Monoxide Exchange Systems

A multistage experiment was performed in which CO dissolved in 0.84 *M* CuCl and 3 *M* HCl exchanged with gaseous CO at 24°C. Previous experiments[3,4] on this system indicated that the

[1] L. L. Brown, *Chemical Separation of Isotopes Section Semiann. Prog. Rep. June 30, 1956*, ORNL-2176, p 23 (Classified).

[2] L. L. Brown, *Chemical Separation of Isotopes Section Semiann. Prog. Rep. June 30, 1955*, ORNL-2005, p 23 (Classified).

[3] L. L. Brown, *Chemical Separation of Isotopes Section Semiann. Prog. Rep. Dec. 31, 1955*, ORNL-2097, p 34 (Classified).

[4] L. L. Brown, *Chemical Separation of Isotopes Section Semiann. Prog. Rep. June 30, 1956*, ORNL-2176, p 21 (Classified).

single-stage separation factor was too small to be established by a single-stage equilibration. The experiment was performed in a small, complete, isotope fractionation system similar to that used in the early Anco[5] work. Isotopic exchange occurred in a 30-in. section of 1-in. glass pipe, packed with $\frac{3}{32}$-in. glass helices. A 6-in. stage height was assumed, giving a single-stage fractionation factor for this system of the order of 1.006 with O^{18} enriching in the aqueous phase.

ENRICHMENT OF SULFUR ISOTOPES

A. C. Rutenberg

An investigation of systems for enriching the isotopes of sulfur has recently been undertaken. Sulfur has four stable isotopes of masses 32, 33, 34, and 36, with abundances of 95.0, 0.75, 4.2, and 0.02%, respectively. A large number of isotopic exchange studies have been made during the past 20 years with radioactive S^{35} as a tracer. Exchange between most of the sulfur-containing species was found to be quite slow.

Experimental work in this laboratory has thus far been limited to systems utilizing the exchange between SO_2 gas and addition compounds of SO_2 to amines, ethers, and thio-ethers. This type of system appears to be attractive because it offers the possibility of being thermally refluxed.

Ethylene oxide (bp 10.7°C) was found to form an SO_2 addition compound which boiled at 17°C. If the vapor phase were appreciably dissociated, enrichment could result from the exchange between SO_2 gas and the liquid addition compound. Some ethylene oxide·SO_2 was distilled through a 30-bubble-plate column at atmospheric pressure. The distillation was carried out for 12 hr in order to be sure that equilibrium was attained. The isotopic analyses were performed directly on the addition compound. The sulfur isotopic fractionation for the entire 30-bubble-plate column was 1.008 ± 0.009 with S^{32} enriching at the top of the column. The data for oxygen fractionation in the ether were too poor to be interpreted. In a similar system, Holmberg[6] claims to have enriched sulfur isotopes by distilling $(C_2H_5)_3N{\cdot}SO_2$ at a pressure of 40 mm Hg.

Dimethyl aniline (DMA) has some desirable characteristics for a gas-liquid exchange system. It was found that the addition and removal of SO_2 are quite reversible. Boiling a mixture having the initial composition DMA·1.3SO_2 for a short while left only 13 ppm SO_2 in the DMA. A single-stage equilibration at 0°C indicated that the separation factor (α) was small and that a multistage experiment would be necessary to measure α.

The 30-bubble-plate column used for the ethylene oxide·SO_2 distillation was used for the exchange section of the multistage apparatus. The recombiner was a jacketed section of 34-mm tubing packed with $\frac{1}{8}$-in. glass helices. Dimethyl aniline was fed into the top of the recombiner to provide the only reflux in the system. Sulfur dioxide was fed from a tank (infinite reservoir) through a flowmeter into the bottom of the bubble-plate column.

Samples of SO_2 were periodically taken from the top and bottom of the column. These samples were purified by distillation in a high-vacuum system before mass spectrometer analysis. The DMA flow rate was about 250 ml/hr, and the exchange-column temperature was 24°C. The effluent liquid from the exchange column had a DMA/SO_2 mole ratio of 1.55. The column attained equilibrium in 4 to 5 hr of operation. A total separation of 1.013 ± 0.003 (95% C.I.) was obtained. If a column efficiency of about 50% is assumed, the single-stage separation factor is approximately 1.001 with S^{32} enriching in the gas phase.

A similar experiment with pyridine in place of dimethyl aniline was performed in the same apparatus. The temperature of the exchange column was 22°C and the SO_2/pyridine mole ratio in the liquid effluent from the column was 1.44. A total separation of 1.019 was achieved, with S^{32} enriching in the gas phase as in the DMA experiment; since the column showed no isotopic gradient with time, this value is rather doubtful. It appears that SO_2 addition compounds that can be readily decomposed give little enrichment of sulfur isotopes.

SEPARATION OF BORON ISOTOPES

Laboratory-Scale Anco System

A. A. Palko

Laboratory studies with the completely automatic, small-scale Anco system for enrichment of boron isotopes have continued. A description of

[5] R. M. Healy and A. A. Palko, *Chemical Separation of Isotopes Section Semiann. Prog. Rep. June 30, 1955*, ORNL-2005, p 8 (Classified).

[6] K. Holmberg, British Patent 736,459 (Sept. 1955).

the apparatus and procedure may be found in previous progress reports.[7,8] A number of experiments were performed to evaluate stage heights in the exchange column as a function of flow rate, column diameter, and the type of packing. Within the range of flow rates studied, the stage height was found to increase with increasing flow rate. The smallest stage heights were achieved by using Podbielniak 0.05 × 0.1 × 0.1 in. Helipak stainless steel packing in a 1-in. column. Several runs were made in order to determine the effects of various metals on the rate of solvent decomposition. The effects on the solvent were inconclusive; however, the addition of copper turnings to the system produced precipitates which tended to plug the column.

Heat of Reaction of Anisole with Boron Trifluoride

L. Landau

The vapor pressures of various mixtures of anisole and boron trifluoride were measured at several temperatures. The heat of the reaction anisole + $BF_3 \longrightarrow$ anisole·BF_3 was calculated from the slopes of the lines obtained by plotting $1000/T$ vs log K', where T is the absolute temperature and K' is the vapor pressure multiplied by the mole fraction of unreacted anisole divided by the mole fraction of complex.

The complex was prepared by distilling BF_3 and trapping it in a weighed amount of anisole cooled with an ice bath. A small amount of gas was formed which failed to condense at dry-ice temperatures. This material was probably SiF_4 which formed as a result of traces of moisture in the anisole or adsorbed on the glass. After the initial reaction, no additional uncondensable gas formed. It was assumed that the anisole contribution to the vapor pressure was negligible. The temperatures were kept constant to ±0.02°C and the vapor pressures were reproducible to ±0.5 mm Hg. A heat of reaction of 12.3 ± 0.4 (95% C.I.) kcal/mole at approximately 30°C was obtained for the composition range anisole·(0.21 to 0.92)BF_3. This value for the heat evolved (ΔH) supersedes the values previously reported.[9] The earlier measurements were made by direct calorimetry, and the scatter in the measurements was very much greater than in the present work.

N^{15} SEPARATION

E. F. Joseph G. M. Begun

The Nitrox system for the concentration of nitrogen isotopes employs the isotopic-exchange reaction between the oxides of nitrogen and nitric acid. A detailed report[10] describing both the chemistry and the operation of the system has been issued. The small, two-column enriching cascade has been operated for producing gram quantities of highly enriched N^{15}.

The rate of production of high-purity N^{15} was approximately 1.2 g/day, while the highest assay level attained was 99.7% N^{15}. This concentration of N^{15} was attained while product was being withdrawn; a higher maximum could be reached at total reflux.

On the basis of experience, the Nitrox system is believed to be the most promising presently known system for the concentration of nitrogen isotopes. The apparatus operated unattended at night, with observation and adjustments at intervals on the day shift. It has been found to be entirely feasible to operate a Nitrox cascade system for producing high-purity N^{15} continuously with automatic controls.

[7] A. A. Palko, *Chemical Separation of Isotopes Section Semiann. Prog. Rep. Dec. 31, 1955*, ORNL-2097, p 6 (Classified).

[8] A. A. Palko, *Chemical Separation of Isotopes Section Semiann. Prog. Rep. June 30, 1956*, ORNL-2176, p 2 (Classified).

[9] L. Landau, *Chemical Separation of Isotopes Section Semiann. Prog. Rep. Dec. 31, 1955*, ORNL-2097, p 4 (Classified).

[10] G. M. Begun *et al.*, *Chemical and Isotopic Studies of the Nitrox System for N^{15} Enrichment*, ORNL-2291 (June 6, 1957).

RADIATION CHEMISTRY

EFFECT OF IONIZING RADIATION ON HETEROGENEOUS CATALYSTS

H. W. Kohn E. H. Taylor

Further studies of the effects of ionizing radiation on heterogeneous catalysts, with particular emphasis on H_2-D_2 exchange on catalytic γ-alumina, have shown the following salient points:

1. The radiation effect is a function of the preparative procedure (Table 16).

2. This effect seems to depend upon poisoning by residual gases (principally H_2O). Catalysts prepared at 520°C which show no radiation effect (see Table 16) show a large radiation effect after poisoning with water, hydrogen, or ethylene.

Table 16. Influence of Evacuation Temperature upon Radiation Effect

Temperature of Evacuation (°C)	Approximate Radiation Effect (Activity* After)/(Activity* Before)
200	200
300	4
400	10
450	9
520	1
600	0.5

*H_2-D_2 exchange at −78°C.

3. The disappearance (annealing) of the radiation effect is slow for very active (unpoisoned) catalysts, but rapid for highly (water) poisoned catalysts.

4. For water-poisoned catalysts, the radiation effect is inversely proportional to some function of the temperature of irradiation.

5. The radiation effect approaches saturation in about 1 hr at −78°C at an estimated dose rate of 2×10^{17} ev·g^{-1}·min^{-1}.

6. Heavy-particle (fast neutrons, alpha particles) bombardment gives a radiation effect which does not appear to anneal out at 25°C.

7. *In situ* experiments indicate that short-lived species existing only during radiation do not affect the catalytic activity.

Studies of other catalysts have shown positive radiation effects on ZnO, V_2O_3, and MgO; BaH_2 and LiH show a positive radiation effect when irradiated in H_2-D_2 mixture, but a negative (<1) radiation effect when irradiated *in vacuo*; TiO_2 shows zero effect.

GAS-PHASE IRRADIATION

P. S. Rudolph S. C. Lind

Retardation of Alpha-Ray-Induced Acetylene Polymerization by Benzene Vapor

Lind and Bardwell[1] studied the effect of foreign gases on numerous gas reactions induced by alpha-ray irradiation. The foreign gases invariably increased the reaction rate in these reactions. Since the foreign gases usually had ionization potentials higher than the reactant gases, this increased rate was attributed to charge transfer from the foreign gas ions to the reactant molecules. The only discrepancy to this explanation was the polymerization of HCN and C_2N_2 in the presence of xenon, which has a lower ionization potential than either HCN or C_2N_2 and hence would be expected to reduce the reaction rate, but instead the rate is enhanced.

Work in this laboratory on the radiolysis of CO with and without foreign gases showed further discrepancies to the charge exchange hypothesis. Both xenon (ref 2) and krypton (ref 3) appeared to have no effect on the velocity of the CO radiolysis, although the xenon and krypton have ionization potentials below the potential of CO and hence retardation would be expected.

Although several reactions had been studied wherein the foreign gas had an ionization potential lower than that of the reactant gas, no retardation of reaction rate had been observed. Recent work on the polymerization of mixtures of C_2H_2 and C_6H_6 indicated that C_6H_6 retarded the reaction rate of the polymerization of C_2H_2. In this case

[1] S. C. Lind and D. C. Bardwell, *J. Am. Chem. Soc.* 48, 1575 (1926).

[2] S. C. Lind and P. S. Rudolph, *Chem. Semiann. Prog. Rep. June 20, 1954*, ORNL-1755, p 65.

[3] S. C. Lind, P. S. Rudolph, and A. C. Stewart, *Chem. Semiann. Prog. Rep. Dec. 20, 1954*, ORNL-1832, p 80.

C_6H_6 has the lower ionization potential and could retard the polymerization of C_2H_2 by the charge transfer mechanism.

Although C_6H_6 polymerizes under alpha-ray radiation, its velocity rate is only about $\frac{1}{20}$ that of the acetylene polymerization. Due to the low relative rate of the disappearance of C_6H_6 as compared with the disappearance of C_2H_2, a comparison of rates of pure C_2H_2 and a mixture of C_2H_2 and C_6H_6 during the initial phases of the reaction should indicate the extent of retardation.

Comparative experiments were performed to determine the polymerization rate of C_2H_2 with and without C_6H_6. The reactions were conducted at 100°C in two small spheres of equal volume with equal quantities of radon and C_2H_2. Into one sphere C_6H_6 was added so that the mole ratio of $C_2H_2:C_6H_6$ was 3:1; this gave both gases in the mixture equal stopping power (cf. Table 17). Both spheres were small enough so that all the alpha particles reached the wall; thus the energy absorbed by the acetylene was the same in each sphere. These procedures eliminated the necessity of making any corrections to the data for comparison.

Table 17. Comparative Initial Conditions

Gas	Initial Pressure (mm Hg)		Volume (cc)	Diameter (cm)	Initial Charge (curies)
	C_2H_2	C_6H_6			
C_2H_2	537	0	7.40	2.42	0.0272
$C_2H_2 + C_6H_6$	539	184	7.40	2.42	0.0272

The total gas pressure in each sphere was measured periodically during the course of the reaction. The plots of log P (total pressure) as a function of the radon decayed $(1 - e^{-\lambda t})$ are shown in Fig. 9. The initial slopes indicate that C_6H_6 retards the disappearance of C_2H_2 by 32%.

This is the first reported case of retardation of a gas-phase radiolysis by a foreign gas. Manion and Burton,[4] however, have shown a "protective" action of benzene in the liquid-phase polymerization of cyclohexane.

[4] J. P. Manion and M. Burton, *J. Phys. Chem.* **56**, 560 (1952).

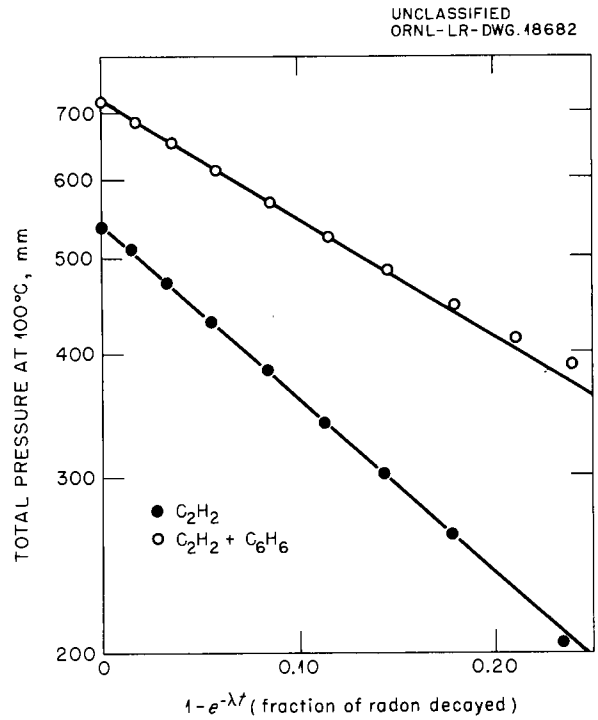

Fig. 9. Comparison of the Rate of Polymerization of C_2H_2 With and Without C_6H_6 Under Alpha Irradiation.

PHOTOREDUCTION OF CERIC ION IN SULFURIC ACID SOLUTIONS – EFFECT OF THALLOUS ION

T. J. Sworski

Evidence has been obtained that the OH radical is an intermediate in the photoreduction of ceric ion in sulfuric acid solutions. The observed chemical reaction in the photolysis of ceric ion–thallous ion mixtures is the oxidation of thallous ion by ceric ion. The initial quantum yield ($\phi_{Ce^{+++}}$) for reduction of ceric ion in the absence of initially added cerous ion is markedly enhanced by thallous ion but is independent of the thallous ion concentration (2×10^{-4} to 2×10^{-2} M). At any particular initial cerous ion concentration, the initial $\phi_{Ce^{+++}}$ decreases with decreasing initial thallous ion concentration. These data obtained in 0.4 M sulfuric acid are quantitatively interpreted by a mechanism in which thallous ion competes with cerous ion for reaction with OH radical. The measured value of 42 for $k_{Tl^+,OH}/k_{Ce^{+++},OH}$ is in agreement with the value of 38 previously determined in 0.4 M sulfuric acid for the radiolysis of ceric ion–cerous ion–thallous ion mixtures with Co^{60} gamma radiation.

WARMING CURVES FOR THE CONDENSED PRODUCT OF DISSOCIATED WATER VAPOR AND FOR HYDROGEN PEROXIDE GLASS

J. A. Ghormley

Water vapor dissociated in an electric discharge and condensed at −196°C forms a glassy product which yields O_2 and H_2O_2 solution when warmed. Warming curves for the discharge product are significantly different from those exhibited by H_2O_2 solution after it has been frozen rapidly to form a glass. The discharge product partially crystallizes between −110 and −75°C, and the resulting crystalline phase begins to melt at about −70°C. When warmed to −60°C the liquid bubbles violently, evolving O_2, and the temperature suddenly rises as much as 120 deg. The resulting H_2O_2 solution when cooled rapidly to −196°C forms a glass which crystallizes, starting at about −110°C, with an abrupt rise in temperature to −56°C, a eutectic for the H_2O_2-H_2O system. This difference in thermal behavior is interpreted as further evidence for the existence at low temperatures of an unidentified species such as H_2O-O, H_2O_3, or H_2O_4. The O_2 evolution reaction is exothermal by about 44 kcal/mole.

FREE-RADICAL AND MOLECULAR YIELDS IN THE GAMMA-RAY DECOMPOSITION OF HEAVY WATER

H. A. Mahlman J. W. Boyle

The radiation decomposition of water and aqueous solutions has been explained in terms of an initial decomposition of water into H, OH, H_2, and H_2O_2. The 100-ev yields are given as G_H, G_{OH}, G_{H_2}, and $G_{H_2O_2}$. The cobalt gamma-ray decomposition of several heavy-water solutions containing 98.8 mole % deuterium has been studied, and the yields of D, OD, D_2, and D_2O_2 have been evaluated. The reactions studied, all in 0.4 *M* sulfuric acid solution, were the formation of D_2 in a degassed dilute bromide solution,[5] the formation of D_2O_2 in an air-saturated solution,[6] the oxidation of aerated ferrous solution,[6] and the reduction of ceric ion.[6] The 100-ev yields of the products were based on the ferrous sulfate dosimeter with a yield[7] of 15.6. On the basis of the reaction mechanisms postulated for light water, the measured yields can be equated to the radical and molecular yields as follows:

$$G(D_2)_{Br^-} = 0.38 = G_{D_2},$$

$$G(D_2O_2)_{air} = 1.24 = G_{D_2O_2} + \frac{1}{2}(G_D - G_{OD}),$$

$$G(Fe^{+++})_{air} = 16.72 = 3G_D + 2G_{D_2O_2} + G_{OD},$$

$$G(Ce^{+++}) = 2.77 = 2G_{D_2O_2} + G_D - G_{OD}.$$

The yields $G(D_2)_{Br^-}$, $G(D_2O_2)_{air}$, and $G(Fe^{+++})_{air}$ give the set of values $G_{D_2} = 0.38$, $G_{D_2O_2} = 0.81$, $G_D = 3.99$, and $G_{OD} = 3.14$. The $G(Ce^{+++})$ provides a substantiating check of the molecular and free-radical yields.

The average value $G(Fe^{+++})_{air} = 16.72$ is in good agreement with the values given by Hardwick[8] (17.05, corrected to a ferrous oxidation rate of 15.6 molecules oxidized per 100 ev) and McDonell[9] (16.36, corrected for the change in the molar extinction coefficient of Fe^{+++} in 0.4 *M* H_2SO_4 heavy-water solution at 25°C), but is in disagreement with the value given by Trumbore and Aten[10] (18.6). Hardwick also observed $G_{D_2} = 0.288$ (corrected to a ferrous oxidation rate of 15.6 molecules oxidized per 100 ev) and calculated $G_D = 4.12$.

For comparison, a similar set of yields was determined for light water, namely, $G(H_2)_{Br^-} = 0.45$, $G(H_2O_2)_{air} = 1.17$, $G(Ce^{+++}) = 2.53$, $G_{H_2} = 0.45$, $G_{H_2O_2} = 0.81$, $G_H = 3.68$, and $G_{OH} = 2.96$.

---

[5] J. A. Ghormley and C. J. Hochanadel, *Radiation Research* **3**, 227 (1955).

[6] A. O. Allen, *Radiation Research* **1**, 85 (1954).

[7] C. J. Hochanadel and J. A. Ghormley, *J. Chem. Phys.* **21**, 880 (1953).

[8] *Progress Report Chemistry and Metallurgy Division, Period Ending October 1, 1956 to December 31, 1956*, P.R.-CM-8A (Classified).

[9] W. R. McDonell, *Radiation Chemistry of Normal and Heavy Water Solutions. I. Radiation-Induced Oxidation of Ferrous Sulfate*, ANL-5206 (Jan. 12, 1954).

[10] C. N. Trumbore and A. H. W. Aten, Jr., *J. Am. Chem. Soc.* **78**, 4179 (1956).

RADIATION-INDUCED NITRITE FORMATION FROM CONCENTRATED NITRATE SOLUTIONS

H. A. Mahlman

The gamma-ray-induced formation of nitrite ion from concentrated nitrate solutions has been extended to include magnesium, zinc, aluminum, and thorium nitrates. The same criteria were used to calculate and interpret the data as were utilized for the alkali-metal nitrates and ammonium nitrate.[11] The nitrite yield can be expressed by the equation

$$G(NO_2^-) = 1.22 \pm 0.02 \log [NO_3^-] + 1.70 \pm 0.01 .$$

EFFECT OF URANYL ION ON THE OXIDATION OF FERROUS SULFATE BY GAMMA RADIATION

J. W. Boyle H. A. Mahlman

The yield for the oxidation of ferrous ion in air-saturated 0.4 *M* H_2SO_4 by Co^{60} gamma rays is reduced by the presence of uranyl ion. The ferric yield drops with increasing UO_2^{++} concentration from a value of 15.6 Fe^{+++} ions per 100 ev with no added UO_2^{++} to a value of 3.0 Fe^{+++} ions per 100 ev with 0.4 *M* UO_2^{++} added.[12] Preliminary work also indicated that the presence of UO_2^{++} enhances the yield for reduction of ceric ion by gamma rays. It had previously been shown[13] that UO_2^{++} lowers the yield of hydrogen in the decomposition of water by radiation. All these observations indicate that UO_2^{++} ions compete for H atoms produced by decomposition of the water.

RADIOLYSES OF COMPOUNDS DISPERSED IN ALKALI-HALIDE MATRICES

A. R. Jones

A new technique which exploits the convenience of absorption spectroscopy in general and the specificity of infrared absorption in particular has been used to investigate the radiolyses of certain solid compounds.

Pressed potassium bromide disks of the type commonly employed in the infrared analysis of solids suffered no changes in absorption over the 4000 to 650 K (ref 14) region when irradiated with 10^{23}-ev/g doses of electrons or gamma rays. Thus it was convenient to determine the effects of such radiation upon milligram samples of organic and inorganic solids suspended in potassium bromide as a matrix by examining the mixture for changes in selective absorption following exposure. Representative compounds were treated to demonstrate the utility of the procedure. Kinetic data on the radiolyses were relatively easy to obtain, and it was possible to determine the initial *G* of disappearance in certain instances: NH_4Br = 0.04, $KBrO_3$ = 0.03, KNO_2 = 0.13, for concentrations of 0.33 wt %, and KNO_3 = 0.05 for a concentration of 0.0033 wt %.

To elucidate the factors determining the stability of the nitrate ion in crystals, pure nitrate salts have been exposed to gamma and ultraviolet radiation by several investigators,[15] and the nitrite ion product has been measured as a function of the energy input. This work was extended by irradiating numerous alkali halides containing nitrate ion impurity. It was found necessary, in order to obtain meaningful values of *G* for nitrite production, to make such calculations on the basis of the energy absorbed in the matrix, rather than on that absorbed in the nitrate ion only, which confirms the existence of a mechanism for the rapid transfer of energy from the host crystal lattice to the impurities. The data of Table 18 are currently being interpreted.

[11] H. A. Mahlman, *Chem. Semiann. Prog. Rep. June 20, 1956*, ORNL-2159, p 25.

[12] J. W. Boyle and H. A. Mahlman, *HRP Quar. Prog. Rep. Oct. 31, 1956*, ORNL-2222, p 165.

[13] J. W. Boyle *et al.*, *Proc. Intern. Conf. Peaceful Uses Atomic Energy, Geneva, 1955* **7**, 576 (1956).

[14] The convention "kayser" (symbol K) as a name for the reciprocal centimeter unit of wave number has been used: see *J. Opt. Soc. Am.* **43**, 410 (1953).

[15] C. J. Hochanadel and T. W. Davis, *J. Chem. Phys.* (in press); L. K. Narayanswamy, *Trans. Faraday Soc.* **31**, 1411 (1935); P. Doigan and T. W. Davis, *J. Phys. Chem.* **56**, 764 (1952); G. Hennig, R. Lees, and M. S. Matheson, *J. Chem. Phys.* **21**, 664 (1953).

Table 18. Values of G^* for the Production of NO_2^- from NO_3^- Dispersed in Matrices of Alkali Halides at a Concentration of 0.33 wt %

	Fluorides	Chlorides	Bromides	Iodides
Lithium			0.044	
Sodium		0.049	0.098	
Potassium	0.092	0.078	0.210	0.581
Rubidium		0.120	0.362	
Cesium		0.033	0.125	

*Based on total energy absorption by the mixture.

Pressed potassium bromide "windows" showed selective infrared absorption after irradiation in the presence of air or oxygen. Nitrate ion and bromate ion were the respective products: the latter was completely absent in the air experiments. It was shown, in agreement with microcrystallographic analyses,[16,17] that the nitrate ion was initially produced in a crystalline environment different from the ordinary birefringent form of potassium nitrate, but that rapid conversion to the normal form followed on standing.

---

[16] R. Blöch, *Österr. Akad. Wiss. Math.-naturw. Kl. Sitzber. Abt. IIa* **162**, 99 (1953).

[17] L. Wieninger and N. Adler, *Acta Phys. Austriaca* **4**, 81 (1950).

ORGANIC CHEMISTRY

THE PINACOL REARRANGEMENT

The Phenyl-di-*p*-tolyl System

L. W. Kendrick, Jr.[1]

The pinacol rearrangement of triaryl-substituted ethylene glycols and the closely related rearrangement of substituted acetaldehydes to ketones have been considered in two papers.[2,3] A mechanism was proposed to explain the apparently anomalous[4,5] migratory aptitudes observed during the conversion of di- and tri-substituted acetaldehydes to their corresponding ketones. Through an application[3] of this mechanism to the rearrangements of diphenyl-*p*-tolylacetaldehyde (I) and the associated glycols II (both threo and erythro forms) and III, it was suggested that the migration ratio of the *p*-tolyl and phenyl groups of aldehyde I during its acid-catalyzed conversion to ketones IV and V was not directly calculable from the ratio of these two ketones formed during the reaction, but was instead equal to $2k_T/k_P$, the ratio k_T/k_P having been evaluated[3] by means of Eq. 1:

$$(1)\quad \frac{k_T}{k_P} = \frac{k_H}{k_\phi} \cdot \frac{k_{Tol}}{k'_H} \cdot \frac{m_e}{m_d} \cdot \left[\frac{1 + (k'_H/k_{Tol})}{1 + (k_H/k_\phi)}\right].$$

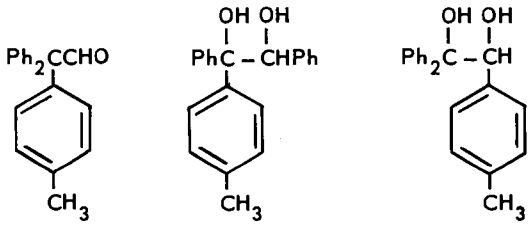

I

II

III

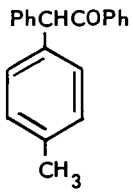

IV

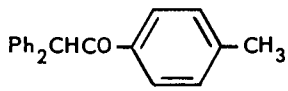

V

By a combination of double-labeling techniques and radioactivity dilution experiments upon appropriately labeled isotope position isomers of I, II, and III, the ratios k_H/k_ϕ and m_e/m_d (m_e = moles of ketone V; m_d = moles of ketone IV) were readily calculated. The ratio k_{Tol}/k'_H, unfortunately, was so large that the error inherent in the experiments precluded its direct experimental determination. It was possible, however, to estimate k_{Tol}/k'_H by an indirect method and thus to conclude that the *p*-tolyl/phenyl migration ratio in the rearrangement of I in cold, concentrated sulfuric acid was about 3, whereas a direct comparison of the ratio of ketones IV and V would definitely indicate that, contrary to all previous experience,[6] this ratio was less than 1.

In order to establish whether the mechanism proposed[3] for the rearrangement of I to the ketones IV and V possesses any degree of generality, several other examples of the aldehyde-ketone rearrangement have been studied. This report includes the results of experiments on compounds VI, VII (both threo and erythro forms), and VIII, in

---

[1] ORINS Fellow, University of Florida.

[2] C. J. Collins, *J. Am. Chem. Soc.* **77**, 5517 (1955).

[3] B. M. Benjamin and C. J. Collins, *J. Am. Chem. Soc.* **78**, 4329 (1956).

[4] G. W. Wheland, *Advanced Organic Chemistry*, 2d ed., p 494–534, Wiley, New York, 1949.

[5] C. K. Ingold, *Structure and Mechanism in Organic Chemistry*, p 479, Cornell University Press, Ithaca, N.Y., 1953.

[6] Previous experimental determinations of the *p*-tolyl/phenyl migration ratio in diverse reactions are found in the following: W. E. Bachmann and R. V. Shankland, *J. Am. Chem. Soc.* **51**, 306 (1929); W. E. Bachmann and J. W. Ferguson, *J. Am. Chem. Soc.* **56**, 2081 (1934), 16; W. E. McEwen, M. Gilliland, and B. I. Sparr, *J. Am. Chem. Soc.* **72**, 3212 (1950), 5.0; J. G. Burr, Jr., and L. S. Ciereszko, *J. Am. Chem. Soc.* **74**, 5426 (1952), 2.0; J. G. Burr, Jr., *J. Am. Chem. Soc.* **75**, 5008 (1953), 2.5; D. Y. Curtin and M. C. Crew, *J. Am. Chem. Soc.* **76**, 3719 (1954), 1.3; S. N. Ege and K. W. Sherk, *J. Am. Chem. Soc.* **75**, 354 (1953), 4.0; R. F. Tietz and W. F. McEwen, *J. Am. Chem. Soc.* **77**, 4011 (1955), 3.44; B. M. Benjamin and C. J. Collins, *J. Am. Chem. Soc.* **78**, 4952 (1956), 1.2.

which were used techniques similar to those previously employed[2,3] in analogous systems:

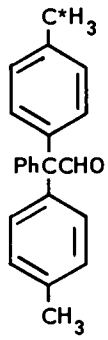

VI

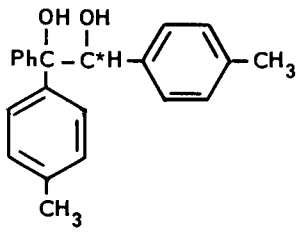

VII*a*

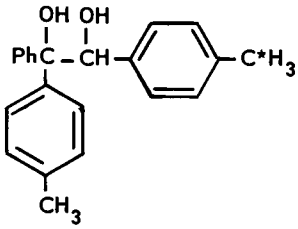

VII*c*

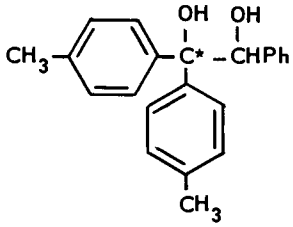

VIII

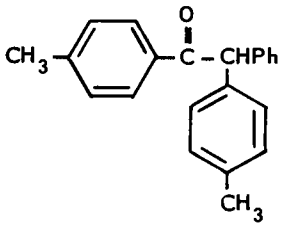

IX

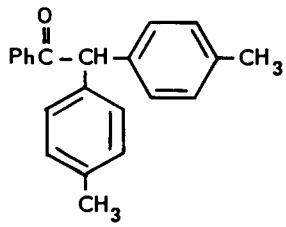

X

The aldehyde VI, the threo and erythro forms of the chain-labeled glycol VII (VII*a*), the threo form of the tolyl-labeled glycol VII (VII*c*), and the chain-labeled glycol VIII were all subjected to rearrangement in cold, concentrated sulfuric acid at 0°C under identical conditions. In each case the yields of ketones IX and X were determined by the C^{14} dilution method.[7] The results of these yield determinations are given in Table 19.

[7]R. H. Mayor and C. J. Collins, *J. Am. Chem. Soc.* 73, 471 (1951).

The fractions of chain label and tolyl label which underwent rearrangement during conversion of the appropriately labeled reactants to the ketones IX and X were determined as follows: (1) alkaline cleavage of the ketones followed by (2) oxidation of the nonacidic fractions to suitable degradation products. These degradation products were then assayed for radioactivity; the results of the radioactivity assays for each fraction are given in Table 20.

In order to have a comparison with the results[3] of the formic acid–catalyzed rearrangements of glycols II and III, the glycols threo-VII*c* and VIII were subjected to rearrangement conditions in 98% formic acid at 25°C. The yields of aldehyde, determined by the radioactivity dilution technique,[7] were 81% (from threo-VII*c*) and 36% (from VIII). These yields permit calculation of a k_{Tol}/k'_H ratio (in formic acid) of 4.3 and a k_ϕ/k_H ratio of 0.56.

Given in Chart 1 is a mechanism for the rearrangements, in concentrated sulfuric acid at 0°C, of aldehyde VI and of threo- and erythro-VII. The yields of ketones IX and X produced from these several reactants (see Table 19) are clearly compatible with the over-all mechanism,[3] thus lending it credence and support, as indicated by the discussion which follows.

If m_A, m_B, m_C, m_D, and m_E are defined respectively as the mole fractions of threo- or erythro-VII which proceed to products through paths A to E (Chart 1), then from Tables 19 and 20 it is possible to calculate values for these mole fractions (m_i). Similarly, if m_F, m'_D, and m'_E (also generalized for purposes of later discussion as m_i) represent the mole fractions of VIII which proceed to products through paths F, D', and E' (Chart 2), then these values likewise may be determined. Now there are several different methods, some of which are nearly independent of each other, by which the various m_i can be calculated. Since it is the purpose here to determine, by the use of Eq. 1, whether, in the rearrangement of VI, the *p*-tolyl/phenyl migration ratio is greater than 1, the data of Tables 19 and 20 have been treated by two different methods.

In the first method the averages of the measurements (Tables 19 and 20) pertaining to the three glycols (i.e., yield data and determinations of chain- and tolyl-label scrambling) have been employed to calculate m_i. In the second method the same data were used as in the first, but the errors probable in each of the measurements of Tables 19

Table 19. Yields of Ketones IX and X from the Action of H_2SO_4 at 0°C upon VI, VII*a*, VII*c*, and VIII

Reactant	Combined Yield (%) of IX + X	Relative Yield (%) IX	Relative Yield (%) X
VI	77.3	52.7	47.3
	87.1	53.3	46.7
		Av 53.0	47.0
VII*a*, threo form[a]	93.3	58.0	42.0
VII*c*, threo form	80.7	59.6	40.4
	88.3	58.4	41.6
	85.9	57.3	42.7
		Av 58.3	41.7
VII*a*, erythro form[b]	74.0	53.4	46.6
VIII	96.1	47.1	52.9
	95.9[c]	48.0	52.0
		Av 47.6	52.4

[a]To test the effect of reduced yield upon the ratio IX/X, one run was carried out at 10°C; combined yield IX + X, 71.7%; IX, 58.3%; X, 41.7%.

[b]The difference in yields of IX and X from the erythro and threo forms of VII is a consequence of different contributions of paths *A* and *B* in the two cases (see Chart 2 and Table 20).

[c]Determined by weight. The yield of X in this case was determined by difference. In a run at 10°C, the combined yields of IX and X were 90%; IX, 49.6%; X, 50.4%.

and 20 have been taken into account, and the assumption has been made that all the errors accumulate in m_C, since the determination of a maximum value for m_C is crucial in estimating, from Eq. 1, a minimum *p*-tolyl/phenyl migration ratio. The results of the foregoing calculations are given in Table 21.

By a method analogous to that previously used,[3] it can be shown that Eq. 1 applies to the mechanism, outlined in Charts 1 and 2, for the rearrangement of aldehyde VI. The symbols employed in the present instance for the specific rate constants and for the various reaction paths of Charts 1 and 2 are the same as those employed in the analogous schemes for the rearrangements of I, II, and III. This has been done to permit an easy comparison of the former[3] work with the data presented in this paper. It must be remembered, however, that these symbols do not possess the same absolute values when used for the two different systems. Given in Table 22 is a summary of the ratios, calculated from Table 21, for use in Eq. 1. Given also in Table 22 are the values for the *p*-tolyl/phenyl migration ratio ($k_T/2k_P$) calculated by means of Eq. 1.

It is apparent from Table 22 that the *p*-tolyl/phenyl migration ratio ($k_T/2k_P$) in the rearrangement of VI cannot be determined with accuracy. This is because of the difficulty involved in calculating m_C, which is so small that its total contribution is about the same size as, or is smaller than, the errors involved in the method of measuring it. Despite this fact, it has been possible through method 2 to set a maximum value (0.046) for m_C and thus to say that $k_T/2k_P$ is probably no less than 2.2. Additional evidence that $k_T/2k_P$ is greater than 2.2 is to be found in unpublished experiments of the Organic Chemistry Group upon the rearrangement of tolyl-labeled tri-*p*-tolylethylene glycol in concentrated sulfuric acid at 0°C; here k_{Tol}/k'_H is much greater than 20, the latter ratio being the minimum value employed in the calculations of method 2.

There is another general method by which m_i and the various specific rate-constant ratios for use in

Table 20. Molar Radioactivities of the Degradation Products of Ketones IX and X Obtained by the Action of H_2SO_4 at 0°C upon VI, VII*a*, VII*c*, and VIII

Reactant	Molar Radioactivity of Degradation Product*			
	From IX		From X	
	Toluic Acid	*p*-Benzoylbenzoic Acid	Benzoic Acid	4,4′-Dicarboxylbenzophenone
VI	0.505			
Threo-VII*a*	0.956	0.039	0.996	0.027
	0.986	0.021	0.963	0.014
Threo-VII*c*	0.491			
	0.478			
	0.476			
	0.483			
	0.492			
	0.511			
Av	0.489			
Erythro-VII*a*		~0.01		0.139
VIII	0.018	0.982	0.0075	0.955
	0.011		0.0092	
Av	0.015		0.0084	

*The molar radioactivities of reactants are taken as 1.000 mc/mole; the molar radioactivities of the degradation products are thus fractions thereof.

Table 21. Summary of Mole-Fraction (m_i) Calculations from the Data of Tables 19 and 20

Mole Fraction (m_i)	Calculated by			
	Method 1		Method 2	
	Threo-VII	Erythro-VII	Threo-VII	Erythro-VII
m_A	0.008	0.065	0.011	0.065
m_B	0.018	0.005	0.023	0.005
m_C	0.005	(–) value	0.046	0.020
m_D	0.409	0.401	0.406	0.401
m_E	0.560	0.541	0.514	0.509
	For Glycol VIII			
m_F	0.177		0.169	
m'_D	0.347		0.355	
m'_E	0.476		0.476	

CHART 1

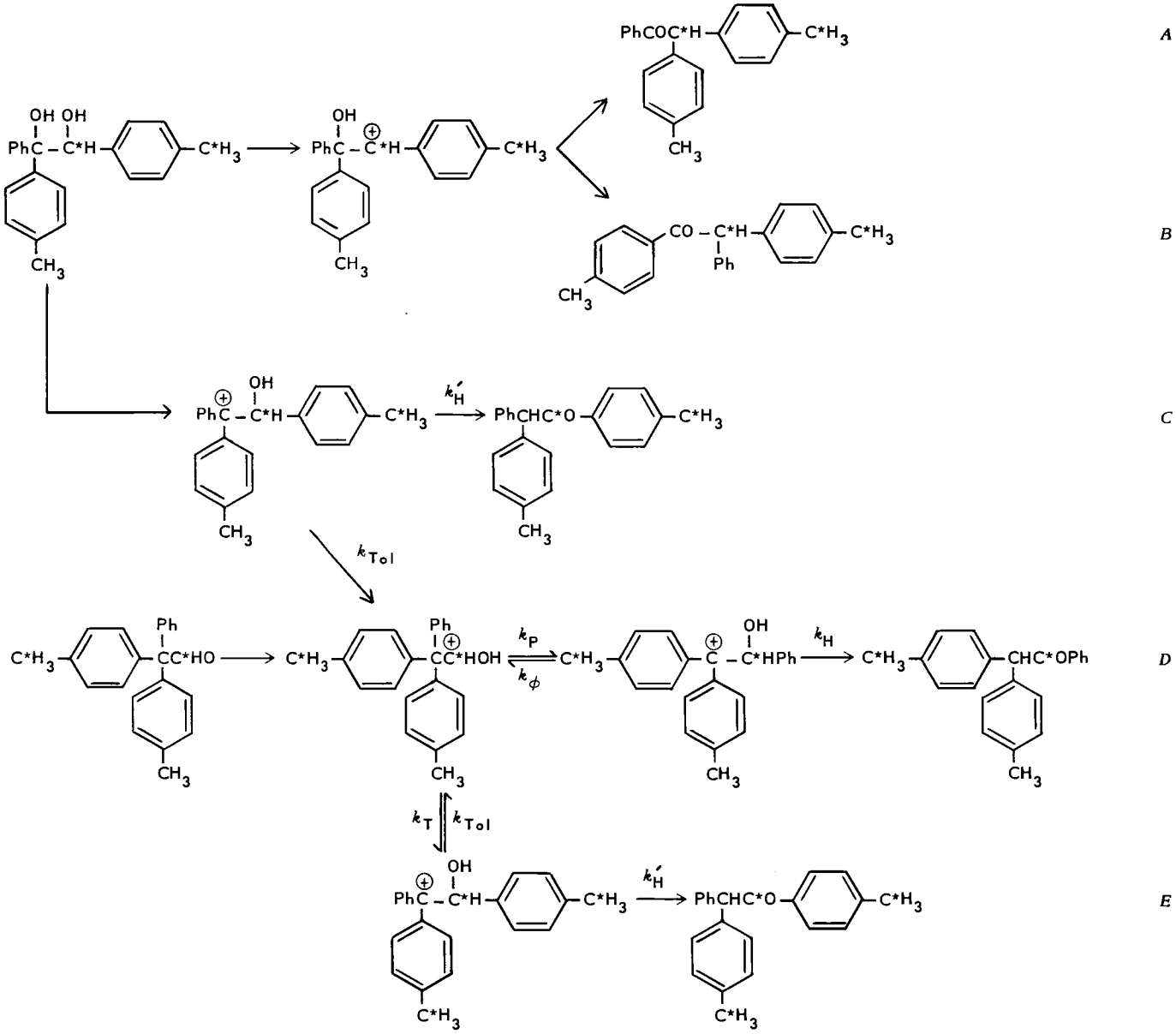

CHART 2

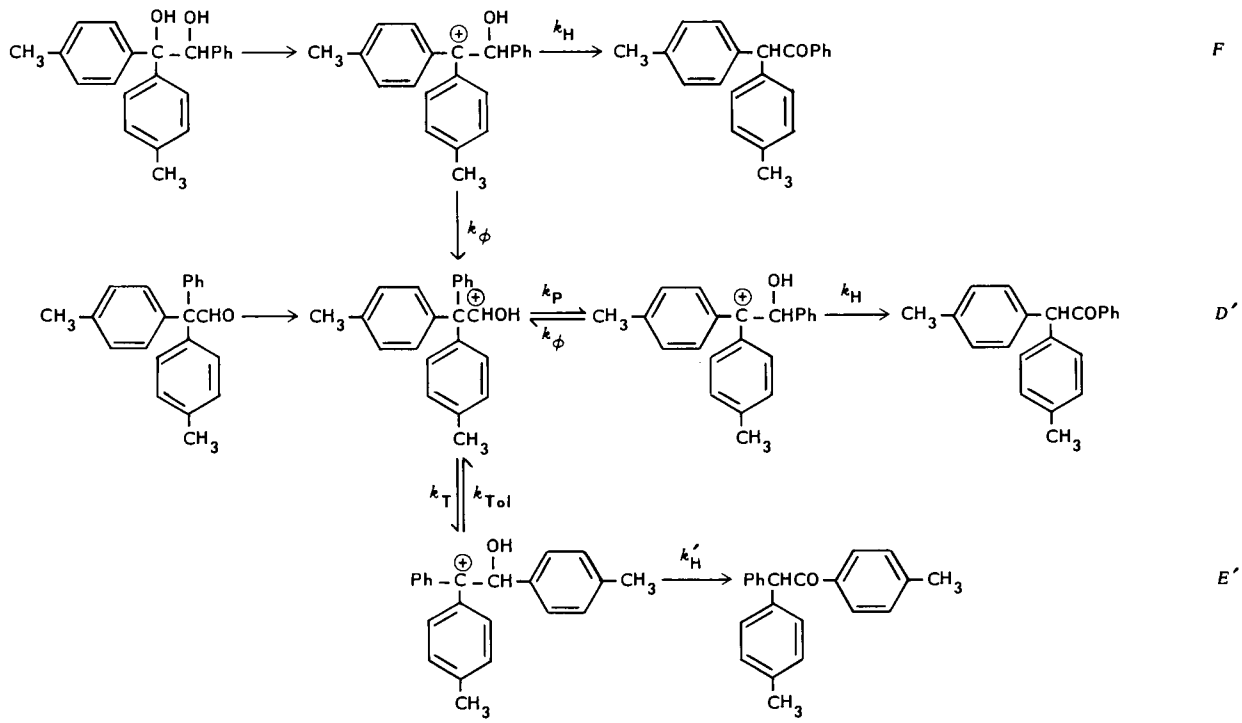

Table 22. Summary of the Ratios Calculated for Use in or by Means of Eq. 1

Ratio	Method of Calculation 1	Method of Calculation 2
m_e/m_d	1.37	1.27
k_ϕ/k_H	4.7	4.9
k_{Tol}/k'_H		
Threo-VII	190	20
Erythro-VII	∞	45
$k_T/2k_P$		
Threo-VII	25	2.2
Erythro-VII	∞	5

Eq. 1 may be calculated, namely, through the use of the ratio (1.13) of ketones IX:X produced when the aldehyde (VI) itself is subjected to rearrangement (see Table 19). By this method, for example, for threo-VII, m_C = yield of IX − m_B − 1.13 × m_D. This method is much inferior, for the present system, to methods 1 and 2, for it involves the subtraction of large numbers in determining the very small m_C and is thus extremely sensitive to small changes in the percentages of ketones produced. This is not true for methods 1 and 2.

The Diphenyl-o-tolyl System

V. F. Raaen

The rearrangements in cold, concentrated sulfuric acid of compounds I, II, and III to the ketones IV and V have been studied:

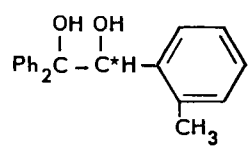

I*a*

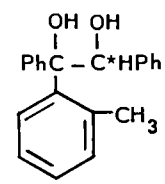

erythro-II*a*

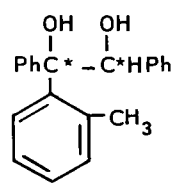

threo-II*ab*

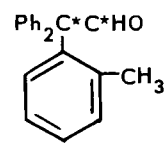

III*ab*

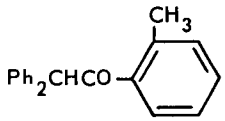

IV

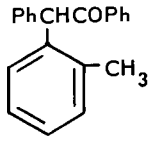

V

This series of compounds[8] was selected in order that a comparison of the *o*-tolyl/phenyl migration ratio in the aldehyde-ketone rearrangement of III might be made with that previously reported[9] (0.82) in the dehydration of 2-phenyl-2-*o*-tolylethanol-1-C^{14}. This seemed to be important, since it has been established[10] that the migration ratios in the aldehyde-ketone rearrangement are not necessarily reversed, as had been assumed,[11,12] and are not directly calculable from the simple product ratio. In two cases[10] involving rearrangements of aldehydes containing the *p*-tolyl and phenyl groups, it has been shown that a *p*-tolyl/phenyl ratio greater than 1 can be justified by means of Eq. 1 (see previous section) if a mechanism is assumed that involves a dynamic equilibrium of three carbonium-ion intermediates. An application of Eq. 1 to the rearrangement of diphenyl-*o*-tolylacetaldehyde (III) should permit a calculation of the *o*-tolyl/phenyl migration ratio in the same fashion in which *p*-tolyl/phenyl migration ratios were previously determined[10] for related systems. The specific rate constants of Eq. 1 have the same significance as in prior work when applied, later in this paper, to the mechanisms of Charts 3 and 4. The value m_e/m_d in the present case is the ratio of ketones IV/V formed when aldehyde III is rearranged in concentrated sulfuric acid.

[8] R. Roger and W. B. McKay, *J. Chem. Soc.*, 332 (1933).

[9] B. M. Benjamin and C. J. Collins, *J. Am. Chem. Soc.* 75, 402 (1953).

[10] B. M. Benjamin and C. J. Collins, *J. Am. Chem. Soc.* 78, 4329 (1956).

[11] G. W. Wheland, *Advanced Organic Chemistry*, 2d ed., p 494–534, Wiley, New York, 1949.

[12] C. K. Ingold, *Structure and Mechanism in Organic Chemistry*, p 479, Cornell University Press, Ithaca, N.Y., 1953.

CHART 3

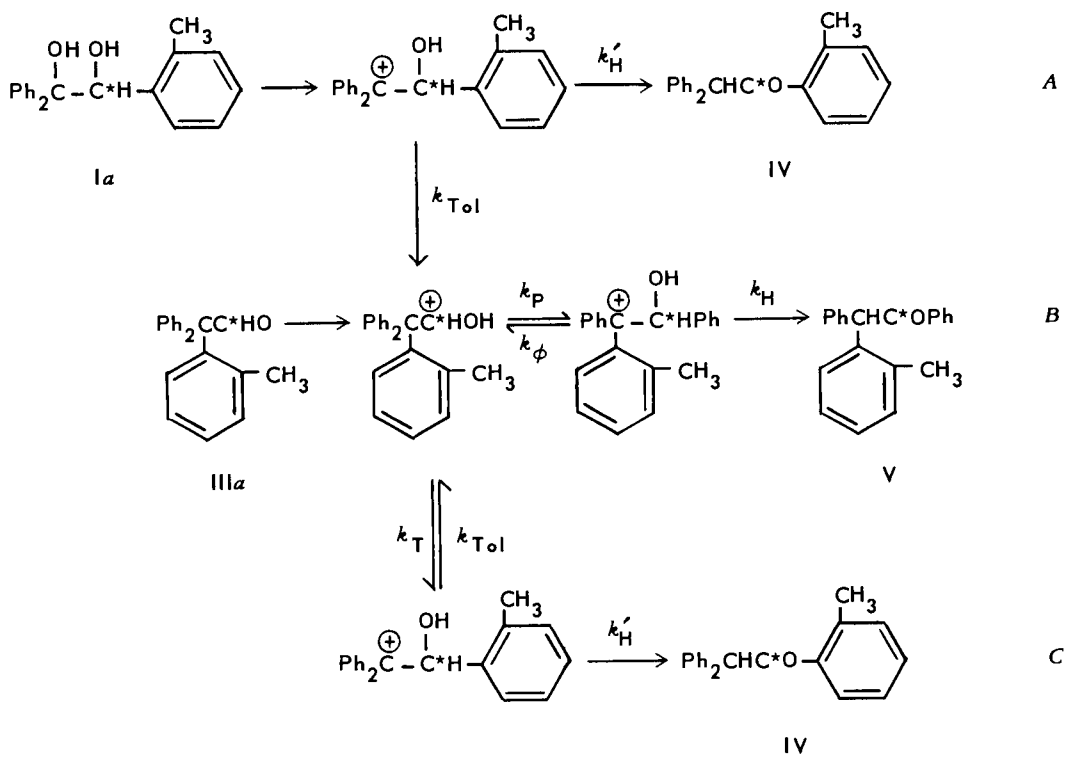

CHART 4

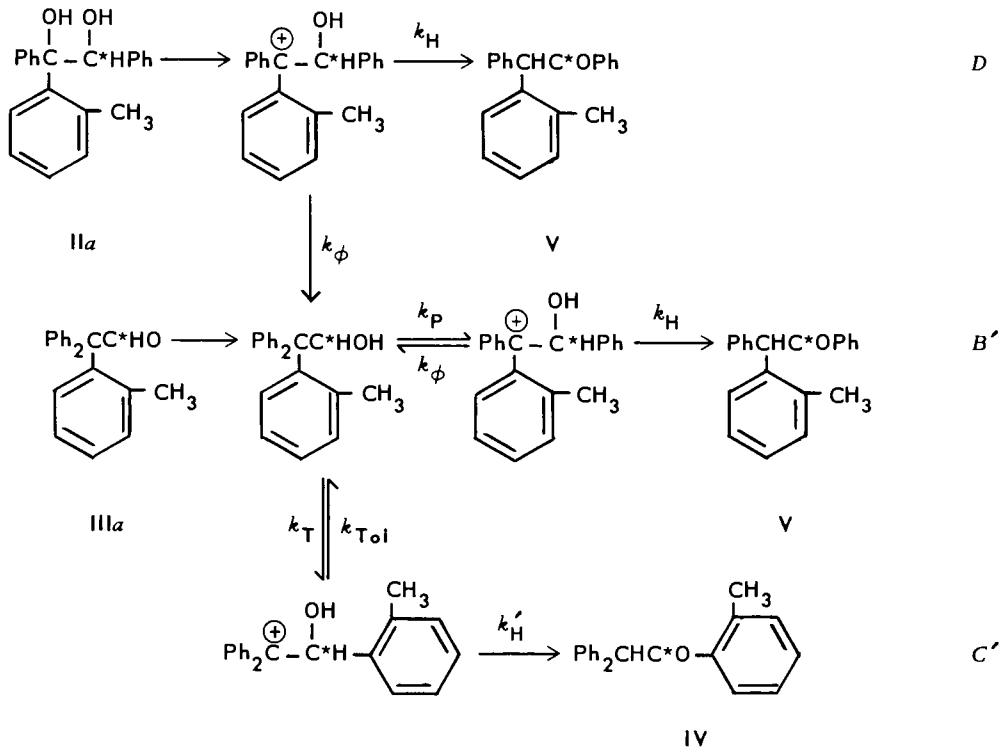

Compounds I, erythro- and threo-II, and III, labeled as shown, were subjected to rearrangement in concentrated sulfuric acid at 0°C. The yields of ketones produced in each case were determined by the isotope dilution method in a manner very similar to that previously described.[10] That no significant fraction of secondary hydroxyl removal occurred from either I or erythro-II under these conditions was demonstrated by alkaline cleavage of the products, followed by radioactivity assay of the purified *o*-toluic acid fractions. It was very difficult to separate benzoic from *o*-toluic acid in the acidic portions of the alkaline cleavage products. The mixed acids obtained from the ketones produced on rearrangement of I, therefore, were assayed for radioactivity, and the isotopic dilution method was then employed to determine the percentage of benzoic acid in the mixture. From these data the molar radioactivity of the benzoic acid was calculated to be the same, within experimental error, as that of the glycol from which it was obtained.

In the case of product IV, from I or from erythro-II, the diphenylmethane fractions obtained upon alkaline cleavage were oxidized to benzophenone fractions, which were then assayed for radioactivity content as the 2,4-dinitrophenylhydrazones. Again, no scrambling of the chain carbons during rearrangement was indicated. To sum up, then, the evidence is that (1) no scrambling of the chain carbons of IV or V took place during rearrangement of glycol I, and that (2) no scrambling of the chain carbons of IV took place during the rearrangement of erythro-II. These data indicate also that there was no scrambling of the chain carbons of ketone V during rearrangement of erythro-II, since the steric requirements of the erythro-isomer are such that if secondary hydroxyl removal takes place, phenyl migration should predominate over *o*-tolyl migration. Since the results demonstrate unequivocally that phenyl migration to C-2 does not occur, it then follows also that there should be no migration of *o*-tolyl to C-2. Threo-II and the aldehyde III were prepared equally labeled in both chain carbons, since for subsequent yield determinations of ketones IV and V produced from these reactants, the distribution of radioactivity was unimportant. That no scrambling of the chain carbons of III took place during the rearrangement follows from the fact that glycols I and erythro-II exhibited no

scrambling of their discrete labels upon rearrangement under identical conditions to IV and V.

It has not been proved rigorously that threo-II undergoes rearrangement with no secondary hydroxyl removal, for all the attempts to prepare this material discretely labeled were unsuccessful. Since both ketones IV and V are obtained from erythro- and threo-II in experimentally identical yields, however, the reasonable assumption has been made that threo-II, even as erythro-II, undergoes no chain scrambling. In Table 23 are given the yields of IV and V obtained from the reactants I, II, or III in cold, concentrated sulfuric acid. In Table 24 is given a summary of experiments upon the deamination of 2,2-diphenyl-2-*o*-tolylethyl-1-C^{14} amine (VI) to the carbinols VII and VIII. The radioactivity dilution method[13] was used in the yield determinations of VII and VIII:

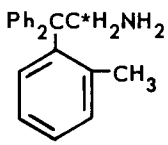

VI

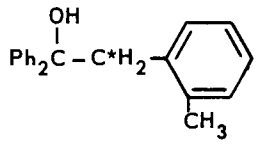

VII

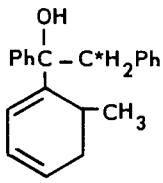

VIII

Finally, the yields of aldehyde III produced upon rearrangement of I and erythro-II in 98% formic acid at 27.6°C were determined by the radioactivity dilution method to be, respectively, 29 and 77%.

In Charts 3 and 4 are given the schemes by which the rearrangements of glycols I and II and of the aldehyde III are presumed to take place. If m_A, m_B, m_C, and, separately, m_D, m'_B, and m'_C are defined as the mole fractions, respectively, of reactants I and II, which proceed to products by the corresponding paths of Charts 3 and 4, then these mole fractions can be calculated to have the following values: m_A, 0.193; m_B, 0.307; m_C, 0.500; m_D, 0.193; m'_B, 0.307; and m'_C, 0.500.

By the same type of mathematical treatment formerly applied[10] to similar schemes, it can be shown that Eq. 1 (see previous section) is applicable to the rearrangement (Charts 3 and 4) of diphenyl-*o*-tolylacetaldehyde (III). The 'symbols employed for the specific rate constants of Charts 3 and 4 are the same as those used in two other cases;[10] again, these identical symbols have been used purposely for the three different systems in order to permit easy comparison. It must be remembered, however, that the symbols do not possess the same absolute values when applied to the three separate and distinct systems.

The specific rate-constant ratios of Eq. 1 may now be evaluated:

$$\frac{k_{Tol}}{k'_H} = \frac{m_B + m_C}{m_A} = 4.18$$

$$\frac{k_H}{k_\phi} = \frac{m_D}{m'_B + m'_C} = 0.241$$

Table 23. Yields of Ketones IV and V Produced by the Action of Sulfuric Acid upon I, II, and III

Reactant	Combined Yields (%) of IV and V	Yield* of Ketone (%)	
		IV	V
I	95.0	69.3	30.7
Erythro-II	99.0	50.0	50.0
Threo-II	100.5	49.1	50.9
III	103	62.0	38.0

*Adjusted to 100%.

Table 24. Migration Ratios Observed in the Deamination of VI as Determined by the Isotope Dilution Method

Yield (%)		Total Yield (%) of Carbinols	*o*-Tolyl/Phenyl Migration Ratio
VII	VIII		
16.2	43.6	59.8	0.746
15.1	40.5	55.6	0.746

[13] R. H. Mayor and C. J. Collins, *J. Am. Chem. Soc.* 73, 471 (1951).

From these values and from the ratio r (1.63) it can be shown (by means of Eq. 1) that $k_T/k_P = 1.64$, and thus the o-tolyl/phenyl migration ratio

$$\frac{2k_T}{k_P} \cong 3 .$$

In order to establish whether the value of 3 for $2k_T/k_P$ is a reliable number, the arbitrary and highly improbable assumptions have been made that all the yield determinations given in Table 23 are in error by 2% in such a direction as to make $2k_T/k_P$ a minimum; thus it has been shown that if such be the error, the $2k_T/k_P$ becomes 1.4. If the assumption is made, conversely, that all the yield determinations given in Table 23 are in error by 2% in such a direction as to make $2k_T/k_P$ a maximum, then this value becomes 9.7. From these data, therefore, it is inferred that the o-tolyl group migrates in preference to phenyl during the rearrangement of III in cold, concentrated sulfuric acid.[14] Because of this fact, the deamination of 2,2-diphenyl-2-o-tolylethyl-1-C^{14} amine (VI) to the carbinols VII and VIII was undertaken, since III and VI contain identical tri-substituted carbon atoms, and might thus be expected to exhibit similar migration ratios. From Table 24, however, it appears that VI undergoes deamination with an o-tolyl/phenyl ratio of 0.8. Since the combined yields of VII and VIII are only 56 to 60%, some caution must be used in transposing the data of Table 24 into migration ratios. In a study of the deamination of 2,2-diphenyl-2-p-tolylethyl-1-C^{14} amine,[15] however, it is possible to establish that the ratio of yields of the two carbinols produced was invariant, even though in separate runs the combined yields varied from 42 to 74%.

The reasons for the foregoing results may now be sought through a consideration of the various conformations of the conjugate acid of diphenyl-o-tolylacetaldehyde which may be formed from I, II, and III (Chart 5). Now it is only through C and

[14] An o-tolyl/phenyl ratio of 3.6 in the solvolyses of o-methylphenyldimethylcarbinyl chloride and phenyldimethylcarbinyl chloride has been reported by H. C. Brown *et al.*, *J. Am. Chem. Soc.* 79, 1897 (1957).

[15] B. M. Benjamin and C. J. Collins, *J. Am. Chem. Soc.* 78, 4952 (1956).

CHART 5

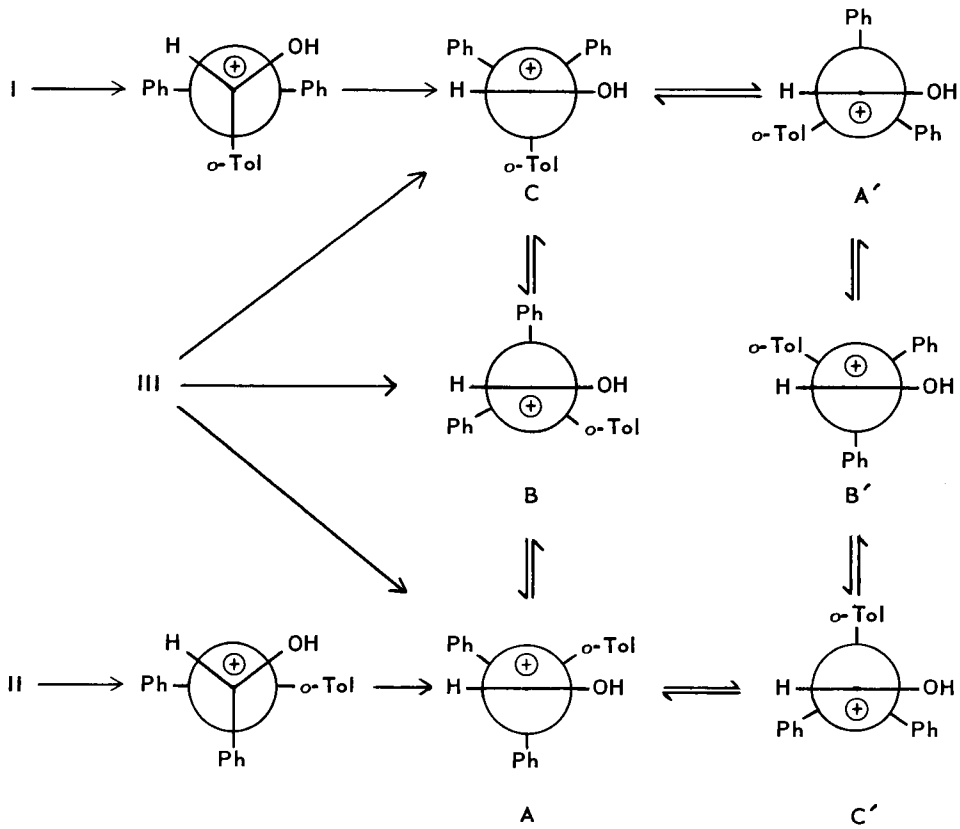

C′ that the shift of o-tolyl can take place. It is likely, however, that

$$A \rightleftharpoons B \rightleftharpoons C \rightleftharpoons A' \rightleftharpoons B' \rightleftharpoons C' \rightleftharpoons A$$

are all in a rapid, reversible equilibrium because of stabilization by solvent (cold, concentrated sulfuric acid) and by the electron-rich hydroxyl group. The relative proportion of o-tolyl which migrates, therefore, will not be limited by the populations of C and C′, but will be determined by the electrical properties and the steric "requirements" of the o-tolyl group.[14] Additional support for the concept that sulfuric acid, being capable of stabilizing the ionic intermediates, thus removes the steric restriction to o-tolyl migration imposed by conformational control is to be found in a comparison of the following ratios:

$$\frac{k_{Tol}}{k'_H} = \frac{k_\phi}{k_H} = 4.2 \quad \text{(in sulfuric acid)},$$

$$\frac{k_{Tol}}{k'_H} = 0.41\,; \quad \frac{k_\phi}{k_H} = 3.3 \quad \text{(in formic acid)}.$$

Steric effects must be quite important, for considerable strain must be relieved through o-tolyl shift, as compared with the shift of a phenyl group; the preference, then, for o-tolyl migration does not seem at all unusual when examined in the light of these circumstances. The question now arises, however, as to the preference for phenyl over o-tolyl migration during the deamination of VI. Shown in Chart 6 are the three conformations (VI-1, VI-2, and VI-3) for 2,2-diphenyl-2-o-tolylethyl amine. From molecular models it seems likely that the equivalent conformations VI-1 and VI-2 are sterically more compatible, and thus more likely than conformation VI-3. Upon deamination these conformations yield, respectively, ionic conformations D, E, and F. Ion DEF, being primary, is much less stable than ion ABC of Chart 5. Further, the environment of the deamination reaction (water–acetic acid) is much less able to stabilize a carbonium ion than is the sulfuric acid environment used in the rearrangements (Charts 3 and 4) of compounds I, II, and III. It is proposed therefore that the interconversions

$$D \rightleftharpoons E \rightleftharpoons F \rightleftharpoons D \quad \ldots$$

are slow, compared with the rates at which phenyl and o-tolyl migrate to produce product. Here the populations of the conformations D, E, and F control the relative amounts of the products, and since conformation F through which the o-tolyl shift occurs, is less important than the two equivalent conformations D and E, o-tolyl migrates less frequently than either of the two phenyls.

This explanation finds much support in the observations (see next section) on the deamination of optically active, stereospecifically phenyl-labeled 1,1-diphenyl-2-aminopropanol-1. By this work it was demonstrated that the labeled phenyl migrates during deamination to yield product of

CHART 6

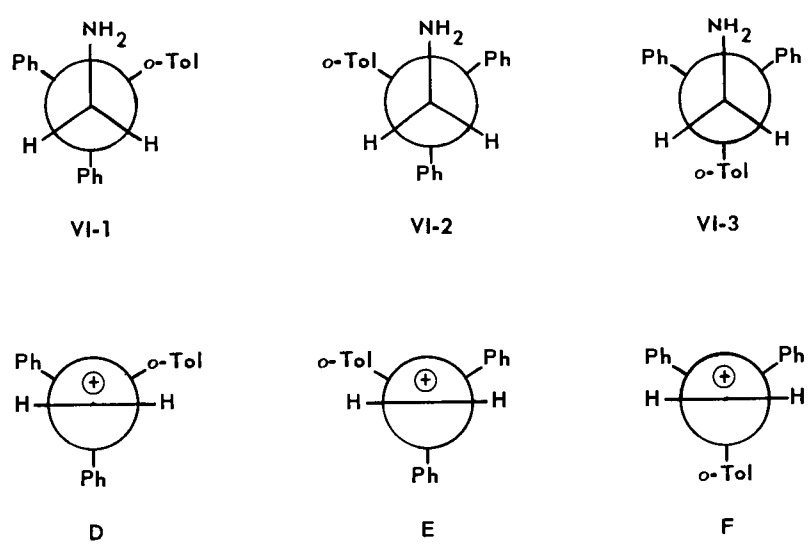

inverted configuration at the migration terminus, whereas the unlabeled phenyl migrates to produce product whose configuration is *retained*, thus demonstrating that the ionic intermediate does not achieve rotational equilibrium prior to its destruction by the entering hydroxyl group.

THE AMINO-ALCOHOL REARRANGEMENT

The Deamination of 1,1-Diphenyl-2-amino-1-propanol

B. M. Benjamin

In the rearrangement of amino alcohols of general structure I with nitrous acid, the following has often been assumed: (1) that ion II is first formed, followed by a concerted migration of R_1 or R_2; (2) that the rate of rotation about the bond connecting the two central carbon atoms is very fast compared with rearrangement; and (3) that the steric factor, called the "*cis*-effect" by Curtin *et al.*,[16] "is a function only of the difference in free energy between the two transition states for the rearrangement step and is independent of the relative populations of the conformations of the initial molecule":[17]

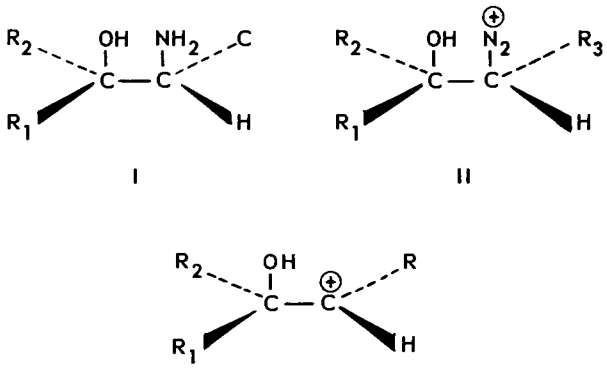

I II III

In the rearrangements of the erythro (I, R_1 = anisyl, R_2 = phenyl, R_3 = methyl) and threo (I, R_1 = phenyl, R_2 = anisyl, R_3 = methyl) isomers of 1-*p*-anisyl-1-phenyl-2-amino-1-propanol, studied by Curtin and Crew,[18] the ratios of the two ketones produced (*p*-anisylphenylethyl ketone to phenyl-α-*p*-anisylethyl ketone) were, respectively, 88:12 and 6:94. It appeared that there is a striking parallel between these results[18] and those obtained by McKenzie and his co-workers[19] in the deamination[20] of optically active 1,1-diphenyl-2-amino-1-propanol (IV), since it was clearly shown[21] by McKenzie that the product consisted of a mixture of the enantiomeric ketones (VII) in the ratio of approximately 88:12.

The stereochemical relationships of (+)- and (−)-IV and (+)- and (−)-VII have been worked out by Bernstein and Whitmore.[22] If the mechanism[16,23] generally accepted is the correct one for the deamination of IV, then both phenyls must migrate in such a way that the configuration of the migration terminus is *inverted*. The considerable amount of racemization (about 25%) which attends this reaction would then be required to arise through instability of the reactant (IV) or product (VII) to the reaction conditions. Since both product and reactant are presumed[24] to be unracemized under the conditions of the deamination reaction, however, the approximately 12% of product (VII) with retained configuration[21] must be a consequence of the conversion VI ⟶ (+)-VII, presuming the reacting amino alcohol IV to have the

[16] P. I. Pollak and D. Y. Curtin, *J. Am. Chem. Soc.* 72, 961 (1950); D. Y. Curtin and P. I. Pollak, *J. Am. Chem. Soc.* 73, 992 (1951); D. Y. Curtin, E. E. Harris, and P. I. Pollak, *J. Am. Chem. Soc.* 73, 3453 (1951).

[17] Quoted from D. Y. Curtin and M. C. Crew, *J. Am. Chem. Soc.* 77, 355 (1955); W. C. Dauben and K. S. Pitzer, *Steric Effects in Organic Chemistry* (ed. by M. S. Newman), pp 11, 44, Wiley, New York, 1956.

[18] D. Y. Curtin and M. C. Crew, *J. Am. Chem. Soc.* 77, 354 (1955).

[19] A. McKenzie, R. Roger, and G. D. Wills, *J. Chem. Soc.* 779 (1926); H. I. Bernstein and F. C. Whitmore, *J. Am. Chem. Soc.* 61, 1324 (1939).

[20] This is a classic reaction which has been widely quoted as evidence for inversion at the migration terminus: C. K. Ingold, *Structure and Mechanism in Organic Chemistry*, p 504–5, Cornell University Press, Ithaca, N.Y., 1953; D. J. Cram, *Steric Effects in Organic Chemistry* (ed. by M. S. Newman), p 253, Wiley, New York, 1956; P. D. Bartlett, *Organic Chemistry* (ed. by H. Gilman), vol III, p 59–60, Wiley, New York, 1953.

[21] A. McKenzie, R. Roger, and G. D. Wills, *J. Chem. Soc.* 779 (1926).

[22] H. I. Bernstein and F. C. Whitmore, *J. Am. Chem. Soc.* 61, 1324 (1939).

[23] D. Y. Curtin and M. C. Crew, *J. Am. Chem. Soc.* 77, 354 (1955); W. C. Dauben and K. S. Pitzer, *Steric Effects in Organic Chemistry* (ed. by M. S. Newman), p 11, 44, Wiley, New York, 1956.

[24] C. K. Ingold, *Structure and Mechanism in Organic Chemistry*, p 504–5, Cornell University Press. Ithica, N.Y., 1953.

(+)-configuration, as shown in the accompanying formulas:

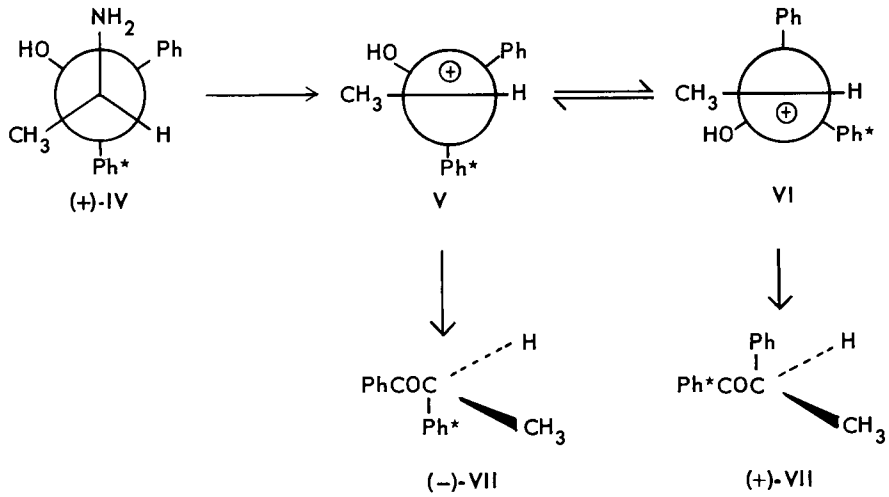

This hypothesis has now been tested and found to be correct by the synthesis of, and subsequent deamination experiments with, the enantiomorphs of IV labeled with C^{14} in only one of the two phenyls. Racemic IV was prepared by the addition of phenylmagnesium bromide to the stannic chloride complex salt of 2-aminopropiophenone-phenyl-C^{14}. Resolution of IV was accomplished through the *d*-10-camphorsulfonate. The optically pure amino alcohols were deaminated by the procedure of McKenzie, Roger, and Wills.[21] In experiments 1 and 2 the ketonic products, produced quantitatively, were cleaved with isoamyl nitrite in ethanolic alkali to yield benzoic acid and acetophenone oxime, which were assayed for radioactivity content. In experiment 3 the product was resolved by repeated crystallization from ethanol into a (–) ketone and into an almost completely racemic fraction. Both these fractions were cleaved as before to yield the degradation products benzoic acid and acetophenone oxime, which likewise were assayed for radioactivity. The results of all these experiments are given in Table 25.

In order to test the generality of the extremely high degree of stereospecificity noted in the addition of phenylmagnesium bromide to α-aminopropiophenone-phenyl-C^{14}, *p*-tolylmagnesium bromide was added to the stannic chloride complex of α-amino-(propio-1-C^{14})-phenone, and the yields of erythro- and threo-1-phenyl-1-*p*-tolyl-2-amino-1-propanol-1-C^{14} (ref 25) were determined by the isotope dilution method. In this way it was shown that the product of this reaction consisted almost exclusively of erythro-1-phenyl-1-*p*-tolyl-2-amino-1-propanol, since there was not more than 1% of the threo isomer produced.

From the foregoing data the following conclusions may be drawn:

1. The addition of Grignard reagents to the stannic chloride salts of α-aminopropiophenone is highly stereospecific. This follows from experiment 3 of Table 25 (cf. footnote *a*) and from the fact that upon addition of *p*-tolylmagnesium bromide to the α-amino-(propio-1-C^{14})-phenone–stannic chloride salt, only the erythro amino alcohol was produced.

2. During the deamination of (+)-IV, Ph* (labeled) migrates nearly exclusively to yield product of *inverted* (–) configuration, whereas Ph (unlabeled) migrates nearly exclusively to yield product of *retained* (+) configuration. The formation of (+)-VII thus is not the result of the decomposition of intermediate II with a simultaneous, concerted migration of Ph, since Ph (unlabeled) approaches the migration terminus from the same side as that occupied by the amino group, and not, as has been assumed,[23] through a transition state

[25] The terms erythro and threo have been employed for these compounds in the same sense as that used by Curtin and Crew (see ref 18, footnote 4).

Table 25. Summary of Deamination Experiments upon (+) and (–) IV

Experiment No.	$[\alpha]_D^{24}$ of		Retention (%)	C^{14} (%) in	
	Reactant IV	Product VII		Ph*COOH[a]	Ph*$COCH_3$
1	–59.3	+158.5	12.5	11.1	89.9
2	–59.3	+158.3	12.5	13.3	89.9
3	+59.3	–161.6	11.5	44.3[b]	53.0[b]
				4.4[c]	98.0[c]

[a]The molar radioactivity of the acetophenone-C^{14} oxime is more reliable than that of the benzoic-C^{14} acid, since during the cleavage of VII, some of the acetophenone fragment is oxidized to benzoic acid. This accounts for the fact that the sum of radioactivity content of the two fractions is usually greater than 100%. The radioactivity assay (exp No. 3) of the acetophenone oxime from (–)-VII is proof that the initial Grignard addition to α-aminopropiophenone was at least 98% stereospecific. This high degree of stereospecificity is consistent with the observations of Curtin and Crew (ref 23) upon similar Grignard addition reactions.

[b]From nearly racemic fraction of product, $[\alpha]_D^{24} = -1.6$ deg.

[c]From fraction of product whose $[\alpha]_D^{24} = -210$ deg.

in which methyl and phenyl are in a *cis*-configuration. It is felt, therefore, that the present data refute the *cis*-transition state proposed by Curtin *et al.*[16,18]

3. Because of the high degree of stereospecificity associated with the additions of phenylmagnesium bromide and *p*-tolylmagnesium bromide to α-aminopropiophenone (see paragraph 1), it is almost certain that the addition of phenyl-C^{14}-magnesium bromide to α-aminodesoxybenzoin to yield 1,1,2-triphenyl-2-aminoethanol (VIII*c*) proceeds also with 98 to 99% stereospecificity. In the deamination of VIII*c*, therefore, it is proposed that Ph (unlabeled) migrates to the opposite side of the migration terminus originally bonded to nitrogen, whereas Ph* (labeled) migrates to the same side of the migration terminus originally bonded to nitrogen.

4. Although these data do not rule out the intervention of ions of general structure II during the deamination of amino alcohols, it is believed that the simplest general explanation of the data of Table 25 is one in which (a) ions of type II are unimportant, (b) the open carbonium ions V and VI are formed, and (c) the equilibrium V ⇌ VI, involving rotation about the central carbon-carbon bond, is not extremely fast, compared with the rate of phenyl migration.

THE HYDROGEN/DEUTERIUM ISOTOPE EFFECT (k_H/k_D) IN THE REARRANGEMENT OF TRIARYLETHYLENE GLYCOLS

W. T. Rainey B. B. Smith

The rates of acid-catalyzed rearrangement, in 3.13 *N* H_2SO_4 (aqueous ethanol) at 43.2 ± 0.2°C, of a series of tri-substituted glycols have been determined. The compounds subjected to study were I, I*d*, II, II*d*, threo-III, and erythro-III:

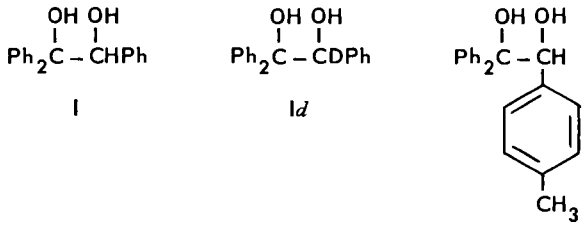

I I*d* II

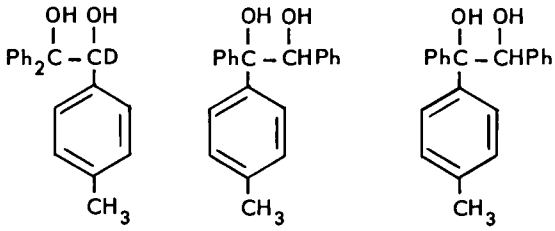

II*d* threo-III erythro-III

The method used for the rate studies was that of Lane and Walters,[26] in which the glycol is recovered quantitatively from aldehyde and ketone products by means of chromatographic separation on alumina. A minimum of five and a maximum of seven points were taken for each kinetic run. The results, expressed as first-order rate constants, were treated by the method of least squares and are summarized in Table 26. In each of these reactions, two products, an aldehyde and a ketone, were formed. The production of aldehyde is a result of aryl migration, whereas the production of ketone is the result of hydrogen (or deuterium) migration:

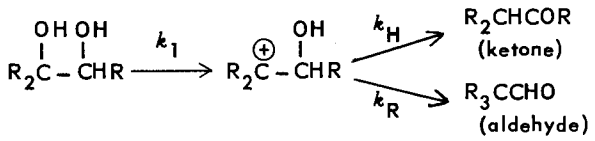

By means of (1) the C^{14} dilution method or (2) an ultraviolet absorption method, the ratios

$$\frac{\text{moles of aldehyde}}{\text{moles of ketone}}$$

were determined at the completion of the reaction. Thus it was possible to determine the H/D isotope effect, with respect to I and I*d*, for example, by the following relation:

$$\frac{k_H}{k_D} = \frac{\text{moles of aldehyde produced from I}}{\text{moles of ketone produced from I}} \times \frac{\text{moles of ketone produced from I}d}{\text{moles of aldehyde produced from I}d}.$$

It was possible, further, to determine the rate of appearance of ketone (k_b or k_d) for the glycols I, I*d*, II, and II*d* by the following relations:

$$k_b = \frac{k_1 \times (k_H/k_R)}{1 + (k_H/k_R)},$$

$$k_d = \frac{k_1 \times (k_D/k_R)}{1 + (k_D/k_R)}.$$

Given in Table 27 are the results of these determinations. Finally, the unreacted glycols from kinetic runs with threo-III and erythro-III were recovered after approximately 10 and 20% reaction, and the yields of threo and erythro isomer were determined in each sample by the C^{14} dilution method. These results are given in Table 28.

From the foregoing data it can be concluded that the mechanism of the rearrangement of glycols I, II, and III involves a rapid and reversible removal of hydroxyl group (undoubtedly as a water molecule) followed by hydrogen migration or aryl migration, the latter steps being rate-determining.

[26] J. F. Lane and D. R. Walters, *J. Am. Chem. Soc.* 73, 4234, 4238 (1951).

Table 26. Summary of Kinetic Data for the Rearrangement, in 3.13 *N* H_2SO_4, of I, I*d*, II, II*d*, Threo-III, and Erythro-III

Reactant	$k_1 \times 10^5$ min^{-1}
I	12.04 ±0.22 11.94 ±0.14*
I*d*	7.03 ±0.25
II	39.5 ±0.6
II*d*	32.9 ±0.003
Threo-III	70.4 ± 1.9
Erythro-III	68.5 ±0.9

*First-order rate of racemization of (+)-1,1,2-triphenylethylene glycol [(+)-I].

Table 27. Comparison of k_H/k_D for I, I*d*, II, and II*d*

Reactant	Aldehyde/Ketone Ratio	k_H/k_D	k_b/k_d
I	0.278	3.1 ±0.4	2.6 ±0.4
I*d*	0.907		
II	2.58	3.0 ±0.4	2.9 ±0.4
II*d*	7.74		

Table 28. Summary of Data Showing Extent of Isomerization of Threo-III and Erythro-III Under Rearrangement Conditions

Reactant	Completion of Reaction (%)	Threo-III (%)	Erythro-III (%)
Erythro-III	10	42	58
	22	54	46
Threo-III	11	61	39
	10	63	37
	22.5	54	46
	24.5	56	44

STEREOCHEMISTRY OF THE SOLVOLYTIC AND DEAMINATION REACTIONS OF 1,2,2-TRIPHENYLETHYL DERIVATIVES[27]

C. T. Lester C. J. Collins

The solvolytic and deamination reactions of 1,2,2-triphenylethanol and its derivatives, previously[28] reported with respect to radiochemistry, have now been subjected to stereochemical studies. It has been found (1) that the products of hydrolysis of 1,2,2-triphenylethyl tosylate and (2) that the deamination product from the reaction between 1,2,2-triphenylethylamine and nitrous acid are formed with some racemization plus retention of configuration. The (–)-1,2,2-triphenylethanol-1,2-C_1^{14} obtained from deamination of the (–)-amine at 36.5°C was resolved into a fraction of $[\alpha]_D^{25}$ = –119 deg and into a racemic fraction. It was found that the extent of C^{14} rearrangement of the former (20.6%) and of the racemic (24.5%) fraction was consistent with a mechanism involving the equilibrating of classical carbonium ion intermediates. These data, however, exclude bridged ions as the cause of configuration retention. Evidence is thus presented that the rate of rotation about the carbon-carbon bond is comparable with the rate of phenyl migration.

The compound (–)-1,2,2-triphenylethylamine (ref 28), $[\alpha]_D^{25}$ = –69.5 deg (ethanol), was obtained by fractional crystallization of the (+)-camphor-10-sulfonic acid salt. The dextrorotatory enantiomer was obtained in slightly lower purity, $[\alpha]_D^{25}$ = +65.4 deg (ethanol), by recrystallization of the tartaric acid salt of the amine recovered from the mother liquors of the first resolution. When either enantiomeric amine was deaminated with nitrous acid under the conditions previously employed,[28] the 1,2,2-triphenylethanol resulting was found to be optically active and to have the same sign of rotation as its amine precursor. The attempts to resolve the *dl*-carbinol with alkaloids via its half-succinate, half-phthalate, etc., were unsuccessful; so the carbinol obtained from deamination of the optically active amine and the acetate derived therefrom were subjected to fractional crystallization in a variety of solvents. It was found that samples of 1,2,2-triphenylethyl acetate, enriched in one optical isomer, could be further enriched to a constant optical rotatory power by fractional crystallization from ethyl alcohol, the racemic form of the acetate being considerably less soluble than either enantiomorph. In this way, (–)-1,2,2-triphenylethyl acetate of $[\alpha]_D^{25}$ = –60 deg, (+)-1,2,2-triphenylethanol acetate of $[\alpha]_D^{25}$ = +61.4 deg, (–)-1,2,2-triphenylethanol of $[\alpha]_D^{25}$ = –119 deg, and (+)-1,2,2-triphenylethanol of $[\alpha]_D^{25}$ = +122 deg were obtained.

Given in Table 29 is a summary of the stereochemical results for (1) the deamination of optically active 1,2,2-triphenylethylamine and (2) the hydrolysis and (3) the acetolysis of optically active 1,2,2-triphenylethyl tosylate. Included also are the radiochemical results for these same reactions. The products obtained from hydrolysis and acetolysis of the tosylate are certainly of the same configuration as that of the carbinol used in the preparation of the tosylate. These reactions, therefore, have proceeded with predominant *retention* of configuration. The carbinol produced through deamination of (+)- or (–)-1,2,2-triphenylethylamine is presumed also, by an application of Freudenberg's displacement rule,[29] to have been formed with

[27] This work was done in collaboration with W. A. Bonner of Stanford University as a continuation of the work done by him in this laboratory in 1952–1953.

[28] W. A. Bonner and C. J. Collins, *J. Am. Chem. Soc.* 75, 5372 (1953); C. J. Collins and W. A. Bonner, *J. Am. Chem. Soc.* 75, 5379 (1953); C. J. Collins and W. A. Bonner, *J. Am. Chem. Soc.* 77, 92 (1955); W. A. Bonner and C. J. Collins, *J. Am. Chem. Soc.* 77, 99 (1955); W. A. Bonner and C. J. Collins, *J. Am. Chem. Soc.* 78, 5587 (1956).

[29] K. Freudenberg, *Sterochemie*, p 699 ff, F. Deuticke, Liepzig and Vienna, 1933; compare also G. W. Wheland, *Advanced Organic Chemistry*, 2d ed., p 278–9, Wiley, New York, 1949.

Table 29. Summary of Stereochemical and Radiochemical Results for Solvolytic and Deamination Reactions of 1,2,2-Triphenylethyl-1-C^{14} Derivatives

Run No.	Reaction	Conditions	C^{14} Rearrangement[a] (%)	Inversion (%)
1	Deamination	–2°C	22.5	28
2	Deamination	–2°C		25
3	Deamination	–2°C	22	23
4	Deamination	12.5°C		31
5[b]	Deamination	36.5°C	24.4	33
6[b]	Deamination	36.5°C		36
7[b]	Deamination	36.5°C	20	30
8[c]	Tosylate hydrolysis	Acetone-H_2O, reflux	22	
9	Tosylate hydrolysis	Acetone-H_2O, reflux		37
10[c]	Tosylate acetolysis	HOAc, NaOAc, 85°C	40	
11	Tosylate acetolysis	HOAc, NaOAc, 85°C		45
12	Tosylate acetolysis	HOAc, NaOAc, 85°C		47
13	Tosylate acetolysis	HOAc, NaOAc, 85°C		47

[a]Of the chain label in 1,2,2-triphenylethyl-1-C^{14}-amine.

[b]In the runs at 36.5°C, in addition to 4% olefin, there was produced 8% of triphenylethyl acetate (see Table 30). When the product was separated from olefin the $[\alpha]_D^{24}$ of the mixed carbinol and acetate was not appreciably different from that of the carbinol obtained upon reduction of this mixture with $LiAlH_4$.

[c]Taken from ref 28.

predominant *retention* of configuration. The discretely labeled carbinol was shown to be unrearranged under the conditions of the deamination, stability tests upon the solvolysis products having been reported previously.[28]

Given in Table 30 is a summary of some experiments which were performed upon (–)-1,2,2-triphenylethyl-1-C^{14}-amine. In this study the labeled, partially racemic product of deamination was resolved into a fraction of $[\alpha]_D^{25}$ = –119 deg and a racemic fraction of no observable optical rotation. These fractions were then oxidized to benzophenone and benzoic acid, and the per cents of C^{14} rearrangement were determined as before.[28] Also included in Table 30 are the per cents of C^{14} rearrangement of two carbinol fractions of $[\alpha]_D^{25}$ = –91 deg and $[\alpha]_D^{25}$ = –5.4 deg and similar data for the acetate and olefin fractions produced during the same deamination.

STEREOCHEMICAL STUDY OF THE ACETOXYL EXCHANGE REACTION OF 1,2,2-TRIPHENYLETHYL ACETATE[30]

C. J. Collins C. A. Krauth

The rate of racemization (k_r) of 1,2,2-triphenylethyl acetate has been determined under conditions previously[31] used to study the rates of isotope position isomerization (k_I, chain label equilibration, and k_{II}, phenyl label equilibration) and acetoxyl exchange (k_{III}) of this same compound.

[30]This work was done in collaboration with W. A. Bonner of Stanford University as a continuation of the work done by him in this laboratory in 1952–1953.

[31]W. A. Bonner and C. J. Collins, *J. Am. Chem. Soc.* **75**, 5372 (1953); C. J. Collins and W. A. Bonner, *J. Am. Chem. Soc.* **75**, 5379 (1953); C. J. Collins and W. A. Bonner, *J. Am. Chem. Soc.* **77**, 92 (1955); W. A. Bonner and C. J. Collins, *J. Am. Chem. Soc.* **77**, 99 (1955); W. A. Bonner and C. J. Collins, *J. Am. Chem. Soc.* **78**, 5587 (1956).

Table 30. Summary of Radiochemical Data for Various Fractions Obtained on Deamination of (–)-1,2,2-Triphenylethyl-1-C^{14}-amine at 36.5°C

Product	Yield (%)		$[\alpha]_D^{25}$ (deg)	C^{14} Rearrangement (%)
$Ph_2C^* = C^*HPh$	4			37
(–)-$Ph_2CH(OCOCH_3)C^*HPh$	8		–23[a]	13[b]
(–)-$Ph_2C^*H(OH)C^*HPh$	88[c]	Fraction 1	0	24.5
		Fraction 2	–5.4	24.6
		Fraction 3	–91	20.7
		Fraction 4	–119	20.6

[a]This value is calculated from $[\alpha]_D^{25}$ determinations of three different fractions.
[b]This value was obtained by oxidation of fraction 1, whose $[\alpha]_D^{25}$ was –3 deg.
[c]In addition to fractions 1 through 4, there were several intermediate fractions.

Kinetic Determinations

The compound (+)-1,2,2-triphenylethyl-1-C^{14} acetate (3.000 g, $[\alpha]_D^{24.7} = +42.9$) was dissolved in 70.0 ml of glacial acetic acid, and the flask containing the solution was placed in a thermostatted bath at 54.6 ± 0.3°C. After thermal equilibrium had been reached, 6 ml of a catalyst solution prepared from 16.55 g of dry *p*-toluenesulfonic acid 54.4 ml of acetic acid, and 6.72 ml of acetic anhydride was added. The catalyst solution had been placed previously in the same thermostatted bath. Aliquots of the reaction mixture were removed at given time intervals and were quenched by adding them to excess aqueous sodium bicarbonate. The acetate was recovered quantitatively, in each case, by ether extraction and then clarified and dried *in vacuo* over Drierite. The specific rotation of each acetate fraction was then observed.

The acetate fractions were treated with lithium aluminum hydride, and the specific optical rotations of the recovered carbinol fractions were determined. Each carbinol fraction was then oxidized to benzophenone and benzoic acid by a method previously described.[32] The benzophenone fractions were converted to 2,4-dinitrophenylhydrazones, which were crystallized three or four times from dioxane, and then assayed for radioactivity.

[32]W. A. Bonner and C. J. Collins, *J. Am. Chem. Soc.* 78, 5592 (1956).

Racemization rates were calculated from the $[\alpha]_D^{25}$ values of both the acetate and carbinol fractions by means of the equation

$$k_r = \frac{1}{t} \ln \frac{\alpha_0}{\alpha_t} .$$

The rate of equilibration of the chain label was calculated by means of the equation[31]

$$k_I = \frac{1}{t} \ln \frac{x_e}{x_e - x} .$$

The acetoxyl exchange rate (k_{III}) was determined in two additional experiments as reported previously,[31] and was calculated by means of the equation

$$k_{III} = \frac{1}{t} \ln \frac{a}{a - x} .$$

The results, based on nine observations each for k_I and k_r, and six observations each for the newly determined values of k_{III}, were calculated by the method of least squares. These results are shown in Table 31, in which are given also the rate constants (k_I, k_{II}, and k_{III}) previously[31] determined, and recalculated by the least-squares method.

The ratio of k_r(av) to k_I is 1.23. The presently determined value (1.961×10^{-2} hr^{-1}) for k_I is in good agreement with the least-squares values

Table 31. Summary of Determinations of Rate Constants k_I, k_{II}, k_{III}, and k_r

	Rate Constant $\times 10^2$ hr^{-1}	Reference	Average
k_I[a]	2.065 ±0.013	31	
	2.064 ±0.067	31	2.030
	1.961 ±0.0005	This section	
k_{II}	1.940 ±0.029	31	1.922
	1.903 ±0.017	31	
k_{III}	1.862 ±0.039	31	
	1.807 ±0.077	This section	1.846
	1.869 ±0.055	This section	
k_r	2.36 ±0.05	This section[b]	2.42
	2.48 ±0.041	This section[c]	

[a]The radioactivity assay of I was originally reported as 2.161 mc/mole (ref 31). When k_I is calculated by the least-squares method with 2.161/2 as x_e, $k_I = 2.138 \pm 0.015 \times 10^{-2}$ and $2.136 \pm 0.067 \times 10^{-2}$ hr^{-1}. Later, the average of many determinations of the radioactivity assay of derivatives of I gave a value of 2.192 mc/mole. It is the later value which has been used in calculating the first two values of k_I.

[b]From carbinol data. Precision to be rechecked.

[c]From acetate data.

(Table 31) for k_I, k_{II}, and k_{III} previously[31] obtained. Since the two values of k_r and one of the values above for k_I were all obtained from a single-flask experiment, the external error due to lack of duplicability of experimental conditions between separate runs has been eliminated. In the determination of k_I the error arising from an isotope effect in the degradative method[31] was corrected. The method employed was that used for the degradation of the deamination product of 1,2,2-triphenylethyl-1-C^{14}-amine to benzophenone and benzoic acid. During the previous application[31] of this method the yields were essentially quantitative, and the isotope-effect error was negligible. The time and effort required, however, to achieve quantitative yields during the present study was not deemed practicable. The maximum isotope effect, owing to the degradation of 1,2,2-triphenyl-2-C^{14}-ethanol to benzophenone-C^{14}, by this method is 6%. The yields obtained during the degradation of each aliquot varied from 35 to 65%, corresponding to errors for each aliquot of 3.5 to 4.5% in the radioactivity assays. In determining the value for k_I reported in this paper, an isotope-effect correction of 4% for the degradative method was applied to each benzophenone derivative obtained for each of the nine aliquots.

This correction was not necessary in the determination of k_{II} and k_{III}, for I is the only isotope position isomer of 1,2,2-triphenylethyl acetate whose isotopic bond is involved during the acetoxyl exchange reaction. Conceivably, an isotope effect during the migration of the labeled phenyl groups of II might be possible. Since the phenyl of II, however, is randomly labeled, the total observed error owing to such an isotope effect would be very small. The label in III, being in the methyl group, should never be directly involved in a bond-breaking reaction during acetoxyl exchange, and thus should not contribute any error through the operation of an isotope effect.

It is clear, therefore, that within the limits of the experimental method, k_I, k_{II}, and k_{III} are identical and slower than the rate of racemization, k_r, in the ratio of 1/1.23. This fact is compatible with the mechanism previously proposed[31] for the acetoxyl exchange reaction, with the modification that some steric shielding by the leaving acetoxyl groups prevents a completely random approach by the entering acetoxyl groups.

STUDY OF THE ABSOLUTE AND RELATIVE RATES OF DECARBONYLATION OF FORMIC ACID AND FORMIC-*d* ACID IN CONCENTRATED SULFURIC ACID

G. A. Ropp

As a continuation of an earlier study of isotope fractionation in the decarbonylation of formic acid,[33] the absolute rate of reaction of formic-*d* acid (95 to 100% pure by mass spectrometric analysis) has been measured at two temperatures under conditions very similar to those used earlier.[33] Formic-*d* acid was synthesized by the following series of processes: (1) hydrolysis of sodium cyanide in pure deuterium oxide at 180 to

[33]G. A. Ropp, A. J. Weinberger, and O. K. Neville, *J. Am. Chem. Soc.* 73, 5573 (1951); H. Eyring and F. W. Cagle, Jr., *J. Phys. Chem.* 56, 889 (1952).

200°C, (2) distillation of the resulting anhydrous sodium deuteroformate with 85% phosphoric acid in high vacuum, and (3) fractionation of the aqueous formic-*d* acid solution in a 40-in. Vigreux column, yielding a 72% solution of formic-*d* acid, bp 105 to 106°C at 730 mm Hg, $d^{20°} = 1.17$. For comparison the rates of decarbonylation were measured under the same conditions for (1) formic acid prepared by dilution of cp formic acid with water to 72% and (2) formic acid synthesized from sodium cyanide and water by a procedure exactly parallel to that used to prepare the formic-*d* acid.

The pseudo first-order rate constants for the decarbonylation of the three acid samples were measured by using approximately 500-fold excess by weight of 96.2% sulfuric acid. The results of ten runs are summarized in Table 32. At each temperature the rate constants of formic acid derived from sodium cyanide are slightly lower than those of formic acid derived from cp formic acid. This is apparently due to the fact that the acid from sodium cyanide contained slightly more water, which could dilute the sulfuric acid and thus lower the reaction rate. Since the strength of the formic acid derived from cp acid was adjusted so that it equaled that of the formic-*d* acid, the values of k_H/k_D were calculated by using k_H determined with formic derived from cp acid. Nevertheless, the reasonable agreement of the rate constants from the two samples of formic acid indicates that the lower rate of reaction with formic-*d* acid does not result from the presence of chemical impurities in one acid sample and not in the other. The variation of the value of k_H/k_D with temperature also supports this belief. The variation of this isotope-effect ratio with temperature is in the direction normally found for isotope effects.

A tentative interpretation of this measured deuterium isotope effect, which is too small to represent the maximum possible deuterium fractionation which could result if cleavage of the carbon-hydrogen bond were rate-determining, may be made in terms of the mechanism proposed by Hammett.[34] Formic acid is assumed to be rapidly and reversibly protonated in strong sulfuric acid, yielding a definite equilibrium concentration of a positively charged ion which then loses water in the subsequent rate step involving cleavage of the carbon-oxygen bond:

$$\left[HC \begin{matrix} \diagup O \\ \diagdown OH_2 \end{matrix}\right]^+ \xrightarrow{A} \left[\begin{matrix}\text{activated}\\ \text{complex}\end{matrix}\right] \longrightarrow [HCO]^+ + H_2O$$

The $[HCO]^+$ fragment, if it exists at all, would be assumed to be too unstable to build up to any

[34] L. P. Hammett, *Physical Organic Chemistry*, 1st ed. p 283, McGraw-Hill, New York, 1940.

Table 32. Rates of Decarbonylation of Formic Acid and Formic-*d* Acid in 96.2% Sulfuric Acid

Thermostat Temperature (°C)	Acid Sample	k ($min^{-1} \times 10^4$)	Mean ($k \times 10^4$)	k_H/k_D
25.2	From cp HCOOH	1370	1400 ± 30	
	From cp HCOOH	1430		
	HCOOH from NaCN	1320		1.49
	DCOOH from NaCN	921	939 ± 20	
	DCOOH from NaCN	957		
0.15	From cp HCOOH	64.5	64.0 ± 0.5	
	From cp HCOOH	63.6		
	HCOOH from NaCN	60.5		1.72
	DCOOH from NaCN	36.6	37.2 ± 0.6	
	DCOOH from NaCN	37.7		

appreciable concentration. Under these conditions no isotope fractionation would occur during the breakup of this ion.

Thus both the large C^{14} isotope effect observed[33] and the deuterium fractionation factor reported here would remain to be accounted for in terms of the activation process, *A*. It would therefore be assumed that the carbon-to-oxygen bond is nearly completely lost in the activated complex, while the carbon-to-hydrogen bond is only weakened.

CRACKING PATTERNS OF FORMIC ACID, FORMIC ACID-*d*, AND FORMIC-*d* ACID IN THE MASS SPECTROMETER

C. E. Melton G. A. Ropp

During assay of the isotopic composition of the formic-*d* acid used in the isotope-effect study described above, it was found convenient to make a comparative study of the cracking patterns of formic acid and the two possible monodeuterated formic acids in the mass spectrometer. The conditions used in this study were as follows:

Ionization chamber temperature	100°C
Energy of ionizing electrons	75 ev
Ionic energy	5.1 kev
Trap current	10 μa

Although the data reported in Table 33 are subject to further verification, the agreement among the three patterns of heights of peaks not involving hydrogen (underlined) is very good and indicates that the instrument was operating in such a way that the heights of other peaks may be compared among the three cracking patterns. The relative heights of the mass-45 and mass-46 peaks indicate that the mass-45 peak, CHO_2^+, in the pattern from HCOOH probably arises partly from loss of hydrogen from the carbon atom and partly from loss of the other hydrogen atom. In the breakup of formic-*d* acid, cleavage of the carbon-oxygen bond predominates, while in the breakup of formic acid-*d*, cleavage of the carbon-hydrogen bond contributes the greater effect. It therefore appears that deuterium bond-breaking isotope effects are operating. With further more careful experimental work it may be possible to make definite statements about the occurrence of isotope effects and the origins of the mass-29 and mass-13 peaks as well as the mass-45 peak in formic acid. Formic acid-*d* was synthesized from sodium formate and deuterophosphoric acid.

PREPARATION OF ALKYL PHOSPHINATES BY THE GRIGNARD REACTION

C. E. Higgins W. H. Baldwin

The formation of carbon-to-phosphorus bonds by the reaction of Grignard reagents with phosphorus chlorides has received attention in many reactions. The reaction of alkyl dichlorophosphates with Grignard reagents has not been generally exploited. However, the reaction has been used here to prepare phosphinate esters in the following manner:

$$ROP(O)Cl_2 + 2R'MgX \longrightarrow R'_2P(O)OR + 2MgXCl$$

In the method typically used here alkyl dichlorophosphate in ether was added to an ether solution of a standardized Grignard reagent. After the addition the reaction mixture was refluxed for 1 hr, hydrolyzed with cold aqueous HCl, and the product isolated in the usual manner (the aqueous solution was separated and washed with ether; the combined ether layers were washed with alkali, then with water, were dried over anhydrous sodium sulfate, then fractionated). The esters listed in Table 34 have been prepared.

In a modification of the above procedure, four molar equivalents of octylmagnesium bromide was added to ethyl dichlorophosphate. The reaction mixture was treated in the above manner and yielded 37% ethyl dioctylphosphinate (based on $EtOPOCl_2$) and a fraction of higher-boiling material (solid at room temperature) whose analysis has not been completed but which appears to be trioctyl phosphine oxide formed by the replacement of the ethoxy group with octyl in the following over-all fashion:

$$EtOPOCl_2 + 3\ OcMgBr \longrightarrow Oc_3PO + EtOMgBr + 2\ MgBrCl$$

ACID FORMATION DURING THE RADIOLYSIS OF ORGANOPHOSPHORUS COMPOUNDS

W. H. Baldwin

Part of the current work has been summarized in ORNL CF-57-4-9,[35] where it has been reported that the strong acid, dibutyl hydrogen phosphate, was formed with essentially the same yield in the presence and in the absence of oxygen. However,

[35] W. H. Baldwin, *Acid Formation in the Radiolysis of Phosphorus Esters*, ORNL CF-57-4-9 (April 3, 1957).

Table 33. Cracking Patterns of Formic Acid and Deuteroformic Acids

Mass	HCOOH		HCOOD*		DCOOH	
	Possible Ions	Relative Abundance	Possible Ions	Relative Abundance	Possible Ions	Relative Abundance
12	C^+	0.92	C^+	1.07	C^+	1.01
13	$C_{13}^+ + CH^+$	0.52	$C_{13}^+ + CH^+$	0.63	$C_{13}^+ + CH^+$	0.15
14	$CH_2^+ + CO^{++}$	0.18	CD^+ or CO^{++}	0.08	CD^+ or CO^{++}	0.91
15	COH^{++}	0.77	COH^{++}	0.06	COH^{++}	0.17
15.5			COD^{++}	0.05	COD^{++}	0.05
16	O^+	2.51	O^+	2.61	O^+	2.79
17	OH^+	3.53	OH^+	1.21	OH^+	3.33
18	HOH^+	15.91	HOH^+ and OD^+	7.16	HOH^+ and OD^+	6.76
19	?	0.46	DOH^+	18.18	DOH^+	14.03
20			?	0.28	?	0.86
22	CO_2^{++}	0.33	CO_2^{++}	0.36	CO_2^{++}	0.33
28	CO^+	22.25	CO^+	22.07	CO^+	23.19
29	HCO^+	88.19	HCO^+	90.57	HCO^+	23.44
30	$HC_{13}O^+$	1.81	DCO^+	14.05	DCO^+	93.79
31			$DC_{13}O^+$	0.67	$DC_{13}O^+$	1.44
44	CO_2^+	37.12	CO_2^+	37.85	CO_2^+	34.14
45	CHO_2^+	77.97	$HCOO^+$	26.91	$COOH^+$	45.17
46	$HCOOH^+$	100.00	$COOD^+$	85.13	$DCOO^+$	57.07
47	$HC_{13}OOH^+ + ?$	3.77	$HCOOD^+$	100.00	$DCOOH^+$	100.00
48			$HC_{13}OOD^+ + ?$	2.06	$DC_{13}OOH^+$	15.72
49			$HCO_{18}OD^+$	0.54	$HCO_{18}OD^+ + ?$	1.08

*Corrected for 26% HCOOH impurity.

Table 34. Properties of Phosphinate Esters

Phosphinate	Yield (%)	Boiling Point (°C)	N_d^{25}	d_4^{25}
Butyldibutyl-	76	151–153 at 10 mm	1.4421	
Ethyldibutyl-	44	80–81 at 1 mm	1.4387	0.9356
Ethyldioctyl-	42	152–154 at 1 mm	1.4499	0.8967

in the presence of oxygen a weaker acid component appeared. It is likely that this weaker component is a carboxylic acid rather than monobutyl dihydrogen phosphate.

The yield of acid from equimolar solutions of tributyl phosphate and water is about half that from the pure ester.

Less acid results from dibutyl butylphosphonate, but the yield is about the same from dibutyl phenylphosphonate as from tributyl phosphate. Other structures will be tested and other products will be sought from the radiolytic decomposition.

DIBUTYL PHOSPHONOACETIC ACID

R. W. Higgins[36] W. H. Baldwin

Dibutyl phosphonoacetic acid, represented by the formula $(BuO)_2P(O)CH_2COOH$, was synthesized as a complexing agent for the extraction of metallic cations. The acid contains the anion for the neutralization of the cation, as well as the phosphoryl group ($P \longrightarrow O$) for coordination with the cation. The acid has been shown to extract uranyl ion from aqueous uranyl nitrate solution better than does tributyl phosphate.

Attempts to isolate the uranyl salt have yielded a yellow glass that swells and eventually disperses in benzene. Cryoscopic determination of the molecular weight in benzene shows the uranyl salt to be associated. The polymer contains 10 to 15 uranyl groups. The acid itself is associated in benzene, containing about three units in the polymer. The phosphoryl group is thereby shown to be capable of coordinating with cations of other salt molecules and to be capable of forming polymeric chains.

Two well-known synthetic paths produced the same amide, $(BuO)_2P(O)CH_2CONH_2$, that was deamidated by a mixture of formic acid and butyl nitrite.

Yields for the deamidation step itself averaged about 70%. Some unreacted amide was recovered. The corresponding tributyl ester was isolated; it presumably resulted from ester interchange between the formed dibutyl phosphonoacetic acid and butyl nitrite.

Dibutyl phosphonoacetic acid was obtained from the evaporation of solvents from solutions. The yellow color associated with it was probably due to an impurity. The following properties have been observed:

d_{24}^{24}	1.0918
N_D^{24}	1.4448
Molar refractivity	
Calculated	60.8
Found	61.5
Phosphorus, %	
Calculated	12.35
Found	12.03
Rate of decarboxylation	7% in 8 hr at 175°C
Equivalent weight	
Calculated	252
Found	252
pK_a	~4.4 (70% ethanol)

COMPOSITION OF AMSCO 125-82

A. D. Horton[37] W. H. Baldwin

Amsco 125-82 is a paraffinic hydrocarbon reportedly made by the polymerization of butenes and pentenes, followed by hydrogenation. The chemical composition of Amsco 125-82 is of considerable interest to process development, since

[36] Summer research participant, June to September 1956.

[37] Analytical Chemistry Division.

it is currently used as a diluent for tributyl phosphate in solvent extraction processes. The structures of the components are important, since they are related to radiolytic decomposition and chemical reaction. The following carbon skeletons represent types of hydrocarbons that have been reportedly identified[38] in such polymerization mixtures and which are expected to boil within the range of Amsco 125-82:

2,3,4,4-tetramethyl hexane
2,3,3,4-tetramethyl hexane
2,3,4-trimethyl-3-ethyl pentane
2,2,4,6,6-pentamethyl heptane
2,2,4,4,6-pentamethyl heptane
2,2,3,5,6-pentamethyl heptane
2,2,4,5,6-pentamethyl heptane

It can be readily seen that the hydrocarbons in Amsco 125-82 are likely to be highly branched chains. Chemically, the tertiary hydrogen atoms are sites of attack by chemical oxidation and nitration. The angular methyl groups are likely to provide much methane during radiolysis.

The Amsco 125-82 is being distilled at 18 mm Hg pressure. The course of the separations is being followed by gas chromatography. In the starting material at least ten fractions are detected by the chromatograph. Distillation has yielded one fraction that is chromatographically pure. The physical properties of this hydrocarbon are being determined in order to aid in the elucidation of the structure.

The fractional distillation of the Amsco 125-82 is being continued to obtain other components in relatively pure form. When the types of the compounds that are present have been established, it is expected that synthesis will make available model compounds of several of these types.

PREPARATION AND PROPERTIES OF URANIUM- AND THORIUM-CONTAINING ORGANIC COMPOUNDS

W. H. Baldwin C. E. Higgins

Wendlandt[39] has examined several organic derivatives of thorium in the thermobalance. The tetrabenzoate was the most stable compound that was examined. Several chelates and alkoxides of U(IV) and U(VI) have been prepared and examined at elevated temperature. Particular emphasis was placed on volatility.[40] The high-temperature (300°C) behavior of thorio- and urano-organic compounds is but little known. Among the properties that are of particular interest are the following:

1. solubility in nonpolar solvents, such as molten diphenyl, up to 300°C,
2. chemical changes occurring in such solutions at elevated temperatures,
3. radiolytic decomposition at elevated temperatures.

The compounds prepared so far include salts of carboxylic acids, chelates with 1,3-diketones, and addition compounds. The methods of preparation of the salts and chelates were well-known procedures that are found in the chemical literature. The addition type of compound is generally prepared by mixing the reactants in alcohol or in aqueous alcohol and then cooling to crystallize the product.

Solubility in molten diphenyl (by the synthetic method) of a few thorium compounds is shown in Table 35. The salts, benzoate and mercaptobenzothiazole, are insoluble. The chelates with acetyl acetone and dibenzoyl methane are soluble in diphenyl. This observation supports the idea that solubility in nonpolar solvents is greater for those compounds that exhibit less ionic character. Thermal decomposition of the chelates occurred on prolonged heating at elevated temperatures. This thermal decomposition was evidenced by darkening and an increase in viscosity. It will be of interest to observe the rate of precipitation of thorium both thermally and radiolytically.

Among the uranyl compounds tested (Table 36), the acetate and benzoate were insoluble. The octanoate dispersed in diphenyl in what appeared to be a colloidal manner. The dispersion became cloudy at 210°C. The single chelate tested (acetyl acetonate) was not soluble to the extent of 235 g per kilogram of mixture. The solubility will be examined at lower concentrations.

The addition compounds formed between uranyl salts and phosphine oxides show remarkable solubility and stability. Nitrate, acetate, and sulfate salts have been tested with tributyl and triphenyl

[38] F. C. Whitmore and P. L. Meunier, *J. Am. Chem. Soc.* 63, 2197 (1941); F. C. Whitmore *et al.*, *J. Am. Chem. Soc.* 63, 2035 (1941); G. C. Johnson, *J. Am. Chem. Soc.* 69, 146 (1947).

[39] W. W. Wendlandt, *Anal. Chem.* 29, 800 (1957).

[40] H. I. Schlesinger *et al.*, *J. Am. Chem. Soc.* 75, 2446 (1953); H. Gilman *et al.*, *J. Am. Chem. Soc.* 78, 2790, 4285, 4287 (1956).

phosphine oxides. In general, the tributyl phosphine oxide addition compounds appear to be more soluble. The sulfate, in qualitative tests, is more stable thermally than nitrate or acetate.

The solution containing 2 moles of tributyl phosphine oxide per mole of uranyl sulfate (18 g of U per kg of solution) was heated at 250°C for 24 days. At the end of 11 days a coke had formed in the flask. When filtered and washed with benzene, the coke was shown to contain 3% of the total uranium that was used in the experiment.

Qualitative tests under other conditions revealed black solids precipitating from solution within $2\frac{1}{2}$ hr in the temperature range of 330 to 360°C. Exposure in the cobalt gamma source for a total of 6×10^{19} ev/ml at 120°C produced a black precipitate in the diphenyl solution. This was assumed to be similar to the coke formed thermally.

The thermal reaction forming coke will be studied further to find the mechanism whereby uranium becomes included in this insoluble residue.

Table 35. Solubility of Thorium Compounds in Diphenyl

Compound	Grams of Th per kg of Mixture	Solution Temperature (°C)	Remarks
Pentaacetylacetonate	150	100	Darkened at 160°C
Tetrabenzoate	32		No detectable solubility at 200°C
Tetrabisbenzoylmethane	110	175	3 hr at 290 to 310°C produced darkening
	205 (undiluted compound)	191	3 hr at 290 to 310°C coused product to become dark and viscous
Tetramercaptobenzothiazole	17		No detectable solubility at 250°C

Table 36. Solubility of Uranyl Compounds in Diphenyl

Compound	Grams of U per kg of Mixture	Solution Temperature (°C)	Remarks
Diacetate·$2H_2O$	18		At 215°C, not detectable
Dioctanoate	13	195	Swelled; cloudy at 210°C
Dibenzoate	15		At 260°C, not detectable
Diacetylacetonate	235		At 160°C, incomplete, dark
$UO_2(NO_3)_2 \cdot 2Ph_3PO$	6 18	178 200	At 210 to 215°C, darkened
$UO_2(NO_3)_2 \cdot 2Bu_3PO$	32	70	Solubility complete at melting point of mixture
$UO_2(OAc)_2 \cdot 2Ph_3PO$	28 66	175 180	
$UO_2(NO_3)_2 \cdot x Bu_2SO_2$	18		At 215°C, insoluble
$UO_2SO_4 \cdot 2Bu_3PO$	18	70	At 250°C, coking after 11 days

CHEMISTRY OF AQUEOUS SYSTEMS

SPECTROPHOTOMETRY OF AQUEOUS SOLUTIONS

W. C. Waggener R. W. Stoughton

Adaptation of a Cary Model 14M Recording Spectrophotometer for Measurements of Aqueous Spectra at Elevated Temperatures and Pressures[1]

Early in 1955 a program was initiated to elucidate any changes with temperature in the relative stabilities of neptunium valence states in aqueous solutions. In particular, it was anticipated that aqueous uranyl sulfate media would be included in the study and that the temperature range covered would be from 0 to 250°C. The (III), (IV), and (V) valence states were known[2] to have distinguishing absorption bands in the region 0.5 to 1.05 μ (5000 to 10,500 Å) at room temperature, and there was some evidence that the spectra of lanthanide and actinide species did not change drastically with temperature. It thus appeared feasible to analyze an Np(III), (IV), (V), and (VI) mixture [getting the (VI) by difference if necessary, i.e., total neptunium less the (III), (IV), and (V)] as a function of temperature by using a spectrophotometer; there was no other known method for conducting such an analysis. As will be described below, a distinctive absorption band has been found in this study for Np(VI) at 1.22 μ. This avoids the necessity of analyzing for this species by difference.

Since the neptunium valence states showed distinctive bands in the visible and near-infrared region above 0.5 μ, and since uranyl sulfate showed negligible absorption in this region, the spectrophotometric method appeared to be a good method, as well as the only known method, for conducting such analyses in aqueous uranyl sulfate solutions. Accordingly a Cary model 14M recording spectrophotometer, a new and highly versatile commercial instrument, was purchased and has been adapted for conducting precision measurements of aqueous spectra at elevated temperatures and pressures.

The first absorption cell designed has a working range of 0 to 250°C and 0 to 1000 psi. It has operated successfully over this range in preliminary runs. The following is a brief description of the apparatus.

Layout of Equipment. – The photograph, Fig. 10, shows the layout of equipment. The chassis on the left contains measurement and control instrumentation for absorption cell and reservoir temperatures and pressures. The portable aluminum hood and mount facility is in the center. The recorder and the monochromator housing are table-mounted immediately above the power supply for the hydrogen and tungsten lamp sources (left) and vacuum gages (right). The cell chamber and the phototube compartment are located inside the hood and attach to the right end of the monochromator, which extends through a seal in the wall of the hood. Piping and other equipment visible in the hood are used in filling and emptying the cell. Pump assemblies for evacuating the cell-chamber and cell-reservoir systems are behind the hood doors. Utilities are controlled from the panel in the lower left corner of the hood-and-mount facility.

Sample Cell. – The photograph, Fig. 11, shows the mounting of cell and reservoir in the cell chamber. The cylindrical body of the cell is made of titanium. The windows are polished cylindrical disks of colorless, artificial sapphire.

The window mount is of a new type. The principle involves a spring-loaded, Teflon-ring seal in an annulus between the polished cylindrical wall surface of a window disk and a titanium recess. The seal against pressure is made quite independent of the mount which holds the window against the end of the cell. Component tests proved the design to be leak-tight at 1000 to 1200 psi of helium with repeated temperature cycling between 30 and 250°C.

Uniform heating and cooling are accomplished by means of an embedded heater winding and a cooling coil attached to a concentric annulus of copper which surrounds the titanium core. This assembly, in turn, is "canned" in a gold-plated

[1] The equipment has been developed with the invaluable assistance of A. M. Tripp and members of his group of the Special Engineering and Design Section of the Engineering and Mechanical Division; J. F. Potts and C. N. Inskeep of the Instrumentation and Controls Division; and W. A. Blevins and W. L. Van Hoozier of the Chemistry Shops Section of the Central Machine Shops. Mr. Van Hoozier fabricated most of the components and has helped with their assembly.

[2] B. B. Cunningham and J. C. Hindman, Chap. 12 in *The Actinide Elements*, NNES vol IV-14A, p 456, McGraw-Hill, New York, 1954.

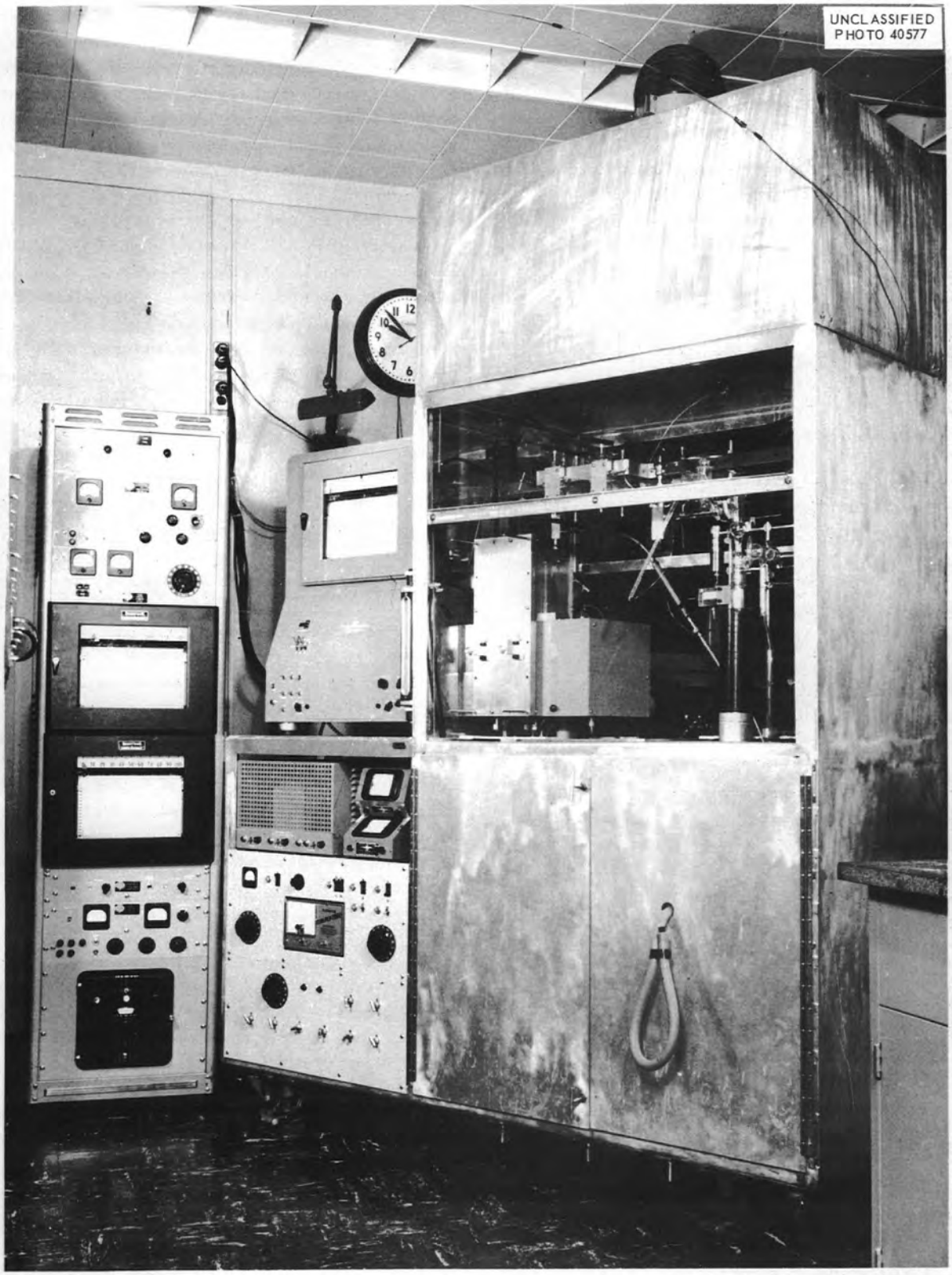

Fig. 10. Equipment for Measurement of Aqueous Spectra at Elevated Temperatures and Pressures.

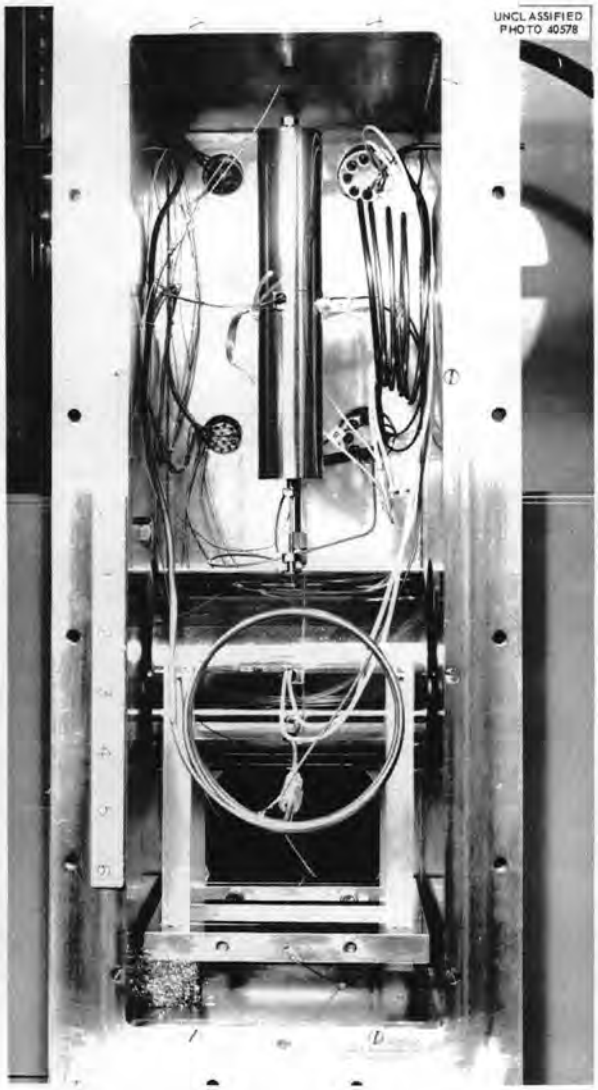

Fig. 11. Closeup of Absorption Cell and Reservoir in Place in Vacuum Chamber.

radiation sheath. The ends of the cooling coil communicate to the walls of the cell chamber by means of helical coils of thin-wall nickel tubing (visible in center-front and upper-right side of the open chamber, Fig. 11). Satisfactory cooling has been obtained with liquid-nitrogen-cooled helium.

A stable, adjustable mount is achieved by cradling the cell on four fused-quartz legs with Inconel X trunnions screwed into the cell body. The fused-quartz legs are fastened to a gold-plated metal base which is kinematically located on three pins. The height of each pin is adjustable under the vacuum chamber by means of a micrometer screw and bellows assembly.

Reference Cell. – The reference cell is mounted in the reference beam, which is parallel to, and exactly 7 in. behind, the sample beam and cell as viewed in Fig. 11. Its housing is light-tight and fitted for continuous purging with dry nitrogen. Geometry and materials of construction of the cell space are identical with the sample cell. It is thermostatted by circulating H_2O (at 25 ± 0.01°C) through an annular space in the titanium body.

Annealed titanium capillary tubing has been used to connect the absorption cell and reservoir with the sample transfer apparatus and Baldwin pressure cell outside the cell chamber. However, the titanium tubing is presently being replaced with heavy-wall platinum capillary for increased safety against corrosion by sulfuric acid solutions at elevated temperatures.

Reservoir. – The reservoir located above the absorption cell in Fig. 11 is used as an expansion chamber and pressurizer. It consists of a titanium core and heater winding with a radiation sheath similar to that of the cell.

The thermal isolation of cell and reservoir is achieved by a chamber vacuum of 1 to 5 μ, and the radiation sheath allows excellent temperature control over the entire design range.

Instrumentation. – The absorption cell uses a self-heating resistance-thermometer temperature controller.[3] In principle, the heater winding is used as one leg of a Wheatstone bridge. Slight unbalance in the bridge (due to changes in wire temperature of the order of 0.1°C) is amplified and made to modulate continuously the impedance of the heater supply circuit to correct the unbalance.

The reservoir heater is energized independently in three sections to provide an adjustable temperature gradient from bottom to top. Reservoir temperature is tied to cell temperature by a Leeds & Northrup Electromax hooked up to control on the temperature difference (range of settings, 0 to 50°C) sensed by a pair of resistance thermometers mounted on cell and reservoir, respectively.

Twelve thermocouples (iron-constantan) located in the cell assembly are monitored by a Brown

[3] J. F. Potts and C. N. Inskeep, *Instrumentation and Controls Semiann. Prog. Rep. July 31, 1956*, ORNL-2234, p 9.

multipoint strip recorder with a range of 0 to 300°C.

The pressure in the absorption cell and reservoir system is recorded continuously by means of a 0 to 1000 psi Baldwin cell with a standard transducer and a Brown recorder.

Hastings thermocouple gages are used to indicate the vacuum (1 μ to 1 atm) at five points in the equipment.

The two face plates of the cell chamber opposite the ends of the absorption cell are held at 25 ± 1°C by circulating water in an interspace around each window. Satisfactory control has been obtained by manual adjustment of water flow and electrical input to a simple 800-w water preheater.

Safety Controls. – An alarm circuit and a heater-power cutoff circuit are actuated respectively by a pair of limit switches on both temperature and pressure recorders. The power cutoff circuit is also actuated by a Simplytrol unit connected to the Hastings thermocouple gage which measures the vacuum in the cell-reservoir chamber. A rise in pressure due to a sudden leak in the absorption cell assembly will immediately trip the power cutoff circuit.

Differential Temperature Absorption of Heavy and Light Water in the Visible and Near-Infrared Regions

Ordinary water begins to absorb appreciably above 0.7 μ (7000 Å), in just the region of occurrence of many of the sharpest absorption bands of the ions of Np(III), (IV), (V) (ref 4), and (VI) (see "Extension of Measurements of the Aqueous Absorption Spectra of Neptunium Ions," this report). For example, the strongest bands for Np(IV), (V), and (VI) ions in 1 *M* $HClO_4$ occur at 0.96, 0.98, and 1.22 μ, respectively, whereas the first prominent water-band maximum occurs at 0.96–0.97 μ. More important, the temperature coefficient of this band is strongly positive. Since our first high-temperature absorption cell is rather long (7.62 cm) and will be compared with a solvent cell of identical geometry maintained at room temperature, the above effect is a serious complication to measurements.

[4] R. Sjoblom and J. C. Hindman, *J. Am. Chem. Soc.* 73, 1744 (1951).

Equipment. – The absorption data presented in Fig. 12 were taken with the Cary model 14M recording spectrophotometer, provided with its regular thermostatted cell compartment (25°C), and separately thermostatted sample cell holder (~8 to 85°C). Two standard 10-cm fused-quartz cells were equipped with long necks, and a No. 30 iron-constantan thermocouple junction was mounted in each cell by means of a small platinum well extending through a Teflon stopper. The thermocouples were calibrated against an NBS certified thermometer. Temperatures of sample and reference cell were recorded with a Brown strip chart recorder having a 0 to 100°C (ion-constantan) range. During measurements, the entire optical system was purged continuously with dry nitrogen. Undispersed radiation was passed through the cells, and the slits operated automatically to provide constant power signal from the reference beam to the PbS detector.

Ordinary distilled water was used without further purification except for removal of part of the dissolved gas by heating the cells at the boiling point to preclude bubble formation during an experiment. Two stocks of D_2O of nominal 99.8% assay were used. The older of the two had been in the laboratory for a number of years, and was used in making the first measurements with heavy water. The newer stock, recently obtained (from the ORNL S. F. Accountability Office) is Savannah River product, having an assay of 99.78 mole % D_2O. By assuming this assay to be correct, and comparing the absorbances of the two stocks at 1.667 μ and at 1.41 μ (see "A Spectrophotometric Method for Determination of H_2O in D_2O," this report), a figure of 99.0 mole % is estimated for the older stock.

Results and Discussion. – Two types of absorption measurements are illustrated in Fig. 12. The *A* curves represent conventional technique, the absorbance of water being measured against nonabsorbing gas and corrected for surface reflections in the cell. The energy response of the instrument in the near-infrared is 3 to 4 absorbance units with slits operating from 0.05 to 3.0 mm, whereas the measurement scale span is 2 absorbance units. By interposing a neutral filter having an absorbance, $A \sim 2$, in the reference beam, the high absorbance portions of the *A* curves of Fig. 12 were measured.

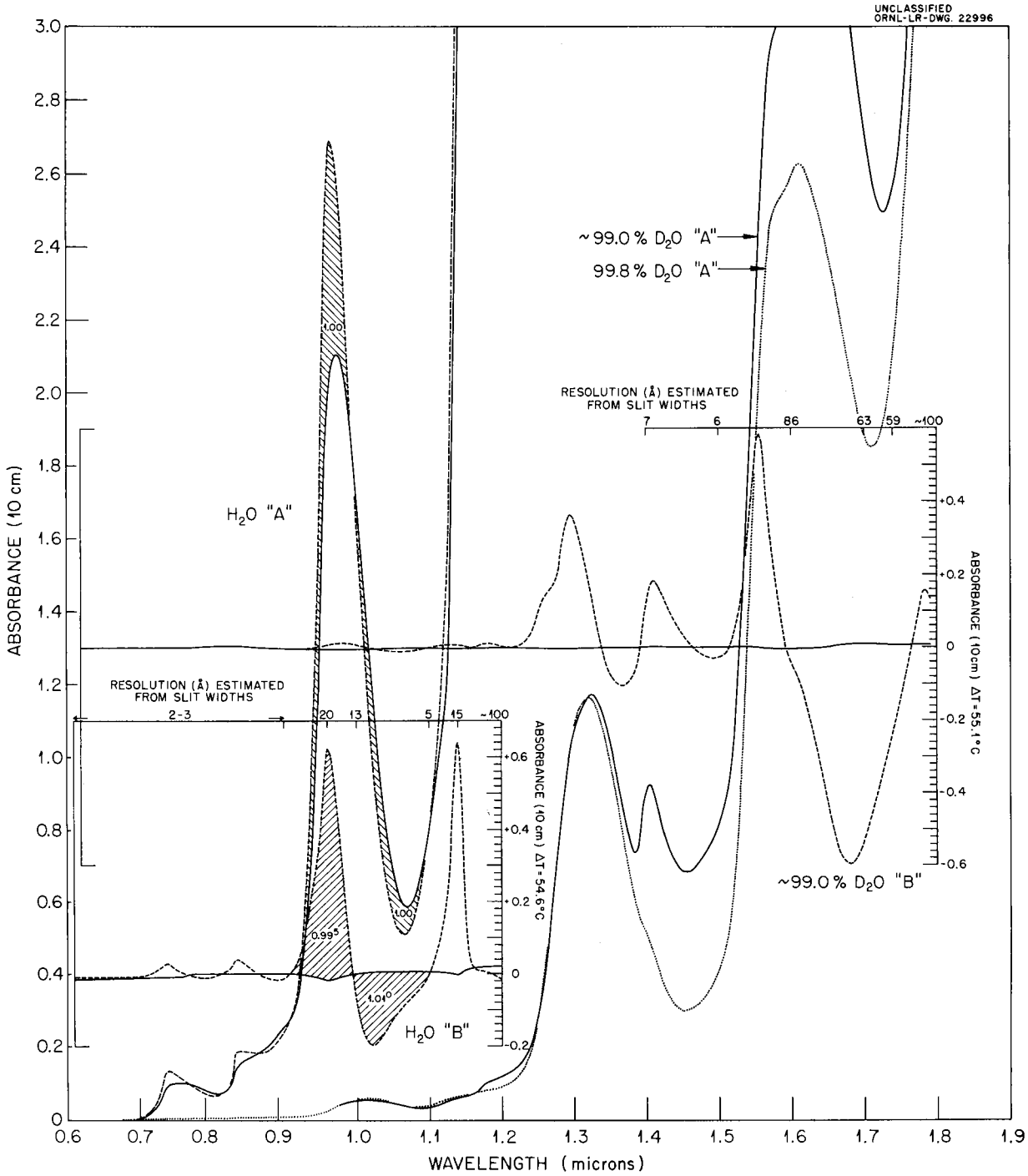

Fig. 12. Absorbance and Differential Temperature Absorbance of 10 cm of $H_2O(l)$ and $D_2O(l)$ (Estimated 99.0 Mole %) from 0.6 to 1.8 μ (or 6×10^3 to 18×10^3 Å). Curve ———, 10-cm sample at 27 to 28°C vs (A) $N_2(g)$ and (B) an identical 10-cm sample in the reference beam at 27 to 28°C; curve – – – – –, 10-cm sample at 82 to 83°C vs (A) $N_2(g)$ and (B) an identical 10-cm sample in the reference beam at 27 to 28°C. Curve ..... is for a 10-cm sample of 99.8 mole % $D_2O(l)$ at room temperature vs $N_2(g)$ reference. The A curves are corrected for cell reflections. Resolution data given above each B curve were estimated from observed slit widths and the dispersion curve for the instrument.

The data for H_2O are in good agreement with those of Collins[5] and with the results of later work by Curcio and Petty.[6]

The *B* curves represent differential temperature absorbance of the sample cell at a series of temperatures (two shown) vs a reference cell of identical geometry and filling. This type of measurement seems not to have been reported previously in the literature. Since the use of this arrangement of cells is proposed in connection with studies of aqueous neptunium ions at 250°C, the curves *A* and *B* have been compared over the region of the first prominent absorbance maximum and minimum for water. The corresponding shaded areas were carefully measured with a planimeter, and the areas of the *B* curves relative to unit area of the *A* curves are given in Fig. 12. These areas are equal within the probable error of measurement, though the small differences in the figures are in the direction expected from a downward shift in wavelength of the maximum and minimum absorbance with increasing temperature.

With the *B* method, families of curves are obtained similar to the two shown in Fig. 12. In these, envelopes of maximums and minimums appear above or below zero absorbance as the sample cell temperature is greater or less than the temperature of the reference cell, respectively.

The position of the differential temperature maximum lies between the respective absorption maximums for water vs dry nitrogen at two temperatures. It is interesting to note that the separation of band maximums for H_2O and D_2O are roughly 1600 and 1200 cm^{-1}, respectively, which is suggestive of harmonics of the symmetrical bending modes given[7] as 1615 and 1220 cm^{-1} for H_2O and D_2O.

The 10-cm absorbance of H_2O and D_2O reaches the practical energy limit for the instrument ($A > 3$) at 1.14 μ and 1.77 μ, respectively. Above 0.7 μ for H_2O and 1.2 μ for D_2O, measurements are complicated by differential temperature absorption of the solvent. Consequently, for study of aqueous solutions at elevated temperatures in the range 0.7 to 1.14 μ for H_2O and 1.22 to 1.77 μ for D_2O, it appears necessary to thermostat both sample and reference cell at the temperature of measurement.

The gain in changing from H_2O to D_2O solvent is indeed significant! Since the spectrum of D_2O corresponding to H_2O is shifted into the near-infrared by a factor of $\sqrt{2}$, the region available to spectrophotometric study in aqueous media is similarly extended (see "Extension of Measurements of the Aqueous Absorption Spectra of Neptunium Ions," this report).

Aside from the practical aspects considered above, the marked changes in the absorption of H_2O and D_2O with temperature are interesting in their relation to modern theory of the structure of water in the liquid state. A family of eight differential-temperature-absorption curves has been obtained in the range of 25 to 223°C vs 25°C by using the 7.62-cm absorption-cell assembly described in the preceding section. The continued sharpening of the bands (increasing maximums, decreasing minimums) plus a general shift toward shorter wavelengths suggest a lessening of the short-range intermolecular attractive forces which are thought to be responsible for the anomalous behavior of water between its freezing point and 100 to 150°C.

Results of the first run of D_2O into the high temperature range are sufficiently interesting that they are presently being extended to cover the range from 4 to 250°C.

A Spectrophotometric Method for Determination of H_2O in D_2O

The Cary model 14M recording spectrophotometer is suitable for differential photometry of H_2O and D_2O in the near-infrared region.

Nine D_2O solutions containing from 0.22 to 15.65 mole % H_2O were prepared by adding weighed amounts of ordinary distilled H_2O to a D_2O stock having an assay of 99.78 mole % D_2O. The 1-cm absorbance of each solution was measured relative to the stock in the near-infrared region from 0.7 to 1.85 μ.

Two pronounced sets of absorption maximums were found – at 1.41 and 1.667 μ. Both have been previously identified with HOD vibrational modes.[7,8] Absorbances of the more intense, symmetrical maximums at 1.667 μ are given in

[5] J. R. Collins, *Phys. Rev.* 26, 771 (1925).

[6] J. A. Curcio and C. C. Petty, *J. Opt. Soc. Am.* 41, 302 (1951).

[7] J. W. Ellis and B. W. Sorge, *J. Chem. Phys.* 2, 559 (1934).

[8] J. Lecomte, M. Ceccaldi, and E. Roth, *J. chim. phys.* 50, 166 (1953).

Table 37. Differential-Absorbance (1 cm) and Concentration Data for Mixtures of H_2O and D_2O Run at 1.667 μ with a Cary Model 14M Spectrophotometer

Solution	H_2O (Mole %)		H_2O (M)	Absorbance (1 cm)
	Total	Sample – Reference	Sample – Reference	
Stock (D_2O)	0.22	0.00	0.00	0.000
1	0.44	0.22	0.12	0.025
2	0.68	0.46	0.25	0.051
3	1.16	0.94	0.52	0.105
4	1.94	1.72	0.95	0.184
5	3.85	3.63	2.00	0.403
6	7.73	7.51	4.14	0.811
7	15.63	15.41	8.51	1.536

Table 37. Figure 13 indicates that the data in this concentration range are in reasonable agreement with Beer's law.

The simplicity and sensitivity of this analytical method might well lend itself to rapid estimation of changes in the H_2O content of deuterated aqueous solutions in the presence of solutes such as uranyl sulfate and sulfuric acid (see also "Differential Temperature Absorption of Heavy and Light Water in the Visible and Near-Infrared Regions" and "Extension of Measurements of the Aqueous Absorption Spectra of Neptunium Ions," this report).

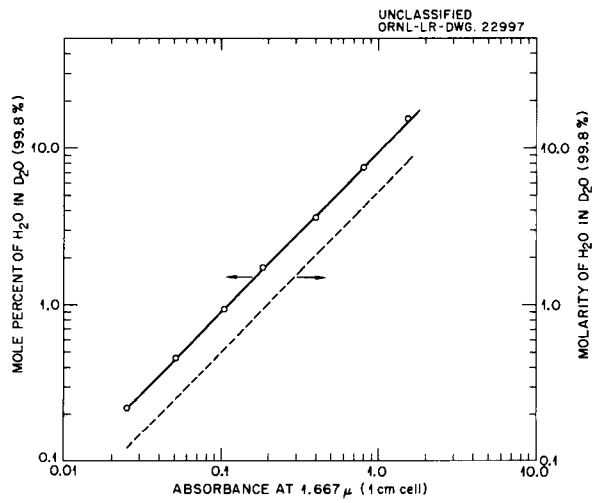

Fig. 13. The 1-cm Absorbance of H_2O-D_2O Mixtures vs D_2O at 1.667 μ as a Function of H_2O Concentration.

Extension of Measurements of the Aqueous Absorption Spectra of Neptunium Ions

During the first measurements of a neptunium solution (0.032 *M* Np^{237} in 1 *M* HNO_3, prepared by P. Lantz) using the Cary model 14M recording spectrophotometer, a strong, previously unreported absorption maximum was noted at 1.223 μ, just below the absorbance cutoff for 1 cm of H_2O. The spectrum below 1 μ indicated about 6% Np(V), and the remainder was deduced as Np(VI) from the broad, low maximums at 0.55 and 0.47 μ, and from the rapidly increasing absorbance toward the ultraviolet. A second solution was prepared as Np(VI) in 0.5 *M* $HClO_4$, and the peak at 1.223 μ ($\epsilon \simeq 45$) was tentatively assigned to the NpO_2^{++} ion.

Further confirmation of the Np(VI) band at 1.223 μ and the discovery and assignments of nine additional new absorption maximums (see Table 38) have been made by following the progressive catalytic reduction of a solution of $NpO_2(ClO_4)_2$ in 1 *M* $DClO_4$-D_2O over the range from 0.35 to 1.85 μ.

The neptunium solution used was prepared by fuming a 30-mg sample of Np^{237} (obtained from P. Lantz and G. W. Parker) to dryness twice with $HClO_4$. An excess of $HClO_4$, then added, was converted to $DClO_4$ by repeated dilution and evaporation with D_2O (99.8%). Finally, constant-boiling acid was evaporated to requisite weight for dilution to unit molarity in $DClO_4$.

Table 38. Estimated Molar Absorptivities and Valence Assignments of New Neptunium Maxima Below 1.85 μ

λ (μ)	Valence	ϵ
1.800	4	5
1.697	4	49
1.620	5	4
1.480	6	5
1.360	3	43
1.223	6	45
1.180	3	3
1.145	4	11
1.117	5	6
1.096	5	23

The concentration of Np^{237} in the deuterated sample was 0.0276 *M* by radiometric assay. One-molar $DClO_4$ for the reference cell was prepared from $HClO_4$ in the manner described for the neptunium sample.

A conventional 1-cm fused-quartz sample cell was fitted with a long neck and a Teflon stopper. Reduction of the sample was done outside the spectrophotometer by inserting a fine platinized platinum capillary helix through which a slow stream of $D_2(g)$ was passing.

The instrument was used with cell compartments thermostatted at 25°C. Undispersed radiation was passed through the cells, and slit operation was automatic, providing a constant power signal from the reference beam to the PbS detector.

Background absorbance was determined from 0.35 to 1.85 μ with 1 *M* $DClO_4$ in both cells. The oxidized sample was then scanned and reduced alternately until the neptunium was 98% converted into the III state.

The spectral curves in Fig. 14 represent the maximum concentration recorded, respectively, for Np(VI), (V), (IV), and (III) ions in the deuterated medium during reduction.

The valence composition given in Fig. 14 for each curve was determined from our data with aid of published results[9] for neptunium ions in 1 *M* $HClO_4$. Beer's law behavior and a negligible effect of change of solvent were assumed. The molar absorptivities computed for 19 bands between 0.428 μ and 1.023 μ are in reasonable agreement with the data of Sjoblom and Hindman if their curve for Np(V) is dropped 4 absorptivity units: $\epsilon_{obs}/\epsilon_{S.\,and\,H.} = 0.95 \pm 0.05$. We have found no evidence for this background absorption, either in $HClO_4$ or $DClO_4$ solutions, which also is not shown by the spectrum of Np(V) in HCl as measured by Hindman and co-workers.[10]

As yet we have not tested any of the absorption maximums for constancy of ϵ. However, the intensities of the sharpest bands, for example, 0.9600 μ and 0.9800 μ of Np(IV) and (V), respectively, did not appear to be sensitive to appreciable changes in slit width.

In line with a desire eventually to study neptunium ions in uranyl sulfate solutions, we have measured the 1-cm absorbance of 0.17 *M* UO_2SO_4 (40 g of U per liter) (furnished by S. H. Wheeler, Reactor Experimental Engineering Division) over the spectral region from 0.35 to 1.85 μ. The UO_2^{++} ion does not absorb appreciably between 0.5 μ and 1.85 μ ($\epsilon < 0.06$) and presumably will not interfere with estimation of neptunium ions or H_2O (see "A Spectrophotometric Method for Determination of H_2O in D_2O," this report) in deuterated media.

This preliminary work suggests a fruitful extension for spectrophotometry of aqueous solutions in general. There is little doubt but that many ions have characteristic absorption bands which occur in the spectral range accessible with deuterated aqueous solutions.

THE CELL Pt, H_2, $HCl_{(m)}$, AgCl, Ag AT HIGH TEMPERATURES

R. S. Greeley
M. H. Lietzke
W. T. Smith[11]
R. W. Stoughton

For over a year, work[12] has been proceeding on the problem of measuring the thermodynamic properties of dilute aqueous HCl solutions at elevated temperatures by using emf measurements of the

[9] R. Sjoblom and J. C. Hindman, *J. Am. Chem. Soc.* 73, 1744 (1951).

[10] J. C. Hindman, L. B. Magnusson, and T. J. La Chappelle, paper 15.2 in *Transuranium Elements*, NNES, vol IV-14B, Book II, p 1039, McGraw-Hill, New York, 1949.

[11] Chemistry Department, University of Tennessee.

[12] R. S. Greeley, Ph.D. thesis problem (University of Tennessee).

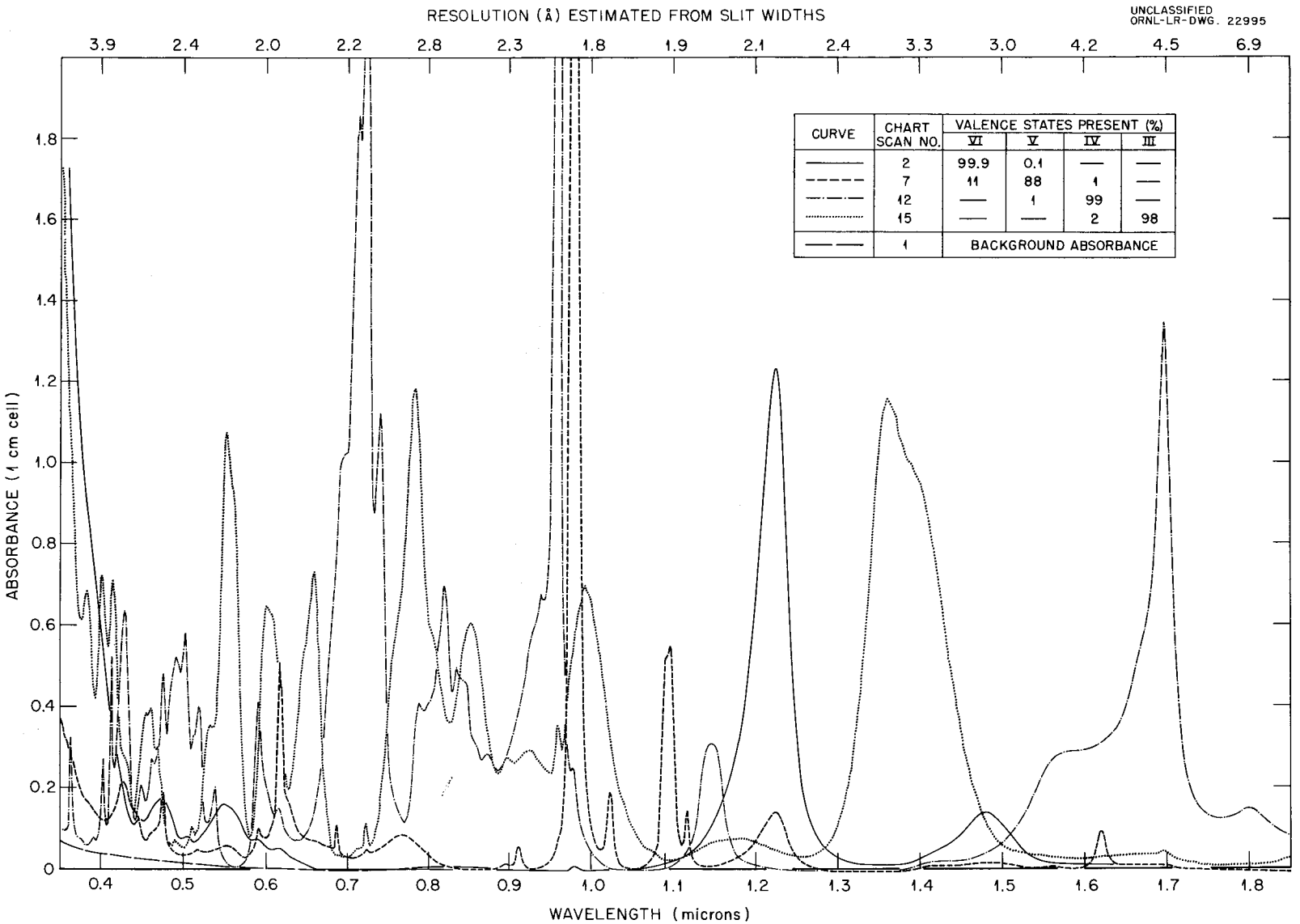

Fig. 14. Absorption Spectra of 0.0276 *M* Neptunium Perchlorate in 1 *M* $DClO_4$–D_2O from 0.35 to 1.85 μ.

hydrogen electrode vs the Ag-AgCl electrode. The apparatus has been assembled and final calibrations are now being carried out.

Preliminary runs have indicated two major problems:

1. If neglected, the increased solubility of AgCl at high temperatures may introduce a serious error in the calculations. Hence, it will be necessary to determine the solubility of AgCl in HCl as a function of acid concentration and temperature. If the AgCl solubility becomes high relative to the acid concentration, it will be necessary to evaluate the data in terms of a mixed AgCl-HCl electrolyte system.

2. The error in the emf readings may be as high as ±0.3 mv unless more complete shielding of the electrode leads is possible. Consultation with and help from the Instrumentation and Controls Division should solve this problem.

A HIGH-TEMPERATURE GLASS ELECTRODE

M. H. Lietzke R. W. Stoughton

A high-temperature pH meter (Canadian Aviation Electronics, Ltd.) will be used to study the pH of uranyl sulfate solutions, both with and without the addition of other electrolytes, as a function of temperature. The manufacturer claims that the electronic circuit of the amplifier has been so designed that it will provide an electrical output proportional to the "true pH" of the solution measured. Actually their temperature compensation device was designed to correct for the coefficient (RT/nF) of the log term in the Nernst equation only. However, it was found necessary in setting up the equipment to make several modifications so that it would function reproducibly. These modifications will be described in a separate memorandum.

The pH of solutions of ~0.01 m HCl and ~0.01 m H_2SO_4 has been studied over the range of 25 to 135°C. The observed pH of the ~0.01 m HCl increased from 2.13 to 2.17 as the temperature was increased from 25 to 123°C. The change predicted from activity-coefficient considerations amounts to +0.03 pH unit; hence the instrument seems to be functioning properly. The pH of the ~0.01 m H_2SO_4 solution increased from 2.06 to 2.45 as the temperature was increased from 25 to 135°C. In this case an increase in pH is to be expected since the second dissociation constant of the H_2SO_4 decreases appreciably with temperature. A program of high-temperature runs with uranyl sulfate solutions will be started soon.

THE CELL Pt, PbO_2, $PbSO_4$, $H_2SO_{4(m)}$, Ag_2SO_4, Ag AS A FUNCTION OF TEMPERATURE

J. V. Vaughen[13] M. H. Lietzke

A study has been made of the effect of dissolved Ag_2SO_4 on the activity of H_2SO_4 solutions by means of emf measurements. The results have been described in a paper[14] due to appear in September 1957. In this work the cell Pt, PbO_2, $PbSO_4$, $H_2SO_{4(m)}$, Ag_2SO_4, Ag was used and the thermodynamic functions were referred to an H_2SO_4 solution saturated with Ag_2SO_4. Figure 15 shows the variation of

$$k_m^{-1}\,\frac{a_{H_2SO_{4(m)}}}{a_{H_2SO_{4(0.3)}}}$$

as a function of temperature and H_2SO_4 concentration, both in the presence and absence of Ag_2SO_4,

[13] Stetson University.

[14] J. V. Vaughen and M. H. Lietzke, *J. Am. Chem. Soc.* (in press).

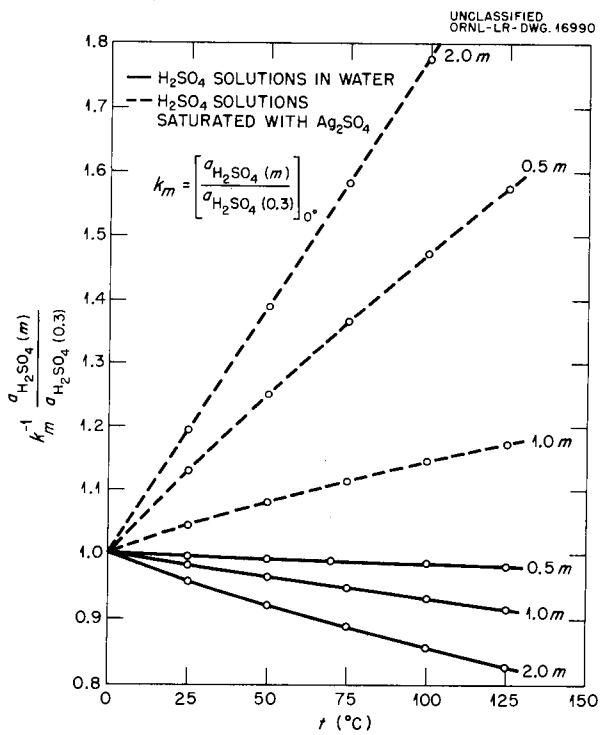

Fig. 15. Relative Activities of H_2SO_4 vs Temperature and Molality.

where

$$k_m = \left[\frac{a_{H_2SO_{4(m)}}}{a_{H_2SO_{4(0.3)}}}\right]_{0°C}$$

It is seen that in the absence of Ag_2SO_4 the values of the normalized ratios decrease as the temperature is raised and that values of the ratios at higher concentrations of H_2SO_4 decrease more than those at lower concentrations. In the presence of Ag_2SO_4, values of the activity-ratio function increase with temperature at all the concentrations studied. However, when the H_2SO_4 is saturated with Ag_2SO_4, the plot of the 2.0-*m*/0.3-*m* ratios lies above the other two plots, while the 1.0-*m*/0.3-*m* plot lies below that for 0.5 *m*/0.3 *m*. Although the activity ratios vary almost linearly with temperature in the presence of Ag_2SO_4, no simple relationship between activity and molality could be found based only on the assumption that H_2SO_4 acts like a 1-to-1 electrolyte and that the only important ionic species in solution are H^+, HSO_4^-, SO_4^{--}, and Ag^+. This is not surprising, however, since the HSO_4^- is slightly dissociated in the concentration range studied, the dissociation being larger at the lower concentrations of H_2SO_4. Moreover, the enhanced solubility of Ag_2SO_4 in the H_2SO_4 means a further change of species in solution, while the effect of ionic strength on the second dissociation constant of H_2SO_4 provides an additional complication. No completely satisfactory explanation of the inversion in order of the plot of

$$k_m^{-1}\ \frac{a_{H_2SO_{4(2)}}}{a_{H_2SO_{4(0.3)}}}$$

in the presence of Ag_2SO_4 could be obtained, although it may be tied in with the fact that the change of solubility of Ag_2SO_4 with H_2SO_4 concentration goes through a maximum in this range. The values of the H_2SO_4 activity ratios in the absence of Ag_2SO_4 were taken from the work of Harned and Hamer.[15]

[15] H. S. Harned and W. J. Hamer, *J. Am. Chem. Soc.* 57, 27 (1935).

A HIGH-TEMPERATURE ISOPIESTIC UNIT

B. A. Soldano R. J. Fox[16]
R. W. Stoughton

The following is a shortened version of an invited paper presented at an international Symposium in Theoretical Electrochemistry at the 111th Meeting of the Electrochemical Society in Washington, D.C., May 12–16, 1957. An expanded version of the material presented here will be submitted for publication with all the papers presented at the Symposium.

In view of the increasing emphasis being placed on high-temperature aqueous chemistry and in view of the success demonstrated for the isopiestic method at and near room temperature, it seemed highly desirable to investigate the feasibility of making isopiestic measurements at temperatures up to and above 100°C. One of the more common methods of obtaining such data at lower temperatures is to equilibrate dishes of solutions at constant temperature, then to open the equilibration vessel and rapidly put covers on the dishes, which are subsequently weighed. At elevated temperatures, however, such a procedure is not feasible because of the loss of solvent to the atmosphere when the equilibration vessel is opened. Therefore it was necessary to modify the method such that either the dishes would be sealed vapor-tight by remote control and then removed from the vessel and weighed, or that the dishes would be weighed inside the vessel. The latter alternative appeared both easier and more versatile; it held out the advantage of knowing that equilibrium had been attained before the dishes were removed from the elaborate vessel and thermostat. Also it held out the advantage of removing solvent vapor after equilibrium is established and before re-equilibrating, thereby covering both a temperature and concentration range before opening the vessel. The balance decided upon was in essence a magnetic balance developed by Stevens and Fox[17] for weighing in vacuum at room temperature, although major modifications had to be made for adaptation to a high-temperature, high-humidity environment.

[16] Engineering and Mechanical Division.

[17] D. K. Stevens and R. J. Fox, private communication.

The Apparatus

Figure 16 is a brief schematic diagram of the isopiestic unit, in which various parts are not necessarily drawn to scale. Figure 17 shows the equilibration vessel in more detail. The equilibration vessel is placed inside a thermostatted tank which is surrounded by an insulated box. The tank was made to hold oil although it has so far been used as an air thermostat. During equilibration the 19 silver dishes rest on a copper block which is supported on three legs, its only direct contacts with the equilibration vessel; an additional dish containing one of the standard weights rests on the balance. By means of the manipulating devices, a wheel is raised which catches the dishes by the lips and raises them off the copper block. Turning the wheel by means of the central shaft (Fig. 17) moves the dishes in a circle; then by means of the shaft lever the wheel may be lowered so that the index finger precisely fixes the circular motion into an exact new position. Each cog on the gear corresponds to a dish and a dish position, so that when the index finger has been in each position around the gear, each of the dishes has been brought in turn onto the balance. The seal of the shaft going through the head is made by means of a bellows and a conical, rotating vacuum seal, the latter involving three silicone rubber O-rings. The bellows permits the vertical movement of the shaft and the ring seal permits the rotation. Between the top two O-rings is an opening to permit application of an inert gas at a pressure roughly equal to the pressure inside the vessel in case this should be necessary in order to eliminate vapor loss through the conical seal. The stainless steel head is sealed to the vessel by means of a thin silicone-rubber gasket and 20 bolts (not shown). Also in the head is a tube with valve for evacuating the vessel at the start of a run or for removing vapor during a run. In the side of the equilibration vessel are two pipe leads. The one with a valve could be used to open the vessel to another one of known vapor pressure if feasible and if desired, and the other is used as a shield for wires which go through the vessel by means of a Kovar seal.

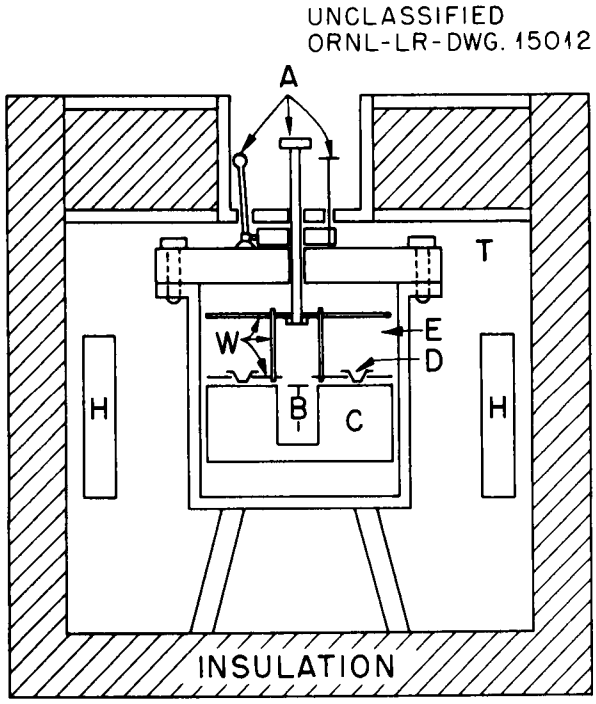

Fig. 16. Diagramatic Sketch of High-Temperature Isopiestic Unit. (*A*) Manipulating devices for transferring dishes; (*B*) magnetic balance; (*C*) copper block; (*D*) silver dish; (*E*) equilibration vessel; (*H*) heaters; (*T*) thermostatted tank; (*W*) wheel for transferring dishes.

Figure 18 shows a detailed drawing of the magnetic balance. The balance is constructed mostly of titanium, a nonferro magnetic corrosion-resistant metal. One of the pans contains a titanium tare which is approximately equal to but less than the weight of a silver dish. The weight on the dish is balanced by means of a magnetic field pushing upward on an Alnico magnet fastened to the beam. The strength of the field is proportional to the current flowing through a Teflon-covered silver-wire coil. The required current is effectively measured by reading, with a Rubicon B potentiometer, the potential drop across a standard resistance in series with the coil. The null position of the balance is determined by means of a microformer pickup. Both the balance beam and the pan are supported by Elgiloy ribbon fibers. In order to avoid excessive loss of sensitivity due to the rigidity of the beam fiber, the center of gravity is kept above the fiber by means of the sensitivity and buoyancy bobs. By a proper set of these bobs a partial correction for buoyancy is also effected. An error also results from the fact that the positioning of the dishes on the pan is not quite perfectly reproducible. This error is minimized by mechanically twisting the pan fiber before inserting it, so that its spring constant is effectively lessened considerably.

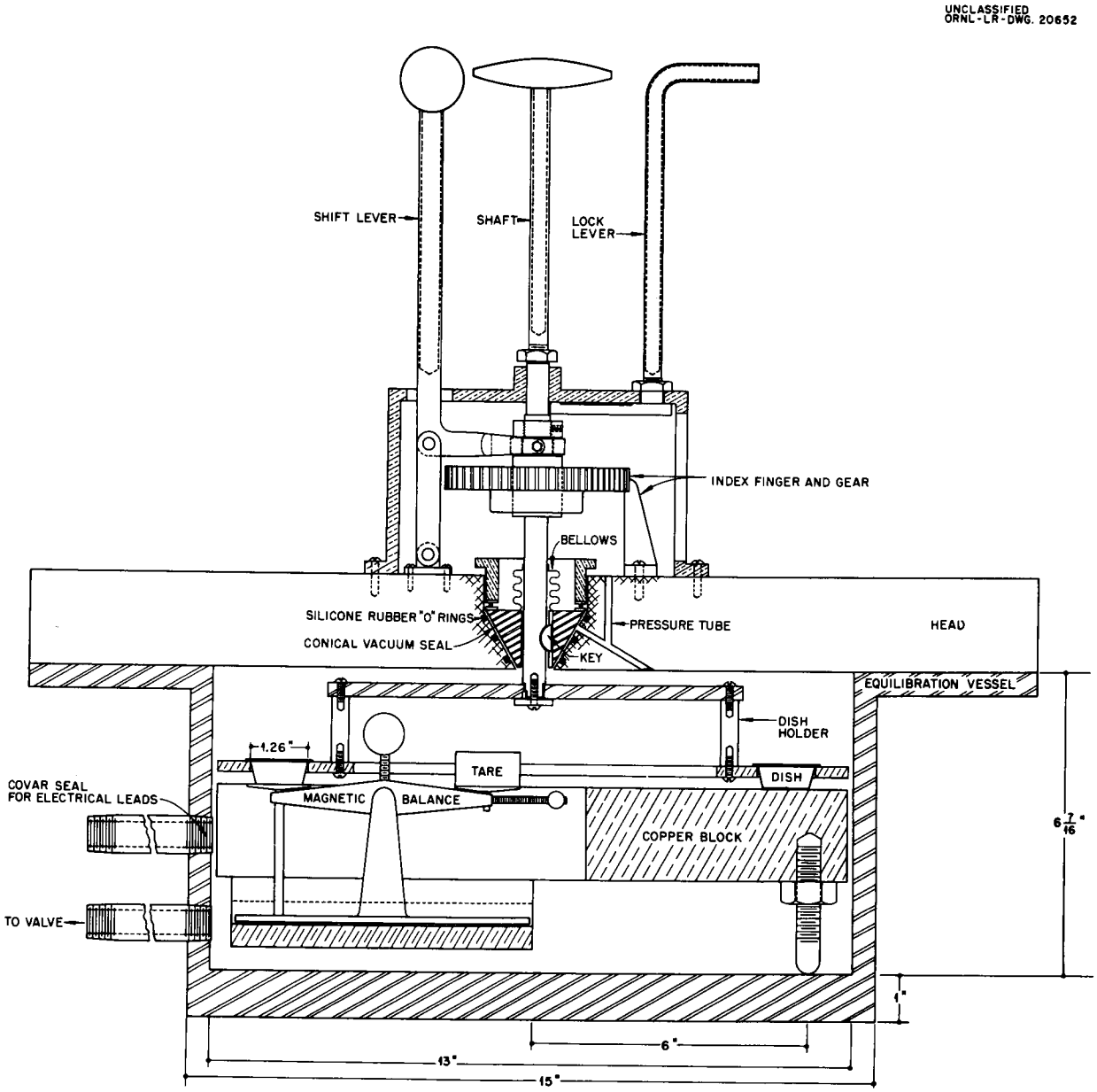

Fig. 17. Equilibration Vessel for Isopiestic Unit.

Figure 19 is an abbreviated schematic diagram of the null-point-detecting equipment of the balance. The microformer comprises a soft iron core which is moved by the balance "pointer" along the axis of three adjacent coils. The two outermost coils are in series but are wound in opposite directions so that current will tend to flow in one direction or the other through both these coils whenever the iron core is not exactly centered. The condition of balance is then read with a Brown amplifier and detector. It is, in principle, possible by electronic compensation to use the balance even though the electronic and geometric null points do not coincide. However, in actual practice it was found that the

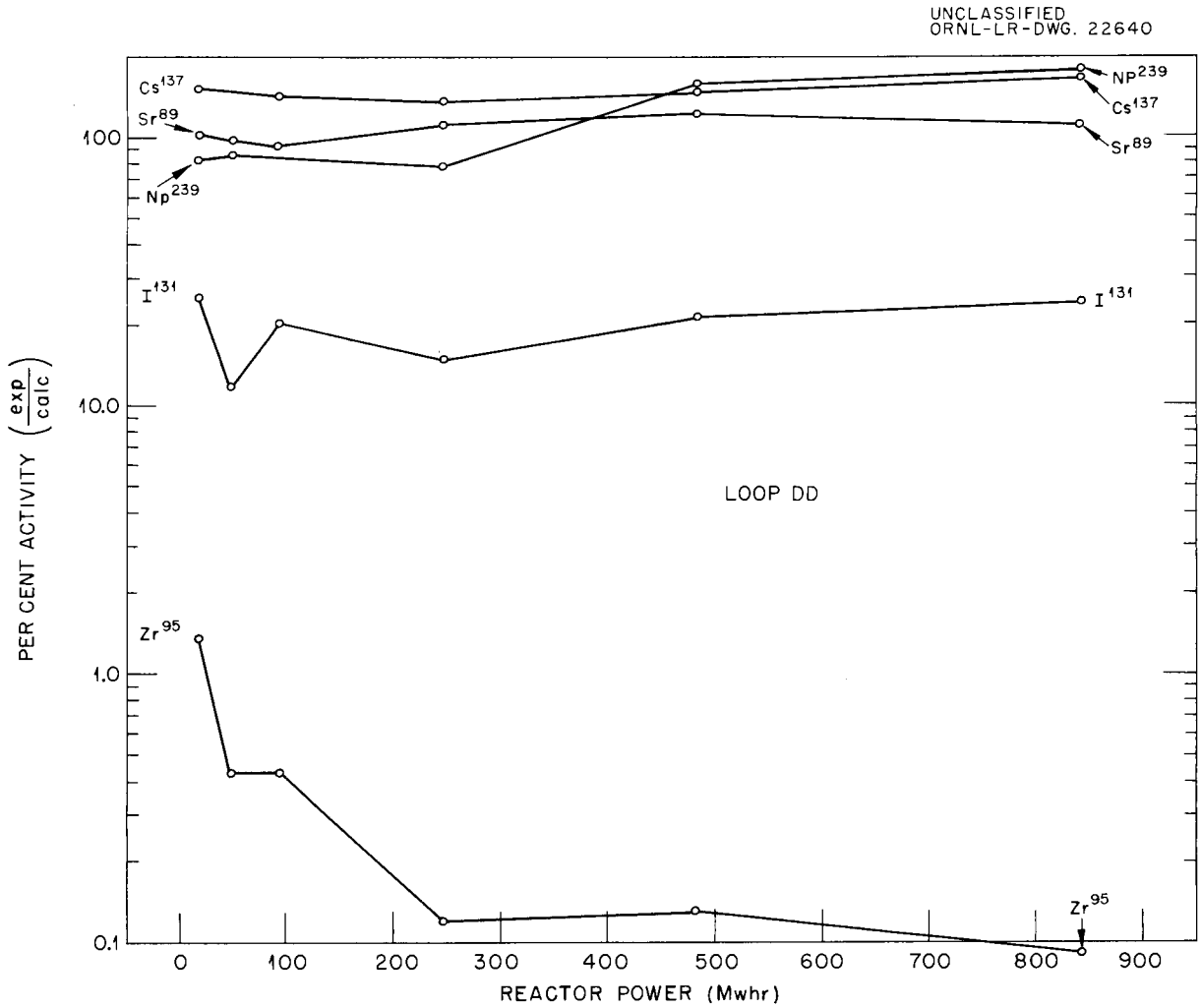

Fig. 18. Magnetic Balance for Isopiestic Unit.

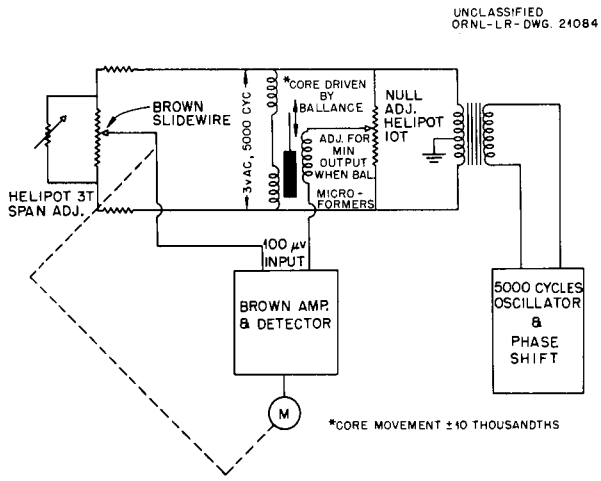

Fig. 19. Diagramatic Sketch of Magnetic Balance Null-Point Detector.

two null points must coincide (or very nearly coincide) or the balance performance is markedly adversely affected.

Operability and Results

The operability of the equipment has been tested up to 140°C with evacuation, with air present, and in the presence of water vapor (slightly less than the pressure in equilibrium with pure water), but without samples in the dishes.[18] The short-time operability appeared to be entirely satisfactory without samples in the dishes. A test of the water transfer rate was then made at 83°C by starting with several dishes containing 2.45 *N* NaCl and

[18] B. A. Soldano and R. W. Stoughton, *Chem. Semiann. Prog. Rep. June 20, 1956*, ORNL-2159, p 56–59.

several containing 0.49 N NaCl. At this temperature, equilibrium appeared to be attained in from one to two weeks. Since no mechanism for stirring the solutions had been incorporated into the design except that incidentally incurred during the manipulations for weighing, the time required for attaining equilibrium was undoubtedly limited by the rates of diffusion in the liquids. In order to get a measure of the effective rates of attaining equilibrium vs temperature, runs were planned for temperatures of about 45, 80, and 105°C. In the first of these runs some 17 salt solutions including alkali halides at about 1 N, and Na_2SO_4, $MgSO_4$, and UO_2SO_4 solutions along with NaCl standards and a large reservoir of 0.5 N NaCl were equilibrated at 46.5°C. This run was purposely started at conditions far from equilibrium in order to test equipment operability; it is well known that the required time can be greatly decreased by starting at concentrations very near to the anticipated equilibrium values.

After about six weeks the solutions were still a few per cent off their anticipated equilibrium values, and at this point a spill inside prevented further equilibration. As a result of these observations and further runs at 75, 83, 92, and 105°C, it appears that the required times of equilibration are roughly 60, 10, and 3 days at 45, 85, and 105°C, respectively. While the times required near 100°C are satisfactorily short, those around 45°C are undesirably long, and it is preferred that data also be obtained at the lower temperatures. Two relatively simple methods of providing a greater measure of stirring are now being considered for incorporation into the present unit. It is anticipated that with these changes and by starting with more favorable concentrations, the unit will operate satisfactorily throughout the temperature range mentioned as well as at still higher temperatures.

So far the emphasis has been on testing operability over a wide range of conditions. Attempts have not yet been made to push the sensitivity, accuracy, and the lowest feasible concentrations to the limit, although such tests will be made in the future. As will be seen below, the osmotic coefficients of the alkali chlorides and bromides (except for the lithium salts) change very little with temperature, and hence considerable accuracy will be required to determine their temperature changes.

Figure 20 shows the equilibrium molalities of several salts vs the molality of KCl at 91.5°C.

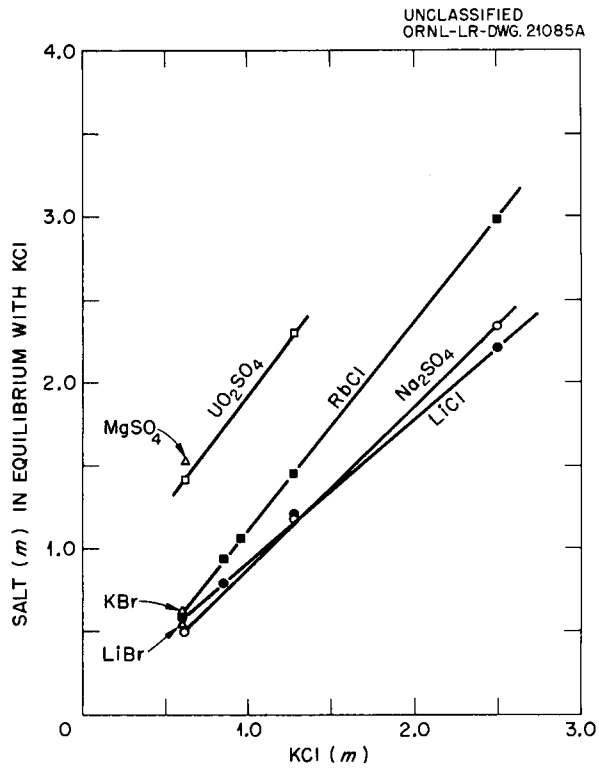

Fig. 20. Solution Behavior as a Function of Concentration at 91.5°C.

Tables 39 and 40 show the relative osmotic coefficients of several salts compared with KCl at 91.5 and 104.6°C at arbitrary concentration values. These were calculated from the equilibrium data as follows.

By definition, for any solute in water,

$$\nu m\phi \equiv -\frac{1000}{M_w} \ln a_w ,$$

where ν is the number of ions per mole in the assumed standard state, m is the molality of solute, ϕ is the osmotic coefficient, M_w is the molecular weight of water, and a_w is the activity of water. It then follows that at equilibrium the products $\nu m\phi$ for all solutes in different solutions in the same vessel are equal. Hence the ratio R of the osmotic coefficient of any solute to that of a standard is given by the inverse ratios of the νm products:

$$R = \frac{\phi}{\phi_{std}} = \frac{(\nu m)_{std}}{(\nu m)} .$$

Table 39. Comparative Osmotic Coefficient Ratios at 25 and 91.5°C

$$R = (\nu m)_{KCl}/(\nu m)_{salt}$$

Salt	25°C*		91.5°C	
	m	R	m	R
KCl	(0.610)	(1.000)	0.610	1.000
RbCl	0.618	0.988	0.616	0.99
CsCl	0.635	0.961	0.620	0.984
NaF	0.622	0.981	0.579	1.055
LiBr	0.561	1.088	0.544	1.123
NaBr	0.585	1.043	0.580	1.050
KBr	0.606	1.007	0.617	0.990
$MgSO_4$	1.038	0.588	1.505 1.520	0.403
UO_2SO_4	1.091	0.559	1.455	0.419
Na_2SO_4	0.532	0.765	0.500	0.813

*Data from R. A. Robinson and R. H. Stokes, *Electrolyte Solutions*, Academic Press, New York, 1955.

Table 40. Comparative Osmotic Coefficient Ratios at 25 and 104.6°C

$$R = (\nu m)_{KCl}/(\nu m)_{salt}$$

Salt	25°C*		104.6°C	
	m	R	m	R
$LiClO_4$	0.848	1.158	0.813	1.208
LiCl	0.880	1.114	0.755	1.301
NaCl	0.992	1.064	0.926	1.060
KCl	0.982	(1.000)	0.982	(1.000)
RbCl	0.996	0.986	1.015	0.968
CsCl	1.030	0.953	1.035	0.949
NaF	1.010	0.972	0.962	1.021
$MgSO_4$	1.515	0.648	2.15 2.18 2.01	0.464
Na_2SO_4	0.907	0.719	0.835 0.845	0.779

*Data from R. A. Robinson and R. H. Stokes, *Electrolyte Solutions*, Academic Press, New York, 1955.

The values of R at 25°C were calculated from data published by Robinson and Stokes,[19] and these are shown in Tables 39 and 40 for comparison at the same KCl concentrations. Robinson and Stokes' data at 25°C and in the range of 60 to 100°C also show that the osmotic coefficients of NaCl and KBr change very little with temperature (at least in this range), and hence the conclusions drawn from Tables 39 and 40 concerning the values of R also hold for the values of ϕ.

It is seen that the osmotic coefficients of the alkali chlorides and bromides (except for the lithium salts) change relatively little with temperature; that those of lithium chloride, bromide, and perchlorate as well as those of sodium fluoride and sulfate increase appreciably with temperature; and those of magnesium and uranyl sulfate decrease markedly with increasing temperature.

In three cases in Tables 39 and 40 the molalities are shown for the weights in duplicate or triplicate dishes. In the values for $MgSO_4$ at 104.6°C the weights of solution were only about 0.3 g (i.e., about 0.2 g of water and 0.1 g of salt) out of about 13.1 g for dish plus solution, and hence they represent an unfortunately low sample-to-dish-weight ratio. In general, duplicate dishes show weights of solutions which agree to within 1% or better. In the same dish, weight changes of about 0.1% of the solution weight can be detected.

The factors which appear to limit the accuracy at the present time are the following:

1. The temperature control is not adequate and appears to be erratic in its behavior. Long-term instabilities are reflected as weight changes and frequently can be detected. Better means of controlling the temperature are now being discussed with members of the Instrumentation and Controls Division.

2. Some sort of stirring or agitation is required at least for the lower temperature work. Simple steps are now planned for improving this situation.

3. Corrosion of dishes and spilling of liquid are perhaps the next most important items. It is well known that R. H. Stokes reported corrosion problems with silver dishes – particularly with bromide salts – at room temperature, and it is unreasonable to hope that corrosion will not be a greater problem

[19] R. A. Robinson and R. H. Stokes, *Electrolyte Solutions*, Academic Press, New York, 1955.

at higher temperatures. Platinum dishes of a new design are now being considered.

4. There are a number of miscellaneous problems concerned with optimizing the material of construction and the shape of the head gasket, sheathing and insulation for the wire leads and the balance coil, etc. These will be solved in the natural course of events.

All the above factors were anticipated; however, in an attempt to minimize costs, known risks were taken. The indicated steps are now being considered to correct all these factors.

THE BASE-SATURATED REGION OF THE SYSTEM CuO-UO_3-SO_3-H_2O AT 100°C

F. E. Clark R. Slusher C. H. Secoy

In a previous report[20] the results of a series of equilibration experiments in the four-component system, CuO-UO_3-SO_3-H_2O, were reported. In this earlier work the identification of solid phases depended entirely on the extrapolation of tie lines and microscopic observation of the solids. A new series of equilibration studies has now been completed in which synthetic compositions were selected so as to extend the concentration range and to supply further information concerning regions left in doubt by the earlier work. Furthermore, x-ray powder patterns of the solids were obtained in most cases to contribute to their identification.

The experimental procedure was identical with that followed in the earlier work. Equilibration times varied from about 70 to 190 days. Synthetic mixtures were prepared by mixing appropriate amounts of stoichiometric uranyl sulfate solutions with stoichiometric copper sulfate solutions and adding solid $UO_3 \cdot H_2O$ in excess of saturation. The use of CuO as a saturating solid was discontinued (except for mixes containing no uranium) because of its tendency to form clumps which would not readily mix with the solution. The equilibration vessels were sealed pyrex glass tubes.

After the equilibration period, liquid-phase samples and wet-solid residues were analyzed for uranium, copper, and sulfate by methods described previously.[20] Comparison of the x-ray powder patterns for the various solid residues with ASTM standards served to identify three crystalline species in the system. These were (1) α-$UO_3 \cdot H_2O$, (2) $3CuO \cdot SO_3 \cdot 2H_2O$, mineral name, antlerite,[21] and (3) the basic complex salt with the mineral name johannite,[22] $CuO \cdot 2UO_3 \cdot 2SO_3 \cdot 7H_2O$. In addition, the pattern for some of the solids, particularly those containing α-$UO_3 \cdot H_2O$, showed a set of lines which was not immediately identified. The first clue to the identity of the substance contributing these lines came when it was noted that the pattern matched that reported by Dawson and co-workers[23] for a solid they obtained by heating UO_3 slurries in glass-lined autoclaves. They called the substance phase III oxide and concluded that it was a new crystal modification of a hydrated UO_3. It was noted also that the x-ray pattern was very similar to, but not identical with, that reported by Marshall and Gill[24] for uranyl orthosilicate trihydrate which they prepared by the action of uranyl fluoride solution on glass at 300°C. All lines seemed to be shifted in position relative to those reported by Marshall and Gill.

A study of the behavior of liquidus points with respect to the equilibrated solids gave a strong indication that this new solid phase was an "impurity" in the four-component system. In the previous work just such an indication was explained away by assuming the existence of a solid solution. In order to verify these suspicions, several of the solids in which the presence of the "impurity" had been disclosed by the diffraction pattern were analyzed for silica. In all cases it was found to the extent of several per cent, an amount sufficient to account for the solid as a mixture of α-$UO_3 \cdot H_2O$ and $(UO_2)_2SiO_4 \cdot 3H_2O$.

The preparation of the silicate by the action of uranyl fluoride on glass was repeated by following the procedure of Marshall and Gill exactly. The diffraction pattern for this preparation was identical with that of the unknown. As to why the pattern for the original silicate preparation was slightly shifted, one can only speculate. Perhaps the material was actually different or perhaps the

[20] F. E. Clark, R. Slusher, and C. H. Secoy, *Chem. Semiann. Prog. Rep. June 20, 1955*, ORNL-1940, p 79.

[21] E. Posnjak and G. Tunell, *Am. J. Sci.* 218, 1–34 (1929).

[22] C. S. Hurlbut, Jr., *Am. Mineralogist* 35, 531–5 (1950).

[23] J. K. Dawson *et al.*, *Some Aspects of the System UO_3-H_2O*, AERE-C/R-1703 (Sept. 14, 1955).

[24] W. L. Marshall and J. S. Gill, *J. Am. Chem. Soc.* 79, 1300 (1957).

machine calibration was in error. The position and relative intensities of the lines of the new diffraction pattern are given in Table 41.

Although the composition of the liquid phase has probably not been greatly changed by the presence of the silicate in the solids, the data will not be reported until the magnitude of this effect has been determined by experiments in an inert vessel. Figure 21 shows the projections of the liquidus binaries on the UO_3-CuO and UO_3-SO_3 faces of a three-dimensional model. The liquidus-composition regions for the stable existence of each of the solid phases are indicated as well as the region in which the solids were contaminated by the presence of the silicate.

Table 41. X-Ray Powder Pattern for Uranyl Silicate

d	*I*	*d*	*I*
6.30	S–	1.90	S–
4.79	M	1.85	S–
4.66	VW	1.83	VW
4.50	S	1.76	M–
3.95	VW	1.73	W
3.75	M–	1.70	M
3.30	S+	1.66	M+ (B)
3.25	M–	1.64	M
2.97	M	1.59	M
2.79	M	1.58	M
2.70	M+	1.55	W
2.65	W	1.51	M– (B)
2.46	S–	1.49	VW
2.39	VW	1.47	W
2.31	W	1.44	VW
2.24	M–	1.40	M (B)
2.20	M–	1.37	W
2.14	VW	1.35	M
2.08	M	1.34	M–
2.06	W	1.33	M–
2.03	M	1.30	VVW
1.97	S–	1.28	VVW

The extensive x-ray studies made in connection with this work were by R. L. Sherman of the Analytical Chemistry Division and by R. D. Ellison of the Chemistry Division. The valuable assistance of both is gratefully acknowledged.

CHARACTERIZATION OF SLURRY FLOCCULATION BY pH MEASUREMENTS

F. H. Sweeton

The peptization states of ThO_2 slurries, which are being studied for use as reactor blankets, are difficult to characterize. At the present time H_2SO_4 is commonly added to control the peptization state, but reproducible results are difficult to obtain. The acid is thought to affect peptization by reacting with the ThO_2 surface to change its electrostatic potential and also the ionic atmosphere associated with the charged surface.

Determination of the pH of such slurries appears to be a way to improve the characterization of their peptization states. The pH reading indicates the effective acid concentration in the solution, and this acid is in equilibrium with the acid that is associated with the ThO_2 surface and which is a major factor in determining the peptization state.

The measurement of the pH of a ThO_2 slurry does not appear to be simple. In order to use a calomel electrode, which can have junction-potential errors when used in a slurry, measurements need to be made in the supernatant phase that is in equilibrium with the slurry. Since the supernatant is very dilute until a considerable amount of acid has been added, the measurements can be expected to be very sensitive to small amounts of impurities such as CO_2 from the air.

The objective of the present study is to develop the apparatus and techniques necessary for making room-temperature pH measurements of ThO_2 slurries to which acid has been added. If the results are sufficiently precise, the methods would be available to use in the slurry program for correlating pH measurements with the slurry-handling properties. The initial work has been confined to the preparation and measurement of purified water, which should be at least as difficult to handle as the slurry supernatants.

A variety of cells for measuring pH have been tried, all using small, commercial glass and calomel electrodes (Beckman numbers 290 and 270). The first cells were constructed of pyrex glass, the electrodes being held in rubber stoppers. The

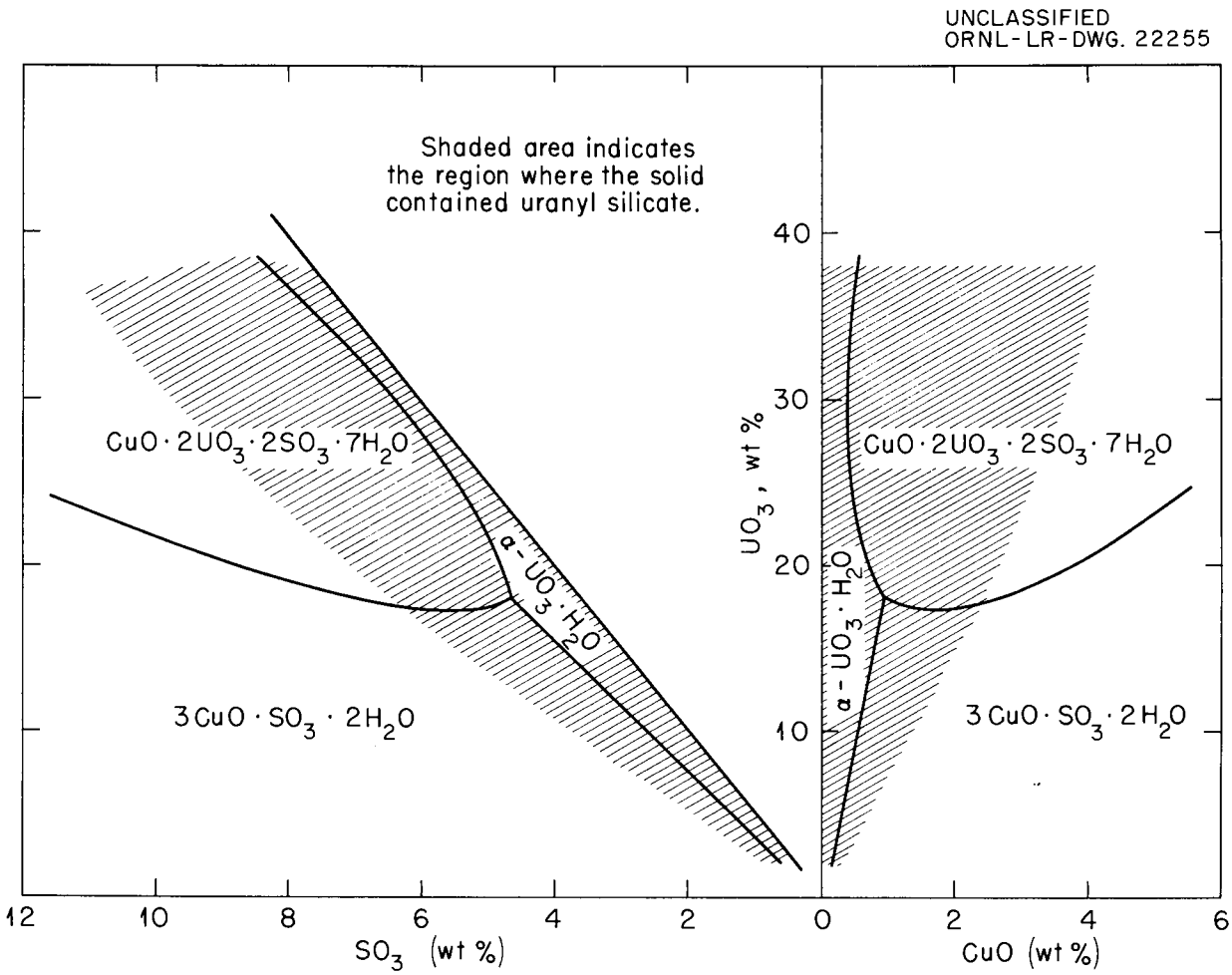

Fig. 21. Projections of the Liquidus Surfaces in the System $CuO-UO_3-SO_3-H_2O$ at 100°C.

next cell was of silica glass with the electrodes held in Teflon sleeves. The final model was itself constructed of Teflon.

Water was prepared in several ways. Purification of laboratory-distilled water by passage through a "Deeminizer" ion-exchange column gave water with pH readings between 5.3 and 6.0. A single distillation of the laboratory-distilled water from alkaline $KMnO_4$ in a one-stage still gave a product with a pH reading as high as 8.2 in the early part of each batch. When the water was first distilled from H_2SO_4, the final product varied between 5.8 and 7.7.

In order to get more consistent results, a two-stage still was set up in which water was first distilled from alkaline $KMnO_4$ and then from H_3PO_4. The second condenser was constructed of platinum. The pH cell was permanently attached to the still system in order to eliminate the chance of CO_2 contamination during transfer of the distillate from the still to the cell. The pH of the water from this system varied between 6.0_5 and 6.7. The pH reading could be raised to between 6.9 and 7.0 by bubbling purified air through the water. These results are being accepted as sufficient to show that the methods used are now ready for trial with slurry supernatants.

Apparatus has been designed, fabricated, and assembled for determining a titration curve for a slurry prepared from ThO_2 recalcined in a vacuum. Provision has been made for excluding carbon dioxide from the air throughout the process.

HOMOGENEOUS CATALYSIS OF THE HYDROGEN-OXYGEN REACTION IN AQUEOUS SOLUTIONS

H. F. McDuffie H. H. Stone

Study of the hydrogen-oxygen reaction, catalyzed by dissolved copper salts, was resumed during the past year after a lapse of several years. Although the previous work provided an adequate basis for application of the reaction to the internal recombination of radiolytic gas produced in a homogeneous reactor, and for application to the operation of in-pile corrosion test loops under nonexplosive conditions, many details of the reaction remained to be elucidated. Questions concerning the effects of higher acidity on the reaction rate were raised as the HRP found excess acid necessary for phase stability of reactor-fuel solutions at progressively higher temperatures. Information concerning reaction rates in heavy-water systems was desired for use in the design of larger reactors, while information concerning the effects of various additives, proposed for corrosion control, became of interest in order to permit the evaluation of a wider range of possible fuel and blanket systems. The otherwise desirable characteristics of the uranium carbonate system called for a search for a suitable homogeneous catalyst for this system.

During the interim period following publication of the now-declassified recombination information,[25] there has been much interest in the homogeneous catalysis of reactions involving dissolved molecular hydrogen. Winfield[26] has reviewed the general field of these reactions. Halpern and coworkers from the University of British Columbia have published extensive studies of copper-catalyzed reactions of hydrogen in aqueous solutions – studies which, although at lower temperatures than those of reactor interest and under somewhat different conditions, have, nevertheless, confirmed and extended the ORNL results and have provided stimulating evidence in support of a proposed mechanism for the reaction.

Studies in the Perchlorate System

Cupric perchlorate was tested in the previous ORNL work in hopes of thus obtaining a measurement of the catalytic activity of uncomplexed copper ions at 250°C. The specific reaction-rate constant was reported[25] as being 5000 $M^{-1}hr^{-1}$, and there was no indication that perchloric acid in excess of that required for phase stability affected the rate of the reaction. Peters and Halpern[27] studied the reaction of hydrogen with acidified dilute cupric perchlorate solutions over the temperature range of 80 to 140°C and reported that the specific reaction-rate constant was expressed by the equation,

$$(1) \quad k = 1.0 \times 10^{13} \exp \frac{-26{,}600}{RT} \; M^{-1} \min^{-1}$$

Figure 22 illustrates the excellent agreement between an extrapolation of this equation to 250°C and the results of ORNL measurements at this temperature.

[25] H. F. McDuffie *et al.*, ORNL CF-54-1-122 (Jan. 26, 1954) (Classified).

[26] M. E. Winfield, *Rev. Pure and Appl. Chem.* 5, 217 (1955).

[27] E. Peters and J. Halpern, *J. Phys. Chem.* 59, 793 (1955).

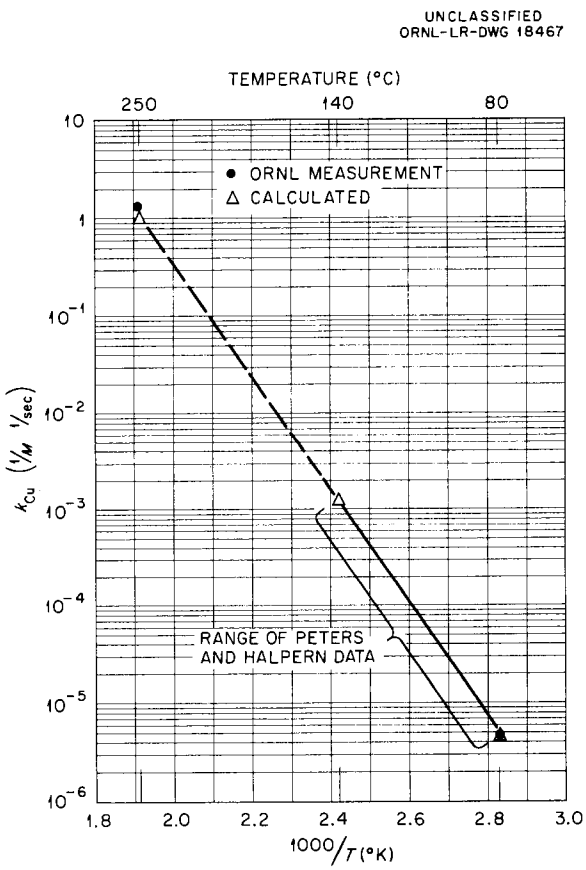

Fig. 22. Homogeneous Catalysis by Cupric Perchlorate.

When Halpern, Macgregor, and Peters[28] tested the effect of added perchloric acid (up to 1.0 *M*) upon the catalytic activity of cupric perchlorate at 110°C, they found a substantial lowering of the rate as the acidity was increased. Moreover, they found that at high acidity the rate was dependent upon the second power of the copper concentration, whereas it had been known that at low acidity the rate was dependent upon the first power of the copper concentration. They have interpreted their data in terms of a mechanism involving the species CuH^+ as a postulated intermediate, as indicated by the following equations:

$$(2) \qquad Cu^{++} + H_2 \underset{k_{-1}}{\overset{k_1}{\rightleftharpoons}} CuH^+ + H^+$$

$$(3) \qquad CuH^+ + Cu^{++} \xrightarrow{k_2} 2\,Cu^+ + H^+$$

$$(4) \qquad 2\,Cu^+ + \text{oxidant} \xrightarrow{\text{fast}} 2\,Cu^{++}$$

It will be observed that the hydrogen ion, H^+, can participate in the reaction because of its presence in the equilibrium; the extent of its participation will depend on its concentration and the magnitude of the constant k_{-1} vs the concentration of Cu^{++} and the magnitude of the constant k_2. Based on a steady-state treatment of the intermediate CuH^+, Halpern *et al.*,[28] derived the following kinetic expression for the rate of the reaction:

$$(5) \qquad \text{Rate} = \frac{-d[H_2]}{dt} = \frac{k_1\,[Cu^{++}]^2\,[H_2]}{[Cu^{++}] + \frac{k_{-1}}{k_2}\,[H^+]}$$

Inverting this expression gives the following equation, which is in suitable form for displaying and interpreting experimental results:

$$(6) \qquad \frac{1}{R} = \frac{1}{k_1\,[Cu^{++}]\,[H_2]}\left[1 + \frac{k_{-1}}{k_2}\,\frac{[H^+]}{[Cu^{++}]}\right]$$

At low acidity the rate should be proportional to the first power of the copper concentration, and at high acidity the rate should become proportional to the second power of the concentration of copper; this was observed by Halpern *et al.* At a constant copper concentration a plot of $1/R$ vs acidity should give a straight line with a slope proportional to the ratio k_{-1}/k_2. Halpern's data indicated that, at 110°C, the value of this ratio was 0.25. The ORNL studies of cupric perchlorate plus perchloric acid (up to an acid-to-copper ratio of 50) did not show any indication of an acid effect; that is, the k_{-1}/k_2 ratio was zero. Although there was no demonstrated inconsistency, since the temperatures were different, it appeared to be desirable to conduct additional work so as to provide either confirmation of this mechanism or the basis for an alternative explanation of the data. It is not unlikely that the explanation lies in the effect of temperature upon the three rate constants involved; this effect could easily be such as to suppress k_{-1} relative to k_2 as the temperature is raised. Experiments with the perchlorate system at intermediate temperatures are now in progress to furnish the desired information.

Studies in the Sulfate System

It had already been reported[25] that the addition of up to 0.05 *M* sulfuric acid to solutions containing 0.001 *M* cupric sulfate reduced the catalytic activity of these solutions at 250°C as the acidity was increased. A plot of the experimental data covering the range of 0.005 to 0.050 *M* sulfuric acid in the form of $10^5/k_{Cu}$ vs the molar concentration of acid is presented as Fig. 23. (Sulfuric acid is treated as a monobasic acid because the second ionization constant becomes very small at

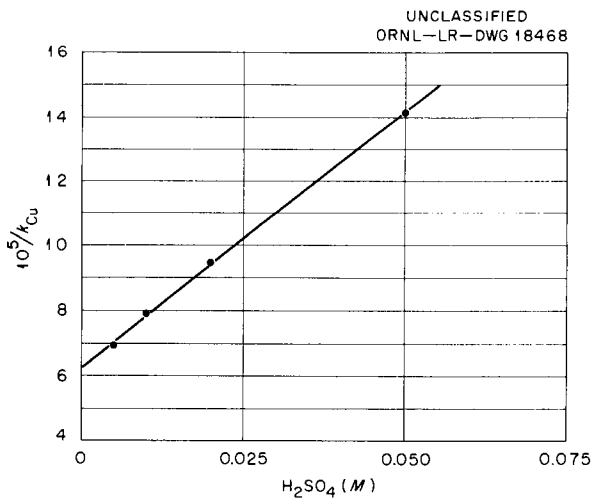

Fig. 23. Effect of Acidity upon the Catalytic Activity of 0.001 *M* Cupric Sulfate at 250°C.

[28] J. Halpern, E. R. Macgregor, and E. Peters, *J. Phys. Chem.* 60, 1455 (1956).

the elevated temperatures.) The observed relationship between the reciprocal rate, $10^5/k_{Cu}$, and acidity appears quite linear, and would be consistent with the type of explanation for the reaction mechanism advanced by Halpern. The ratio of k_{-1}/k_2 calculated from these results is 0.0258, indicating that although the effect of acid is quite noticeable in the sulfate system at 250°C, the actual value of k_2 is far larger (38.75 times) than k_{-1}. Since ORNL already had considerable experience with the sulfate system, and since an acidity effect at 250°C had been demonstrated in this system but not in the perchlorate system, a series of experiments at intermediate temperatures was planned to determine the effects of acidity and copper concentration. The techniques and nomenclature are the same as those previously reported[25] except that titanium bombs, fittings, and capillary tubing are being used in order to minimize corrosive interference.

The interpretation of the experimental results is based on the previously derived[25] relationship between the experimentally observed first-order rate of pressure decrease, k_π, and the experimentally established ratio of gas volume to liquid volume:

$$\frac{1}{k_\pi} = \frac{1}{k_{sol}} + \left(\frac{V_g}{V_l}\right)\left(\frac{\alpha}{RTk_{sol}}\right) .$$

The value of k_{sol}, the reaction-rate constant for a particular solution, is obtained by extrapolating the least-squares line through the experimental points to the condition $V_g/V_l = 0$, that is, where there would be no gas phase present from which hydrogen would have to be transferred to the solution during the reaction. A value for the solubility, α (concentration of dissolved hydrogen $= P/\alpha$), is obtained from the slope of the least-squares line and the extrapolated value for k_{sol}. It has been assumed that the solubility and the solution-rate constant are essentially independent of each other and that agitation of the solution has been sufficient to maintain, throughout the solution, the equilibrium concentration of dissolved hydrogen required by the experimentally determined value for α. It has also been assumed that the rate of approach to the solubility equilibrium is very fast relative to the subsequent rate of reaction of the dissolved hydrogen with the copper-catalyst species.

It will be noted that the necessity for extrapolating to obtain k_{sol} introduces more variance into the estimate of this value than is contained in the slope itself; subsequent use of k_{sol} with the slope to obtain α means that this additional variance is also introduced into the measurement of α. As a practical matter it is fortunate that the slope contains the product of the solubility and rate effects in such a combination that it can be used for reactor calculations (based on hydrogen pressure) with less variance than either of the two ultimate quantities of interest to kineticists. Experiments with the sulfate system (cupric sulfate–sulfuric acid) have been performed at 175 and 200°C over a range of copper concentrations and added acid concentrations.

The experimentally determined solution-rate constants are presented in Figs. 24 and 25 as $k_{sol}/[Cu]$ vs nominal acidity for 175 and 200°C. The number of experiments which were used in the least-squares line is indicated by each datum point. The correction for copper concentration is based on the simplest assumption, that the activity of the solution is directly proportional to the copper concentration. The decrease in activity with increasing acidity up to about 0.05 *M* (nominal – at room temperature) appears real; above this acidity the activity may be constant within experimental error. It has tentatively been speculated that there may be more than one catalytically active copper species and that the effect of increasing acidity is to convert the various more-active species into some one less-active species.

When the solubility values associated with these solutions were examined (in terms of $10^4/\alpha$ so that an increase in solubility would show as an increase in the value), it appeared that, for a given acidity and temperature, the solubility was proportional to the square root of the copper concentration; therefore, the experimental-solubility values were divided by the square root of the copper concentration in order to obtain the values plotted vs nominal acidity at 175 and 200°C in Figs. 26 and 27. The internal consistency of the results is considered satisfactory support of the choice of the square-root function. The substantial effect of acidity on the solubility, with maximal solubility at around 0.05 *M* nominal sulfuric acid concentration, suggests that changes in the responsible species are occurring as the acidity is changed.

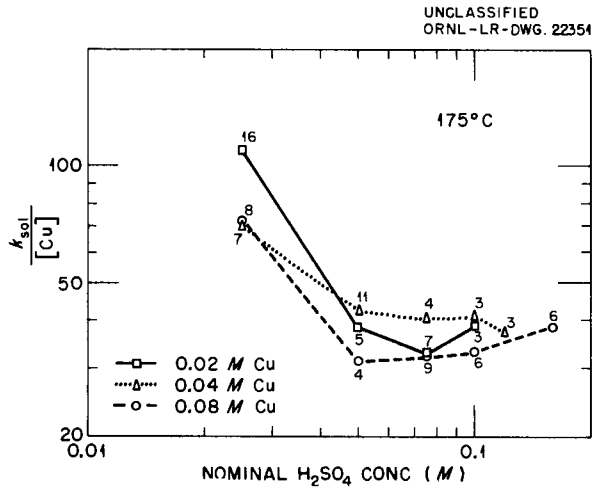

Fig. 24. Homogeneous Catalytic Activity at 175°C.

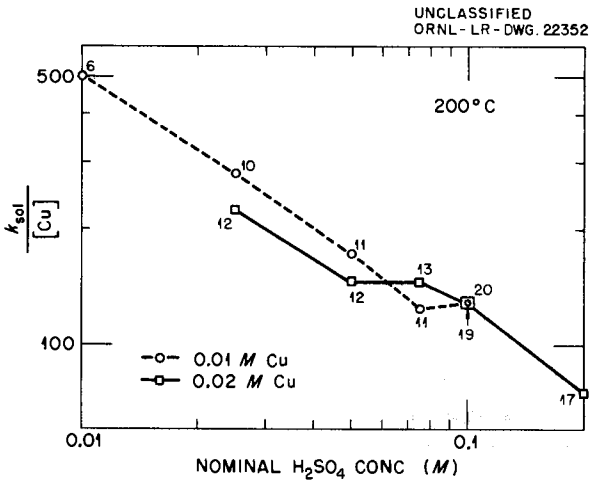

Fig. 25. Homogeneous Catalytic Activity at 200°C.

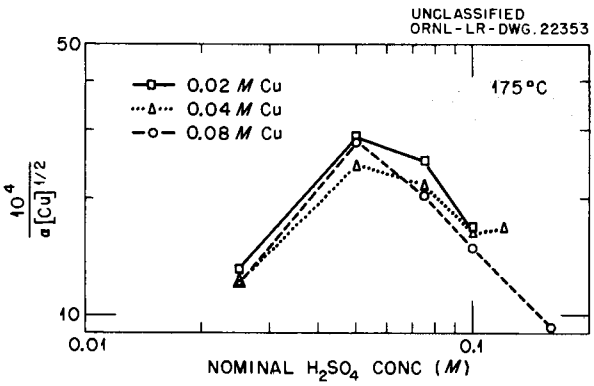

Fig. 26. Experimental Solubility Parameter at 175°C.

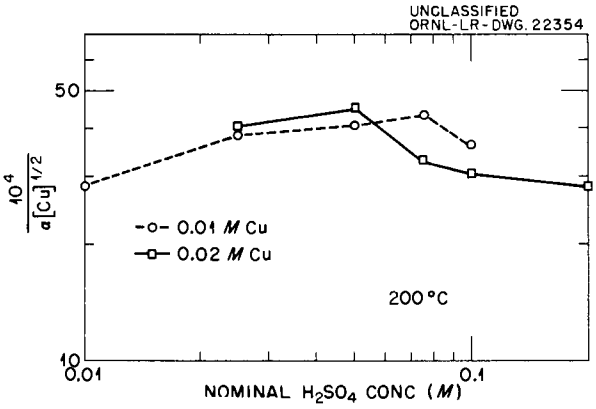

Fig. 27. Experimental Solubility Parameter at 200°C.

The square-root dependence on copper concentration and the first-power dependence on hydrogen pressure suggest that a copper dimer could possibly be involved, but no specific species is proposed at this time.

Additional experiments extending the range ot acidity, copper concentration, and temperature are under way to provide a firmer basis for understanding the reaction mechanism. Preliminary studies in the perchlorate system at 175°C have indicated that this system differs substantially from the sulfate system. Studies in mixed perchlorate-sulfate systems appear necessary in order to elucidate the role of the sulfate ion (or bisulfate, as it probably exists).

Studies in the Deuterium–Heavy-Water System

A few experiments using deuterium gas instead of hydrogen, both with light and with heavy water as the solvent for the copper catalyst, have confirmed the previous report[25] that the combination of rate and solubility effects gives only 30 to 60% as much activity for the deuterium-oxygen reaction as is found in the hydrogen–light-water systems. It remains to be discovered whether the decrease in activity is due to changes in the rate or the solubility function, or both.

Attention has been called[29] to one implication of the equilibrium postulated in Halpern's mechanism (Eq. 2). If deuterium gas is used in the presence of a light-water solution, any deuterium ions formed in the equilibrium will exchange very rapidly with

[29] P. H. Emmett, consultant, Johns Hopkins University.

the hydrogen in the water; the subsequent reaction of hydrogen ions with the CuD^+ intermediates, to regenerate the starting materials, would furnish HD instead of D_2, and would ultimately convert the deuterium into hydrogen. It has been pointed out[29] that it should be possible to detect the isotopic exchange by sampling the gas phase during the course of the reaction. Although such experiments had not yet been performed, other experiments had been performed with the use of deuterium gas and light-water solutions at 250°C, as indicated previously,[25] and detailed rate data were available for the course of these reactions. If deuterium reacts more slowly than hydrogen, and if the equilibrium with acid is such as to permit the k_{-1} reaction to compete with the k_2 reaction, then the conversion of a substantial amount of deuterium into hydrogen during the course of the reaction should lead to an accompanying increase in the experimentally measured rate constant. Examination of our plots of dP/dt vs P did not reveal the curvature which would have been expected. This finding is in agreement with the lack of acid effect in the perchlorate system and the relative unimportance of k_{-1} as compared with k_2 in the sulfate system at 250°C. If conditions can be established under which the acidity effect is so great as to represent a substantial competition with the forward reaction, the expected curvature in the rate plots will again be sought by experiments making use of deuterium gas and a light-water system.

CRITICAL PHENOMENON IN BINARY AQUEOUS SOLUTIONS – THE SYSTEM SO_3-H_2O

J. E. Stuckey C. H. Secoy

A background study of the general field of critical phenomena reveals the limited knowledge of critical data concerning aqueous solutions. The high temperatures and pressures developed in the critical region and the highly corrosive nature of many aqueous solutions make ordinary experimental techniques useless.

In this work experimental techniques and apparatus were designed for obtaining data on the SO_3-H_2O system. No satisfactory apparatus was conceived whereby direct simultaneous measurements of pressure, temperature, volume, and composition could be made; therefore, measurements were made in two separate experiments and the data correlated by means of a parameter, the ratio of liquid volume to vapor volume.

The first series of experiments was designed to correlate temperature, composition, and the fraction of a fixed volume occupied by the liquid phase. A modification of the phase-study apparatus for semimicro experimentation developed by Marshall, Wright, and Secoy[30] was employed. This apparatus was satisfactory to temperatures near 550°C but higher temperatures required a furnace of similar design but machined from electrode graphite.

Sample tubes were constructed from 4-in. lengths of 1-mm-ID–3-mm-OD quartz tubing. Solutions of known concentrations were sealed in the tubes and a Gaertner micrometer-slide comparator was used to measure the liquid-fraction filling of each tube. The center of each tube was marked as a reference point and the tube was placed inside the furnace at a temperature near the critical region. The tube was agitated by means of a rod connected to a Vibra-tool. The temperature at which the meniscus disappeared and reappeared was determined by potentiometric readings of voltage output from calibrated iron-constantan thermocouples. The position, relative to the center of the tube, at which the meniscus vanished was determined by observation of the tube through a telemicroscope. This permitted calculation of the relative volumes of each phase at the temperature at which the meniscus vanished.

This semimicro apparatus required only a small solution sample in tubes which could be easily prepared. The tubes could withstand high temperatures and pressures without special apparatus and techniques. The use of a telemicroscope gave increased visual perception of phase changes within a sample tube while it was held inside the furnace in a constant temperature region. The apparatus was inexpensive and readily assembled. The chief limitations were imposed by delays during the frequent calibrations of thermocouples and by their limit of accuracy. The corrosion of the quartz tubes, particularly by lower sulfur trioxide concentrations, had to be carefully evaluated.

The critical temperature of the binary solution was arbitrarily defined as the temperature at which the meniscus disappeared and reappeared at the center of the experimental sample tube. Data appears in Table 42 and is plotted in Fig. 28.

[30] W. L. Marshall, H. W. Wright, and C. H. Secoy, *J. Chem. Educ.* 31, 34 (1954).

Table 42. Summary of Critical Temperatures

Mole Fraction SO_3	Room Temperature Fraction Filling of Sample Tube	Critical Temperature (°C)
0.0000	0.32	374.2*
0.0193	0.393	404.2 ± 1.0
0.0419	0.396	447.4 ± 1.0
0.0654	0.376	482.8 ± 1.0
0.0938	0.353	526.1 ± 1.0
0.1251	0.336	562.0 ± 1.0
0.1643	0.333	592.2 ± 1.0
0.2084	0.314	621.0 ± 1.0
0.2664	0.293	646.8 ± 1.0
0.3368	0.283	665.4 ± 1.0
0.4353	0.280	666.4 ± 1.0
0.5591	0.331	637.2 ± 1.0
1.0000	0.336	218.3**

*K. A. Kobe and R. E. Lynn, Jr., *Chem. Revs.* **52**, 117–236 (1953).

A. Berthoud, *J. chim. phys.* **20, 77–86 (1923).

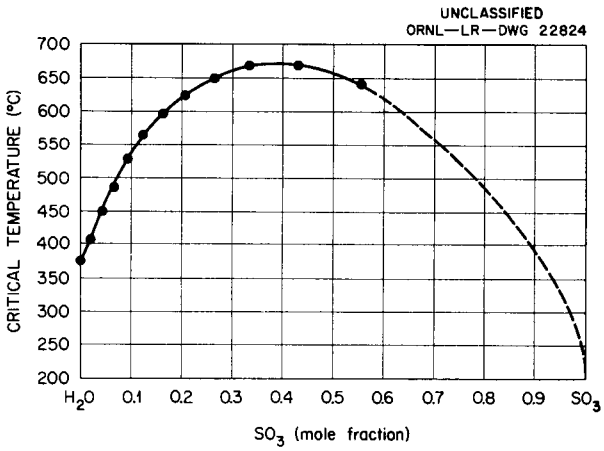

Fig. 28. Critical Temperature for the System SO_3-H_2O.

Since the pressure was unknown but specific for each point, the plot is a projection of the critical curve on a constant-pressure plane in the three-dimensional pressure, temperature, composition diagram.

Data on the SO_3-rich side were limited by the experimental techniques involved and the extreme difficulty of handling highly volatile and corrosive SO_3. Further study in this region will require construction of special equipment to handle sulfur trioxide.

The second series of experiments involved the design and construction of apparatus capable of measuring pressures of the highly corrosive solutions at elevated temperatures. The principle, developed by Richardson,[31] of measuring the pressure of an enclosed system by the displacement of a restrained diaphragm was the basis for the design of a special pressure measuring apparatus suited to high temperatures, relatively high pressures, and highly corrosive solutions.

Figure 29 shows a schematic diagram of the platinum-lined, stainless steel pressure vessel which was constructed. The distinctive feature of the apparatus was the bimetallic diaphragm in the bomb head which was limited in displacement by a platinum-iridium retainer plate and the concave bomb head. The diaphragm was constructed of two 5-mil, well-bonded sheets of metal; one was type 347 stainless steel and the other was platinum. It was stamped in a concave press corresponding to the bomb head with three concentric corrugations to ensure even displacement with no "cricket" snapping.

The diaphragm was backed up by a mercury system connected to a high-pressure piston-type pressure generator. Volume reduction of the slightly compressible mercury system increased the external pressure on the diaphragm. When the external pressure became slightly greater than the internal pressure of the acid solution, the diaphragm was displaced from the bomb head toward the retainer plate. Further rotation of the pressure-piston handle moved the diaphragm but resulted in only a slight increase in the pressure of the mercury system. This pressure plateau (Fig. 30) could be used to determine the internal pressure on the bomb.

The pressure on the mercury system was measured by two Baldwin SR-4 pressure transducers. One supplied its potential to a Brown recorder for a continuous pressure reading while the potential from the other cell was determined precisely and recorded in the data. The maximum accuracy of this cell was obtained by supplying a constant

[31] D. M. Richardson, *Pressure Measurement by Displacement of a Restrained Diaphragm*, ORNL CF-56-2-168 (1956).

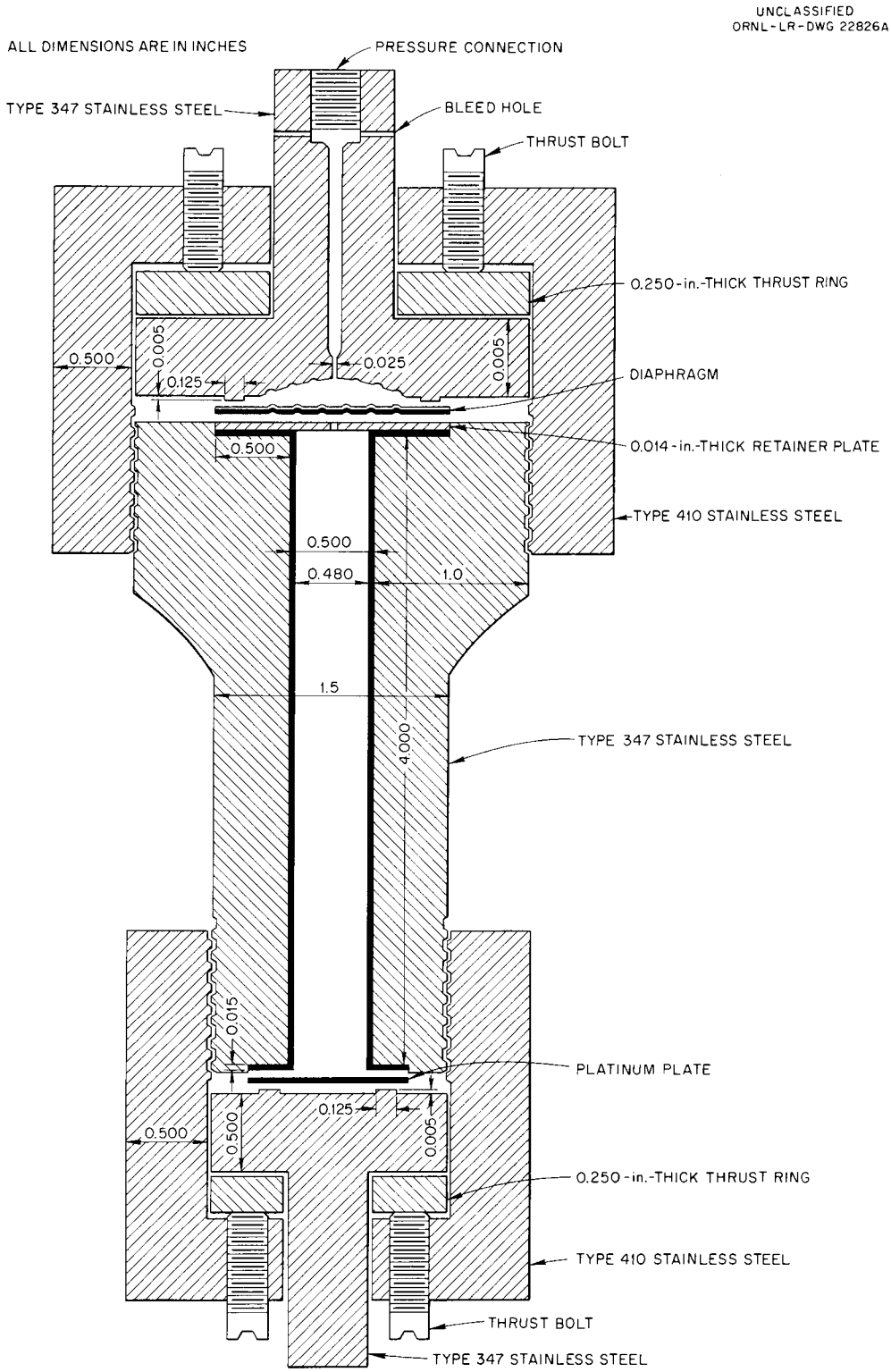

Fig. 29. High-Pressure Bomb.

input voltage from a Willard low-discharge battery, by temperature control of the cell itself, and by careful reading of its output voltage on a Rubicon potentiometer. Figure 31 shows a schematic diagram of the Baldwin cell instrumentation as well as the Pt, Pt–10% Rh thermocouple instrumentation used to record the temperature of the bomb.

The bomb was heated in a modified Marshall furnace whose power was supplied from two sources. One supplied base heat through a constant current regulated by a 20-amp Variac to give a temperature about 20°C below that desired. The second source supplied current through a step-down transformer for the remaining heat required to give the desired temperature. A constant temperature was obtained by the on-off action of a d'Arsonval millivolt vane-type controller operating through a modified Electron-O-Therm. The modification included an auxiliary Wheatstone bridge containing a platinum resistance-controlling thermometer and a control-point adjustment. Figure 32 gives a schematic diagram of the instrumentation.

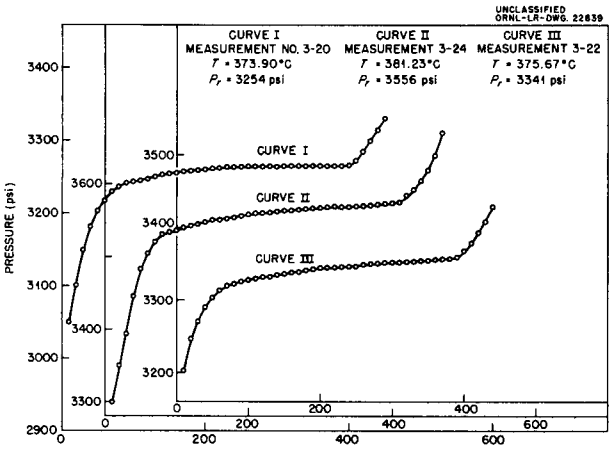

Fig. 30. Pressure as a Function of Volume Reduction.

Figure 33 shows the experimentally determined vapor pressures of pure water compared with the values of Keenan and Keyes.[32] Most of the experimental values are within 0.5% of the standard values.

Further exploratory work is being carried out with the apparatus before pressures of the SO_3-H_2O system are measured. (An absolute calibration of the bimetallic diaphragm, as well as the effects of continued mechanical working, is under study.) The effect of repeated temperature cycling on various bomb parts is also being noted.

[32] J. H. Keenan and F. G. Keyes, *Thermodynamic Properties of Steam*, Wiley, New York, 1936.

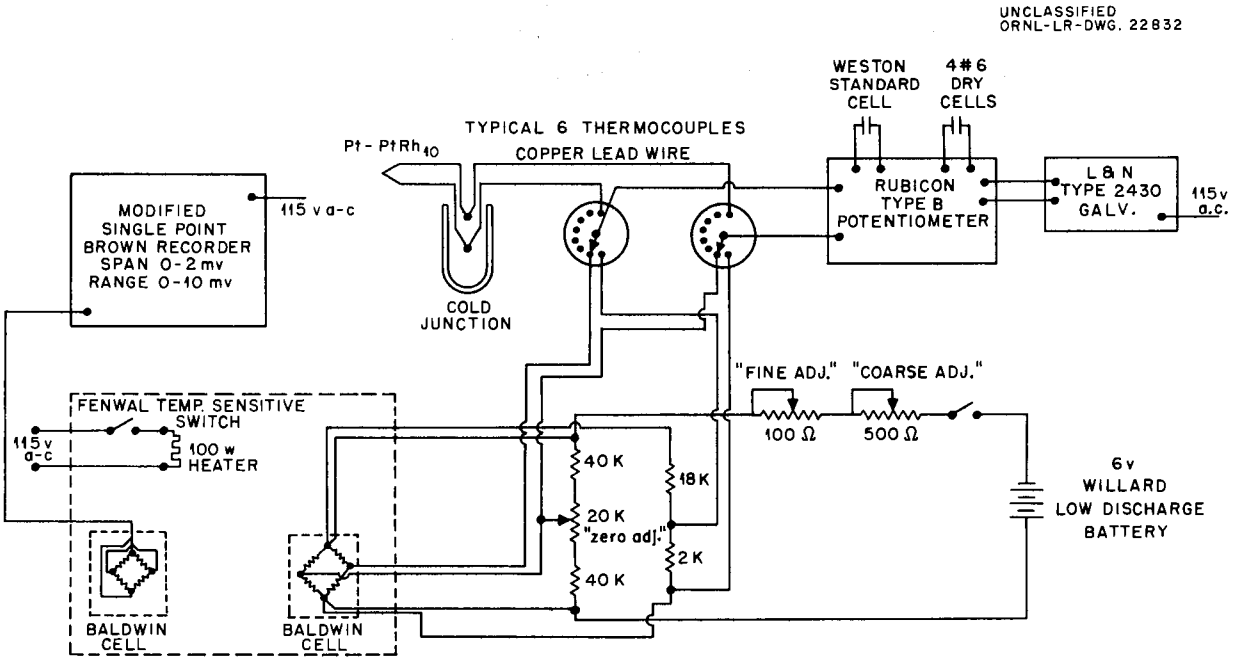

Fig. 31. Schematic Diagram of Instrumentation.

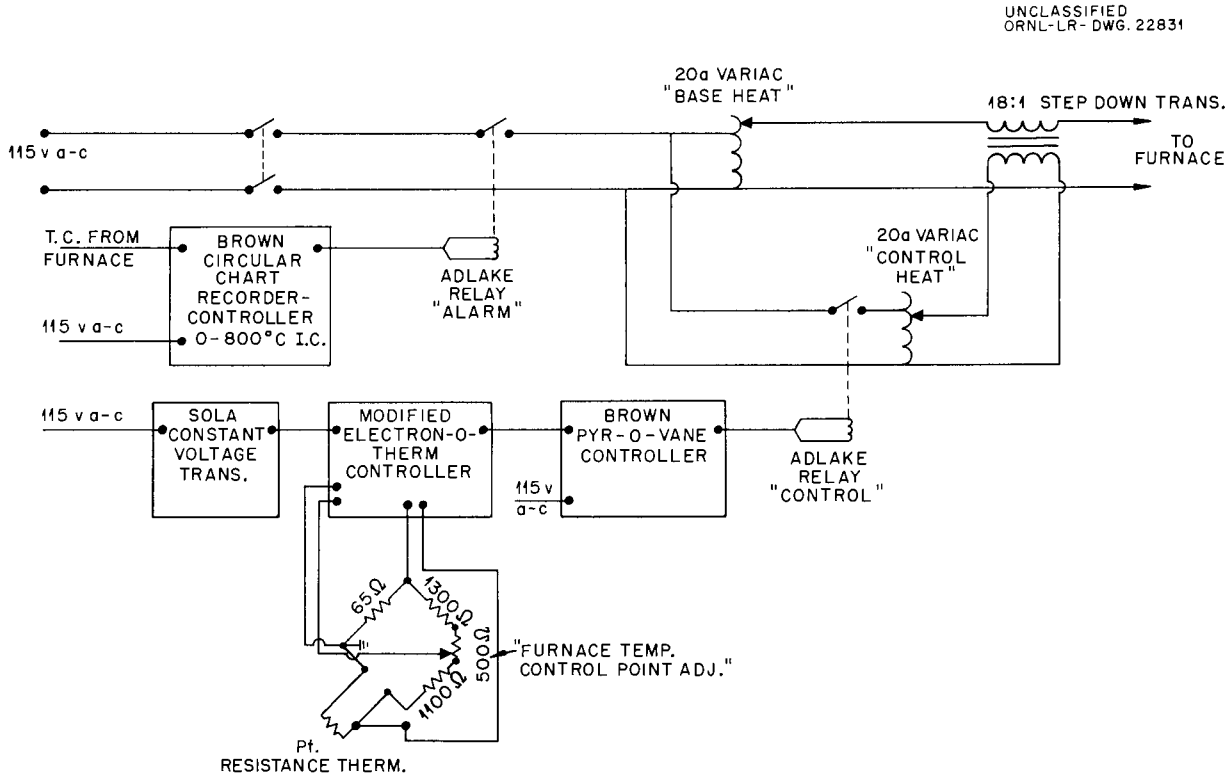

Fig. 32. Schematic Diagram of Instrumentation.

THE DENSITIES OF HEAVY-WATER LIQUID AND SATURATED VAPOR AT ELEVATED TEMPERATURES

G. M. Hebert H. F. McDuffie C. H. Secoy

In connection with other work it became desirable to know the densities for the liquid and saturated vapor of heavy water at temperatures above 250°C. Previous studies of the density of heavy water had provided data for the density of the liquid up to 250°C (ref 33), and for the critical properties of heavy water.[34] No data concerning the vapor density of heavy water over the temperature range appeared to be available.

The experimental method used for determining the volume of uranyl sulfate solutions as a function of concentration, temperature, and fractional filling of sealed quartz tubes[35] appeared suitable for application to the determination of the fractional filling, at various temperatures, of tubes containing heavy water. It is easily shown, by mass-balance equations, that the relationship between the fractional filling at room temperature, F_0, and that at some other temperature, F_T, is expressed by

$$F_0\left(d_{l_0} - d_{v_0}\right) + d_{v_0} = F_T\left(d_{l_T} - d_{v_T}\right) + d_{v_T} ,$$

where

d = density,
l = liquid,
v = vapor.

The reasonable assumption that $d_{v_0} \cong 0$ reduces the expression to a simple linear relationship:

$$F_0 d_{l_0} = F_T\left(d_{l_T} - d_{v_T}\right) + d_{v_T} .$$

It is also assumed that only one component (D_2O) is present in the tubes and that the air included when the tubes were sealed has only a negligible effect. Values for d_{v_T} and d_{l_T} were obtained by graphical or mathematical extrapolation of this

[33] J. R. Heiks *et al.*, *J. Phys. Chem.* 58, 488 (1954).

[34] P. A. Lottes, chap. 1.3, sec 1, in *Reactor Handbook* (declassified edition), ed. by J. F. Hogerton and R. C. Grass, Technical Information Service, AEC, 1955.

[35] G. M. Hebert, D. W. Sherwood, and C. H. Secoy, *HRP Quar. Prog. Rep. Oct. 31, 1954*, ORNL-1813, p 164.

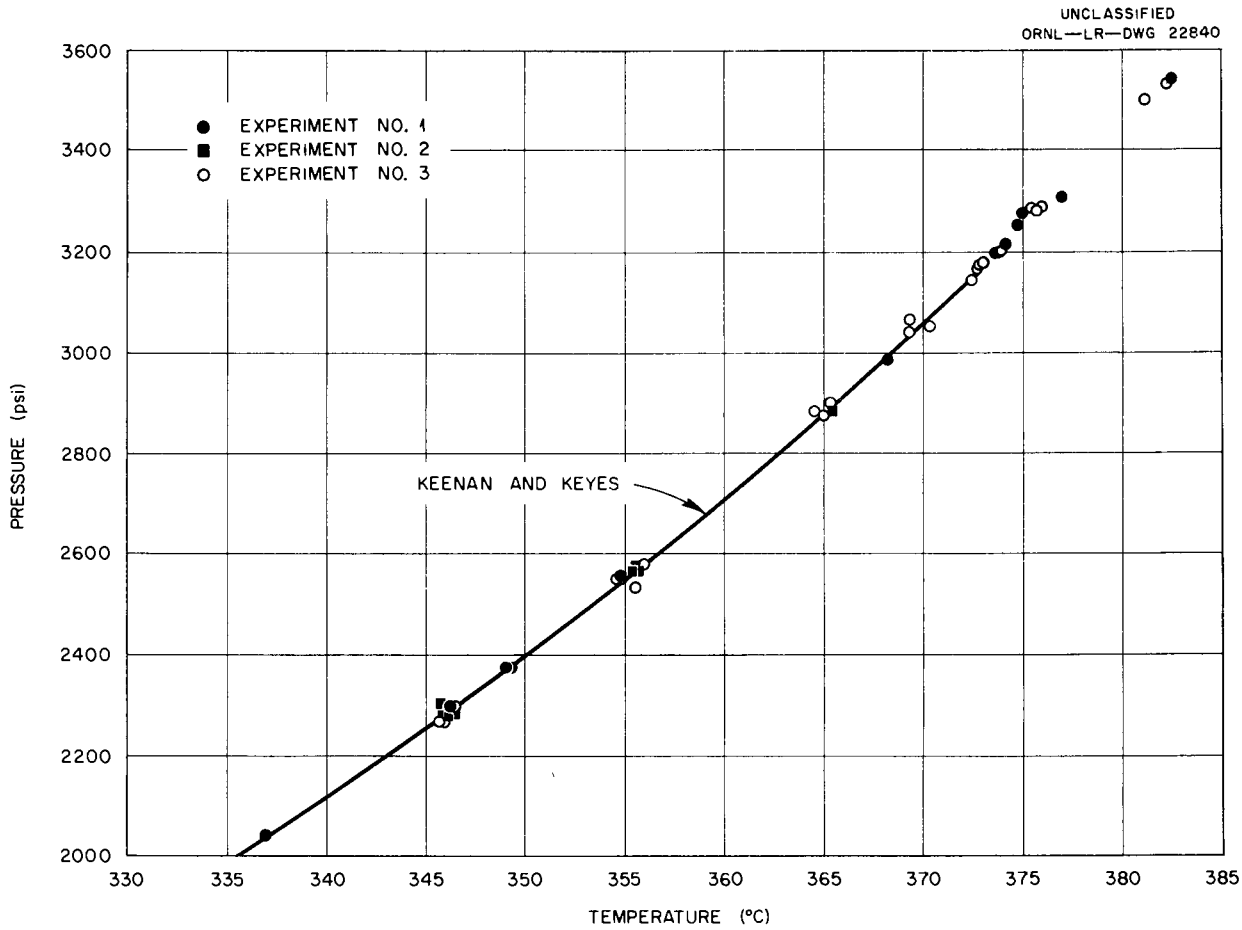

Fig. 33. Pressure-Temperature Isochor of Water.

relationship to the extremes where $F_T = 0$ and $F_T = 1$, respectively. Four quartz tubes, of differing F_0 values, were used for all determinations except that at 367°C, where only two of the tubes retained observable liquid phases. As an internal check of the experimental method and interpretation, two tubes containing light water were included for comparison with the known data for water. The experimentally determined values for both light and heavy water are presented in Fig. 34, together with accepted values for each.

ANION EXCHANGE STUDIES

F. Nelson R. M. Rush
K. A. Kraus D. C. Michelson

Work on anion exchange of metal complexes has continued during the last year. Principal emphasis was placed on extension of adsorption studies to complexing systems which had received little attention in the past, on preliminary studies for a general ion exchange separations scheme, on studies of the properties of exchangers in concentrated electrolyte solutions, and on utilization of exchangers for the determination of equilibrium constants and activity coefficients in the aqueous phase. Representative examples of this work will be discussed in the following sections.

Adsorption of Metals from HCl-HF Solutions

This system has received considerable attention in the past because it appears to be very attractive for handling those highly charged metals which, in the absence of strong complexing agents, tend to hydrolyze and polymerize even in very acidic solutions. Fluoride ions effectively prevent these hydrolytic reactions and permit handling of these elements in a reproducible manner. In order to

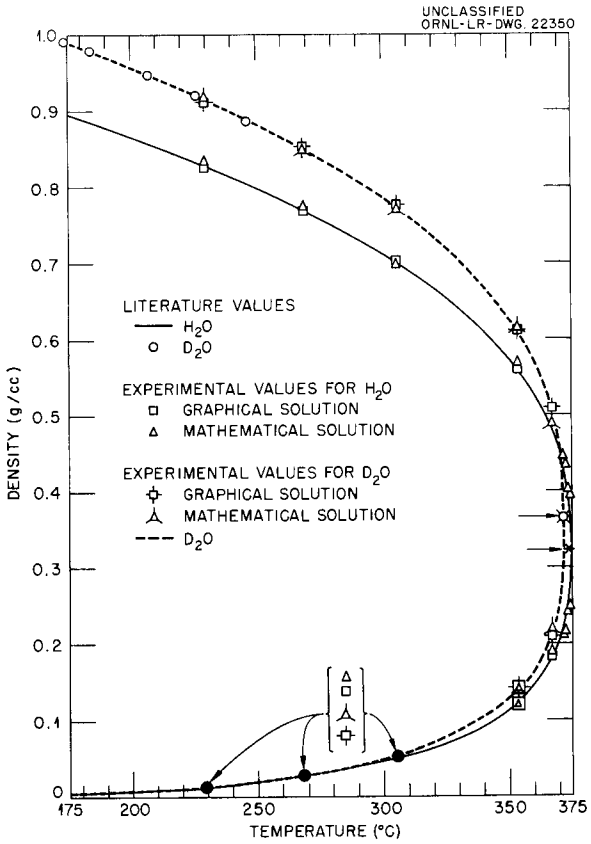

Fig. 34. Liquid and Saturated Vapor Density of H_2O and D_2O.

make this system generally useful and to gather information on fluoride complexing, it is desirable to characterize a large number of elements in this medium, and approximately 20 elements have now been studied in HCl-HF mixtures. During the last year Ti(IV), V(IV), Fe(III), As(III), Sn(II), and Sb(III) have been added to the list, which now contains most of the elements which might show fluoride complexing in HCl solutions. A summary of the new results, as well as of the older ones, is given in Fig. 35, where for comparison the adsorption functions of the same elements in HCl alone (absence of HF) are included.

These studies were carried out at constant HF concentration (1 or 0.5 *M*) and in the HCl concentration range 0.1 to 12 *M*. As shown in Fig. 35, a surprisingly large number of elements [As(III), As(V), In(III), Tl(III), Pb(II), Bi(III)] have essentially the same adsorbabilities in HCl and in HCl-HF. For most of the other elements, addition of HF tends to decrease adsorbabilities at high *M* HCl. This is most pronounced for some of the elements of high oxidation number [Ti(IV), Zr(IV), Hf(IV), Ge(IV), Pa(V)], where, in the presence of 0.5 or 1 *M* HF, adsorbabilities are essentially negligible at high *M* HCl. For many other elements [e.g., Mo(VI), W(VI), U(VI), Fe(III), Ga(III), Sn(II), Sn(IV), Sb(III), Sb(V)] the HCl and HCl-HF adsorption functions approach each other at high *M* HCl, and, at moderate HCl concentrations, the adsorbabilities from HF-containing media are lower than from HCl solutions. In many cases the HCl-HF adsorption functions exhibit minimums, presumably because at low HCl concentrations adsorption of negatively charged fluoride complexes becomes dominant. No adsorption minimums were found for Fe(III) and Ga(III), although in the case of Fe(III) the studies were extended down to 0.01 *M* HCl in 1 *M* HF. This unusual behavior of Fe(III) is extremely useful for many separations involving this element.

A systematic series of measurements has been carried out on the adsorbability of Fe(III) from 2 *M* HCl as a function of HF concentration. The distribution coefficients decrease with increasing HF concentration from $D = 36$ (2.0 *M* HCl, 10^{-3} *M* HF) to 5.8 (2 *M* HCl, 1 *M* HF). Preliminary interpretation of the data indicates that appreciable amounts of FeF^{++} are formed in the solutions at low HF concentration and that, at the highest HF concentrations, some FeF_2^{+} also forms.

Adsorption from EDTA Solutions

A large number of metal ions are not adsorbed by anion exchangers from solutions containing the common inorganic anions such as chloride, nitrate, or sulfate. However, separations involving these metals should be feasible with organic complexing agents. Of the many possible organic ligands, EDTA (ethylenediaminetetraacetic acid) appeared to be particularly suitable. This complexing agent has been used by Samuelson and co-workers[36] for the separation of the alkaline earths as a group from many other metals, and in this laboratory it was utilized for the anion exchange separation of

[36] O. Samuelson and E. Sjöström, *Anal. Chem.* **26**, 1908 (1954); O. Samuelson, E. Sjöström, and S. Forsblom, *Z. anal. Chem.* 144, 323 (1955).

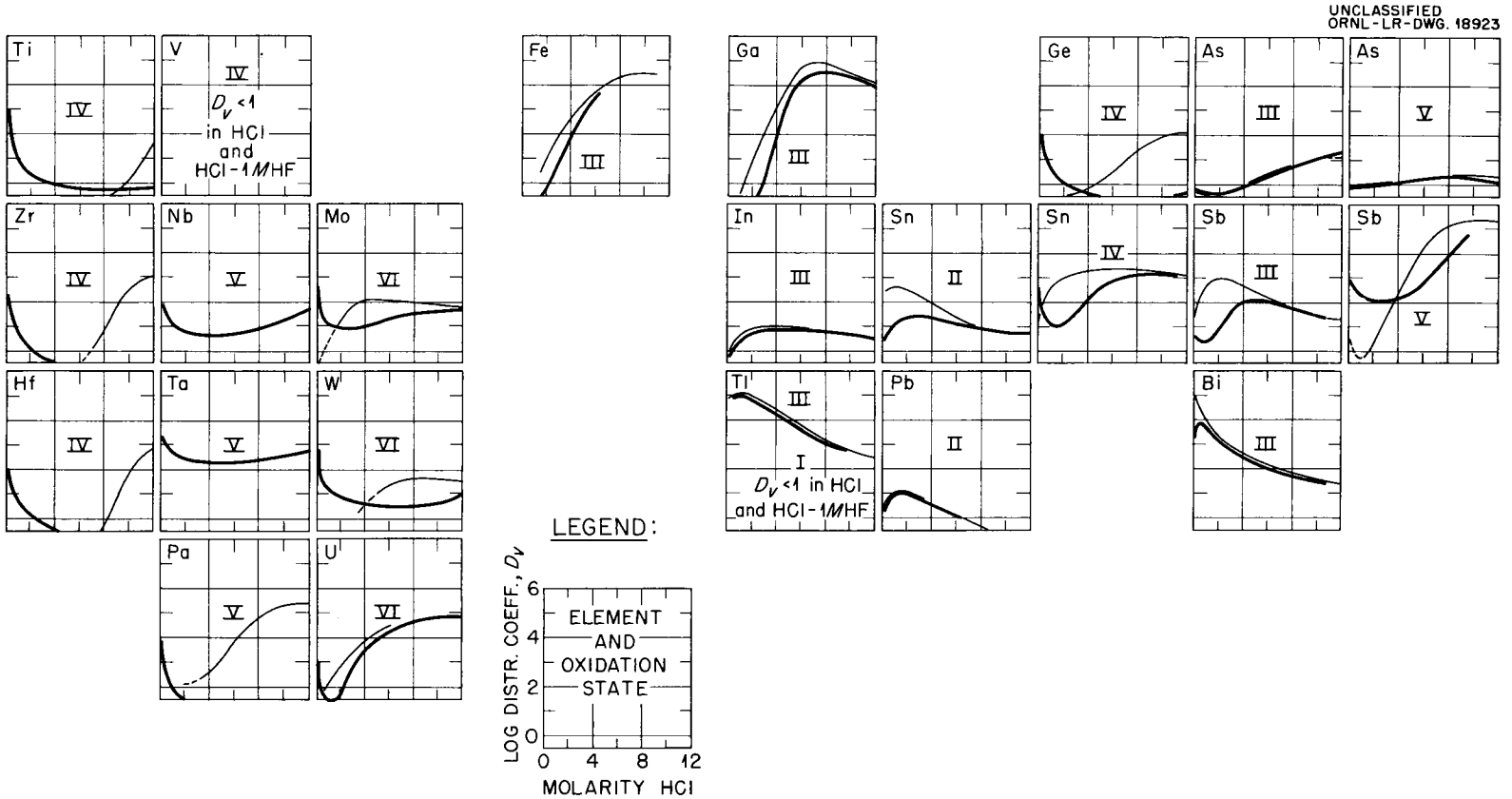

Fig. 35. Adsorption of Some Elements from HCl and HCl-HF Solutions. ——HCl; ——HCl-HF; 1 *M* HF, except Zr(IV), Hf(IV), Nb(V), Ta(V), and Pa(V), where *M* of HF = 0.5.

some alkali metals.[37] During the last year adsorbabilities of a number of metals in EDTA solutions were studied as a function of pH and supporting electrolyte concentration, and a number of anion exchange separations were developed.

The variation of adsorbabilities with pH is illustrated with the alkaline earths in Fig. 36. These measurements were carried out in 0.1 *M* NH_4Cl solutions containing 7.5×10^{-4} *M* EDTA. Under these conditions the resin was found not to take up significant amounts of the complexing agent, that is, to remain substantially in the chloride form. The distribution coefficient measurements may thus be considered to be carried out at constant resin composition and can be used with "standard" methods to obtain the stability constants of the complexes.

[37]F. Nelson, *J. Am. Chem. Soc.* **77**, 813 (1955).

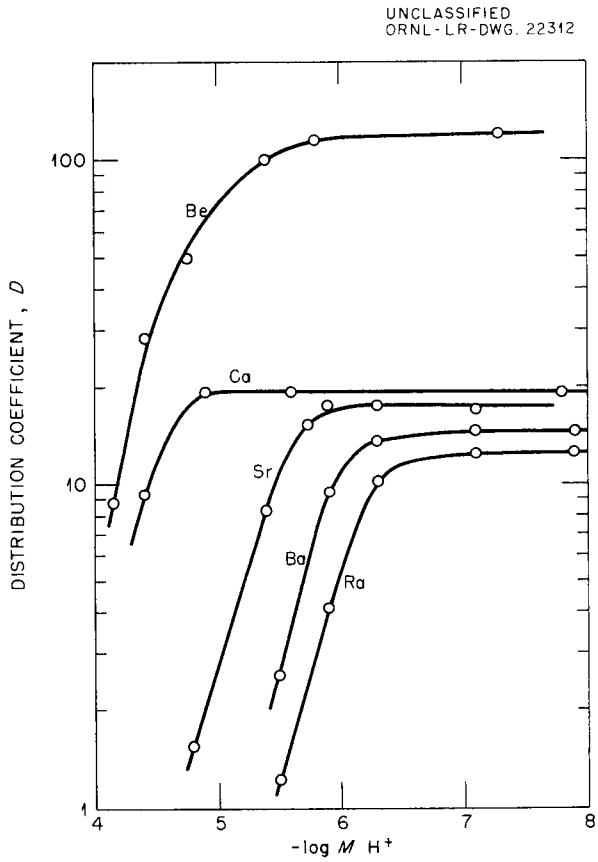

Fig. 36. Adsorption of Alkaline Earths from EDTA Solutions (0.10 *M* NH_4Cl, 7.5×10^{-4} *M* EDTA).

Analysis of the adsorption data of Ca(II), Sr(II), and Ba(II) yielded values of the concentration quotients of the stability constants (k^m_{01}) for the reaction

$$M^{++} + Y^{4-} \longrightarrow MY^{--}$$

where M^{++} is the metal and Y^{4-} is the ligand, which were in substantial agreement with the values reported in the literature. The stability constants for Be(II) and Ra(II), which have not been previously determined, were calculated to be $10^{9.1}$ and $10^{7.1}$, respectively, under the experimental conditions ($\mu = 0.1$).

The adsorbability of a number of elements of the first long period of the periodic table [Ca(II), Sc(III), V(IV), Cr(III), Mn(II), Co(II), Ni(II), Zn(II)] was investigated as a function of NH_4Cl concentration at constant EDTA concentration and constant pH. As mentioned earlier, if the NH_4Cl concentration is large enough, the resin remains substantially in the chloride form, and the activity coefficient quotient in the mass-action expression for the ion exchange equilibrium may be assumed to be constant. Under these conditions, slopes of plots of log *D* vs log *M* Cl^- (the eluting ion) give the average charge of the metal in the aqueous phase. It was found that for *M* $NH_4Cl \geqq 0.1$, the slopes $d \log D/d \log M\ NH_4Cl$ became essentially constant with values approximately −1 or −2, depending on the element. For *M* $NH_4Cl < 0.1$ the slopes were less negative, presumably because a significant portion of the resin became converted to the EDTA form. The slopes for *M* $NH_4Cl \geqq 0.1$ are summarized in Table 43. Included are the formulas of the complexes which exist in these solutions and the observed distribution coefficients D_v for *M* $NH_4Cl = 0.1$.

From these studies in EDTA solutions it is clear that a very large number of separations are possible through control of EDTA concentration, pH, and eluting ion concentration (e.g., Cl^-). A typical separation is illustrated in Fig. 40, given below.

Adsorption of Gaseous $GeCl_4$ by Anion Exchangers

Adsorption of Ge(IV) by anion exchangers from concentrated hydrochloric acid solutions has been demonstrated earlier.[38] Unfortunately, under the

[38]F. Nelson and K. A. Kraus, *J. Am. Chem. Soc.* **77**, 4508 (1955).

Table 43. Adsorption of Some Elements from EDTA Solutions (0.01 *M* EDTA, pH 4.5)

Element	D_v in 0.1 *M* NH_4Cl	$d \log D_v / d \log M\ NH_4Cl$	Probable Formula of Complex
Ca(II)	10.0	−2	CaY^{--}
Sc(III)	1.7	−1	ScY^{-}
V(IV)	73.6	−2	VOY^{--}
Mn(II)	4.8	−2	MnY^{--}
Cr(III)	8.9	−1	CrY^{-}
Co(II)	10.0	−2	CoY^{--}
Ni(II)	9.6	−2	NiY^{--}
Zn(II)	7.4	−2	ZnY^{--}

same conditions where Ge(IV) may be adsorbed effectively it also tends to volatilize, and hence there is considerable danger of losing some of it during an analytical procedure involving the anion exchange technique. Actually it is possible to remove Ge(IV) from aqueous hydrochloric acid solutions with a gas-sweeping technique. By this method, a new short-period isomer of germanium (Ge^{73m}, $T_{1/2}$ = 0.52 sec) was separated from its arsenic (As^{73}) parent,[39] although the rate of removal of germanium had not been determined accurately. In more recent work it was demonstrated that Ge(IV) can be removed quantitatively by sweeping the solution with an inert gas for 10 to 20 min. Further, this gaseous $GeCl_4$ can quantitatively be adsorbed on a small bed of anion exchange resin in the chloride form. A combination of gas-sweeping and anion exchange adsorption from the gas stream permits isolation of Ge(IV) from a large number of elements. Recovery of Ge(IV) is simple, since it only involves washing of the anion exchange column with dilute hydrochloric acid, from which it does not significantly adsorb.

The technique of adsorbing materials from gas streams on resin beds should be applicable in a large number of cases. In particular, it should permit adsorption of acidic gases by anion exchangers in a suitable salt form. In preliminary experiments satisfactory adsorption of gaseous HCl was demonstrated with the chloride form of Dowex 1, as was excellent adsorption of HF with the fluoride form of the exchanger. Regeneration may be achieved by washing the exchangers with water.

General Separations Scheme

During the last few years a considerable amount of information has accumulated on the anion exchange behavior of the metallic elements in various complexing media. On the basis of this information it now appears feasible to devise a general separations scheme which utilizes almost exclusively strongly basic anion exchangers. As a beginning to this general problem, separation of the metallic elements of the first long period of the periodic table was attempted, and an anion exchange scheme is proposed which separates them first into groups and then, with some exceptions, isolates them individually.

As shown in Fig. 37, the elements are first divided into three major groups: (1) volatile elements (Ge, As), (2) elements adsorbable from 12 *M* HCl (Ti, Fe, Co, Cu, Zn, Ga), and (3) elements weakly adsorbed or nonadsorbable from 12 *M* HCl (K, Ca, Sc, V, Cr, Mn, Ni).

The volatile elements are separated by controlled distillation (Fig. 38) followed by ion exchange. Elements of the second group may be separated from each other by elution with solutions of progressively decreasing HCl concentration (Fig. 39). The elements in the third group are separated from each other or into smaller subgroups by adsorption from EDTA solutions followed by elution at controlled acidity and ionic strength (Fig. 40).

[39] E. C. Campbell and F. Nelson, *Phys. Rev.* (in press).

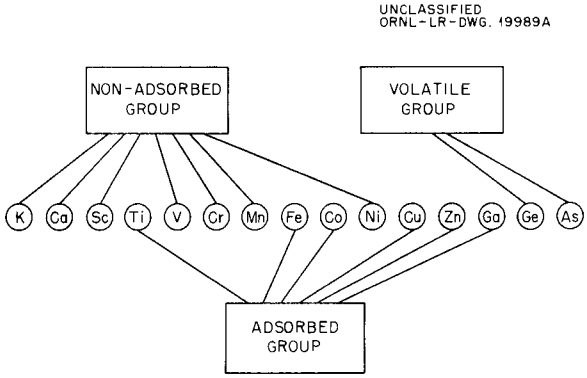

Fig. 37. Group Separation in Concentrated Hydrochloric Acid.

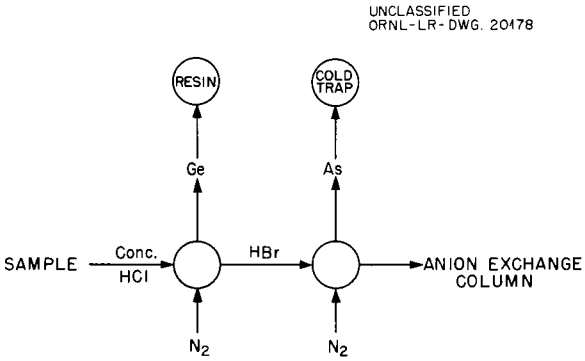

Fig. 38. Separation of Volatile Elements.

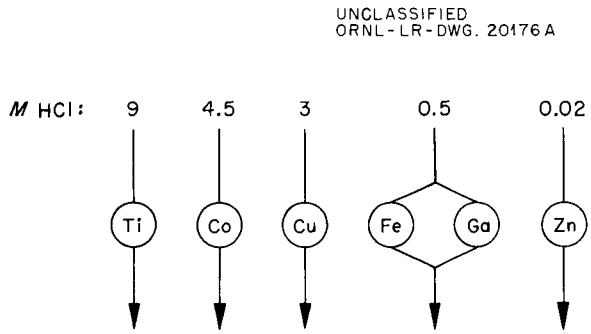

Fig. 39. Separation of Elements Adsorbed from 12 *M* HCl.

Activity Coefficients of Strong Electrolytes in the Resin Phase

The large selectivities for complex ions of anion exchange resins imply that the activity coefficients $\gamma_{\pm(r)}$ for the corresponding distributable components are very much lower in the resin phase than in the aqueous phase $\gamma_{\pm}$. Further, it had been found[40] that the distribution coefficients of many complex ions are very much greater from concentrated LiCl solutions than from HCl solutions. This implies that the activity coefficients of the lithium salts of the complexes in the resin are very much lower than those of the acids, provided that the activity coefficients in the aqueous phase do not differ greatly for these two media, an assumption for which there now seems to be ample evidence.

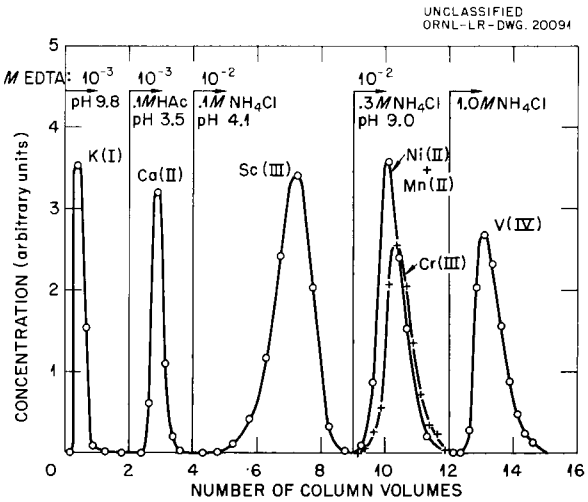

Fig. 40. Separation of a Number of Elements in EDTA Solutions by Anion Exchange.

In order to explain the great selectivity of the exchangers for complex ions, it appeared desirable to measure the activity coefficients in the resin of a number of "simple" electrolytes. Preliminary studies of this type have been reported earlier for HCl.[41] These measurements have now been repeated with somewhat greater precision, and the activity coefficients $\gamma_{\pm(r)}$ have also been determined for LiCl and NaCl. Values of $\gamma_{\pm(r)}$ were computed, choosing the same standard states for the distributable components in both phases and expressing the concentrations in the resin phase in terms of moles per 1000 g of imbibed water. Plots of log $\gamma_{\pm LiCl(r)}$ and log $\gamma_{\pm HCl(r)}$ vs molality of LiCl or HCl in the resin phase were found to be

[40] K. A. Kraus *et al.*, *J. Am. Chem. Soc.* **77**, 1391 (1955).

[41] K. A. Kraus and G. E. Moore, *J. Am. Chem. Soc.* **75**, 1457 (1953).

essentially straight lines. The activity coefficients for HCl in the resin phase at high HCl concentrations are approximately a factor of 2 lower than those in the aqueous phase at the same molality. For LiCl the activity coefficients were essentially the same in both phases. This implies greater interaction of hydrogen ions than of the lithium ions with the resin phase.

A summary of the HCl and LiCl data, as well as those for NaCl, is given in Fig. 41 as plots of log $\gamma_{\pm(r)}$ and log $\gamma_{\pm}$ vs activity of the electrolytes. The similarity of the activity coefficients in the two phases is striking and implies that there is comparatively little interaction between the resin and these strong electrolytes. The high adsorbabilities of complex ions thus imply interactions with the resin which are very much greater than those of "simple" strong electrolytes.

Adsorption of HF by Anion Exchangers

In the course of investigations of anion exchange behavior of complexes in HCl-HF solutions, significant amounts of HF were found to be adsorbed as a neutral component by quaternary amine polystyrene–DVB resins in the chloride form.

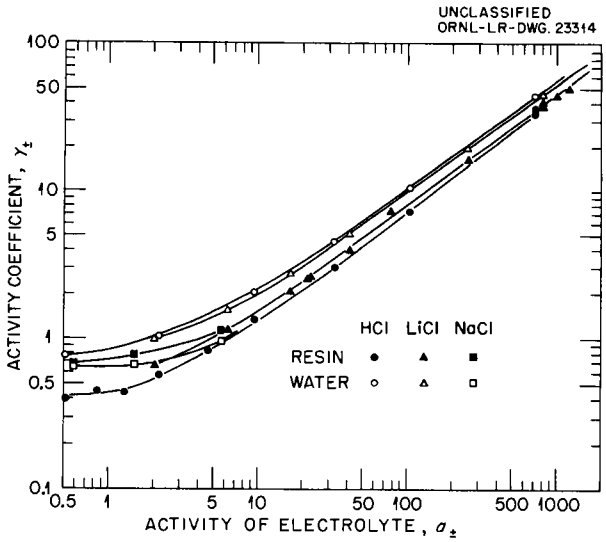

Fig. 41. Activity Coefficients of Strong Electrolytes in the Resin and Aqueous Phases.

Since the selectivity of these resins for fluoride ions is considerably less than for chloride ions[42] and since HF is a weak electrolyte, significant displacement of chloride ions by fluoride ions does not occur in these media, except perhaps if the HF concentration greatly exceeds the HCl concentration.

The partitioning of HF between resin and solution phases was measured in the range 0.1 to 0.5 *M* HCl and 0.025 to 1.03 *M* HF. A single distribution coefficient $D^{*}_{HF} = 3.5 \pm 1$ was found to describe the experimental data satisfactorily. The units chosen are moles of HF adsorbed per 1000 g of imbided water and the molality of the HF in the aqueous phase.

Similar HF adsorption experiments were carried out with the fluoride form of the resins. For these the amount of HF adsorbed was considerably greater than could be attributed to simple partitioning of undissociated HF; however, the results could be interpreted readily as an acid-base reaction

$$F^-_{(r)} + HF_{(r)} \rightleftharpoons HF_2^-{}_{(r)} \qquad (1)$$

for the resin phase. The concentration quotient for the equilibrium constant for this reaction was estimated to be $k^m_{HF_2^-{}_{(r)}} = 6.5$ at 25°C, which does not differ greatly from the corresponding value $k^m_{HF_2^-{}_{(aq)}} = 3.86$, which is given for the aqueous phase.[43] The similarity of these constants again confirms, as did the measurements of the activity coefficients of strong electrolytes (see "Activity Coefficients of Strong Electrolytes in the Resin Phase," above), that activity coefficients "normally" do not differ widely for the two phases.

The acid-base reaction, Eq. 1, provides a mechanism by which substantial amounts of HF can be adsorbed by the fluoride form of the exchangers. This HF uptake may be utilized for many separations involving HF. Two typical examples, separation of HF from a nonadsorbable salt (NaF) and from a weakly adsorbed organic compound (glycerine), are illustrated in Fig. 42.

---

[42] R. M. Wheaton and W. C. Bauman, *Ind. Eng. Chem.* 43, 1088 (1951).

[43] H. H. Broene and T. De Vries, *J. Am. Chem. Soc.* 69, 1644 (1947).

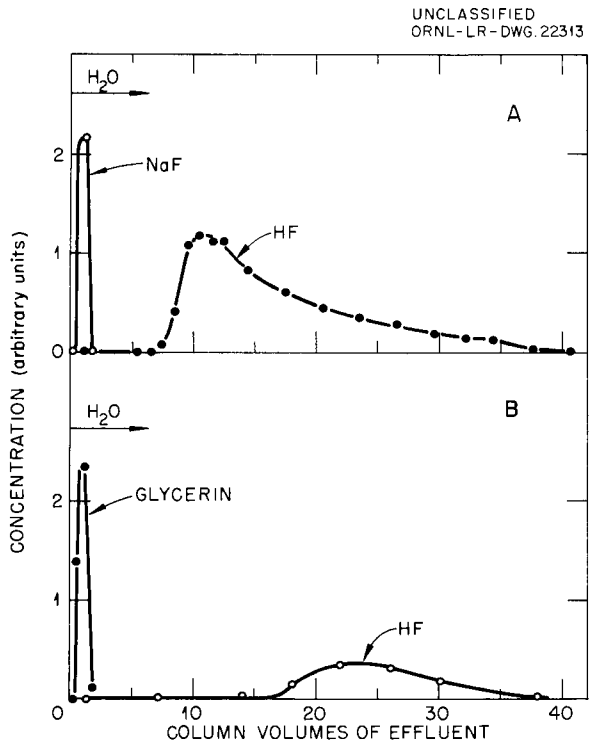

Fig. 42. Separations Involving HF (Fluoride Form of Anion Exchanger, Water Elution). (*A*) Added one column volume 0.5 *M* HF–0.5 *M* NaF; (*B*) added 0.5 column volume 6.2% glycerine–0.25 *M* HF.

ULTRACENTRIFUGATION OF INORGANIC SYSTEMS

J. S. Johnson K. A. Kraus

During the last year, study of hydrolytic polymerization of metal ions by equilibrium ultracentrifugation has continued. Some of the principal results are summarized below.

Interference Optical System

In the past, analysis of the concentration distribution of the solute was obtained by the "schlieren" method, which is based on refractive-index gradients. An interference optical system has now been added to the ultracentrifuge by which differences in refractive index are observed, a considerable theoretical advantage in the nonideal polycomponent systems with which work is being done. In addition, the interference method is expected to be more precise than the schlieren method and should yield satisfactory results at higher dilution. Performance of the equipment has been checked by measurement of the activity coefficients of cadmium iodide in water solutions and of the molecular weight of silicotungstic acid (see the following section).

A cadmium iodide solution of initial concentration 0.05 *M* was centrifuged to equilibrium; the concentration range was about 0.03 to 0.07 *M*. Stoichiometric activity coefficients of cadmium iodide were computed by a method analogous to the one earlier described.[44] These agree to better than 1% with the emf data of Bates,[45] which represents about the same accuracy as attained in earlier measurements with schlieren optics[44] on more concentrated solutions (0.2 to 0.8 *M* CdI_2). Since accuracy should be roughly proportional to concentration, a substantial increase in accuracy is attained with the interference system.

Silicotungstic Acid

If the species of silicotungstic acid ($H_4SiW_{12}O_{40}$) in solution is the same as that in the solid, the analytical ratio of Si/W allows only multiples of the large formula weight (2879) for the molecular weight of the dissolved species. Measurement of its molecular weight by velocity ultracentrifugation[46] has indicated that the species in solution corresponds to the formula weight, and this material should be a suitable standard for checking various methods for molecular weight determination. Measurements of the pH of solutions both in connection with the velocity work[46] and in this laboratory by T. A. Carlson indicated that four moles of protons are ionized per mole of silicotungstic acid.

Three concentrations of silicotungstic acid were centrifuged, 0.0016, 0.0047, and 0.0086 *M*, all in 1 *M* $NaClO_4$. The results indicated a low charge, although the scatter precluded an accurate determination of its value, perhaps because of the low charge/mass ratio. With 4 assumed for the charge, the molecular weight obtained from the results agreed with the formula weight, subject to a maximum uncertainty of ±4%.

---

[44] J. S. Johnson, K. A. Kraus, and T. F. Young, *J. Am. Chem. Soc.* **76**, 1436 (1954).

[45] R. G. Bates, *J. Am. Chem. Soc.* **63**, 399 (1941).

[46] M. C. Baker, P. A. Lyons, and S. J. Singer, *J. Am. Chem. Soc.* **77**, 2011 (1955).

Polymerization of Sn(IV)

Attempts were made to estimate degrees of polymerization of Sn(IV) in HCl and in $HClO_4$ solutions. However, in $HClO_4$ no stable solutions of Sn(IV) could be obtained, and a precipitate slowly separated. An estimate of the degree of polymerization of the order of 1000 was established by ultracentrifugation for the Sn(IV) remaining "in solution" in 3 *M* $HClO_4$. In 0.5 and 1 *M* HCl, Sn(IV) (0.05 *M*) was found not to be polymerized. Extensive aggregation (degrees of polymerization of the order of 1000) occurred when the acidity of the solutions in excess of the component $SnCl_4$ was equal to or less than 0.2 *M*, where a solid also slowly separated.

In sodium hydroxide solutions Sn(IV) (sodium stannate) is apparently not aggregated. In the absence of excess base, low-molecular-weight polymers were found.

The results of the centrifugations in chloride solutions are summarized as a function of acidity in Fig. 43. A steep polymer cliff seems to occur in this system when there is little excess acid or excess base. Outside this polymer region only monomers seem to occur. In this respect Sn(IV) thus differs greatly from other quadrivalent ions studied [e.g., Zr(IV) (ref 47) or Th(IV) (see the following section)], where, in acidic solutions, low molecular polymers have substantial stability ranges.

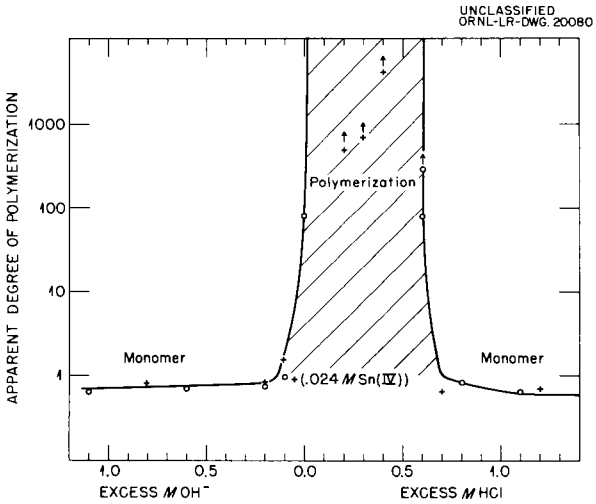

Fig. 43. Polymerization of Sn(IV). Excess acid and base are computed far camponent $Sn(OH)_4$; —+— ultracentrifugation [~0.05 *M* Sn(IV) unless specified]; —o— diffusion coefficient measurements [0.05 *M* Sn(IV)] presented as function roughly proportional to degree of polymerization and normalized to match centrifugatian results in monomer region [see G. Jander, S. Busch, and T. Aden, *Z. anorg. u. allgem. Chem.* 177, 345 (1929)].

Polymerization of Th(IV) in Perchlorate and Chloride Solutions

Earlier studies[48,49] of hydrolytic polymerization of Th(IV) in perchlorate solutions carried out with schlieren optics indicated general agreement with the computations of Hietanen[50] based on emf data, which were interpreted by the continuous polymerization model of Sillen.[51] However, the extent of the agreement remained uncertain because the schlieren method tends to give average molecular weights, which strongly emphasize heavier species. Further, computation of weight average molecular weights is difficult in these polydisperse systems where the assignment of charges to the polymeric species is also uncertain. These complications are lessened if interference optics is used, and after its installation, a new series of centrifugations was carried out. The earlier schlieren results were confirmed, as well as the degrees of polymerization reported by Hietanen.

In a similar recheck of molecular weights in chloride solutions, substantial differences were found between the schlieren and interference methods. The authors had earlier reported that Th(IV) in chloride solutions is highly polydisperse and that the degree of polymerization is considerably larger than in perchlorate solutions of the same hydroxyl number **n**. In a reinvestigation of a 0.015 *M* Th(IV)–1 *M* NaCl solution with **n** = 1.5, results by schlieren and interference optics were compared. Such comparisons can be carried out essentially simultaneously with the machine in this laboratory, since they involve only rotation of the light source by 90 deg. Analysis of the schlieren results gave a degree of polymerization

[47] J. S. Johnson and K. A. Kraus, *J. Am. Chem. Soc.* 78, 3937 (1956).

[48] J. S. Johnson, K. A. Kraus, and R. W. Holmberg, *Chem. Semiann. Prog. Rep. June 20, 1955*, ORNL-1940, p 5.

[49] T. A. Carlson *et al.*, *Chem. Semiann. Prog. Rep. June 20, 1956*, ORNL-2159, p 42.

[50] S. Hietanen, *Acta Chem. Scand.* 8, 1626 (1954).

[51] L. G. Sillén, *Acta Chem. Scand.* 8, 318 (1954).

of about 40, and analysis of the interference results gave a degree of polymerization of only 10 (weight average). The new results again indicate a higher degree of aggregation in chloride than in perchlorate media, but also show that, for such highly polydisperse systems, interpretations based on refractive-index gradients must be made with considerable caution.

Pb(II) in Acidic Solutions

Most of the centrifugation studies of hydrolyzed metal solutions to date have been concerned with ions having charges of +3 or +4 before hydrolysis. Hydrolytic polymers have been reported for some +2 ions, for example, Be(II) (ref 52), Cu(II) (ref 53), and Pb(II) (ref 54). Dilution and titration curves[54] for Pb(II) have been interpreted on the basis of a tetrameric lead species.

Preliminary ultracentrifugation studies of Pb(II) in perchlorate solution indicate that low-molecular-weight polymers are formed in the range of hydrolysis studied, between hydroxyl numbers (n) about 0.5 and 1.4. Interpretation by a simple monomer-tetramer equilibrium does not seem to be adequate, however, since degrees of polymerization higher than 4 are found for $n = 1.4$. Near $n = 1$ the weight average degree of polymerization is about 4, but existence of a predominant tetrameric species has not yet been established.

Search for Hydrolytic Copolymers

Copolymerization of ions of different elements in the course of hydrolytic aggregation is an interesting possibility but is rather difficult to establish. Something of this general nature may occur in the formation of certain inorganic adsorbents, for example, zirconium tungstate, although this is by no means certain. There is some evidence for copolymerization of Zr(IV) and Hf(IV) at low concentrations of one ion in the presence of higher concentrations of the other,[55] but little evidence, to the knowledge of the authors, of such behavior by less similar metal ions, if the heteropoly acids are excepted.

[52]G. Jander and K. F. Jahr, *Kolloid-Beih.* 43, 295 (1936).

[53]C. Berecki-Beidermann, *Arkiv Kemi* 9, 175 (1956).

[54]M. Geloso and J. Faucherre, *Compt. rend.* 227, 200, 430 (1948).

[55]E. M. Larsen and P. Wang, *J. Am. Chem. Soc.* 76, 6223 (1954).

An attempt has been made to find examples by centrifuging mixtures of ions under conditions for which the polymerization of each of the solutes has been studied. If a copolymer of high molecular weight and of stability much greater than the stability of either simple polymer is formed, it should be reflected in observation of much higher molecular weights than would be observed for either ion alone.

The pairs centrifuged were 0.027 *M* Bi(III)–0.021 *M* Zr(IV) in 1 *M* $HClO_4$; 0.025 *M* Bi(III)–0.018 *M* Zr(IV) in 0.5 *M* $HClO_4$–0.5 *M* $NaClO_4$; 0.024 *M* Sn(IV)–0.027 *M* Zr(IV) in 1 *M* HCl; and 0.021 *M* Zr(IV)–0.021 *M* Mo(VI) in 3 *M* HCl. No indication was found for copolymerization in any of these systems.

TEMPERATURE COEFFICIENTS OF ION EXCHANGE EQUILIBRIA

K. A. Kraus R. J. Raridon
D. C. Michelson

A study of the temperature coefficients of ion exchange equilibria has been initiated. It is planned to study a wide variety of ion exchange equilibria with organic cation and anion exchangers, and with some of the inorganic exchangers recently developed in this laboratory.

In the method selected, various solutions are passed through a column containing a bed of uniformly loaded exchanger, and the effluent is analyzed. From these data and from the known composition of the exchangers, distribution coefficients D are obtained, and the concentration quotients $K^{()}$ of the ion exchange equilibria may be computed. At substantially constant resin and solution composition, as is the case here, $K^{()}$ is proportional to D.

The column was provided with a jacket through which a thermostatted liquid was pumped. Measurements have been carried out with two columns. One is made of glass, is not pressurized, and permits measurements up to about 85°C. The other column was specially designed for operation up to 150°C, has stainless steel fittings and a capillary glass column, and can be pressurized.

Trace-Metal Adsorption on a Sulfonic Acid Cation Exchanger

Several series of measurements have been carried out on the temperature coefficient of adsorption of typical trace-metal ions (Na^+, K^+,

Cs^+, Ba^{++}, Co^{++}, Zn^{++}, Eu^{+++}) on the hydrogen and sodium forms of a commercial sulfonic acid–polystyrene–DVB resin (Dowex 50 × 12). The tracers were in acid ($HClO_4$) or sodium salt ($NaClO_4$ or NaCl) solutions of sufficient dilution so that the distribution coefficients D of the trace ions were large and depletion of the columns during an experiment was small. In most cases distribution coefficients were measured at about 20°C intervals from 2 to 145°C and checked at the same temperatures, as the columns were cooled. The two sets of measurements usually agreed within a few per cent, and no detectable destruction of the exchanger occurred during its relatively brief contact time with the aqueous solutions at the elevated temperatures. A series of measurements was usually completed within about 8 hr; contact time above 100°C was about 2 hr, and at 145°C about ½ hr.

Without exception, the logarithms of the distribution coefficients did not vary linearly with $1/T$ as might be expected if the heats of reaction (ΔH) for the ion exchange equilibria were constant and independent of the temperature. Plots of log D vs molarity of supporting electrolyte showed inflection points for some reactions involving the Na^+ form of the exchangers, possibly because of interference from hydrolytic reactions. Before being reported, these experiments will be rechecked. For the equilibria involving the hydrogen-form exchangers, log D seemed to be approximately a quadratic function of $1/T$. Minimums, where $\Delta H = 0$, occurred in several cases in the temperature range studied (see Fig. 44). While the data could reasonably well be fitted to a quadratic in $1/T$, the final function chosen was of the form $\log D = A' \log T + B'/T + C'$, which holds when the differences in heat capacities of the products and reactants are constant. For convenience in computation, this function was rewritten in the form

$$(1) \quad \log \frac{D}{D_0} = A \log \frac{T}{T_0} + B\left(1 - \frac{T_0}{T}\right) ,$$

where T_0 is a reference temperature (here 0°C) and D_0 the distribution coefficient at T_0. The constants A and B were evaluated by a graphical-iterative method and are listed in Table 44. The heats for the reactions

$$(2) \quad M^{z+} + zH^+_{(r)} \longrightarrow M^{z+}_{(r)} + zH^+$$

were obtained by differentiation of Eq. 1 and are tabulated in Table 45.

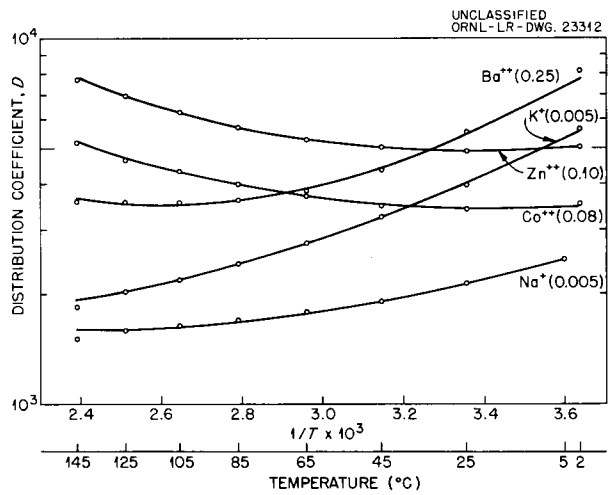

Fig. 44. Temperature Dependence of Cation Exchange Equilibria. Hydrogen form of Dowex 50 × 12; trace concentration of metals; $HClO_4$ solutions with molarity indicated in parentheses; points are experimental data; solid lines are computed with Eq. 1.

Table 44. Temperature Dependence of Ion Exchange Equilibria (Hydrogen Form Dowex 50 × 12) Constants in Eq. 1

Ion	A	B
Na^+	5.240	−3.400
K^+	5.846	−4.485
Ba^{++}	12.67	−7.734
Co^{++}	7.12	−3.286
Zn^{++}	8.56	−4.027

Table 45. Enthalpy Changes for Some Cation Exchange Equilibra (Hydrogen Form Dowex 50 × 12)

Temperature (°C)	ΔH (kcal)				
	Na^+	K^+	Ba^{++}	Co^{++}	Zn^{++}
0	−1.41	−2.43	−2.79	−0.24	−0.39
25	−1.15	−2.14	−2.16	0.11	0.04
50	−0.89	−1.85	−1.53	0.47	0.46
100	−0.36	−1.27	−0.27	1.17	1.31
150	0.16	−0.69	0.99	1.88	2.16
200	(0.68)*	(−0.11)*	(2.25)*	(2.59)*	(3.01)*

*Extrapolated values.

Adsorption of Acids and Bases by Hydrous Zirconium Oxide

Certain oxides such as zirconium oxide can adsorb acids or bases in a manner reminiscent of weakly basic anion and weakly acidic cation exchangers, respectively.[56] The temperature coefficient of these reactions has now been investigated with a hydrous zirconium oxide which was prepared by precipitation of Zr(IV) with ammonia, followed by overnight drying at 105°C.

To convert the oxide to the chloride form containing a known amount of Cl^-, it was first treated with excess ammonia to remove residual chloride ions, washed with water, and then treated with sufficient dilute HCl to make the equilibrium acidity about 10^{-2} *M*. At this point the solid contained 0.799 mole of Cl^- per kilogram of adsorbent. The temperature coefficient of the HCl adsorption reaction was studied at essentially constant Cl^- content of the solid and in the temperature range 25 to 85°C by measuring equilibrium acidities in the presence of an excess of chloride ions (about 0.1 *M* KCl). In various series of experiments, it was found that the logarithm of the acidity varies approximately linearly with $1/T$. Measurements carried out with increasing temperature usually did not follow this linear relationship as closely as those carried out with decreasing temperature, presumably because of an aging of the solid at the higher temperatures. The slopes of plots of log *M* H^+ vs $1/T$ which were obtained in several series of measurements were surprisingly constant and reproducible if the measurements were carried out with decreasing temperature. A typical set of results is illustrated in Fig. 45. From the slope of this plot, $\Delta H = -6.9$ kcal can be calculated for the reaction

$$(3) \qquad H^+ + Cl^- \longrightarrow H^+_{(r)} + Cl^-_{(r)}$$

where (*r*) refers to the solid (exchanger) phase.

A similar series of measurements was carried out with the same hydrous zirconium oxide pretreated with KOH (0.311 mole of OH^- per kilogram of adsorbent). The hydroxide ion concentration of KCl solutions (about 0.1 *M*) in equilibrium with the solid was determined. As in the HCl measurements the data followed a linear relationship

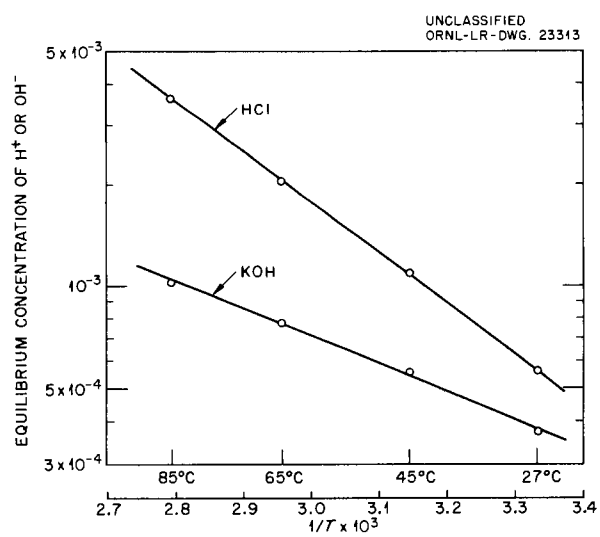

Fig. 45. Temperature Dependence of HCl and KOH Adsorption by Hydrous Zirconium Oxide.

[56] K. A. Kraus and H. O. Phillips *J. Am. Chem. Soc.* 78, 249 (1956).

between log M OH^- vs $1/T$. A typical set of results obtained with decreasing temperature is included in Fig. 45. From these data, $\Delta H = -3.8$ kcal for the reaction

$$K^+ + OH^- \longrightarrow K^+_{(r)} + OH^-_{(r)}$$

can be obtained.

SOLUBILITY OF CHLOROAURATES IN HCl AND IN LiCl SOLUTIONS

K. A. Kraus D. C. Michelson

It was mentioned in the previous report[57] that with packed-column techniques, solubilities could be measured rapidly and conveniently. This method has now been used for measurement of the solubility of $CsAuCl_4$ in HCl and in LiCl solutions from 25 to 75°C. The solubility was substantially constant in HCl solutions (0.1 to 16 m) at constant temperature, but in LiCl solutions (0.1 to 19 m) decreased by approximately a factor of 4. The solubilities increased with temperature in the range studied, and the change of solubility with supporting electrolyte concentration was essentially independent of temperature.

The variation of solubility of $CsAuCl_4$ with HCl and LiCl concentration was compared (at 25°C) with variations of tetramethylammonium chloroaurate, benzyltrimethylammonium chloroaurate, and cesium perchlorate (see Fig. 46). For $CsClO_4$ the solubilities in HCl and in LiCl solutions were practically the same and essentially independent of supporting electrolyte concentration. For $(CH_3)_4NAuCl_4$ the logarithm of the solubility varied approximately linearly with supporting electrolyte concentration, with LiCl solution causing as much salting-out as HCl caused salting-in. For the compound $\phi CH_2N(CH_3)_3AuCl_4$ the results were similar to those for $(CH_3)_4NAuCl_4$, although both salting-in and salting-out were more pronounced. In 16 m solutions the solubility was approximately 100 times greater in HCl than in LiCl. These differences in salting coefficients are remarkably large. They point out dramatically the dangers involved in concluding, from the similarity of the activity coefficients of HCl and LiCl in binary

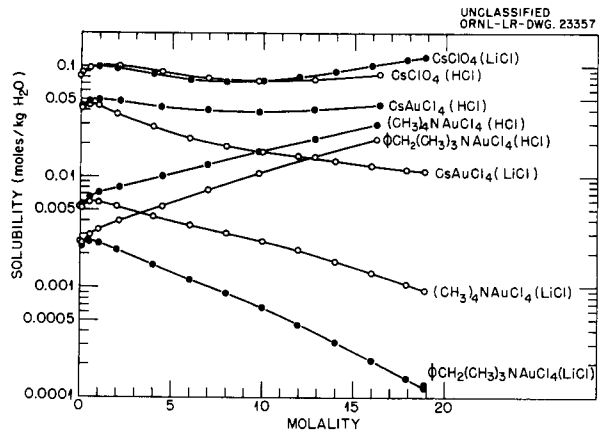

Fig. 46. Solubility of Various Salts in HCl and in LiCl Solutions (Temperature, 25°C).

mixtures, that salts dissolved in these solutions would also have the same activity coefficients. The large differences in activity coefficients of benzyltrimethylammonium chloroaurate in HCl and LiCl solutions are reminiscent of the enormous differences in the adsorbabilities of $AuCl_4^-$ by anion exchangers from HCl and LiCl solutions,[58] although the exact relationship between these two types of measurements is somewhat obscure.

DISPERSIONS OF THORIUM OXIDE

T. A. Carlson J. S. Johnson
K. A. Kraus

Work has continued on the properties[59,60] of concentrated polymer solutions of Th(IV). These polymer solutions or dispersions of thorium oxide are prepared from precipitates of so-called thorium hydroxide dried at moderate temperatures. These solids can readily be dispersed in water to yield "solutions" containing up to 2 kg of ThO_2 per liter. The dispersions seem to contain crystallites of ThO_2 with approximately 1000 Th(IV) ions per particle and with a diameter of 35 Å. The dispersions have high stabilities at room temperature and at slightly elevated temperatures but tend to precipitate or jell within a few minutes at 250°C.

[57] K. A. Kraus and D. J. Coombe, *Chem. Semiann. Prog. Rep. June 20, 1956*, ORNL-2159, p 42.

[58] K. A. Kraus *et al.*, *J. Am. Chem. Soc.* **77**, 1391 (1955).

[59] K. A. Kraus and D. J. Coombe, *Chem. Semiann. Prog. Rep. June 20, 1956*, ORNL-2159, p 42.

[60] K. A. Kraus *et al.*, *HRP Quar. Prog. Rep. Jan. 31, 1956*, ORNL-2057, p 136, esp 139, and previous HRP quarterly progress reports.

Attempts to increase the thermal stability of these dispersions so far have met with only moderate success. A large number of additives were tried, most of which had little or no effect on the rate of precipitation at 250°C. Some increased stability, however, resulted on addition of Mo(VI), W(VI), Bi(III), Zr(IV), and silicates. Most successful of these was W(VI), which, if incorporated in the solid by coprecipitation in amounts of 1 to 5 mole %, prevented precipitation for one to two days at 250°C.

It is to be anticipated that solutions of the polymer would exhibit ion exchange properties similar to those shown by solid oxides. In particular, it is of interest to establish if these polymer solutions which result from dried hydrous oxides lie intermediate in properties between those of insoluble materials dried at lower and higher temperatures. Through emf measurements (activity of HCl) as a function of added NaOH, a substantial buffering region was established for the polymer solutions, and, as long as the solutions are still acidic, the "capacity" of the polymer for chloride ions seems to be intermediate between the capacities of oxides dried at 115 and 500°C. Some differences were found for neutral and basic solutions, but their significance cannot be firmly established as yet.

Measurements are under way to establish the heat of adsorption of HCl by the polymer by measuring the activity of HCl (emf) in chloride-containing polymer solutions as a function of temperature. In preliminary measurements in the range of 25 to 80°C, ΔH for the reaction

$$H^+ + Cl^- \rightleftharpoons H^+_{(p)} + Cl^-_{(p)}$$

where subscript (p) indicates the polymer, was found to be approximately −6 kcal. No measurements have so far been carried out with solid hydrous thorium oxide, although it is of interest to compare the result with the heat of adsorption of HCl on hydrous zirconium oxide (see "Adsorption of Acids and Bases by Hydrous Zirconium Oxide," this report), where $\Delta H = -6.9$ kcal was observed.

ADSORPTION ON INORGANIC MATERIALS

H. O. Phillips K. A. Kraus
T. A. Carlson

The systematic investigation of adsorption and ion exchange properties of inorganic materials, which was initiated several years ago, has continued. As in the past, the principal interest centered around anion and cation exchange properties of hydrous oxides and on the cation exchange properties of certain "acidic salts" such as zirconium phosphate, molybdate, and tungstate.

Anion and Cation Exchange Properties of Hydrous Oxides

The relative importance of anion exchange properties in acidic solutions and of cation exchange properties in basic solutions has now been established for most of the acid-insoluble oxides. The investigations at present include the hydrous oxides of Ti(IV), Zr(IV), Th(IV), Sn(IV), V(V), Nb(V), Ta(V), and U(VI) as well as of Fe(III) and Bi(III). All these oxides except V(V) and U(VI) show, in acidic solutions, good anion exchange properties. The capacities, for example, for chromate, however, differ widely, with the most acidic of these oxides [Ti(IV) and Nb(V)] showing the least capacity. The hydrous oxide of U(VI), which is relatively soluble in acidic solutions, was not studied below pH about 6, where its anion exchange capacity was essentially negligible. All the oxides except those of Bi(III) showed cation exchange properties in strongly basic solutions. Their capacity for alkali-metal uptake varied roughly with the acidity of the oxides and was highest for Ti(IV), Nb(V), and U(VI).

The studies were carried out with oxides fired at various temperatures between 25 and 800°C. The capacity for anions and cations decreases with drying or firing temperature, although this decrease in general is not substantial until the firing temperature exceeds about 300°C. With thorium oxide, anion exchange capacity showed an interesting maximum when the firing temperature was about 300°C. In the case of U(VI) the capacity was not greatly decreased even after firing to 800°C, presumably because this oxide can rehydrate relatively easily on immersion in water.

One of the most characteristic properties of oxides as anion exchangers is their high selectivity for certain polyvalent anions. Compared with singly charged anions the high selectivity for chromates has been mentioned repeatedly in earlier reports, and, indeed, chromate uptake has been used routinely by the authors to determine approximate capacities of the exchangers. The hydrous

oxides also strongly adsorb molybdate and tungstate, sulfate, phosphate and arsenate, and borate and vanadate. Of the singly charged anions, their selectivity for fluoride is remarkably high. In general, they may thus be used for the removal of these anions from various waste liquors. They may be regenerated with sodium hydroxide, and in some cases with ammonia. Separation of the polyvalent anions from each other has so far not been completely satisfactory.

In neutral or basic solutions the oxides can adsorb metals, even those which do not undergo hydrolytic reactions, such as the alkali metals and alkaline earths. Alkali metals can usually be removed with concentrated ammonium salt solutions, while the alkaline earths remain adsorbed. The latter can then be removed with acids. In some cases, alkali metals may be removed with NH_3-NH_4^+ mixtures, the alkaline earths with concentrated NH_4^+ salt solutions, and more hydrolyzable salts (e.g., rare earths) with acids. The oxides thus are very convenient for group separations of the alkali metals, alkaline earths, and rare earths. They may also be utilized for separation of the alkali metals from each other. Interestingly, the oxide of U(VI) is very useful for such purposes, as demonstrated in Figs. 47 and 48, which represent separations with about 3-cm columns of Na^+ from Rb^+ (Fig. 47) and of Cs^+ from Ba^{++} (Fig. 48).

Acid Dependence of Selectivities – Group Separation of Alkali Metals and Alkaline Earths

Exchangers such as zirconium tungstate, zirconium molybdate, and zirconium phosphate have remarkably large selectivities for various elements within a group, and they may be used for separations, for example, of the various alkali metals from each other[61,62] or of the alkaline earths,[63] with moderately short columns. This selectivity is dependent on the H^+ content of the exchangers, which in turn is reflected by the pH of the solutions.

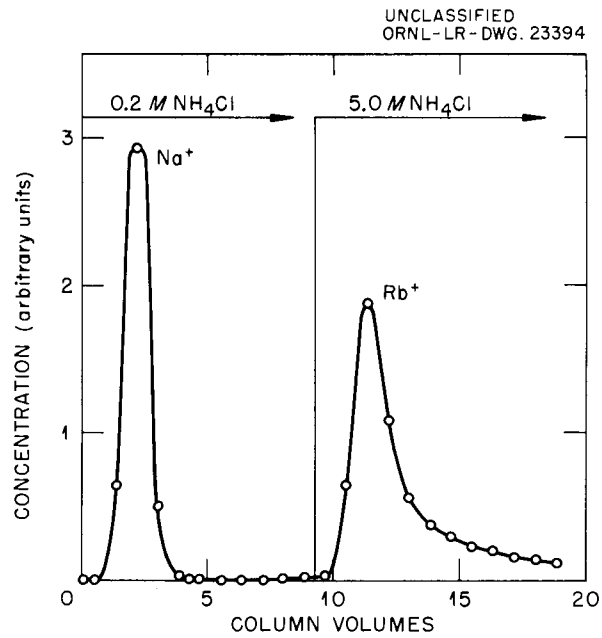

Fig. 47. Cation Exchange Separation of Na^+ and Rb^+ with Uranium(VI) Oxide. Column, 0.2 cm^2 × 3 cm; flow rate, 1 cm/min.

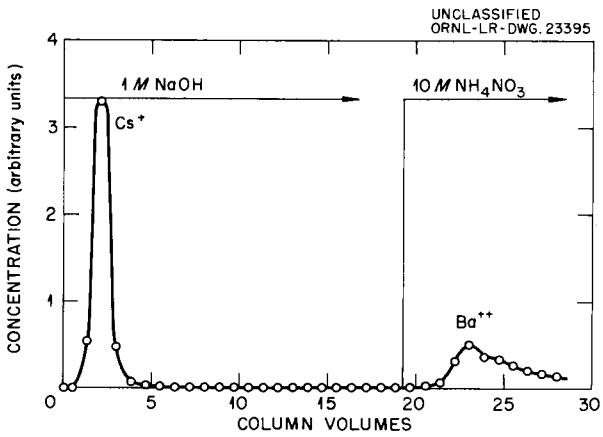

Fig. 48. Cation Exchange Separation of Cs^+ and Ba^{++} with Uranium(VI) Oxide. Column, 0.2 cm^2 × 3 cm; flow rate, 1 cm/min.

The pH dependence of adsorbabilities is illustrated for some alkali metals and "zirconium tungstate" in Fig. 49. The measurements were carried out in 0.45 *M* KCl (Rb^+, Cs^+) and in 0.1 *M* KCl (Na^+). To compensate partially for differences in supporting electrolyte concentration $\left(m_{K^+}\right)$ and

[61] K. A. Kraus and H. O. Phillips, *J. Am. Chem. Soc.* 78, 694 (1956).

[62] K. A. Kraus, T. A. Carlson, and J. S. Johnson, *Nature* 177, 1128 (1956).

[63] T. A. Carlson *et al.*, *Chem. Semiann. Prog. Rep. June 20, 1956*, ORNL-2159, p 40, esp 41.

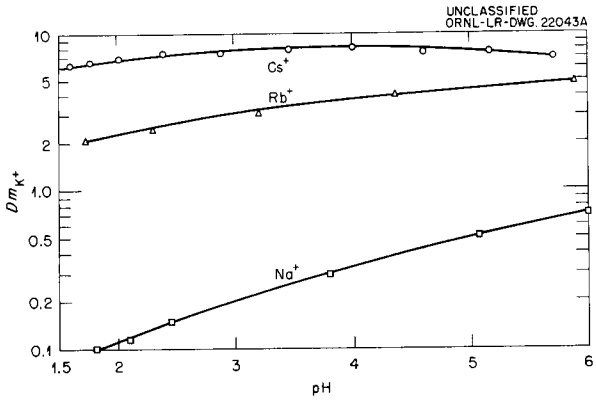

Fig. 49. Adsorption of Alkali Metals by "Zirconium Tungstate."

hence to make the data more directly comparable, Fig. 49 gives plots of log Dm_{K^+} rather than of log D vs pH. Except for Cs^+, the distribution coefficients D rise with increasing pH, and relative adsorbabilities (ratios of distribution coefficients) decrease with pH. Presumably at still higher pH values the adsorbabilities of the various alkali metals will become equal and they will then be elutable as a group in a relative sharp band. Such high pH values cannot be reached with zirconium tungstate because of its instability (loss of tungstate) in basic solutions. With zirconium phosphate, for which stability in basic solutions is very much greater than for the tungstate, a complete loss of relative selectivities was observed for the alkali metals in basic solutions, and it was possible to elute the alkali metals as a group. In neutral or basic solutions, most other metals, including the alkaline earths, become extremely strongly adsorbed by zirconium phosphate, and the specific isolation of the alkali metals from most elements in the periodic table should become feasible.

Utilization of zirconium phosphate in basic solutions for group separations is illustrated in Fig. 50, which shows separation of the alkali metals and the alkaline earths from each other. Zirconium phosphate was first treated with ammonia to convert it to the NH_4^+ form. Alkali metals and alkaline earths were adsorbed from dilute NH_4Cl solutions containing some ammonia. The alkali metals (Na^+, K^+, Cs^+) were removed with 1 *M* NH_4Cl. Under these conditions the alkaline earths are retained strongly by the exchanger. They may readily be removed with 1 *M* HCl. The column was only 2 cm high, and as implied by the wide separation of the groups (Fig. 50) could have been substantially shorter.

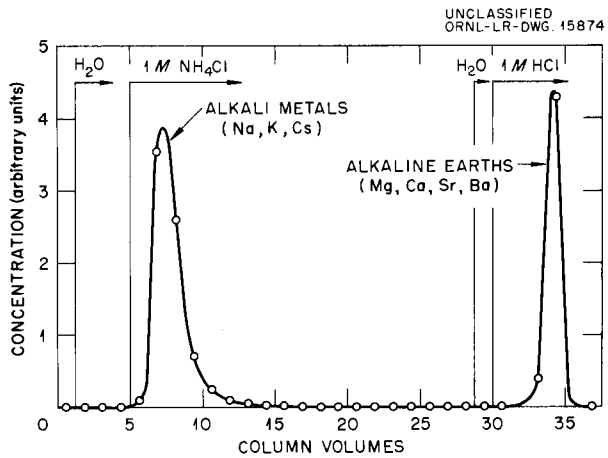

Fig. 50. Group Separation of Alkali Metals and Alkaline Earths with "Zirconium Phosphate." Drying temperature, 25°C; pretreatment, 1 *M* NH_3; column, 0.2 cm^2 × 2.0 cm; flow rate, 1.1 cm/min; loading (per element), 0.025 equiv/kg adsorbent.

CHEMISTRY OF CORROSION

ELECTROCHEMISTRY OF CORROSION SYSTEMS

G. H. Cartledge R. E. Meyer
F. A. Posey R. F. Sympson[1]

The work concerned with fundamental electrochemistry has included studies along three chief lines since its initiation five years ago. These subjects were (1) the electrochemical characteristics of stainless steel and zirconium under a variety of conditions, (2) the action of inorganic inhibitors of corrosion, and (3) the nature of passivity and the passivation process. The principal results of these investigations will be summarized briefly before presenting the more recent work in greater detail.

One study concerns the electrochemistry of stainless steel related to its corrosion. This has involved experiments on the activation and repassivation of specimens initially oxidized superficially in air and then exposed to aerated dilute sulfuric acid at 85°C. It was discovered that there is a "critical recovery potential" above which spontaneous passivation occurs under the conditions of the experiments. This potential was found to coincide, within a few millivolts, with the reversible hydrogen potential in the same environment.[2] The potential-time curves showed characteristic inflections or other features that are related to the corrosion or film-forming processes. Several details of these processes appear to be understood reasonably well. The results account nicely for the fact, observed previously in practice, that there is often a narrow boundary between conditions that passivate stainless steel and those that permit continuous corrosion.

In extension of this work, the effect of numerous ions in low concentrations was investigated. It was found that many reducible ions cause an ennobling of the potential in such a way that, over a considerable range of concentrations, a linear potential-log activity relation is obtained, the slope of which is often near a 2.3 RT/nF value. In addition, one of the systems (addition of Cu^{++}) was carefully examined by potentiostatic and galvanostatic procedures, as well as by use of tracer Cu^{64} (ref 3). These experiments show clearly how cupric ions act in inhibiting the corrosion of stainless steel in sulfuric acid.

The addition of foreign ions, as in the experiments just cited, provides a multiplicity of possible electrode reactions and alters the kinetics of the processes involved in corrosion or in passivation. Hence the absolute rate theory of electrode processes has been amplified to cover the case of independent, simultaneous charge-transfer processes at an electrode, which is considered to have a distribution of activation energies for each process over its surface. The completely general equations derived will be useful in interpreting a variety of electrochemical data. Certain of the equations and their applications are presented in outline in the following section.

Further experiments are being initiated in which irradiated stainless steel will be used, in order to permit measurement of the very slow corrosion rate under passivating conditions by continuous counting of the radioactivity passing into solution. Another problem is to determine the nature of the changes in the surface state of the metal that are associated with the enhanced corrosion rate and dull black color observed when the potential is somewhat more noble than the value at which cathodic protection results.

A brief study of the effect of gamma radiation on the electrochemical behavior of stainless steel was made. It was found that the results could be interpreted in terms of the radiolytic products from the electrolyte and their known effects on the electrode potential.[4]

The studies on stainless steel are being paralleled by a corresponding investigation of the polarization characteristics of zirconium. The measurements are being made over a very wide range of current densities and with extreme precautions as to homogeneity of sample, surface preparation, and purity of electrolyte and atmosphere. A summary of the results thus far obtained is presented below (see "Electrochemistry of Zirconium").

[1] Summer employee, Ohio University.

[2] G. H. Cartledge, *Nature* 177, 181 (1956); *J. Electrochem. Soc.* 104, 420 (1957).

[3] F. A. Posey, R. P. Yaffe, and G. H. Cartledge, to be published in *J. Electrochem. Soc.*

[4] W. E. Clark, to be published in *J. Electrochem. Soc.*

The second general field of investigation has been the action of inorganic corrosion inhibitors. In an attempt to identify the reason for the specificity of the inhibitory property in the XO_4^{n-} particles, a short-range electrostatic interaction arising from polarity within the particle was conceived to be the unique feature. This idea led to the discovery of the strong inhibiting action of the pertechnetate ion.[5] It was shown that even 5 ppm of technetium element (5×10^{-4} *f* $KTcO_4$) inhibited the attack on a 0.1% carbon steel in aerated water at 250°C, as well as at lower temperatures. In a series of studies it was shown, by measurement of beta activity, that inhibition may be achieved under certain very corrosive conditions without depositing more than minute amounts ($\sim 3 \times 10^{12}$ molecules per cm^2) of reduced inhibitor on the metal, and also that there has been no continuing consumption of inhibitor over the 4.5 years during which the activity of the immersed specimen has been followed. It was shown that the inhibition and the noble electrode potential associated therewith are due to a labile and reversible state which depends upon the relative concentration of the anions in solution, exactly as though a competitive adsorption were involved.[6]

A comparative study was made of the XO_4^{n-} particles derived from most of the transition metals of groups V to VIII of the periodic system. These measurements showed that the lability with respect to competing ions also characterized the other effective inhibitors in these groups.[7] The discovery that the perrhenate ion fails to inhibit under any of the conditions in which the pertechnetate ion is effective further emphasized the necessity of seeking the specificity inside the inhibitor particle, rather than in effects to which previous theories ascribed the action.[8] From the standpoint of both theory and observation, it appears not unjustified to say that technetium has the most suitable combination of inhibitory properties of all the elements.

A third series of studies dealing with passivity and the nature of the passivation process is an outgrowth of the work on inhibitors. It was found that a 0.04 *f* solution of osmium(VIII) oxide (OsO_4) passivates iron so completely that the iron indicates the reversible potential of the Os(IV)–Os(VIII) couple, with no detectable polarization due to an anodic corrosion process.[9] The action of OsO_4 resembles that of the other XO_4^{n-} inhibitors in being sensitive to competing ions, still further confirming the view that an adsorption process is involved.

The essential inactivity of iron in the experiments with osmium and technetium led to a new hypothesis regarding the nature of the film on passive iron and a new interpretation of the Flade, or passivation, potential.[10] According to this view, the Flade potential is the reversible potential of the electrode process

$$e^- + H^+ + FeO(OH) \rightleftharpoons \text{"}Fe(OH)_2\text{"}$$

where $E_h^0 = 0.58$ v. The symbol "$Fe(OH)_2$" is used to represent a surface film in contact with the metallic phase and, by this contact, stabilized by about 12 kcal·mole^{-1}, in comparison with bulk ferrous hydroxide. (It is not clear whether anhydrous or hydrated oxides should be represented, although there are some reasons favoring the formulation above. The free-energy relations are not significantly different in the two cases.)

In the measurement of the electrode potential of iron in aerated inhibitor solutions, it was observed[6] that halts in the potential-time curves sometimes occurred at about the value of the Flade potential. This suggested that there is no essential electrochemical difference between the surface film produced under these conditions and that formed by violent passivation procedures, such as by use of concentrated nitric acid or a sufficiently strong anodic polarization. A systematic investigation has shown that this is, indeed, the case, in that the Flade potential was found as a definite halt in the potential-time curves when iron was brought to noble potentials by an aerated inhibitor and then activated by addition of sulfate ions in sufficient concentration.

---

[5] G. H. Cartledge, *J. Am. Chem. Soc.* 77, 2658 (1955); *Corrosion* 11, 335t (1955); *J. Phys. Chem.* 59, 979 (1955).

[6] G. H. Cartledge, *J. Phys. Chem.* 60, 28 (1956).

[7] R. F. Sympson and G. H. Cartledge, *J. Phys. Chem.* 60, 1037 (1956).

[8] G. H. Cartledge, *J. Phys. Chem.* 60, 32 (1956).

[9] G. H. Cartledge, *J. Phys. Chem.* 60, 1468 (1956).

[10] *Ibid.*, p 1571.

The experiments are abstracted below (see "Evidence for a Flade Potential on Inhibited Iron Electrodes").

A review of the work on passivation and a discussion of evidence for the electrostatic point of view and its relevance to corrosion have been prepared.[11] It is shown that the space charge which an adsorbed XO_4^{n-} inhibitor may induce over a distance of a few Angstrom units below the surface of a substrate is of similar character to effects that are of importance in the behavior of heterogeneous catalysts and of semiconductors.

The work, taken as a whole, makes it clear that it is not correct to think of stainless steel as being fundamentally unlike iron or inherently noble, with respect to corrosion. The essential difference is in the greater ease with which the reduction of hydrogen ions may be diminished on stainless steel, so that it may be passivated by oxygen, with consequent greater acid resistance of the film so formed. Further research is therefore planned to study the properties of such films, by treating them as semiconducting oxidation-reduction electrode systems, the composition of which may be varied by "doping" the metal. From the results of such studies it may become possible to control the polarization characteristics, and hence the corrosion rates, by rational means.

STUDIES ON CORROSION SYSTEMS INVOLVING INDEPENDENT, SIMULTANEOUS ELECTROCHEMICAL REACTIONS

F. A. Posey

Numerous investigations have contributed to the foundations and experimental applications of the absolute rate theory of electrochemical reactions,[12] and comprehensive reviews of this work have been published.[13-15] However, in the study of some of the more complex electrochemical systems, such as corrosion systems, there exists a need for a more elaborate formalism than that presented previously in order to interpret the phenomenology. Accordingly, a kinetic treatment of two-phase, multicomponent electrochemical systems has been developed, and the detailed propositions and deductions of this theory will be described elsewhere.[16] The term, multicomponent, as used here, refers to the situation where more than one individual or partial process is occurring at an electrode-solution interphase. Each partial process involving charge transfer between phases is designated as a component of the electrochemical system under consideration. The term, two-phase system, denotes a metallic electrode in contact with an environment in the liquid state capable only of ionic conduction; considerations of measuring instrument and reference electrode circuits are excluded. Particular attention has been devoted to the mechanistic significance of measurable electrochemical quantities and to the kind of information obtainable about multicomponent systems, especially corrosion systems, from some of the usual operations.

Part of the uniqueness of the approach is its concern with variations in partial-process current densities over the surface of an electrode, and with the effect of these variations on observable electrochemical quantities. Three levels of current density are found to be important in electrochemical systems. The first of these levels is expressed by the equation

$$j_i = \lambda_i \mathfrak{F} k_i a_i^{p_i} , \tag{1}$$

wherein the current density, j_i, of the ith partial process at a very small (differential) element of area, dS, on an electrode is related to the absolute value of the net number of charges transferred across the interphase during the course of one reaction sequence (λ_i), to Faraday's constant ($\mathfrak{F}$), to a specific rate constant (k_i), and to the product of the kinetic activities of the reactants (symbolized by $a_i^{p_i}$, where p_i denotes the kinetic order of the reaction with respect to the various reactants). The second level of current density is the net current density, j_σ, at a differential element of area on an electrode, given by the equation

$$j_\sigma = \sum_i (j_{i,a} - j_{i,c}) \tag{2}$$

[11] G. H. Cartledge, to be published in *Z. Elektrochem.*

[12] S. Glasstone, K. J. Laidler, and H. Eyring, *The Theory of Rate Processes*, 1st ed., p 552 ff., McGraw-Hill, New York, 1941.

[13] J. O'M. Bockris, *Modern Aspects of Electrochemistry*, p 180 ff., Academic Press, New York, 1954.

[14] K. J. Vetter, *Z. Elektrochem.* 59, 596 (1955).

[15] H. Gerischer, *Z. Elektrochem.* 59, 604 (1955).

[16] Theoretical and experimental results will be presented in detail in two papers to be submitted for publication to the *J. Electrochem. Soc.*

as the difference in total anodic and total cathodic partial-process current densities. Subscript a refers to an anodic process, entailing a transfer of positive charge from electrode to solution or of negative charge in the reverse direction; likewise, subscript c refers to a cathodic process with a corresponding transfer of negative charge from electrode to solution or of positive charge in the reverse sense. Current densities are denoted here by j, currents by i. Partial-process current densities and currents are considered as positive quantities, and positive or negative signs are affixed according to whether the particular partial processes are anodic or cathodic, respectively. The signs of all other current quantities and derived functions, such as the sign of an externally applied current, are fixed by this procedure.

The sign of j_σ depends on the relative energetics of the various partial processes occurring at dS, on the properties of the rest of the electrode, and on the sign and magnitude of any current applied to the electrode from an external agency. The third important current quantity is the total applied, polarizing, or integral current, i_P, given by Eq. 3, on integrating j_σ over the surface area, S, of the electrode:

$$(3) \quad i_P = \int_0^S j_\sigma \, dS = \int_0^S \left[\sum_i (j_{i,a} - j_{i,c}) \right] dS \; .$$

By use of the form of the specific rate constants, k_i, provided by the absolute rate theory of electrochemical reactions, Eq. 4 follows from Eq. 3:

$$(4) \quad i_P = \mathfrak{F}\left(\frac{kT}{h}\right) \int_0^S \sum_i \left[\lambda_{i,a} K_{i,a} a_{i,a}^{p_{i,a}} \exp\left(-\frac{A_{i,a}}{RT}\right) \exp\left(+\frac{\alpha_{i,a}\lambda_{i,a}\mathfrak{F}}{RT}\Delta\phi\right) - \right.$$
$$\left. - \lambda_{i,c} K_{i,c} a_{i,c}^{p_{i,c}} \exp\left(-\frac{A_{i,c}}{RT}\right) \exp\left(-\frac{\alpha_{i,c}\lambda_{i,c}\mathfrak{F}}{RT}\Delta\phi\right) \right] dS \; .$$

This is the fundamental expression of the present model describing two-phase, multicomponent electrochemical systems under activation control. Here, (kT/h) has its usual significance of the decomposition frequency of activated complexes, K_i is the transmission coefficient of the ith partial process, A_i is the standard chemical free energy of activation, α_i is the electrochemical transfer coefficient, and $\Delta\phi$ is the absolute Galvani potential difference, $\phi_m - \phi_s$, between the interior of the metal electrode and the outermost portion of the diffuse double layer in the solution. In the general case the differential form of the fundamental expression, Eq. 4, is simultaneous with Eq. 5,

$$(5) \quad j_s = -\sigma_s \cdot \nabla\phi_s = \sigma_s \cdot E_s \; ,$$

which functions as a boundary condition, relating the net current density at a differential element of area in the solution, j_s, to the specific conductance, σ_s, and to the gradient of potential in the solution, $\nabla\phi_s$, or to the "solution conductance field," E_s. It can be shown that, for very many cases of interest, the boundary condition may be completely neglected in characterizing electrochemical systems and that the electrode-solution potential difference, $\Delta\phi$, may be taken as being constant over the surface of the electrode to an excellent approximation.

Equations 2 and 4 may be solved exactly for certain quantities of interest in the case of a simple, two-component (one anodic and one cathodic) corrosion system with no externally applied current, where it is presumed that chemical free energies of activation are the only factors varying significantly over the surface of an electrode. Equation 6 gives the electrode-solution potential difference, $\Delta\phi$, of such a system in terms of quantities defined above (the subscript i is dropped in the presentation of equations pertaining to a two-component system):

$$(6) \quad \Delta\phi = \frac{1}{\alpha_a\lambda_a + \alpha_c\lambda_c} \cdot \frac{RT}{\mathfrak{F}} \left[\ln \frac{K_c\lambda_c}{K_a\lambda_a} + \ln \frac{a_c^{p_c}}{a_a^{p_a}} + \ln \frac{I_c}{I_a} \right] .$$

Here,

$$I_c \equiv \int_0^S e^{-A_c/RT}\, dS \ ,$$

$$I_a \equiv \int_0^S e^{-A_a/RT}\, dS$$

are the exceedingly important exponential activation energy integrals which are characteristic of this treatment of systems with activation energy distributions.

Equation 7 is an expression for the total anodic or corrosion current of an electrically isolated, two-component corrosion system:

(7)
$$i_a = \mathfrak{F}\left(\frac{kT}{h}\right)\left(K_c\lambda_c a_c^{p_c}\right)^{\theta_a}\left(K_a\lambda_a a_a^{p_a}\right)^{\theta_c} \cdot I_c^{\theta_a} \cdot I_a^{\theta_c} \ .$$

Here,

$$\theta_a = \frac{\alpha_a\lambda_a}{\alpha_a\lambda_a + \alpha_c\lambda_c} \ ,$$

$$\theta_c = \frac{\alpha_c\lambda_c}{\alpha_a\lambda_a + \alpha_c\lambda_c} \ .$$

The quantities I_a and I_c determine the effect of the activation energy distributions on the observable kinetics. The symmetry of this equation and the interdependence of the kinetic parameters of the two partial processes in determining rates are striking. A similar expression is derivable for i_c. The dependence of the net current density, j_σ, at a differential element of area, on the energetics of the partial processes proceeding over the whole electrode, is given by the equation

(8)
$$j_\sigma = \mathfrak{F}\left(\frac{kT}{h}\right)\left(K_c\lambda_c a_c^{p_c}\right)^{\theta_a}\left(K_a\lambda_a a_a^{p_a}\right)^{\theta_c}\left[\left(\frac{I_c}{I_a}\right)^{\theta_a} e^{-A_a/RT} - \left(\frac{I_a}{I_c}\right)^{\theta_c} e^{-A_c/RT}\right] \ ,$$

where j_σ may be either positive or negative; for this case, $\int_0^S j_\sigma\, dS = 0$. Hence for electrodes with activation energy distributions, the result obtained is that variations, over the electrode surface, of the net current density crossing the interphase arise quite naturally in a kinetic analysis, in the complete absence of any variation of $\Delta\phi$ over the surface. If, as a corollary of Eq. 8, the actual distribution of activation energies were specifiable in algebraic form, so that I_a and I_c could be evaluated, Eq. 9 could be used to calculate the locus of all points where $j_\sigma = 0$ on an electrode surface:

(9)
$$A_a - A_c = RT \ln \frac{I_c}{I_a} \ .$$

This locus represents the boundary between "anodic" and "cathodic" areas, for which j_σ is positive or negative, respectively. In the general case of externally applied current, values of j_σ, and thus the locus of points where $j_\sigma = 0$, are also functions of i_p.

The predictions of previous theories of corrosion reactions in solution have been shown to arise as special cases of the present treatment, and their inadequacies and inconsistencies have been examined. Numerical examples have been developed on the basis of the model which demonstrate the importance of activation energy distributions in electrode systems and which show the effect of the boundary condition of noninfinite solution conductance in a complete system consisting of electrode(s) plus environment. Conditions have been established for the validity of applying classical thermodynamic treatments to corrosion systems or to any system characterized by simultaneous and chemically distinct redox processes at an electrode-solution interphase. It can be shown that the concepts of "equilibrium exchange current density" and "overvoltage," common to many kinetic treatments of electrode processes, lack precise significance in systems possessing activation energy distributions for one or more partial processes.

General expressions for the polarizability of multicomponent electrochemical systems under

activation rate control follow directly from Eq. 4. Because they are dimensionally different, three forms of the polarizability, denoted by P_A, P_B, and P_C, are distinguished and defined by Eqs. 10, 11, and 12:

$$(10)\qquad P_A \equiv \left(\frac{\partial \Delta\phi}{\partial i_P}\right)_{T,a_i,\ldots} = \frac{RT}{\mathfrak{F}}\left[\sum_i\left(\alpha_{i,a}\lambda_{i,a}\int_0^S j_{i,a}\,dS + \alpha_{i,c}\lambda_{i,c}\int_0^S j_{i,c}\,dS\right)\right]^{-1},$$

$$(11)\qquad P_B \equiv \left(\frac{\partial \Delta\phi}{\partial j_P}\right)_{T,a_i,\ldots} = \frac{RT}{\mathfrak{F}}\left[\sum_i\left(\alpha_{i,a}\lambda_{i,a}\overline{j_{i,a}} + \alpha_{i,c}\lambda_{i,c}\overline{j_{i,c}}\right)\right]^{-1},$$

$$(12)\qquad P_C \equiv \left(\frac{\partial \Delta\phi}{\partial \ln i_P}\right)_{T,a_i,\ldots} \equiv \left(\frac{\partial \Delta\phi}{\partial \ln j_P}\right)_{T,a_i,\ldots} = \frac{RT}{\mathfrak{F}}\left[\frac{\sum_i\left(\overline{j_{i,a}} - \overline{j_{i,c}}\right)}{\sum_i\left(\alpha_{i,a}\lambda_{i,a}\overline{j_{i,a}} + \alpha_{i,c}\lambda_{i,c}\overline{j_{i,c}}\right)}\right].$$

Equations 11 and 12 are expressed in terms of the average current densities of the individual partial processes, defined as

$$\overline{j_{i,a}} \equiv \frac{\int_0^S j_{i,a}\,dS}{S}, \ \ldots .$$

The well-known and much-abused Tafel relation is a special case of Eq. 12. Polarizability measurements find importance in estimating rates of electrode processes and in determining the kinetic quantities, $\alpha_i\lambda_i$, which have significance with respect to the mechanisms of the partial processes. It can be shown that polarizability measurements provide diagnostic criteria for reversibility in two-component systems. A relationship (Eq. 13) between the polarizability of a multicomponent corroding electrode at its corrosion potential, $P_{B,0}$, and its corrosion rate, $\sum_i \overline{j_{i,a}}$, follows from Eq. 11 and allows calculation of corrosion rates from polarizability measurements to an accuracy of a small numerical factor, even in the absence of auxiliary knowledge of reaction mechanisms:

$$(13)\qquad \sum_i \overline{j_{i,a}} = \frac{RT}{\mathfrak{F}}\cdot\frac{1}{K}\cdot\frac{1}{P_{B,0}}.$$

Here, K (a function of $\alpha_i\lambda_i$ of the various partial processes) is a constant of the order of magnitude of unity for any system under activation control. This equation quantitatively describes data obtained by some other workers[17,18] on the relationship between corrosion rate and polarizability in certain systems.

The elementary theory of d-c potentiostatic experiments in multicomponent systems has been developed. This technique offers a means for ascertaining the independent simultaneity of all the electrode reactions (i.e., whether or not there exists a nonzero order of at least one partial process with respect to a reactant, product, or intermediate common to at least two partial processes), of establishing the kinetic order of an electrode reaction with respect to (at least one of) its reactants, and of elucidating the mechanism of the electrode reaction itself. A phenomenon observed in corrosion reactions and other multicomponent systems is an effect on the electrode potential of the addition to the solution of some oxidizable or reducible substance. In some cases, with no externally applied current, the electrode potential increases linearly with the logarithm of the concentration of the added (cathodic) component, at least at the higher concentrations.[19,20] This behavior is described quantitatively by the present rate theory in terms of experimentally

[17] K. F. Bonhoeffer and W. Jena, *Z. Elektrochem.* **55**, 151 (1951).

[18] R. V. Skold and T. E. Larson, *Corrosion* **13**, 139t (1957).

[19] R. P. Yaffe, *Chem. Semiann. Prog. Rep. June 20, 1953*, ORNL-1587, p 13.

[20] G. H. Cartledge and R. P. Yaffe, *Chem. Semiann. Prog. Rep. Dec. 20, 1953*, ORNL-1674, p 11.

measurable quantities, and Eq. 14 is a general expression for this effect:

$$(14) \quad S_{jP} \equiv \left(\frac{\partial \Delta\phi}{\partial \ln a_x}\right)_{jP}$$

$$= \mp \frac{RT}{\mathfrak{F}} \left[\frac{p_x \overline{j_x}}{\sum_i \left(\alpha_{i,a}\lambda_{i,a}\overline{j_{i,a}} + \alpha_{i,c}\lambda_{i,c}\overline{j_{i,c}}\right) + \alpha_x\lambda_x\overline{j_x}}\right].$$

Here, subscript x refers to the added constituent, and the minus or plus sign is employed according to whether the additional partial process is anodic or cathodic, respectively. When $\overline{j_x} \gg \sum_i \overline{j_{i,c}}$, and there is only one anodic partial process, Eq. 14 reduces to Eq. 15, which predicts constant S_{jP} when $j_P = 0$; this is also observed experimentally:

$$(15) \quad S_{jP} = \mp \frac{RT}{\mathfrak{F}} p_x \left[\alpha_x\lambda_x + \alpha_a\lambda_a\left(\frac{j_p}{j_x} \mp 1\right)\right]^{-1}.$$

By means of d-c galvanostatic and potentiostatic experiments on the same electrode system, it can be shown that complete characterization of partial-process current densities as a function of electrode potential and of the kinetic parameters, $\alpha_i\lambda_i$, which have mechanistic significance for these partial processes, is possible for cases where it can be demonstrated that all electrode processes are independently simultaneous. The kinetic analysis, although limited to multicomponent systems consisting of activation-controlled electrode reactions in a steady state, can be extended to include partial-diffusion rate control, partial-"reaction" rate control,[21] or other situations of mixed rate control for one or more partial processes, including partial-process reaction sequences involving alternative and/or consecutive reaction paths.

The reduction of cupric ion on the surface of passive stainless steel electrodes in aerated, dilute sulfuric acid has been investigated by using d-c potentiostatic, galvanostatic, and tracer techniques, and the results of these studies have been analyzed on the basis of the theory outlined above. The potentiostatic experiments have established that the order of the reduction reaction with respect to the concentration of cupric ions in solution is unity over an enormous range of concentrations and electrode potentials. In addition, the independent simultaneity of all the electrode reactions in the system (oxidation of steel constituents, reduction of oxygen dissolved in solution, and reduction of cupric ion) has been demonstrated.

The reduction of cupric ion proceeds by way of an intermediate in the cuprous state, and equations have been derived which express the rate of reduction as a function of concentration and electrode potential and the slope of the (electrode potential)–(logarithm of cupric ion concentration) plot as a function of quantities related to the mechanism of the reduction reaction. Evidence has been obtained which argues against the existence of an important potential difference through the oxide film on (passive) stainless steel, as compared with the potential differences at the metal–metal oxide interphase and at the oxide-solution interphase. Excellent agreement has been found between theory and experiment in galvanostatic experiments on the effect of additions of cupric ion to solution on the electrode potential of passive stainless steel. The (electrode potential)–(logarithm of current density) curves for the oxidation of steel constituents and for the reduction of oxygen dissolved in solution have been calculated from experimental data and provide support for the mechanistic interpretations advanced. The results of tracer experiments on the amount of copper retained by the electrode as a function of cupric ion concentration in solution are in good agreement with values calculated on the basis of the proposed reduction mechanism. Thus a self-consistent picture of the present electrochemical system on a mechanistic basis has been obtained. There seems to be little doubt that similar studies, involving the theory and techniques used in this concerted study of a single system, would prove to be valuable in analyzing other multicomponent corrosion systems.

ELECTROCHEMISTRY OF ZIRCONIUM

R. E. Meyer

A program of investigation of the electrochemical behavior of zirconium in sulfuric acid was initiated. Measurements made so far include open-circuit potential-time measurements and d-c polarizabilities.

[21] H. Gerischer and K. J. Vetter, *Z. physik. Chem.* 197, 92 (1951).

The program was begun by investigating the open-circuit behavior of crystal-bar zirconium electrodes in air-saturated sulfuric acid solutions at various temperatures. In general, the electrodes initially exhibited potentials several hundred millivolts below the normal hydrogen electrode. The potentials rose rapidly for several hundred millivolts and then rose slowly until, after several days, rest potentials within 100 mv of the saturated calomel electrode were recorded. The precise behavior was a sensitive function of surface treatment, temperature, and solution composition. The ennobled electrodes were extremely polarizable, which indicates a very low corrosion rate, and changes in pH, addition of Cu^{++}, and other factors which might be expected to change the potential had little or no effect. However, the ennobled electrodes exhibited a sharp drop in potential in the temperature range 80 to 95°C, and at these lower potentials the electrodes responded rapidly to changes in variables in a manner that would be expected from consideration of electrode kinetics. This effect is not fully understood and will be investigated further.

In an effort to learn more concerning the charge-transfer processes occurring at the electrode-solution interface, d-c polarizabilities are also being measured. Since the polarizabilities are very sensitive functions of impurities in solution and of surface preparation, extreme precautions had to be taken. Triply distilled water was used in making up solutions, and extensive pre-electrolysis with platinum electrodes was used. The cell was of all-glass construction with water-sealed ground glass joints and stopcocks. Especial care was taken to prevent contact of the solution with rubber stoppers, stopcock grease, or any other substance that could contaminate the electrode surface. The hydrogen used was passed over Drierite, Hopcalite (to remove CO), Ascarite, palladium and copper catalysts, and through two liquid-nitrogen traps. Surface preparation of electrodes included washing, degreasing, abrasion, chemical polishing to a bright smooth finish, and outgassing and annealing at about 750°C in high vacuum.

The current-voltage relationship at an electrode surface due to a single charge transfer process follows the equation

$$i = i_0 \exp\left[-\alpha\lambda(E - E_0)\frac{F}{RT}\right],$$

where i equals the current, i_0 equals the current when $E = E_0$, E_0 is a fixed potential taken as the reversible hydrogen potential in hydrogen overvoltage studies, λ is the number of units of charge passed, and α is the electrochemical transfer coefficient (to be discussed below). Some pertinent results for hydrogen evolution on zirconium at 25°C are presented in Table 46. In each case a linear plot of log i vs E was obtained.

Another run was made with an electrode annealed for about 6 hr at 750°C so that the grain size was considerably larger than that in the usual fine-grained specimens. This electrode did not give reproducible results, but on $\alpha\lambda$ factor of 0.55 and an i_0 of 1×10^{-8} was estimated from data taken 2 hr after immersion. Electrodes anodized to thick, visible films also gave irreproducible results which changed with time. Initially, however, thick films gave overvoltages at 0.5 ma/cm^2 of about 10 v.

A number of anodization runs were also made. Zirconium forms oxide layers upon anodization, and linear increases of voltage vs time are obtained at constant current density. It soon became evident that more precise instrumentation was necessary than was available at the time. The required equipment has been constructed by the ORNL Instrument Department, and runs will soon be continued.

The experimental data are not yet extensive enough to predict with confidence a model for the zirconium electrode. However, a few general comments can be made. An α factor of about 0.5 is frequently found in hydrogen overvoltage studies.[22] It is explained by assuming that the potential barrier involved is symmetrical and that practically the full change in potential occurs across the Helmholtz double layer at the electrode surface. This is a satisfactory approximation when the electrode is a good conductor like a metal, but probably not a good approximation when the electrode surface is an oxide or other poorly conducting medium. In this case the possibility arises that the double layer may extend into the electrode in a complex manner or that the potential barrier for a reaction may exist within the solid electrode itself. If these considerations are valid, the low α factors and high overvoltages found with oxide-covered electrodes might be expected.

[22] J. O'M. Bockris, *Modern Aspects of Electrochemistry*, Academic Press, New York, 1954.

Table 46. Kinetic Constants for Hydrogen Evolution on Zirconium

Solution Composition	Electrode Pretreatment	$\alpha\lambda$	i_0 (amp/cm^2) (E_0 = −312 vs S.C.E.)
			$\times 10^{-8}$
0.1 N H_2SO_4	Annealed 1 hr at 750°C; immersed 1 day in deoxygenated solution	0.47	1.0
	Same as above but immersed 4 days in oxygenated solution	0.33	1.9
	Anodized to +0.5 v vs S.C.E.	0.27	4.2
0.1 N H_2SO_4 + 10^{-5} M NaF	Annealed 1 hr at 750°C; immersed 2 hr in deoxygenated solution	0.51	1.26

EVIDENCE FOR A FLADE POTENTIAL ON INHIBITED IRON ELECTRODES

G. H. Cartledge R. F. Sympson

Experiments with chromate, phosphate, and pertechnetate ions have agreed in showing that, in aerated solutions, only small amounts of the inhibitor element may be found in the passivated surface, so that the effective film consists essentially of iron oxide. Accordingly, an attempt was made to determine whether the film formed in inhibited solutions behaves electrochemically like the one produced in passivation by nitric acid or like the one produced by anodic polarization in acid solution. The investigation included TcO_4^-, CrO_4^{--}, MoO_4^{--}, and WO_4^{--} in aerated solutions as the inhibiting ions. When the inhibition was destroyed by addition of sufficient sulfate ion, the falling potentials gave a definite halt before reaching the region of corrosion potentials. The acidity was varied between pH values of 5.60 and 7.03 in order to determine whether the halts had the numerical value and pH dependence of the Flade potential, namely, E_f = 0.338 − 0.059 pH at 20°C vs saturated calomel. The average values of the potential during the halts agreed with the calculated value over the pH range investigated, without regard to the identity of the inhibitor. In 21 experiments the average deviation from the theoretical value was 8 mv.

By comparison with the experiments on the passivation of stainless steel,[23] it is therefore concluded that the function of the inhibitor is to suppress reduction of hydrogen ions so that oxygen, as the effective passivating agent, can build a stable film. The detailed results are to be published.[24]

[23] G. H. Cartledge, *Nature* 177, 181 (1956); *J. Electrochem. Soc.* 104, 420 (1957).

[24] G. H. Cartledge and R. F. Sympson, *J. Phys. Chem.* (in press).

NONAQUEOUS SYSTEMS AT HIGH TEMPERATURES

HETEROGENEOUS ISOTOPIC EXCHANGE REACTIONS OF FLUORINE-CONTAINING COMPOUNDS

T. A. Gens[1] A. R. Brosi

Isotopic exchange reactions between solid inorganic fluorides and gaseous fluorocarbons have been studied for the first time. Rates of many of these exchange reactions have been measured at temperatures as low as 0°C. Of the inorganic fluorides studied, the exchange was most rapid with alkali-metal fluorides. Among the alkali fluorides the rate of the exchange reaction increased markedly with increasing atomic number of the cation.

Of the gaseous fluorine-containing compounds studied, the unsaturated fluorocarbon perfluoropropene exchanged more readily than did perfluorodiethyl ether or perfluorobutane, and the latter compounds exchanged more readily than did carbon tetrafluoride. No exchange was observed between fluoroform or sulfur hexafluoride and the alkali fluorides at temperatures below which decomposition occurred. Silicon tetrafluoride exchanged fluorine atoms with alkali fluorides at low temperatures. With the heavier alkali-metal fluorides, complex fluorosilicates were formed at moderate temperatures. In the case of lithium fluoride, although rapid exchange occurred, no detectable stable fluorosilicate was formed at temperatures up to 500°C.

Exchange of fluorine atoms between alkali fluorides and fluorocarbons appeared to proceed by two distinct mechanisms. When fluorocarbon gas first came into contact with alkali fluoride crystals, isotope exchange occurred so rapidly that only quasi-equilibrium data were obtained. The number of fluorine atoms exchanging in this fast reaction was in most cases much larger than the number of fluorine atoms on the alkali fluoride surface. The fraction of the fluorine atoms in the alkali fluoride which exchanged in the fast reaction was an exponential function of the temperature. At any given temperature, after the fast reaction had reached an apparent equilibrium, there was further exchange at a much slower rate. It is postulated that the rate-controlling step in this second stage is ionic self-diffusion of fluoride ions through alkali fluoride crystals. Although the initial rapid reaction is less well understood, it is postulated that rapid transport of fluorine atoms or ions through defect sites in the alkali fluoride crystals may be involved.

A separate report[2] has been issued which gives a complete description of the apparatus and techniques used in this work, along with a discussion of the results.

SELF-DIFFUSION IN MOLTEN SALTS

A. S. Dworkin

The self-diffusion coefficients of the ions in molten $NaNO_3$, KNO_3, and $CsNO_3$ have been measured. The data for $NaNO_3$ and KNO_3 have been reported previously.[3,4] However, since the results for KNO_3 appeared to be in error, this salt was rerun, and the new data appear below. The self-diffusion coefficient of the NO_3^- in $NaNO_3$ was also rerun with the use of the stable isotope N^{15} to follow diffusion rather than with O^{18}, which had been used previously. The capillary method used for the measurement of the self-diffusion coefficients has been described in detail previously.[3]

Some doubt had been raised as to whether the O^{18} could be used as a true indication of the diffusion of the NO_3^-. Since highly enriched N^{15} has recently become available, some of this material was obtained and incorporated in $NaNO_3$. A method of analysis for N^{15} was worked out in which the NO formed upon heating the nitrate was analyzed mass spectrometrically. Six diffusion experiments at three different temperatures were performed. The results of five of these were found to be well within the experimental error of the previously determined line. Since N^{15} could be obtained at a much higher enrichment than O^{18} and could be incorporated in the salts more easily, it was used in all the following nitrate measurements.

[1] ORINS Fellow, 1955–1957, University of Florida.

[2] T. A. Gens, *F^{18} Exchange Between Fluorocarbons and Some Fluorine-Containing Compounds*, ORNL-2363 (Aug. 22, 1957).

[3] A. S. Dworkin and D. Brown, *Chem. Semiann. Prog. Dec. 20, 1955*, ORNL-2046, p 23.

[4] A. S. Dworkin and E. R. Van Artsdalen, *Chem. Semiann. Prog. Rep. June 20, 1956*, ORNL-2159, p 81.

Cesium nitrate containing both Cs^{134} and N^{15} was used in order to obtain the self-diffusion coefficients of both ions with one measurement. Six points were obtained at four different temperatures varying from 425 to 480°C. The data may be expressed in the form of a rate equation:

$$(1) \qquad D = Ae^{-\Delta H^{\ddagger}/RT} ,$$

where D is the self-diffusion coefficient and $\Delta H^{\ddagger}$ is the heat of activation of self-diffusion. The equations for Cs^+ and NO_3^-, obtained by means of least-squares calculations, are shown below:

$$(2) \qquad D_{Cs^+} = 1.127 \times 10^{-3}\, e^{-5608/RT} ,$$

$$(3) \qquad D_{NO_3^-} = 1.777 \times 10^{-3}\, e^{-6279/RT} .$$

The straight lines obtained by plotting log D vs $1/T$ are shown in Fig. 51. The probable error in D_{Cs^+} is ±0.032 (1.2 to 1.6%), while that for $\Delta H^{\ddagger}_{Cs^+}$ is ±0.27 kcal (5%). The probable error in $D_{NO_3^-}$ is ±0.038 (1.4 to 2.0%) and that for $\Delta H^{\ddagger}_{NO_3^-}$ is ±0.38 kcal (6%).

Since in both $NaNO_3$ and $CsNO_3$ the cation diffusion was faster than the anion diffusion (60% faster in the case of $NaNO_3$ and 2% faster in the case of $CsNO_3$), the earlier KNO_3 results,[4] which indicated a faster anion diffusion, appeared to be anomalous. Since some difficulty was also encountered in the O^{18} analysis in this earlier experiment, a new set of measurements was made by using KNO_3 containing K^{41} and N^{15} to follow the diffusion. It was found that the earlier K^+ results were essentially correct but that the NO_3^- results were in error. The new measurements indicated that the K^+ diffusion was about 12% faster than that of the NO_3^-. The equations for K^+ and NO_3^-, obtained by means of least-squares calculations, are shown below:

$$(4) \qquad D_{K^+} = 1.324 \times 10^{-3}\, e^{-5530/RT} ,$$

$$(5) \qquad D_{NO_3^-} = 1.42 \times 10^{-3}\, e^{-5760/RT} .$$

The straight lines obtained by plotting log D vs $1/T$ are shown in Fig. 52. Twenty-one points were used in the calculation of Eq. 4, and 12 points were used for Eq. 5 over a temperature range from 345 to 390°C. The probable error in D_{K^+} is ±0.024 (1.2 to 1.6%) and that for $\Delta H^{\ddagger}_{K^+}$ is 0.20 kcal (3.5%). The probable error in $D_{NO_3^-}$ is ±0.026 (1.5 to 2.0%) and that for $\Delta H^{\ddagger}_{NO_3^-}$ is ±0.26 (4.5%).

It had been noted previously[3] that the heats of activation for the cation and anion were approximately the same within experimental error. As

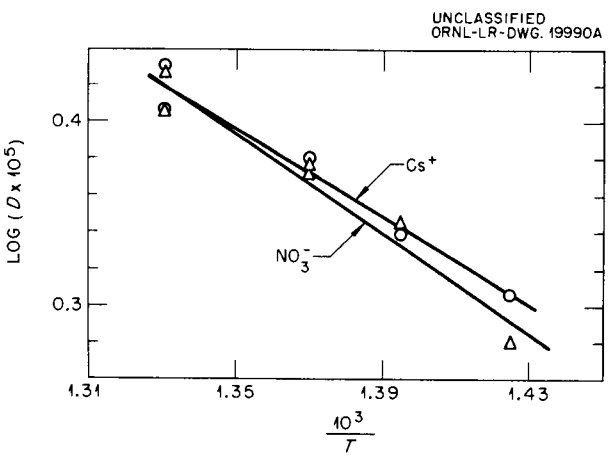

Fig. 51. Self-Diffusion Coefficients in Molten $CsNO_3$.

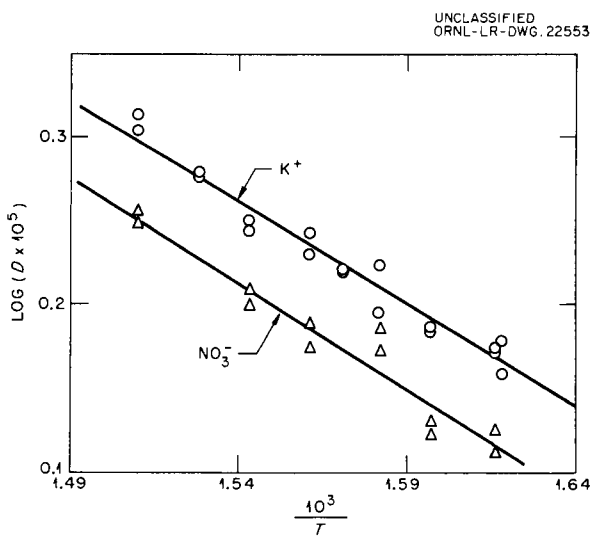

Fig. 52. Self-Diffusion Coefficients in Molten KNO_3.

can be seen from the data given below, the differences between $\Delta H_+^\ddagger$ and $\Delta H_-^\ddagger$ in KNO_3 and $CsNO_3$ are larger than in $NaNO_3$:

	$\Delta H_+^\ddagger$ (kcal)	$\Delta H_-^\ddagger$ (kcal)
$NaNO_3$	4.97 ± 0.08	5.08 ± 0.08
KNO_3	5.53 ± 0.20	5.76 ± 0.26
$CsNO_3$	5.61 ± 0.27	6.28 ± 0.38

However, the probable errors are also considerably larger, so that the above statement still holds true. No significance is attached to the apparent trend in the $\Delta H^\ddagger$ values, since they are all essentially between 5 and 6 kcal and probable errors are fairly large.

The observation was made at the conclusion of $NaNO_3$ measurements[3,5] that the ratio of the absolute rates of self-diffusion of the two ions is approximately proportional to the inverse square roots of their masses. The KNO_3 and $CsNO_3$ measurements reported above indicate that this observation is incorrect. The ratios of the self-diffusion coefficients of the cation to anion in $NaNO_3$, KNO_3, and $CsNO_3$, respectively, are 1.57, 1.13, and 1.02. The values of D for the ions in these three salts at 350 and 450°C are shown in Table 47. The values for $NaNO_3$ and KNO_3 at 450°C are extrapolated above the actual measured temperature range. It will be noted that if the mass relationship held, the diffusion of the K^+ would be about 25% greater than that of the NO_3^- in KNO_3, and the diffusion of the Cs^+ would be considerably less than that of the NO_3^- in $CsNO_3$. The values shown in Table 47 appear to indicate that the relative sizes of the ions are much more important than the relative masses. While there is no apparent direct relation between the ratio of the self-diffusion coefficients and the cation-to-anion radius ratio, the cation radius approaches that of the anion as the self-diffusion coefficient of the cation approaches that of the anion. The self-diffusion coefficients of the ions in $AgNO_3$ are now being measured in an attempt to further clarify this point.

[5] E. R. Van Artsdalen *et al.*, *J. Am. Chem. Soc.* 78, 1772 (1956).

LIQUID METAL–SALT SOLUTIONS[6]

High-Temperature Region of the Sodium–Sodium Halide Systems

M. A. Bredig J. E. Sutherland

In the study of the phase equilibria existing between liquid sodium metal and molten sodium halides, which was the first of a series of investigations concerned with the alkali metals, consolute or critical solution temperatures had been derived through extrapolation of data obtained at lower temperatures.[7] Subsequent measurements of the electrical conductivity (cf. "Electrical Conductivity in Molten Salt–Metal Solutions," this report) gave strong indications that a few of the early data for the solubility of the metal in the molten salt, especially of Na in NaCl, might have been somewhat in error, probably because of unfavorable conditions of specific gravity and surface tension which prevented a clean phase separation before

[6] Frequent discussions with W. T. Smith, Jr., University of Tennessee, consultant, are gratefully acknowledged.

[7] M. A. Bredig, J. W. Johnson, and W. T. Smith, Jr., *J. Am. Chem. Soc.* 77, 307 (1955).

Table 47. Self-Diffusion Coefficients

	350°C		450°C	
	$D_+ \times 10^5$ ($cm^2 \cdot sec^{-1}$)	$D_- \times 10^5$ ($cm^2 \cdot sec^{-1}$)	$D_+ \times 10^5$ ($cm^2 \cdot sec^{-1}$)	$D_- \times 10^5$ ($cm^2 \cdot sec^{-1}$)
$NaNO_3$	2.33	1.48	(4.06)	(2.61)
KNO_3	1.52	1.35	(2.82)	(2.56)
$CsNO_3$			2.28	2.23

phase analysis. Excessively long equilibration periods may have contributed to these errors, since the two liquids tended to be broken up more and more into small droplets that were difficult to remove from the walls of the sampling chamber. Stirring for 1 min or less has now been found to be sufficient for equilibration of these liquids. Following the success of the method of thermal analysis (cooling curves) in the determination of the liquid-liquid phase equilibria in three of the potassium–potassium halide systems,[8] a modification of this method imposed by the considerably higher temperatures was applied to an actual experimental determination of the high-temperature range of the four sodium–sodium halide systems and to a re-evaluation of the equilibria at lower temperatures. Especially for measurements in the fluoride system, temperatures slightly in excess of 1200°C, that is, 400 deg higher than those encountered in the potassium systems, had to be reached. Sodium equilibrium pressures, sometimes in excess of 100 psi inside the test capsules, had to be balanced by an outside pressure of an inert gas. The capsule, with a thermocouple fastened inside a thermocouple well in its bottom, was suspended on a frame inside a tank made of Inconel and pressurized with argon gas. Cooling curves were recorded as previously described.[8]

In Fig. 53 a summary is presented of the results thus obtained, combined with the early data from the equilibration-and-sampling tests. The results of a redetermination of the liquid-liquid phase equilibria of the KF-K system, shown in greater detail in Fig. 54, together with the previously reported data for the other three potassium systems,[8] are also included.

The new values for the solubility of sodium metal in molten sodium chloride are considerably lower than the earlier ones.[9] They are in good agreement with both the observations made during the conductivity measurements (see "Electrical Conductivity in Molten Salt–Metal Solutions," this report) and with a few measurements made elsewhere.[10] Otherwise, the thermal analysis data for the high-temperature range blend smoothly into

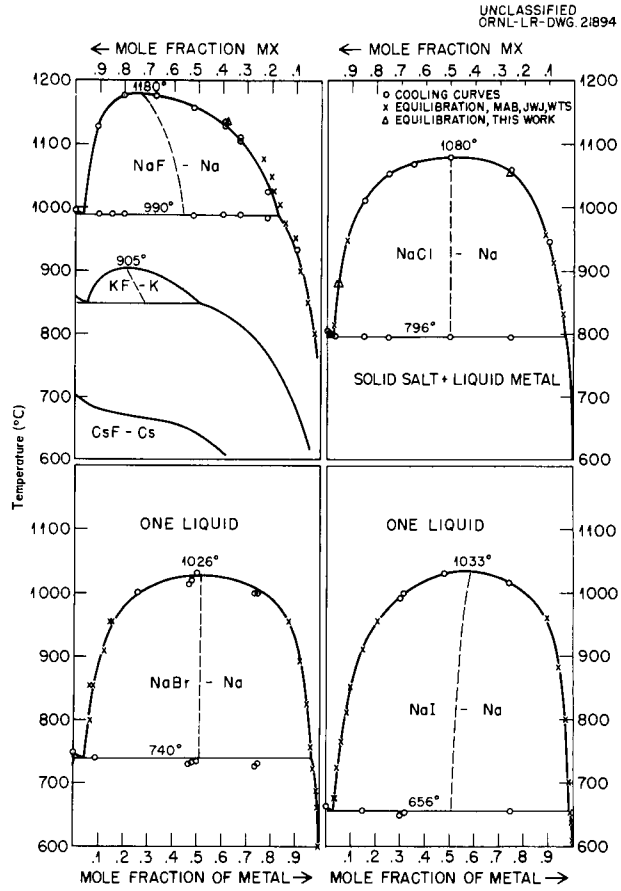

Fig. 53. Phase Equilibria in the Sodium Metal–Sodium Halide Systems.

the earlier lower-temperature data for the solubilities of the salts in the liquid sodium metal and also into those for the metal solubility in the two heavier ones of the molten salts, NaBr and NaI. Only in the NaF-Na system are the older equilibration values for the solubility of NaF in Na slightly higher than those now obtained by thermal analysis, the difference probably being due to distillation of some excess metal from the main tube into the sampling chamber.[11] The new data for the KF-K system are also slightly different from those obtained earlier, but the general conclusions of the earlier discussion and comparison of the three fluoride systems[11] CsF-Cs, KF-K,

[8] J. W. Johnson and M. A. Bredig, *Chem. Semiann. Prog. Rep. June 20, 1956*, ORNL-2159, p 83–84.

[9] M. A. Bredig, J. W. Johnson, and W. T. Smith, Jr., *J. Am. Chem. Soc.* 77, Fig. 2, p 309, and Fig. 3, p 310 (1955).

[10] Personal communication from M. Benedict, MIT, on three experiments, on the diffusion of Na metal into molten NaCl, by F. C. Benner, National Research Corporation.

[11] M. A. Bredig, J. W. Johnson, and W. T. Smith, Jr., *J. Am. Chem. Soc.* 77, Fig. 1c, p 308 (1955).

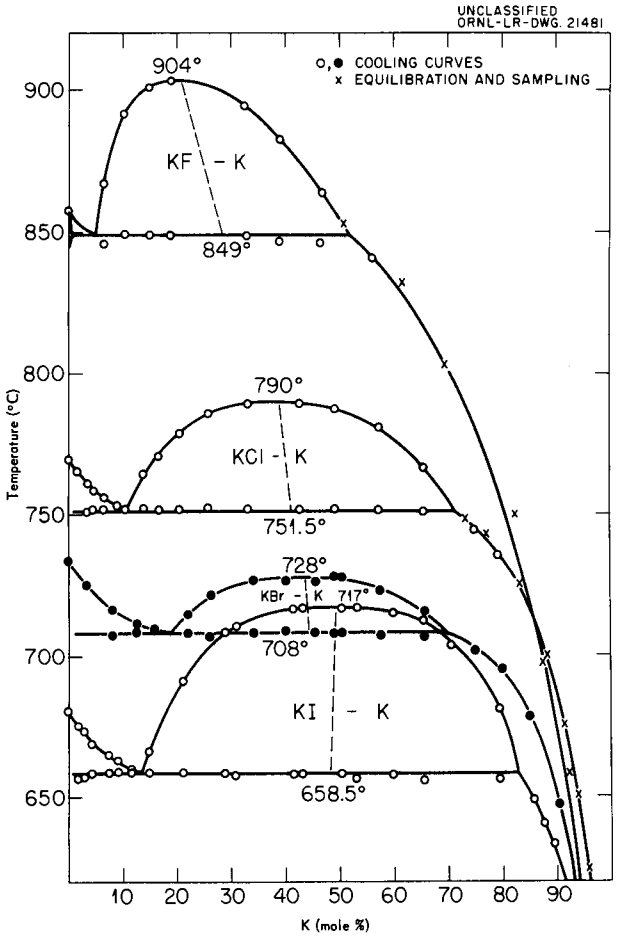

Fig. 54. Phase Equilibria in the Potassium Metal–Potassium Halide Systems.

and NaF-Na are not affected (cf. Fig. 1, upper left-hand diagram, with Fig. 3 of ref 12).

It is interesting to note that the heat of solution at saturation for the solid salt in the liquid potassium metal, as calculated for the straight portions of the solubility curves by the approximate equation

$$\Delta H_{\text{sat. soln}} = \frac{4.575(\log X_2 - \log X_1)}{(1/T_1) - (1/T_2)} ,$$

is lowest for KF, 18.1 kcal as against 20 kcal for the three other halides. This behavior, as expected, is intermediate between that of the NaX-Na and of the CsX-Cs systems. It reflects the operation of at least two factors: (1) the trend in the heats of vaporization (in kcal) of the salts (NaF, 53; NaCl, 40; KF, 41; KCl, 38; CsF, 34; CsCl, 36) and (2) the greater ease with which the smaller F^- anions, or fluoride molecules, may enter the "holes" between the large metal atoms, or, in other words, the importance of the ratio, in size, of the anion and the metal atom.[12]

One significant result of the new measurements is the observation that the ratio $q = V_{MX}/V_M$ of the volumes of the two components in each binary system determines to a large extent the symmetry of the liquid-liquid phase equilibria. This relationship had previously been masked by the errors in the earlier data. If the volume fraction, ϕ, is plotted instead of the mole fraction, X, more symmetrical diagrams result, especially for the fluoride and iodide systems, where the difference in the volumes of the two components is greatest. This is particularly true if, instead of the simple volume fraction,

$$V_{\phi_M} = \frac{X_M V_M}{X_M V_M + (1 - X_M) V_{MX}} = \frac{X_M}{X_M(1 - q) + q} ,$$

with the molar volumes of the pure liquid components calculated from known density values, volume fractions of the salt ions and metal atoms,

$$r_{\phi_M} = \frac{X'_M r_M^3}{X'_M r_M^3 + X'_{M^+} r_{M^+}^3 + X'_{X^-} r_{X^-}^3} ,$$

are used in which r_M, r_{M^+}, and r_{X^-} represent the atomic and ionic crystal radii corrected for thermal expansion of the pure liquids from room temperature to the equilibration temperature. The fact that higher symmetry of the phase diagram is thus obtained than with the bulk volumes of the components might be connected with a possible destruction, on addition of the other component, of the "structure" of the pure liquids, especially of a salt such as NaF, which possesses a particularly large molar volume in the liquid state.

Still better agreement with the rather hypothetical and tentative postulate of a symmetrical phase equilibrium for effective volume fractions

[12] M. A. Bredig, H. R. Bronstein, and W. T. Smith, Jr., *J. Am. Chem. Soc.* 77, 1454 (1955).

is obtained if either of the effective volume ratios above,

$$q_V = \frac{V_{MX}}{V_M} ,$$

$$q_r = \frac{r^3_{M^+} + r^3_{X^-}}{r^3_M} ,$$

is assumed to be a linear function of the concentration, for example, of the mole fraction of the anion. Several explanations seem to be possible for such behavior, among them being the polarization of the very highly polarizable metal atom, or, in other words, the expansion of the wave function of the metal electron in the relatively strong field of F^-, the smallest of the halide anions. These calculations do not appear to warrant further discussion until measurements of partial molar volumes are available.

Rubidium–Rubidium Halide Systems

M. A. Bredig J. W. Johnson[13]

An interpolation of the data obtained for the miscibility of metal with salt, in the liquid state, in the four potassium–potassium halide and the corresponding cesium systems, suggested that, peculiarly, in the intermediate series of the rubidium systems a miscibility gap might *alternately* occur and be absent. This prediction was borne out thus far in the study of the Rb-RbI and Rb-RbBr systems (Fig. 55). A miscibility gap of more than 50 mole % was observed in the Rb-RbI system at a monotectic temperature of 615 ± 1°C, with a consolute temperature of 634 ± 1°C, approximately 14 deg below the melting point of the pure salt. Complete miscibility in the liquid state was found, as expected, in the Rb-RbBr system. The study of the remaining two systems is under way. A miscibility gap is expected to exist in the case of the chloride, but possibly not for the fluoride, if the cohesive energy of RbF, like that of CsF, is low enough as a result of the polarization of the Rb^+ ion by the F^- ion.

[13]Now with Stanford Research Institute.

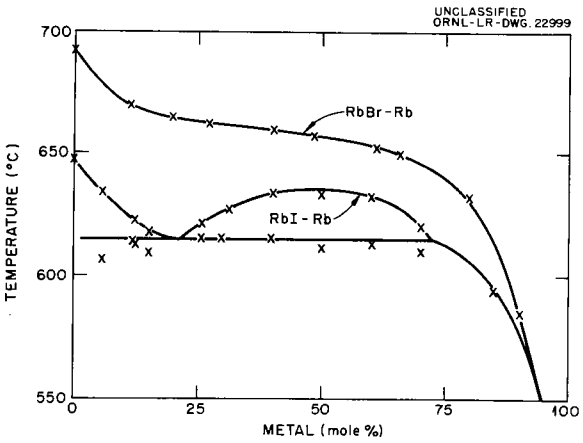

Fig. 55. Phase Equilibria in the Rb-RbBr and Rb-RbI Systems.

Electrical Conductivity in Molten Salt–Metal Solutions

H. R. Bronstein M. A. Bredig

With several improvements, most of which were mentioned in the last progress report,[14] the apparatus (Fig. 56) was found to work quite satisfactorily at temperatures up to 900°C.

The results obtained in the temperature range between 750 and 900°C in the salt-rich regions of the systems Na-NaCl, Na-NaBr, K-KCl, and K-KBr are summarized in Fig. 57, which gives the specific conductivity of the molten mixtures. Figure 58 gives the equivalent conductance of the metal in the solution as calculated by the equation

$$\Lambda_M(X_M) = \frac{\sigma_{soln}}{X_M} (X_M V_M + X_{MX} V_{MX}) - \frac{X_{MX}}{X_M} \Lambda_{MX} ,$$

where Λ, σ, X, and V designate the equivalent conductance ($ohm^{-1} \cdot cm^2 \cdot mole^{-1}$), specific conductance ($ohm^{-1} \cdot cm^{-1}$), mole fraction, and molar volume ($cm^3 \cdot mole^{-1}$), respectively, of the entities indicated by the subscripts (M for metal, MX for halide). Simplifying assumptions are made, in the absence of actual density and viscosity data, namely, of additivity for salt and metal in molar volume and of constant equivalent conductance of the salt. The alkali-metal–halide systems are distinguished from those few metal-salt systems for which data are available in the literature, such

[14]H. R. Bronstein and M. A. Bredig, *Chem. Semiann. Prog. Rep. June 20, 1956*, ORNL-2159, p 85.

UNCLASSIFIED
ORNL-LR-DWG. 16412

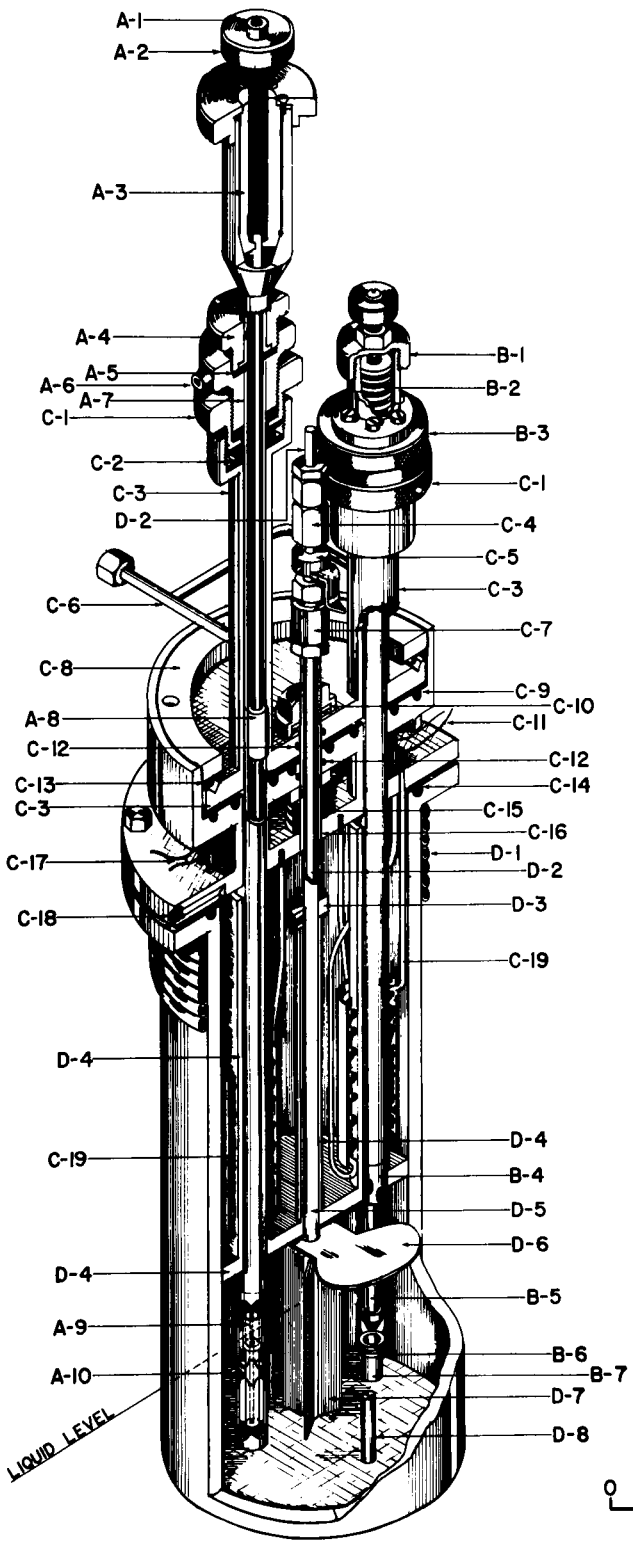

ELECTRICAL CONDUCTANCE APPARATUS FOR ALKALI METAL-ALKALI HALIDE SOLUTIONS

CELL ASSEMBLY
A-1 CENTRAL ELECTRODE TAP
A-2 THREADED CENTRAL ELECTRODE
A-3 TEFLON THREADED INSULATOR AND PRESSURE SEAL
A-4 GASKET TIGHTENER
A-5 RUBBER "O" RING AND TEFLON GASKETS
A-6 OUTER ELECTRODE TAP
A-7 THREADED FLANGE-END OF TUBE ASSEMBLY
A-8 TEFLON INSULATOR AND CENTERING DEVICE
A-9 SAPPHIRE CONDUCTANCE CELL
A-10 CELL HOLDER

SAMPLER ASSEMBLY
B-1 BELLOWS ACTUATING SCREW ASSEMBLY
B-2 STAINLESS STEEL BELLOWS
B-3 SHOULDER OF SAMPLER TUBE
B-4 DETACHABLE AMPULE HOLDER
B-5 VALVE STEM
B-6 SPLIT STEEL RING
B-7 SAMPLE AMPULE

TURRET AND HEATER ASSEMBLY
C-1 GASKET TIGHTENER
C-2 GASKETS-RUBBER "O" RING, TEFLON BUSHINGS & RUBBER SPACER
C-3 ROTATABLE TURRET & ENTRANCE PORTS
C-4 HOUSING FOR PRESSURE & VACUUM SEALS FOR STIRRER
C-5 TURNING DEVICE & POSITION INDICATOR FOR CLOSURE PADS
C-6 VACUUM & PRESSURE LINE
C-7 HOUSING FOR PRESSURE & VACUUM SEALS FOR CLOSURE PAD ASSEMBLY
C-8 RING TIGHTENER FOR TURRET
C-9 TEFLON "O" RINGS
C-10 TENSION NUT & THRUST BEARING
C-11 WIRE LEADS FOR SAMPLER HEATER
C-12 RUBBER "O" RING
C-13 BALL BEARINGS
C-14 TEFLON "O" RING
C-15 WATER COOLING COILS
C-16 CENTERING TUBE FOR TURRET AND MOUNT FOR HOUSING C-7
C-17 WIRE LEADS FOR CELL HEATER
C-18 VACUUM & PRESSURE ENTRY TO TANK
C-19 STAINLESS STEEL SHEATHED, SWEDGED MgO INSULATED NICHROME HEATERS & ASSEMBLY

TANK ASSEMBLY
D-1 WATER COOLING COILS
D-2 STIRRER SHAFT
D-3 RING AND SET SCREW FOR CLOSURE PAD TENSION
D-4 PARTITION PLATE AND SHIELD TUBES
D-5 TUBULAR SUPPORT FOR PADS
D-6 CLOSURE PADS
D-7 STIRRER
D-8 THERMOCOUPLE WELLS

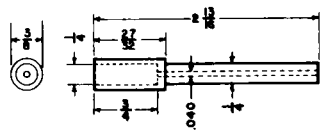

CONDUCTANCE CELL
SYNTHETIC SAPPHIRE

Fig. 56. Apparatus for Measuring Electrical Conductance of Solutions of Metals in Molten Salts.

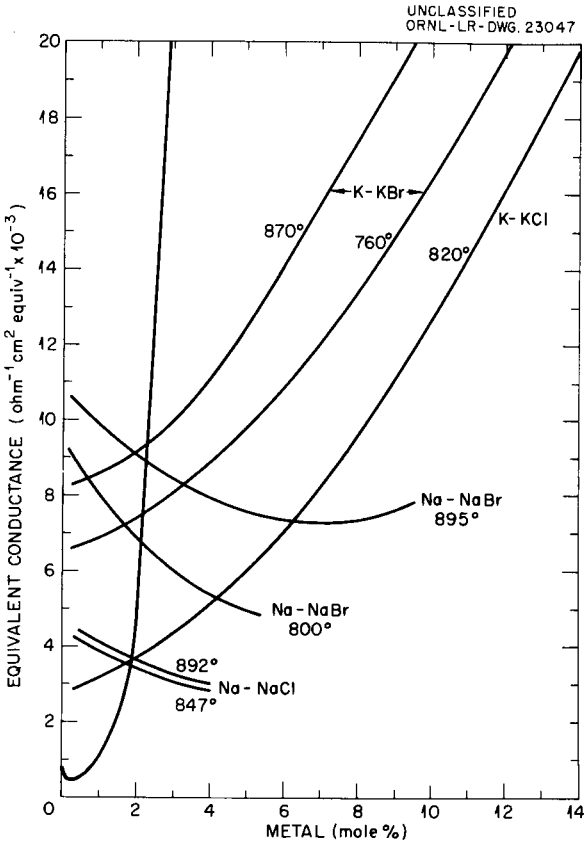

Fig. 57. Specific Conductance of Solutions of Sodium and Potassium Metals in Their Molten Chlorides and Bromides.

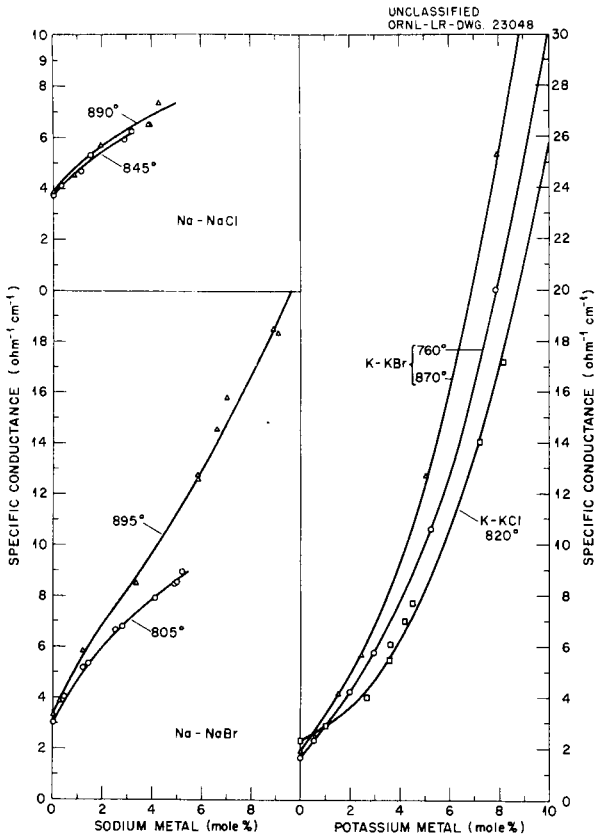

Fig. 58. Equivalent Conductance of Sodium and Potassium Metals in Their Molten Chloride and Bromide Solutions.

as $Cd\text{-}CdCl_2$ and $Bi\text{-}BiCl_3$, by a monotonic increase, instead of an initial decrease, in specific conductance of the solutions of the metal in the fused salt with increasing metal concentration. Thus the electrons of the metal in the dilute solution are not as tightly bound as they are in those few previously known examples where the formation of Cd_2^{++} and Bi^{+} ions from $Cd + Cd^{++}$ and $2Bi + Bi^{+++}$ is assumed to explain the low electronic conductivity.

The equivalent conductance of the metal, however, shows a behavior for sodium which is different from that of potassium. In the sodium systems, an initial decrease in equivalent conductance leads to a minimum in the region of 2×10^3 to 8×10^3 $ohm^{-1} \cdot cm^2 \cdot mole^{-1}$ between 5 and 10 mole % Na. The position of the minimum depends on the temperature and on the nature of the anion; this minimum is followed by a rise toward the much higher equivalent conductance of the pure liquid metal of $\sim 10^6$ $ohm^{-1} \cdot cm^2 \cdot mole^{-1}$. The beginning of this rise was experimentally observed thus far only in NaBr, where the solubility of sodium at the test temperature allowed sufficiently large concentrations of metal to be dissolved in the fused salt. In the potassium systems there is no minimum but a monotonic increase in the equivalent conductance of the metal with its concentration.

It may be too early to attempt a really significant theoretical interpretation of these observations. The difference in the ionization energies of sodium and potassium, approximately 1 ev, does not seem to be an important factor. At infinite dilution the equivalent conductance of the sodium metal is higher than that of potassium by several thousand $ohm^{-1} \cdot cm^2 \cdot mole^{-1}$, even though the ionization potentials are in reverse order. The rapid increase in the equivalent conductance of the metal, after it has passed through the minimum, suggests a

mechanism involving the overlap of the electronic orbitals of the metal atoms or molecules in the gradual establishment of the "conduction band" characteristic of the pure metal. Through this same mechanism, it seems possible to connect the observed difference in the conductance behavior of the sodium and potassium solutions with the differences in the corresponding phase diagrams at the temperature of the conductance measurements. In the case of the two potassium systems, these temperatures were significantly above the consolute (or critical solution) temperatures, where the solutions approach ideality, that is, monatomic dispersion of the potassium metal in the molten salt. Reversely, the test temperatures in the case of the sodium systems were far below the critical solution temperatures. The sodium metal was, therefore, in the condition of a highly nonideal solution most readily explained by a high degree of association, perhaps, to discrete Na_2 molecules. Thus at a given total metal concentration, the average distance between "metallic particles" which may be taken to determine the average amount of electron orbital overlap would depend on the degree of association. While in the case of nonassociated metal atoms (potassium above the consolute temperature) this distance would be essentially proportional to the reciprocal of the cube root of the concentration, it would decrease much more slowly in the case of associating metal atoms, such as sodium, far below the critical solution temperature.

The increase, with the atomic number of the halide ion, in the equivalent conductance of the metal at infinite dilution (e.g., Λ^0_{Na}, in bromide, equal to 10,000, as against 5000 $ohm^{-1} \cdot cm^2 \cdot mole^{-1}$ in chloride) may be related to observations both in aqueous solutions and in solids. Electron transfer between two oxidation stages of a metallic element is known to be greatly facilitated by greater polarizability of the anion, that is, its rate increasing from fluorides to iodides. Even the somewhat smaller difference, at infinite dilution, between the solutions of sodium and potassium in the salts with the same anion seems to demonstrate the stronger effect of the polarization with the smaller cation, Na^+ ($\Lambda^0_{Na} \cong 5000$ against $\Lambda^0_K \cong 3000$, in the chlorides, and $\Lambda^0_{Na} \cong 10{,}000$ against $\Lambda^0_K \cong 7500$ $ohm^{-1} \cdot cm^2 \cdot mole^{-1}$, in the bromides).

For comparison, there is included in Fig. 58 the equivalent conductance of sodium metal in liquid ammonia at −33.5°C, as measured by Gibson and Phipps in 1926. It appears that the state of the electron must be a very different one in the two types of solutions. A conductance minimum was also observed in liquid-ammonia solutions, but at values of concentration and conductance of approximately 0.2 mole % and 500 $ohm^{-1} \cdot cm^2 \cdot mole^{-1}$, much lower than in the molten-salt solutions. The minimum in liquid ammonia is followed by a much steeper rise than in the molten salts. The initial decrease in NH_3 has been attributed to the concentration-dependent, that is, decreasing dissociation of the metal atoms into solvated electrons and sodium ions, while the rise is connected with the rapid establishment of the truly metallic type of conductance by the electrons (large mean free path). The fact that the equivalent conductance of the metal at infinite dilution is very much larger in the molten salt than in NH_3 is perhaps due to the influence of the cations of the salts, which may permit establishment of the metallic type of conduction at much lower metal concentration than in liquid ammonia. Part of the large difference in the metallic type of conductance at higher metal concentrations, with the ratio of the equivalent conductance of the metal in ammonia to that in the molten salt reversed and reaching values in excess of 10, may be attributed to the commonly negative temperature coefficient of metallic conductance, in view of the large difference in the absolute temperature, which is four to five times higher for the molten salts than for the liquid ammonia. However, the very different nature of the solvents, involving also the halide ions, probably is the most important factor.

The present measurements on salt-metal solutions will be extended next to the iodide systems of sodium and potassium, which, from extrapolation of the present data and because of the high polarizability of the iodide ion, are expected to exhibit larger equivalent metal conductances than either the bromide or chloride systems.

EFFUSIOMETRIC DETERMINATION OF THE VAPOR PRESSURE OF NaCl AND KCl. EFFECT OF VAPOR PHASE ASSOCIATION

S. Datz R. E. Minturn

The Knudsen effusion method for the determination of alkali halide vapor pressures has been extended in temperature up through the melting points of the salts and into the liquid region.

The experimental arrangement consists of a metal vacuum chamber containing a salt oven fixed with a small effusion orifice, an oven mount, a mechanical shutter system for interrupting the molecular beam formed at the orifice, and a movable surface ionization gage detector.

The oven (see Fig. 59) consists of a stainless steel block fitted with heaters formed of tungsten wire helices contained in ceramic tubing and inserted into holes in the block (*A*). The salt is

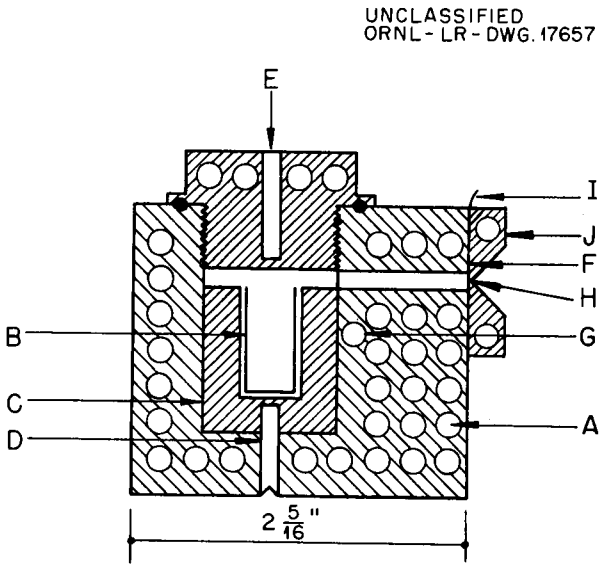

Fig. 59. Schematic Drawing of the Effusion Oven.

contained in a burnished platinum crucible (*B*) which is surrounded by a heavy oxygen-free high-conductivity copper cylinder (*C*) which is pressure-fitted into the stainless steel block. Calibrated Pt, Pt–13% Rh thermocouples are discharge-welded to the oven at points *D*, *E*, and *F*, and a Chromel-Alumel thermocouple located at *G* acts as a sensing element for a pneumatic temperature controller which maintains the temperature to within ±0.2 deg at 1000°K. Effusive flow in the higher pressure regions (~10 mm Hg) was maintained by the use of a very small effusion orifice (0.0004-in.-dia) (*H*) drilled in a 0.001-in. platinum foil (*I*) which is held on the oven face by a heated flange plate (*J*). The oven is mounted on three tungsten pins to diminish heat conduction and is surrounded by a tantalum-sheet radiation shield.

The surface ionization gage used is identical to one described in previous work[15] and is mounted so that it may be moved to obtain maximum beam current. The surface used is a 0.002-in.-dia oxygenated tungsten wire which is maintained at 1500°K while a small amount of oxygen (5×10^{-6} mm Hg) is directed at it. Under operating conditions the surface efficiency is independent of temperature over at least a 200-deg range. The theory of this detector has been discussed by Zimm and Mayer,[16] Cogin and Kimball,[17] and Datz and Taylor.[15]

Heats of sublimation, vaporization, and fusion (by difference) have been determined in two ways from the data shown in Figs. 60 and 61. The first assumes that no association exists in the vapor phase, and the second assumes that association exists to the extent reported by Miller and Kusch.[18] These results are listed in Table 48. The differences in the literature values for the heats of sublimation (determined by effusion) and

[15] S. Datz and E. H. Taylor, *J. Chem. Phys.*, **25**, 389 (1956).

[16] B. H. Zimm and J. E. Mayer, *J. Chem. Phys.* **12**, 362 (1944).

[17] G. E. Cogin and G. E. Kimball, *J. Chem. Phys.* **16**, 1035 (1948).

[18] R. C. Miller and P. Kusch, *J. Chem. Phys.* **25**, 860 (1956).

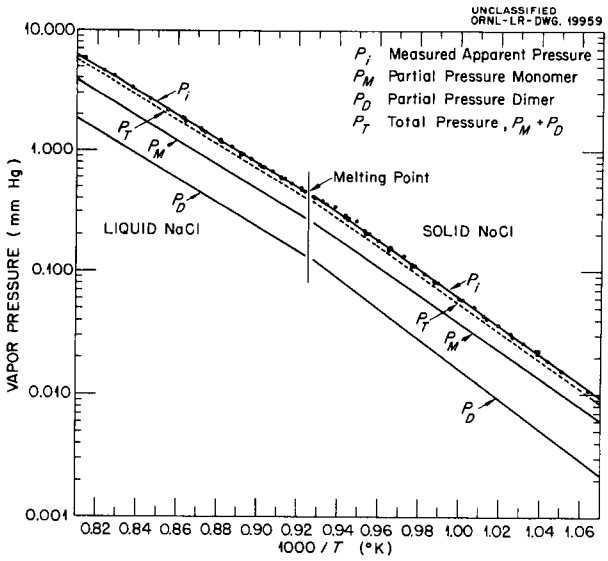

Fig. 60. Log *P* vs 1000/*T* Plot for NaCl.

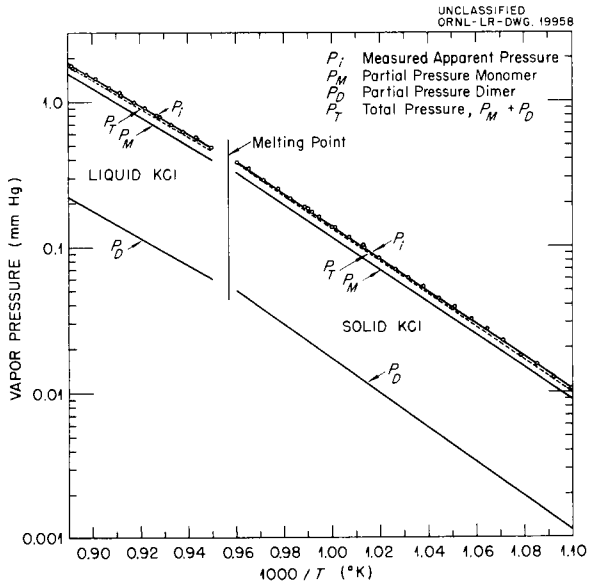

Fig. 61. Log P vs 1000/T Plot for KCl.

the heats of vaporization (obtained by static methods) do not agree with the calorimetrically determined heats of fusion.

The values obtained from data here, assuming that no dimer is present, are in good agreement with these heats of fusion, but the assumption of association destroys this agreement. These data therefore infer that there is little or no association in the gas phase. Recent investigations by Klemperer and Rice on the vapor-phase infrared spectra of the lithium halides[19] and other alkali halides[20] have also indicated no association. To resolve this question, experiments are proceeding on the measurement of alkali-halide vapor densities.

[19] W. Klemperer and S. A. Rice, *J. Chem. Phys.* **26**, 618 (1957).

[20] S. A. Rice and W. Klemperer, private communication.

Table 48. Thermodynamic Values Derived from Vapor Pressure Measurements

	NaCl (1081°K)			KCl (1045°K)		
	ΔH_{sub}	ΔH_{vap}	ΔH_{fus}	ΔH_{sub}	ΔH_{vap}	ΔH_{fus}
Literature	53.0 ± 0.45[a]	45.34[b]	7.1 ± 0.3[c]	51.2[a]	43.28[c]	6.265[d]
Zero association	53.12 ± 0.23	46.11 ± 0.18	7.01 ± 0.29	51.34 ± 0.13	44.88 ± 0.33	6.46 ± 0.35
Monomer (MX)	51.10	46.99	4.11	50.64	45.71	4.93
Dimer $(MX)_2$	55.65	46.90	4.38	53.65	43.42	5.12
From P_T (one formula wt of MX)	39.81 ± 0.18	34.83 ± 0.21	4.98 ± 0.23	45.20 ± 0.12	39.59 ± 0.26	5.61 ± 0.28

[a] B. H. Zimm and J. E. Mayer, *J. Chem. Phys.* 12, 362 (1944).

[b] E. F. Fiock and W. H. Rodebush, *J. Am. Chem. Soc.* 48, 2522 (1926).

[c] K. K. Kelly, *U.S. Bur. Mines, Bull.* 383 (1936).

[d] T. B. Douglas, National Bureau of Standards, private communication.

CHEMICAL PHYSICS

MICROWAVE AND RADIO-FREQUENCY SPECTROSCOPY

Hydrogen Gas and Atomic Hydrogen Yields from Irradiated Acids

A. Weinberger R. Livingston

Work on the measurement of gas yields from various acids irradiated with gamma rays from Co^{60} has been reported previously.[1] The study was being carried out to see if the bulk gas yield in any way correlated with the yield of atomic hydrogen found in these same materials by paramagnetic resonance measurements on samples irradiated at a low temperature (77°K). It has now been found that there is a correlation.

Measurements of yields of molecular hydrogen and oxygen have now been completed on several concentrations of sulfuric and perchloric acids, and work is starting on orthophosphoric acid. In each case the acid was irradiated at 77°K in order to duplicate the conditions used for studying stably trapped atomic hydrogen by the paramagnetic resonance method. After irradiation the samples were warmed above the melting point, and the hydrogen and oxygen were collected and assayed by using conventional vacuum-line techniques.

Sulfuric acid, especially in concentrations above 10 mole % acid, may be cooled either quickly to give a glassy solid or very slowly with temperature cycling to give a polycrystalline material. Quite unexpectedly, the gas yields were found to be manyfold higher in the glassy material. The hydrogen results are summarized in Fig. 62. Although there is considerable scatter in the experimental data, the effect is easily seen from the points which have been fitted by curves in a somewhat arbitrary manner. The curve for the glassy material has been made broken at concentrations below 0.1 mole fraction acid, since in this range clear glasses could not be made, and the material was likely partly crystalline. The molecular oxygen yields showed a similar trend and were roughly one order of magnitude smaller than the corresponding hydrogen yields.

A few preliminary atomic-hydrogen yield measurements on sulfuric acid have been made, and the data, at best, are only approximate, but the correlation with the gas yield data of Fig. 62 is striking. Three rough comparisons can be made. First, in the original[2] atomic-hydrogen work it was found that the yield was a maximum for about 0.17 mole fraction glassy acid, with a lower yield for more concentrated glassy acids and a very much lower yield for much more dilute, crystalline acids. This is in general agreement with the

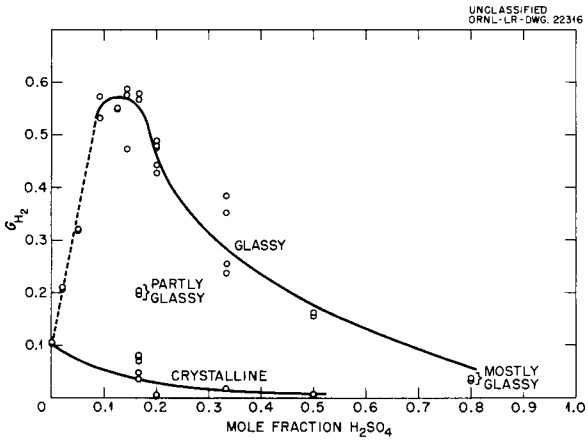

Fig. 62. Hydrogen Gas Yields (Molecules/100 ev) After Irradiation of Aqueous H_2SO_4 at 77°K with Co^{60} Gamma Rays.

glassy curve of Fig. 62, although at extreme dilution there is no correspondence, since atomic hydrogen could not be stably trapped in ice at 77°K, whereas molecular hydrogen appears with a yield of 0.1 (molecules per 100 ev of absorbed energy). Second, the ratio of yields for atomic hydrogen for glassy to crystalline material was determined at each of three concentrations, 0.17, 0.33, and 0.5 mole fraction acid. The yields for glassy material were much higher than for crystalline, and the ratios were in rather good agreement with the ratios of yields for molecular hydrogen deduced from Fig. 62. Finally, the early[2] order-of-magnitude estimate of the absolute atomic-hydrogen yield has been somewhat refined and is more in

[1] A. Weinberger and R. Livingston, *Chem. Semiann. Prog. Rep. June 20, 1956*, ORNL-2159, p 89.

[2] R. Livingston, H. Zeldes, and E. H. Taylor, *Discussions Faraday Soc.* 19, 166 (1955).

keeping with the molecular-hydrogen yield. The absolute yield of atomic hydrogen measured on 0.17 mole fraction glassy acid was about twice as large as was needed to account for the hydrogen gas formed. Although this could mean that not all hydrogen atoms form molecules of hydrogen when they react in the solid, it could also reflect the very large uncertainty in absolute yield measurements at the present state of refinement.

Molecular-hydrogen and-oxygen gas yields for irradiated perchloric acid do not depend upon whether the state of the material is glassy or crystalline. In going to higher acid concentrations the hydrogen gas yield slowly rises from 0.1 (molecules per 100 ev of absorbed energy) for ice to about 0.4 for 0.13 mole fraction acid and then abruptly drops at higher concentrations so that it is about 0.1 for 0.16 mole fraction and about 0.002 for 0.25 mole fraction. The molecular-oxygen yield shows a similar increase in going to higher concentrations, rising from about 0.2 at mole fraction 0.02 to about 1.2 at 0.15 mole fraction acid, but then it shows a sudden rise in the more concentrated acids, becoming about 2.1 in the 0.25 mole fraction acid.

Paramagnetic Resonance Studies

H. Zeldes R. Livingston
R. Holmberg

A variety of single crystals have been irradiated at 77°K and their paramagnetic spectra examined with varying degrees of thoroughness. Some of the more interesting cases are presented here. Work is continuing on several of the crystals. Calcium hydroxide single crystals were discussed in some detail previously.[1] Several additional measurements have been completed. These include a location of the principal axis system for the *g*-value tensor of the species considered earlier[1] to be an interstitial, and as a result possible locations of the species in the lattice are suggested. The main species found[1] in the irradiation disappears with third-order kinetics with respect to unpaired electron concentration, with an activation energy of 12 kcal/mole. These and other details of the calcium hydroxide work are now being prepared for publication elsewhere.

Two groups of lines that appear in gamma-irradiated calcium tungstate crystals have been measured. Each group consists of four main lines, and their behavior for various crystal orientations is completely described by crystal symmetry operations and elements of a *g* tensor that have been deduced for each group of lines from the measurements. In addition, each set of lines shows a number of weaker lines, and for one set these have been measured and interpreted as W^{183} hyperfine structure. The weaker lines associated with the other set have not yet been obtained with sufficient intensity and resolution for good measurements, but work is continuing.

Single crystals of essentially 100% hydrogen peroxide have been grown and the spectra of the irradiated material examined. At least two distinct species have been produced. One species formed in high yield by gamma irradiation at 77°K gives rise to a closely spaced, not completely resolved group of lines. This species persists even after the sample is warmed to much above dry-ice temperature. Ultraviolet irradiation of hydrogen peroxide crystals, on the other hand, gives rise to an entirely different spectrum, and in this case the spectrum disappears with first-order kinetics at 77°K with a half life of a little over 1 hr. For this reason relatively small concentrations of the species were obtained in the initial work. However, with a lower-temperature (pumped nitrogen) irradiation, much higher steady-state concentrations could be produced after prolonged irradiation, and strong spectra were obtained. A number of the features of the spectrum have been measured for a few known crystal orientations, but an interpretation has not yet been attempted. The disappearance of the species was found to follow first-order kinetics at three different temperatures, and the activation energy was 5 kcal/mole. Upon extremely heavy ultraviolet irradiation a second species appears which may be the same as the gamma-ray-produced material. The initial ultraviolet-produced spectrum might also appear under gamma irradiation if either a lower temperature or higher gamma intensity is used.

Single crystals of the mono- and the dihydrate of sulfuric acid have been grown, gamma-irradiated at 77°K, and examined. Both crystals, in addition to showing weak atomic-hydrogen hyperfine lines, show a complex group of lines near the free-electron *g* value. In both cases the lines show anisotropy in the *g* values. This more or less confirms an early notion that the central broad line[2] in the irradiated sulfuric acid spectrum was actually an average over several lines showing anisotropy and that a single crystal would be

needed for detailed study. The spectrum of the monohydrate consists of at least two species that disappear at different temperatures upon warming. The spectrum, not too well resolved, does not appear well suited for study. The spectrum of the dihydrate, on the other hand, appears to be more favorable for study, and additional observations are under way.

A single crystal of perchloric acid monohydrate (hydronium perchlorate) was grown, but unfortunately it underwent a phase transition and shattered when cooled to 77°K, so studies on it have been postponed.

In addition to the single-crystal studies, work has been started on a new type of irradiation experiment. An effort will be made to find a paramagnetic resonance spectrum in a substance while it is being irradiated at nominally room temperature. Intense electron-beam irradiation will be used in the hope that a high enough steady-state radical concentration can be obtained to make detection possible. A magnet has been designed and constructed with features that are intended to make it possible to get the focused electron beam into the magnetic field. The equipment has not yet been assembled at a Van de Graaff generator.

Nuclear Magnetic Resonance

R. Livingston J. J. McBride

A survey study on the applicability of nuclear magnetic resonance for elucidating basic properties of fused salt systems has been started as a cooperative venture with members[3] of the Metallurgy Division. Much of the work to date has been instrument development, and initial observations have been made on molten sodium hydroxide at about 350°C. Both the proton and sodium resonance were seen with a Pound-Watkins type of spectrometer, but the lines were artificially broadened by the spectrometer. Bridge-circuit spectrometers have now been built, and the magnet has been shimmed to give greatly improved homogeneity. The proton resonance in molten sodium hydroxide has been examined with the bridge circuit, and development is now under way to refine the circuitry for observing the sodium resonance. The plan is to survey the nature of the resonances in alkali halide systems at somewhat higher temperatures as soon as the instrumentation is refined.

[3] J. J. McBride is spending essentially full time on the program.

NEUTRON AND X-RAY DIFFRACTION STUDIES

Effect of Thermal Motion on the Diffraction Measurement of Bond Lengths in Crystals

W. R. Busing H. A. Levy

Because the atoms of a crystal are in constant thermal vibration, the position coordinates of an atom as determined from a diffraction study represent only the maximum density or the centroid of a distribution of matter. It has been common practice in the past to call the distance between two such atomic "positions" a "bond length." As the accuracy of experimental techniques has improved, however, it has become clear that there may be discrepancies between spectroscopic and diffraction measurements of bond lengths, and that some of these errors can be attributed to the effect of thermal motion on the atomic positions observed in diffraction work. Cox, Cruickshank, and Smith[4] have shown that an error in the determination of the C-C distance in benzene resulted from a large torsional oscillation of the molecule about its sixfold axis, and Cruickshank[5] has discussed in detail the effect of angular oscillation on the position of a Fourier maximum. The authors have used[6] two different methods to correct a measurement of the O-H distance in $Ca(OH)_2$ for the libration of the OH^- ion.

Unfortunately, the way in which these corrections should be made is not clear-cut, since it depends on an understanding of the thermal motions in solids which is not yet available in general form. The purpose of this report is to present some formulas which may be useful for correcting the estimations of bond lengths if certain assumptions about the atomic motions are accepted. The proof of the expressions is presented below.

Case 1. – Suppose that atom A is heavy enough for its motion to be negligible and that atom B undergoes a thermal motion which can be approximated by a Gaussian distribution with root-mean-square displacements along its principal axes of

[4] E. G. Cox, D. W. J. Cruickshank, and J. A. S. Smith, *Nature* 175, 766 (1955).

[5] D. W. J. Cruickshank, *Acta Cryst.* 9, 757 (1956).

[6] W. R. Busing and H. A. Levy, *J. Chem. Phys.* 26, 563 (1957).

μ_1, μ_2, and μ_3. A plausible assumption is that the desired bond length, A-B, is the mean distance, $\bar{r}$, from the point A to the distribution B. This is given by the approximate expression

$$(1)\quad \bar{r}^2 \cong r_0^2 + \left(1 - \gamma_1^2\right) \mu_1^2 + \left(1 - \gamma_2^2\right) \mu_2^2 + \left(1 - \gamma_3^2\right) \mu_3^2 ,$$

where r_0 is the distance from the point A to the centroid of B (i.e., the uncorrected "bond length") and where the γ_i's are the direction cosines of the vector $\vec{r}_0$ referred to the principal axes of the Gaussian distribution. Note that $(1 - \gamma_i^2)\ \mu_i^2$ is the square of the projection of the vector $\vec{\mu}_i$ on a plane perpendicular to $\vec{r}_0$.

Case 2. – Suppose that atom A is a moderately heavy atom with some thermal motion and that atom B is a light atom attached only to A so that it "rides" on A and exhibits thermal motion which is the convolution of its independent motion and that of A. Let μ_{A1}, μ_{A2}, μ_{A3}, and μ_{B1}, μ_{B2}, μ_{B3} be the root-mean-square displacements of the Gaussian distributions of A and B as determined by experiment. Then, by accepting the assumption of case 1, the desired bond length is the mean distance from the centroid of A to a third Gaussian distribution centered at B and would be obtained by unfolding the observed distributions. It is not necessary to perform this unfolding, however, and the desired distance is given by

$$(2)\quad \bar{r}^2 \cong r_0^2 + \left(1 - \gamma_{B1}^2\right) \mu_{B1}^2 + \left(1 - \gamma_{B2}^2\right) \mu_{B2}^2 + \left(1 - \gamma_{B3}^2\right) \mu_{B3}^2 - \left(1 - \gamma_{A1}^2\right) \mu_{A1}^2 - \left(1 - \gamma_{A2}^2\right) \mu_{A2}^2 - \left(1 - \gamma_{A3}^2\right) \mu_{A3}^2$$

Proof of Eqs. 1 and 2. – Assume that a Cartesian coordinate system is coincident with the principal axes of a normalized Gaussian distribution, $\rho(x,y,z)$. Let (x_0, y_0, z_0) be a fixed point at distance r_0 from the origin, and let

$$(3)\quad r(x,y,z) = \left[(x - x_0)^2 + (y - y_0)^2 + (z - z_0)^2 \right]^{1/2}$$

be the distance of an arbitrary point (x,y,z) from (x_0, y_0, z_0). The quantity to be calculated is

$$(4)\quad \bar{r} = \iiint r(x,y,z)\ \rho(x,y,z)\ dx\ dy\ dz\ .$$

Expanding $r(x,y,z)$ in a Taylor series about the origin and substituting in Eq. 4 gives

$$(5)\quad \bar{r} = r(0,0,0) + r_{xx}(0,0,0)\ \overline{x^2} + r_{yy}(0,0,0)\ \overline{y^2} + r_{zz}(0,0,0)\ \overline{z^2} + \ldots$$

where the terms in r_x, etc., have dropped out because the axes were chosen to make $\bar{x} = \bar{y} = \bar{z} = 0$, and where the terms in r_{xy}, etc., are zero because $\overline{xy} = \overline{xz} = \overline{yz} = 0$ for a Gaussian distribution in the principal axis system. Differentiating Eq. 3 gives

$$(6)\quad r_{xx}(0,0,0) = \frac{1}{r_0} - \frac{x_0^2}{r_0^3} ,$$

with similar expressions for the other derivatives. Since $r(0,0,0) = r_0$ and $\overline{x^2} = \mu_1^2$, etc., it is possible to obtain

$$(7)\quad \bar{r} = r_0 + \frac{\mu_1^2 + \mu_2^2 + \mu_3^2}{2r_0} - \frac{x_0^2\mu_1^2 + y_0^2\mu_2^2 + z_0^2\mu_3^2}{2r_0^3} + \ldots .$$

Squaring Eq. 7 and neglecting higher-order terms gives

$$(8)\quad \bar{r}^2 = r_0^2 + \left(1 - \frac{x_0^2}{r_0^2}\right) \mu_1^2 + \left(1 - \frac{y_0^2}{r_0^2}\right) \mu_2^2 + \left(1 - \frac{z_0^2}{r_0^2}\right) \mu_3^2 + \ldots ,$$

which is identical with Eq. 1, since $\gamma_1 = x_0/r_0$, etc.

Three theorems which will be useful in deriving Eq. 2 will be stated without proof.

Theorem 1. – Given any distribution $\rho(x,y,z)$ in an orthogonal coordinate system, and r the distance of a point from the origin, then $\overline{r^2} = \overline{x^2} + \overline{y^2} + \overline{z^2}$.

Theorem 2. – Given any distributions $\rho_1(x,y,z)$ and $\rho_2(x,y,z)$ and their convolution $\rho(x,y,z)$, with $\xi(x,y,z)$ the component in a specified direction of the displacement of the point (x,y,z) from the centroid $(\bar{x},\bar{y},\bar{z})$ of a distribution, and $\overline{\xi^2}$, $\overline{\xi_1^2}$, and $\overline{\xi_2^2}$ the mean square values of this variable over ρ, ρ_1, and ρ_2, respectively, then $\overline{\xi^2} = \overline{\xi_1^2} + \overline{\xi_2^2}$.

Theorem 3. – Given $\overline{r_1^2}$, $\overline{r_2^2}$, and $\overline{r^2}$, the mean square distances from the centroids of ρ_1, ρ_2, and ρ, where the ρ's are defined as in theorem 2, then $\overline{r^2} = \overline{r_1^2} + \overline{r_2^2}$.

For a Gaussian distribution the mean square displacement in any direction defined by the direction cosines γ_1, γ_2, and γ_3 is

$$\overline{\xi^2} = \gamma_1^2\mu_1^2 + \gamma_2^2\mu_2^2 + \gamma_3^2\mu_3^2 , \tag{9}$$

so that, by using theorem 1, Eq. 1 reduces to

$$\overline{r}^2 \simeq r_0^2 + \overline{r^2} - \overline{\xi^2} , \tag{10}$$

where $\overline{r^2}$ is the mean square radius of the Gaussian and $\overline{\xi^2}$ is the mean square displacement along the vector $\vec{r}_0$.

Now if ρ_B is assumed to be the convolution of ρ and ρ_A, then, from theorems 2 and 3,

$$\overline{r}^2 \simeq r_0^2 + \left(\overline{r_B^2} - \overline{r_A^2}\right) - \left(\overline{\xi_B^2} - \overline{\xi_A^2}\right) , \tag{11}$$

which is equivalent to Eq. 2.

Crystal Structure of Acetylglycine

H. A. Levy S. W. Peterson
V. Schomaker

A weighted least-squares refinement of previous neutron diffraction measurements on acetylglycine has been carried out. Data from $[0kl]$ and $[hk\overline{2h}]$ zones, 279 measurements in all, were utilized; 104 independent parameters were determined. The parameters were broken up into three groups which were handled separately in a refinement cycle; three cycles were required for convergence. Weights were assigned to measured structure factors according to the usual scheme

$$W^{-1} = \text{var } F = [E + 2B + (0.02E)^2] \frac{k^2}{4F^2} .$$

The precision of the determination may be judged from the resulting value of

$$\left[\frac{\Sigma W(F_o - F_c)^2}{m - n}\right]^{1/2} ,$$

the standard deviation of an observation of unit weight, which is 2.8. The R factor

$$\frac{\Sigma \,|\,|F_o| - |F_c|\,|}{\Sigma |F_o|}$$

is 9.7%.

The results of the analysis are best indicated by the diagram in Fig. 63 and by Tables 49, 50,

Table 49. Bond Lengths in Acetylglycine

Bond	Length (Å)	
	X Ray*	Neutron
C_1-C_2	1.506	1.470
C_2-N	1.448	1.464
N-C_3	1.323	1.364
C_3-C_4	1.503	1.491
C_1-O_1	1.312	1.331
C_1-O_2	1.192	1.180
C_3-O_3	1.243	1.214
$O_1 \cdots O_3$	2.558	2.547
N$\cdots O_2$	3.030	3.035

*G. B. Carpenter and J. Donohue, *J. Am. Chem. Soc.* 72, 2315 (1950).

Table 50. Bond Angles (deg) in Acetylglycine

Angle	X Ray	Neutron
O_1-C_1-C_2	111.5	111.1
O_1-C_1-O_2	124.2	124.8
O_2-C_1-C_2	124.3	124.0
C_1-C_2-N	110.2	109.8
C_2-N-C_3	119.6	119.9
N-C_3-C_4	117.7	116.4
N-C_3-O_3	121.3	120.3
O_3-C_3-C_4	121.0	123.4

UNCLASSIFIED
ORNL-LR-DWG. 22197

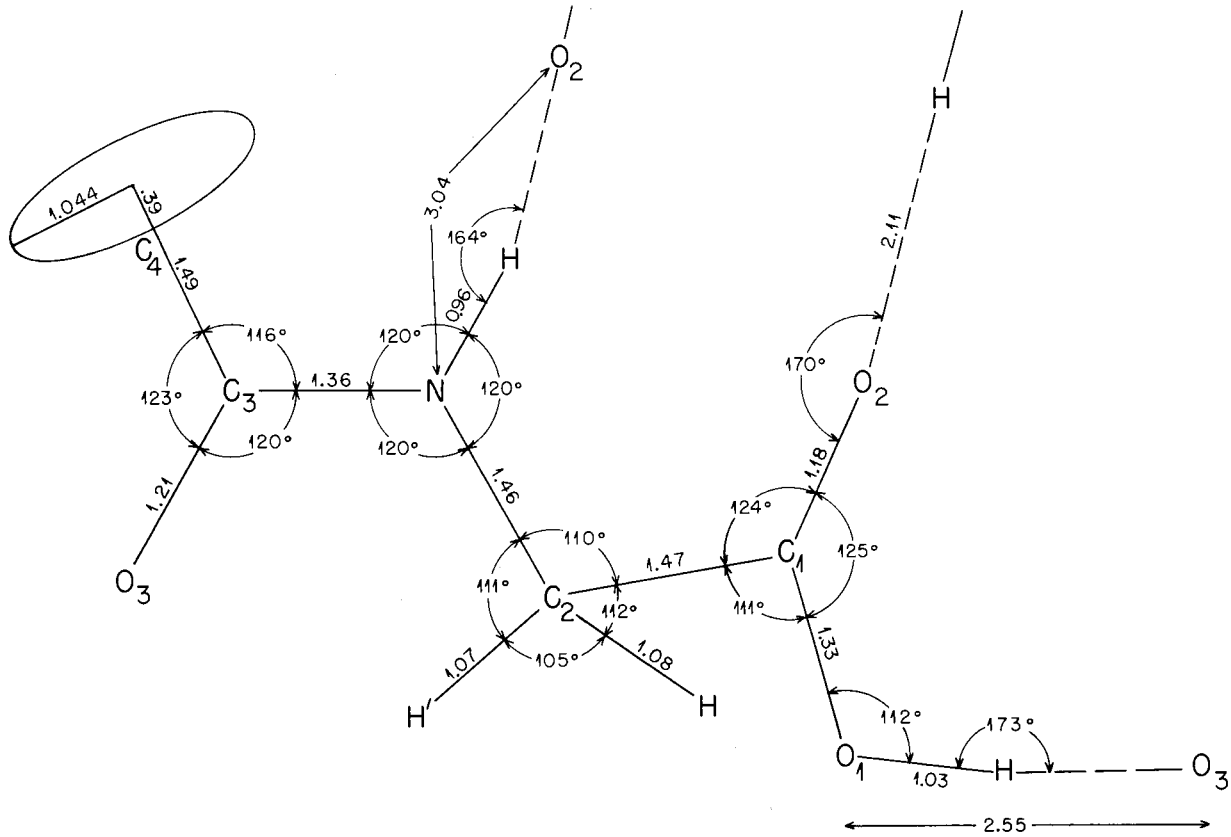

Fig. 63. Acetylglycine Dimensions.

and 51, which list bond distances and angles. The acetylglycine molecule is nearly planar, the methylene and methyl hydrogen atoms being the only ones markedly out of the molecular plane. The main points of interest in the analysis are as follows:

1. the nature of the peptide link,
2. the methyl group,
3. the hydrogen atom locations.

The peptide link is characterized by the trigonal and planar grouping around N, the angles about N being almost exactly 120 deg. The C_2-N bond distance is about normal for a single bond, but the C_3-N is short, indicating some double-bond character. The peptide hydrogen lies near the N-H· · ·O hydrogen bond line, as expected. The N-H distance, 0.95 Å, is shorter than the corresponding distances in urea (0.99), ammonia (1.01), and ammonium ion (1.03).

A distribution of methyl hydrogen atoms suggesting a rotating methyl group was indicated by Fourier analysis early in the investigation. In the least-squares analysis, the methyl hydrogen atoms were approximated by placing 12 one-quarter hydrogen atoms at equal spacing around a circle and adjusting the following seven parameters describing the configuration: the polar and azimuthal angles of the axis of the circle, the radius, three coordinates of the center, and one temperature factor. Estimates of the C-H distance and H-C-H angle from the resulting parameters are 1.11 Å and 104 deg.

The amide hydrogen atom, as already mentioned, is in its expected position on the N-H· · ·O hydrogen bond. The carboxyl hydrogen atom is located, also as expected, close to the O-H· · ·O hydrogen bond line, with an O-H distance of 1.028 Å, correlating well with the moderately short

Table 51. Hydrogen Bond Lengths and Angles in Acetylglycine

Bond	Length (Å)	Bond	Angle (deg)
O_1-H_O	1.028	C_1-O_1-H_O	111.8
N-H_N	0.956	O_1-H_O· · ·O_3	173.2
C_2-H_C	1.078	C_1-C_2-H_C	111.5
C_2-H_C'	1.067	C_1-C_2-H_C'	112.4
H_O· · ·O_3	1.520	H_C-C_2-H_C'	104.9
H_N· · ·O_2	2.106	N-C_2-H_C	107.4
Me C-H	~1.11	N-C_2-H_C'	110.6
		H_N-N-C_2	119.9
		C_3-N-H_N	119.8
		N-H_N· · ·O_2	163.7
		H_N· · ·O_2-C_1	169.8

O· · ·O distance of 2.55 Å. The methylene hydrogen atoms are situated so as to make the environment of C_2 essentially tetrahedral, with C-H distances of 1.08 and 1.07 Å.

The standard deviations of distances not involving hydrogen atoms are about 0.02 Å; those in distances involving one hydrogen atom are about 0.03 Å.

Neutron and X-Ray Diffraction Studies on Urea

H. A. Levy S. W. Peterson
R. D. Ellison

A neutron diffraction study of urea at this Laboratory[7] revealed the positions of hydrogen atoms and gave a partial description of thermal motion. The results of this study differed somewhat from those of an earlier x-ray study,[8] although the differences were not far outside the quoted experimental error of the latter. Grenville-Wells[9] has emphasized that the differences, particularly with regard to thermal parameters, are disturbing and raise the question as to whether neutron and x-ray results in general are strictly concordant. An important aspect of any real difference between neutron and x-ray results is the possibility of deriving information concerning the distribution of electrons in crystals, as distinct from the distribution of the atomic nuclei. In order to explore and clarify these aspects of the urea problem and of the neutron and x-ray diffraction methods in general, the following studies were undertaken.

Extension of the Neutron Study to Three Dimensions. – In the previous study, data were collected from only one zone, [010]; these were sufficient to fix all position parameters, but left one thermal parameter for each atom, β_{bk}, undetermined. The [001] and [110] zones have now been measured, and these data, together with the older set, have been refined by means of least squares, leading to the following agreement criteria:

$$\frac{1}{2}\left(\frac{\Sigma|F_c^2 - F_o^2|}{\Sigma F_o^2}\right) = 3.0\% \; ; \qquad \sigma_1 = 2.25 \; .$$

The parameters are listed in column 1 of Table 52, where they are compared with other sets to be described later. The position parameters are little different from those obtained earlier;[7] the additional thermal parameters confirm the existence of a large rotary amplitude about the C=O bond direction.

Test of the Neutron Parameters Against the X-Ray Data. – The question of concordance between neutron and earlier x-ray results was directly tested by computing x-ray structure factors from the above neutron parameters. The agreement criterion

$$\frac{1}{2}\left(\frac{\Sigma|F_c^2 - F_o^2|}{\Sigma F_o^2}\right)$$

was 8%, as compared with 6% for the Vaughan and Donohue[8] parameters (obtained by Grenville-Wells,[9] who corrected an error in the original work). Inspection of individual structure-factor agreement showed that the fit was less than satisfactory.

[7] J. Worsham, H. A. Levy, and S. W. Peterson, *Acta Cryst.* 10, 319 (1957).

[8] P. Vaughan and J. Donohue, *Acta Cryst.* 5, 530 (1952).

[9] H. J. Grenville-Wells, *Acta Cryst.* 9, 709 (1956).

Table 52. Crystal Parameters for Urea

		Neutron	X Ray		
			Vaughan and Donohue	Spectrometric	
				All Data	Selected Data
C	z	0.3335	0.3291	0.3317	0.3330
	β_{bb}	0.01639	0.02255	0.02247	0.02308
	β_{bk}	0.00156	−0.00233	−0.00008	−0.00321
	β_{ll}	0.00892	0.03044	0.02260	0.01939
O	z	0.5969	0.6008	0.5976	0.5974
	β_{bb}	0.02727	0.03397	0.03531	0.03474
	β_{bk}	0.00295	0.00447	0.00417	0.00150
	β_{ll}	0.00897	0.01558	0.01864	0.01787
N	x	0.1431	0.1423	0.1422	0.1427
	z	0.1829	0.1850	0.1839	0.1824
	β_{bb}	0.03893	0.04507	0.04369	0.04413
	β_{bk}	−0.02204	−0.01976	−0.02084	−0.02132
	β_{ll}	0.01562	0.02389	0.02548	0.02490
	β_{bl}	−0.00122	−0.00133	0.00051	0.00128
H_1	x	0.2537			
	z	0.2830			
	β_{bb}	0.05494			
	β_{bk}	−0.02853			
	β_{ll}	0.05494			
	β_{bl}	−0.01184			
H_2	x	0.13889			
	z	−0.02733			
	β_{bb}	0.04762			
	β_{bk}	−0.02075			
	β_{ll}	0.01997			
	β_{bl}	0.00090			
Scale factor (for F^2)			1.15	1.20	1.22

Refinement of Parameters from the Vaughan and Donohue X-Ray Data. – The analysis of Vaughan and Donohue did not include a complete treatment of asymmetric thermal motion, as did the neutron study (see "Extension of the Neutron Study to Three Dimensions"). In order to bring x-ray and neutron analyses to a comparable basis, the Vaughan and Donohue data were submitted to a general least-squares refinement in which all thermal and position parameters, except those for hydrogen, were included; these latter were held at the neutron-derived values. The quantity minimized was

$$\Sigma w(F^2)\left[F_c^2 - F_o^2\right]^2 ,$$

and weights were assigned according to the formula

$$w^{-1} = \sigma^2(F^2) = (0.1F^2)^2 + 0.2^2 .$$

The resulting agreement criterion

$$\frac{1}{2}\left(\frac{\Sigma|F_c^2 - F_o^2|}{\Sigma F_o^2}\right)$$

was 4.3%; the quantity σ_1 was 1.75. This considerably improved agreement is primarily the result of more general thermal parameters and a revised scale factor; the position parameters were little changed from those of Vaughan and Donohue. Parameters obtained by this treatment are also listed in Table 52 (column 2).

As a result of this refinement, there can be no doubt that the neutron and the published x-ray data yield significantly different parameters, both for positions and for thermal displacements; the differences are as large as six standard deviations. The two estimates of the C=O bond length, for example, differed by 0.02 Å.

Collection and Analysis of Counter X-Ray Data. – For a reliable comparison of x-ray and neutron results, the use of spectrometric x-ray data is highly desirable, since counting techniques afford both higher precision and reliable estimates of experimental error. A set of counter-measured intensities was collected from a spherically ground urea specimen, mounted on a Weissenberg x-ray goniometer equipped with a scintillation counter. Three-dimensional data were obtained with molybdenum $K\alpha$ radiation monochromatized by reflection from NaCl.

Comparison of the counter data with those of Vaughan and Donohue, after scaling both sets in accordance with the least-squares scale factors listed in Table 52, yields the following measure of agreement:

$$\frac{\Sigma|F^2_{\text{V. and D.}} - F^2_{\text{counter}}|}{\Sigma F^2_{\text{V. and D.}}} = 6.6\% ,$$

omitting values for (110) and (111). These two reflections are open to question because of extinction and because in the Vaughan and Donohue set they are derived from powder measurements. In general, this agreement is considered to be satisfactory.

These new data were analyzed by means of least squares, with weights assigned that are consistent with the formula

$$\sigma^2(E) = (0.02E)^2 + E + 2B ,$$

E being the integrated intensity and B the background measurement. The agreement criteria achieved were

$$\frac{1}{2}\left(\frac{\Sigma|F_c^2 - F_o^2|}{\Sigma F_o^2}\right) = 3.3\% ; \quad \sigma_1 = 1.26 .$$

These remarkably small values attest to the value of counter data and the power of the least-squares refinement method.

The resulting parameters (Table 52, column 3) show two important points: (1) the position parameters are identical within experimental error with the neutron values, and (2) the thermal parameters differ from the corresponding neutron results to a highly significant degree, being uniformly larger than the latter.

Test of the Effect of Distortion of the Outer Electrons. – An interpretation of the difference between neutron and x-ray results might lie, as mentioned earlier, in the details of the distribution of electrons about the atomic nuclei. The x-ray results have thus far been analyzed in terms of electron distributions for isolated atoms; if serious distortions of these distributions exist in urea, produced for example by bonding or hybridization of orbitals, the effect might possibly be simulated by apparent thermal parameters that are different from those describing nuclear displacement. A

test of this interpretation was made in the following way. A selection of the x-ray data including only reflections at low and high scattering angles was analyzed by means of least squares. These particular data are least sensitive to electron distortion effects; those at low angle depend substantially only on the total number of electrons per atom, while those at high angle depend mostly on the K electron distribution. The exact criterion used was rejection of reflections for which $2 < f_o < 6$.

The resulting parameters (Table 52, column 4) differed very little from those resulting from analysis of the entire set of data. It must be concluded, therefore, that electron distortion is not the principal cause of nonconcordance between the x-ray- and neutron-derived thermal parameters.

The studies described above show good agreement between position parameters for atoms in urea obtained by neutron and x-ray diffraction methods, but leave a pronounced disagreement in thermal parameters. It was further shown that the disagreement is not principally a reflection of electronic distortion.

Elucidation of this disagreement must await further study. However, a possible line of investigation may be suggested. The thermal displacements in urea are unusually large, and these displacements give rise to diffuse scattering of x rays, and presumably also of neutrons. It seems quite possible that a portion of the diffuse neutron scattering might occur at angles only slightly displaced from Bragg directions and, with typical neutron spectrometer resolution, be measured along with Bragg intensity. The corresponding effect in the x-ray measurement would not occur because of the higher resolution of that measurement. The over-all result might then be an apparent reduction in the thermal displacements deduced from neutron measurements.

Preliminary Neutron Diffraction Study of Solid H_2O_2

W. R. Busing H. A. Levy

An x-ray study[10] has shown that solid H_2O_2 is tetragonal and that it has space group $D_4^4 - P4_12_1$, with four molecules in a cell of dimensions a = 4.06 Å and c = 8.00 Å. It was postulated that the hydrogen atoms lie on the line connecting two oxygens, separated by 2.78 Å, and in positions which would make the dihedral angle between planes containing H_1-O_1-O_2 and O_1-O_2-H_2 equal to 94 deg.

A 56-mg single crystal of H_2O_2 was grown in a sealed quartz tube by R. W. Holmberg, and the neutron diffraction intensities of 16 nonequivalent $hk0$ reflections were measured at −25°C, as described elsewhere.[11] Experimental structure factors were found in the usual way, and an $hk0$ Fourier projection was made by using signs calculated from the x-ray structure and postulated hydrogen positions. This projection indicated that the model was essentially correct, and a least-squares refinement was made by varying the two position parameters and three temperature factor coefficients of the oxygen and of the hydrogen and an over-all scale factor. A weighted discrepancy factor in F^2,

$$\left[\frac{\Sigma w\left(F_o^2 - F_c^2\right)^2}{\Sigma w F_o^4}\right]^{1/2},$$

of 6.1% was obtained.

The position parameters resulting from the least-squares refinement are in good agreement with those from the x-ray determination, and they are listed together in Table 53 for comparison. Work

[10] S. C. Abrahams, R. L. Collin, and W. N. Lipscomb, *Acta Cryst.* 4, 15 (1951).

[11] S. W. Peterson and H. A. Levy, *J. Chem. Phys.* 20, 704 (1952).

Table 53. The Fractional Position Parameters of H_2O_2

		X-Ray* Diffraction	Neutron Diffraction
O	x	0.071	0.072
	y	0.172	0.170
	z	0.217	
H	x	0.24**	0.220
	y	0.44**	0.460
	z	0.37**	

*See ref 10.

**Estimated by assuming the postulated model and by using an O-H distance of 1.0 Å.

on another zone is now in progress, and this should give the z coordinates of the atoms as well as a complete description of their thermal motion.

MASS SPECTROMETRY AND RELATED TECHNIQUES

Dissociation of CO^+ and CO^{++} Ions by Collision with Neutral Molecules

C. E. Melton G. F. Wells

Ion-molecule reactions between ions of CO and the following molecules were investigated with a mass spectrometer: He, D_2, H_2, N_2, CO, A, and Kr. The reactions studied were

(1) $CO^+ + M \rightarrow C^+ + O + M$

(2) $CO^+ + M \rightarrow C + O^+ + M$

(3) $CO^{++} + M \rightarrow CO^+ + M^+$

(4) $CO^{++} + M \rightarrow C^+ + O + M^+$

where M is any neutral molecule. These reactions were investigated as a function of the energy of the CO ions over the range of 1000 to 5100 ev. The relative cross sections normalized to helium for dissociation of 5100-ev CO^+ ions are shown in Table 54.

The predominant ion resulting from dissociation of CO^{++} is C^+, suggesting a charge-exchange dissociation reaction. This is supported by the observation that neutral molecules having high ionization potentials such as helium and neon do not produce dissociation in CO^{++}. Relative cross sections normalized to krypton for CO^{++} are shown below for the reaction

$$CO^{++} + M \rightarrow C^+ + O + M^+$$

Neutral Molecule	Relative Cross Section
He	0
Ne	0
D_2	67
H_2	67
N_2	50
CO	94
A	83
Kr	100

These data suggest that the energy for dissociation of the CO^{++} ions is derived completely from electronic energy, in opposition to the dissociation of CO^+ ions, which requires the conversion of kinetic energy to vibrational energy. These dissociation studies indicate that the fragmentation of a molecule is dependent on the structure of the molecule rather than on the method of excitation. A more complete treatment of this problem has been submitted for publication.[12]

Calculations for the absolute cross sections were made by using for the pressure the uncorrected values as read by the ion gage. Also, equal collection efficiencies were assumed for

[12] C. E. Melton and G. F. Wells, *J. Chem. Phys.* (to be published).

Table 54. Relative Cross Sections for Dissociation of CO^+

$CO^+ + M \rightarrow C^+ + O + M$		$CO^+ + M \rightarrow C + O^+ + M$	
Neutral Molecule	Relative Cross Section	Neutral Molecule	Relative Cross Section
He	100	He	100
D_2	82		
H_2	81	H_2	24
N_2	73		
CO	68	CO	38
A	55	A	34
Kr	34	Kr	14

the primary and secondary ion beams. Results of these calculations are shown in Table 55 and are compared with those obtained by Kuprianov[13] and co-workers in Russia.

Research Mass Spectrometer, RS 1

G. F. Wells C. E. Melton

The single-stage 6-in.-radius mass spectrometer shown in Fig. 64 has been in continuous use to investigate ion-molecule collision reactions. Some of the operating characteristics are illustrated by data from the following tests.

Measurements of the diffusion of gases from the analyzer tube to the ionization chamber and vice versa indicate that the following pressure ratios can be maintained: $(P_i/P_t)_S = 200$ and $(P_t/P_i)_T = 58$, where P_i is the ionization chamber pressure, P_t is the analyzer tube pressure, S indicates source admission of the gas, and T indicates tube admission of the gas.

By utilizing these ratios, a knowledge of the per cent dilution of a gas in one region by the gas in the other region may be obtained as illustrated below:

	Pressure with Source Admission (mm Hg)	Pressure with Tube Admission (mm Hg)	Dilution (%)
	$\times 10^{-5}$	$\times 10^{-5}$	
Ionization chamber	4.0	0.04	1.0
Analyzer tube	0.02	2.3	0.87

[13] S. E. Kuprianov *et al.*, *J. Expl. Theoret. Phys.* 30, 569 (1956).

The previously calculated maximum resolution[14] of 730 based on a mercury spectrum has been checked with a gas mixture of CO and C_2H_4. The difference in mass, Δm, of these two molecules is 0.036 mass unit at mass 28. To resolve completely these two masses would require a resolution of 778. As shown in Fig. 65, the two peaks are readily identified, although they are not completely separated.

As a final check of the ability of the instrument to operate as designed, a study was made of the ion-molecule collision reaction

$$N_2^+ + M \longrightarrow N^+ + N + M$$

where M is any atom or molecule. Figure 66 shows some results of this study. The relative abundance of the N^+ ion to its parent ion, N_2^+, is plotted as a function of the analyzer gas pressure, P_t, for various gases. The N^+ ion was not diluted below a value of $P_t = 1 \times 10^{-6}$ mm Hg. The linear increase in N^+ above this value is in agreement with the well-known mechanism of formation of this ion, which is the product of a single-collision reaction with an atom or molecule of the analyzer tube gas.

Two-Stage Mass Spectrometer, RS 2

G. F. Wells C. R. Baldock

The two-stage mass spectrometer analyzer tubes and vacuum system previously described[15] have now been fabricated, and the initial phases of the vacuum testing have begun.

[14] G. F. Wells and C. E. Melton, *Stable Isotopes Semiann. Prog. Rep. Nov. 30, 1956*, ORNL-2236, p 28.

[15] G. F. Wells and C. R. Baldock, *Stable Isotopes Semiann. Prog. Rep. May 20, 1956*, ORNL-2114, p 17–19.

Table 55. Absolute Cross Sections for Dissociation of CO^+

Reaction	Source of Data	Value (cm^2)
$CO^+ + CO \longrightarrow C^+ + O + CO$	ORNL	0.2×10^{-17}
	Kuprianov	1×10^{-17}
$CO^+ + CO \longrightarrow C + O^+ + CO$	ORNL	0.02×10^{-17}
	Kuprianov	0.1×10^{-17}

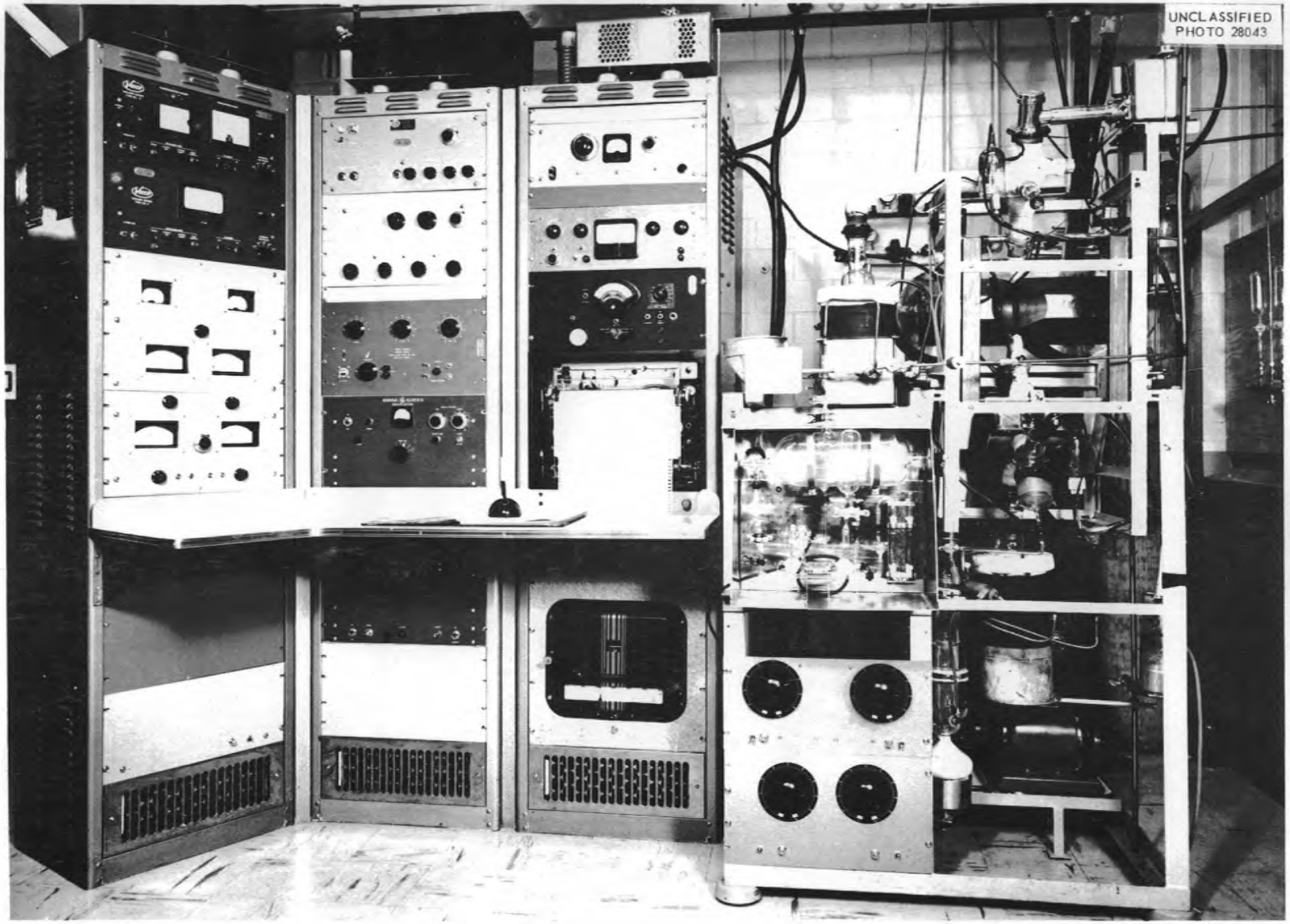

Fig. 64. Research Mass Spectrometer, RS 1.

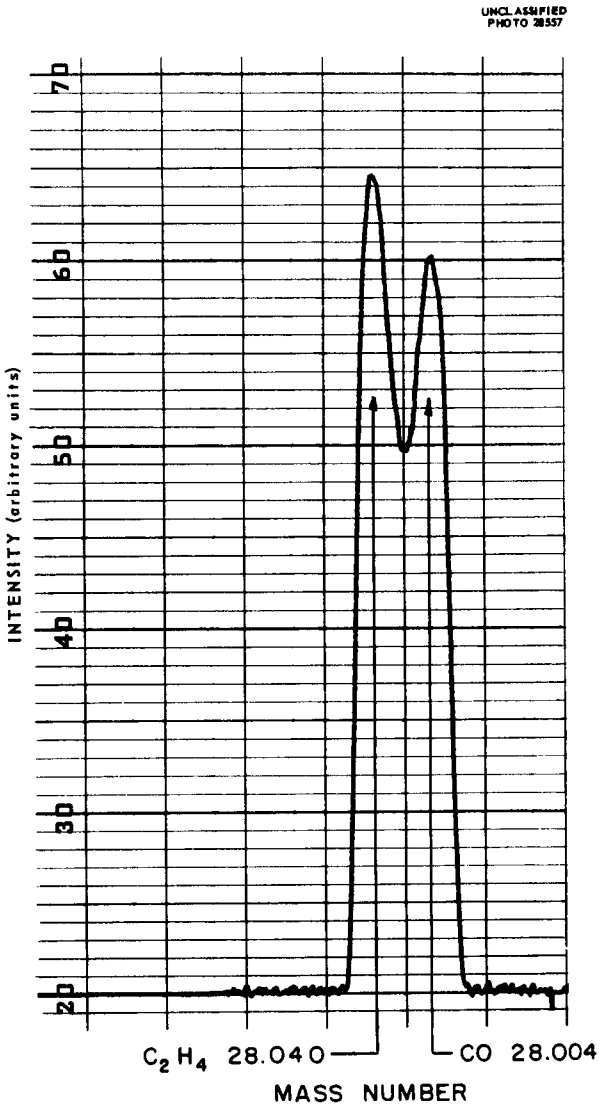

Fig. 65. Resolution of CO and C_2H_4.

FUNDAMENTAL VIBRATIONAL-ROTATIONAL BAND OF $N^{15}O$

W. H. Fletcher[16] G. M. Begun

Nitric oxide is the only stable diatomic molecule which possesses an unpaired electron. Because of this odd electron NO has a resultant orbital angular momentum of 1 and a spin angular momentum of $\pm\frac{1}{2}$ (in units of $h/2\pi$). This results in a doublet Π ground state, and in the case of NO the two components are only slightly separated. These properties produce an interesting and unique infrared spectrum and important perturbations in the microwave spectrum which are associated with the nuclear magnetic moment and the quadrupole moment of the nitrogen. The availability of high-purity N^{15} from the Nitrox process has made it possible to examine the infrared spectrum of $N^{15}O$. The rotational structure of the fundamental vibrational band has been studied.

Nitric oxide containing 95% N^{15} was prepared from nitric acid by reaction with SO_2. The spectroscopic measurements were made on the University of Tennessee grating spectrometer[17] with a 7500-line/in. Bausch and Lomb replica grating and a Golay detector. Gas pressures ranging from 6 to 30 cm in a 10-cm cell were used. Measurements were made on slow traces in which the resolution of all but two of the spin-doubled R lines was easily seen, and a number of lines in the Q branch were also resolved.

The two sub-bands and the Q branch were analyzed mathematically, and observed and calculated frequencies for the lines were tabulated. The molecular constants of $N^{15}O$ (cm^{-1}) determined are summarized below:

$B_{01} = 1.6146$	$B_{02} = 1.6577$
$B_{11} = 1.5984$	$B_{12} = 1.6410$
$D_{01} = D_{11} = 3 \times 10^{-6}$	$D_{02} = D_{12} = 8 \times 10^{-6}$
$(B_{01} - B_{11}) = -0.01631$	$(B_{02} - B_{12}) = -0.01695$
$G_1(1 \leftarrow 0) = 1843.05$	$G_2(1 \leftarrow 0) = 1842.79$
$B_e = 1.6446$	$\alpha_e = 0.0170$

The anharmonic constants[18] for $N^{14}O$ were employed to calculate the corresponding constants for $N^{15}O$. The calculated band centers for several vibrational transitions for $N^{15}O$ and the anharmonic constants are given in Table 56. The data from the fundamental vibration-rotation band of $N^{15}O$ yield a value of 0.0166 cm^{-1} for α_e', but since this is based on only one band it is less reliable than the value of 0.0170 cm^{-1} which is calculated from the isotopic relation. The difference is, however, within experimental error.

[16] Consultant, Chemistry Department, University of Tennessee.

[17] A. H. Nielsen, *J. Tenn. Acad. Sci.* **22**, 241 (1947).

[18] J. H. Shaw, *J. Chem. Phys.* **24**, 399 (1956).

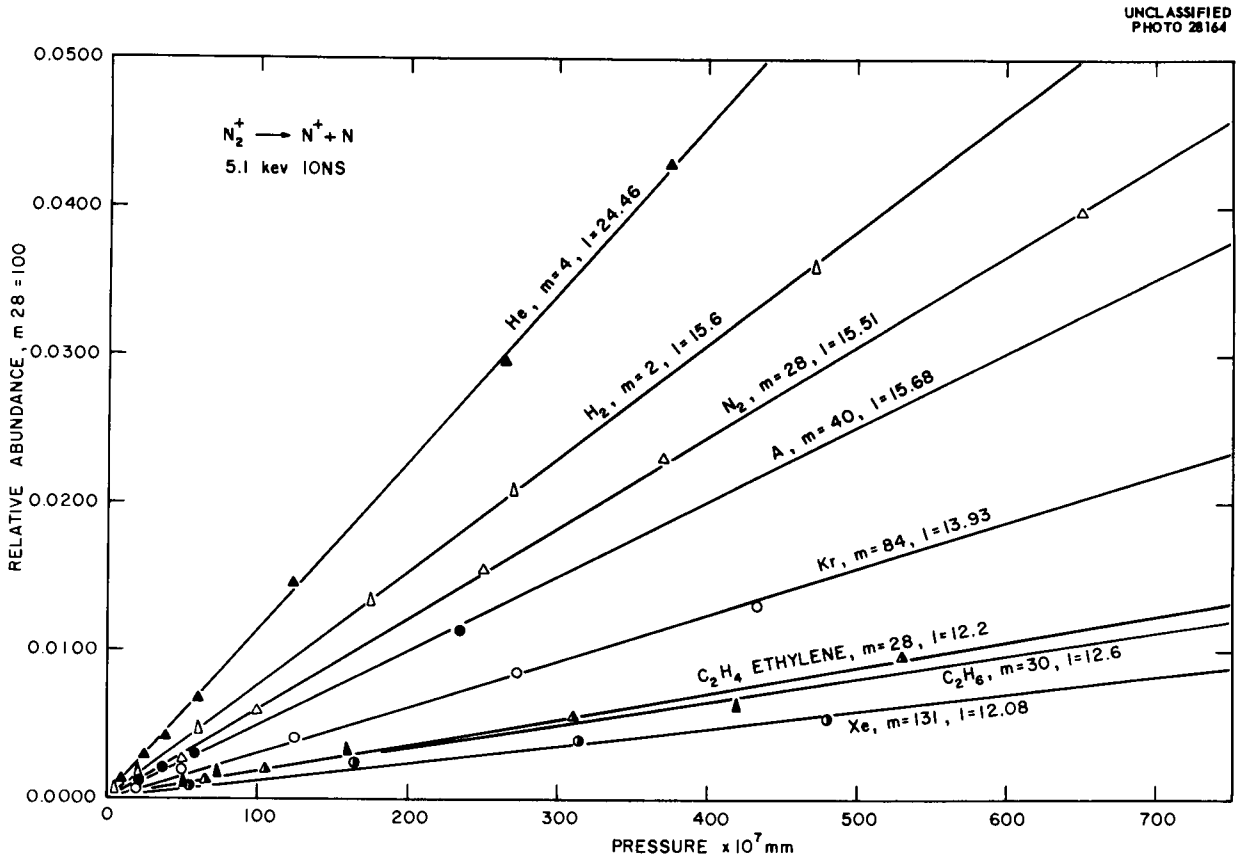

Fig. 66. Relative Abundance of the Collision-induced N^+ Ion as a Function of the Pressure of Various Gases.

Table 56. Calculated Anhormonic Constants and Vibrational Transitions for $N^{15}O$ (cm^{-1})

Band	$\Omega = 1/2$	$\Omega = 3/2$
(1 – 0)	1843.04	1842.70
(2 – 0)	3659.12	3658.44
(3 – 0)	5448.25	5447.23
(4 – 0)	7210.42	7209.06
$\omega'_{e1} = 1869.98$	$\omega'_e x'_e = 13.47$	
$\omega'_{e2} = 1869.64$	$\omega'_e y'_e = -0.00114$	

It is planned to investigate the infrared spectra of the various N^{14} and N^{15} species of N_2O, and these compounds have been synthesized from high-purity N^{15}.

BEAM STUDIES IN CHEMICAL KINETICS

S. Datz E. H. Taylor

A new branch of study has been undertaken in which a beam of low-energy, simple ions will be made to collide with a molecular beam. The composition and angular distribution of products will be observed by means of a small mass analyzer rotating about the scattering center. The first ion-molecule study will be the reaction of the protium ion with the deuterium molecule.

In order to study collisions of chemical interest, the ion beam required is in the very low energy region of from 0.1 to about 5 ev, and the energy spread should be as small as possible ($\Delta E/E$ = 0.01) to facilitate interpretation of the angular distribution. To accomplish this the ion source and monochromator described below was designed and constructed.

The ion source utilizes a radio-frequency discharge tube of the type developed for use as a Van de Graaff source[19] which can deliver sustained proton currents of 500 to 1000 μa. The scheme employed is illustrated in Fig. 67. A beam of protons is extracted at 2000 to 5000 v from the ion source A, is bent through magnet section B, passes through grid C, and experiences a retarding potential at grid D. The retarding potential is adjusted so that those protons which are formed in the discharge in the high half of the energy distribution will be transmitted through grid D, reaccelerated by grid E, and discarded. Those protons formed in the low half of the energy distribution are reflected from equipotential planes between C and D and are reaccelerated in the opposite direction. Since the sense of the current is now opposite, the reflected beam will be bent by magnet B so that it passes through the grid system F, G, H. The grid G is set at a retarding potential slightly less than D so that only those protons will be transmitted through the entire system which have an energy spread equal to the difference in potential between D and G. The beam is then slowed to low energies by a retarding grid just before collision. Electrostatic lenses L_1, L_2, and L_3 are used to maintain focusing through the system. This system is presently undergoing tests.

UNCLASSIFIED
ORNL-LR-DWG. 22315

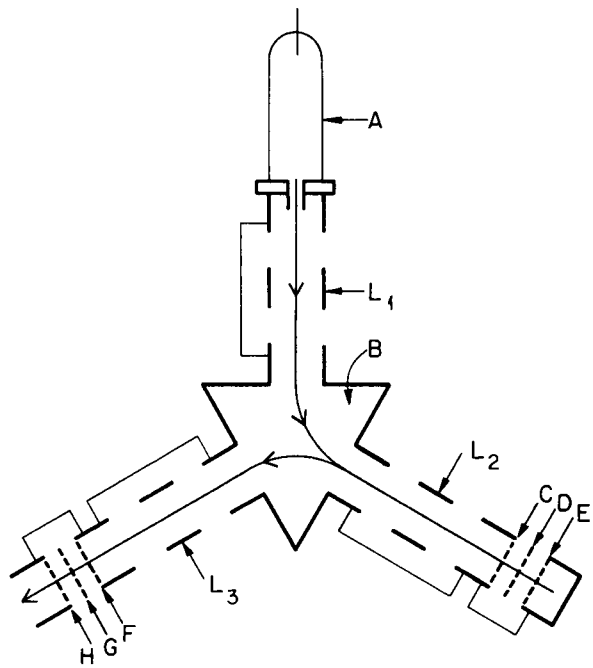

Fig. 67. Ion Source and Monochromator.

[19] C. D. Moak, H. Reese, and W. M. Good, *Nucleonics*, 9(3), 18 (1951).